DISSERTATION

MULTI-MODAL INVESTIGATION OF TENDON HEALING: TENDINOPATHIC INJURY

MODELS TO NOVEL REHABILITATIVE STRATEGIES

Submitted by

Sherry Johnson

Department of Clinical Sciences

In partial fulfillment of the requirements

For the Degree of Doctor of Philosophy

Colorado State University

Fort Collins, Colorado

Fall 2022

Doctoral Committee:

      Advisor: David Frisbie
      Co-Advisor: Melissa King

      Kurt Selberg
      Adam Chicco

ABSTRACT

MULTI-MODAL INVESTIGATION OF TENDON HEALING: TENDINOPATHIC INJURY

MODELS TO NOVEL REHABILITATIVE STRATEGIES

For decades, superficial digital flexor tendon (SDFT) injuries have been a source of debilitating morbidity and significant economic loss for the equine industry. The high rate of equine tendon re-injury is believed to be due to the inferior biomechanical properties of the damaged tendon and the higher compensatory stresses and strains of the adjacent transitional areas between healthy and pathologic tissues. Even following periods of extended convalescence, diagnostic imaging and clinical evaluations often suggest that tendons have adequately healed, but neither can consistently predict physiologic preparedness to return to work. These shortcomings have motivated investigations to explore advanced diagnostic imaging methods' correlation to lesion staging and quality of healing. Additionally, when exercise can be initiated following SDFT injury, it is usually at a much lower intensity than pre-injury, with little known about efficacy of specific therapeutic exercise prescriptions. Subsequent rehabilitation strategies have remained imperfect, with few proving superior to that of rest and controlled exercise. Orthopedically, humans face similar challenges with injury often leading to cyclic pain, disuse and ultimately loss of function. Blood flow restriction (BFR) training has become increasingly utilized by human physical therapists to prescribe controlled exercise following injury due to the ability to increase strength via low intensity training to a level typically only achieved with mid to high intensity training. Such a rehabilitative modality in horses may be highly beneficial, but little is known about modernized BFR application in the horse.

The compilation of studies described herein aims to advance the understanding of tendinopathy by first investigating the utility of advanced diagnostic imaging methods in various experimental tendinopathic models, then exploring the role of exercise variables in a translational murine model of tendon injury, and lastly investigating the safety and musculoskeletal effects of a novel orthopedic rehabilitative modality for horses, that of blood flow restriction (BFR) training. It is through this series of investigations that improvements in the management of tendinopathy from diagnosis to rehabilitation have been realized.

The objective of the first study was to obtain a better understanding of the complex interplay between multi-modal diagnostic imaging and tendon tissue characteristics. Specifically, computed tomography (CT), magnetic resonance imaging (MRI), and ultrasound (US) evaluations were compared to outcome measures for histologic, biochemical and biomechanical parameters using an equine surgical model of tendinopathy. Lesions were surgically created in both forelimb SDFTs of eight horses and imaged using MRI, CT and US at seven time points over twelve months. Imaging characteristics were then correlated to end point histologic, biochemical and biomechanical data using lasso regression. Interestingly, lesion isoattenuation on CT evaluation suggested suboptimal healing, while T2-weighted hyperintensity indicated hypercellular tendinopathy even in chronic stages of healing. Non contrast-enhanced MRI and CT evaluation correlated most closely to cellular characteristics of surgically damaged tendons assessed over this twelve month study period. Ultrasonographic evaluation was found to significantly underestimate true lesion size.

In the second study, the ability of elastography to differentiate tissue deformability characteristics associated with treatment and biochemical properties using a prospective, experimental study design was evaluated. Tendinopathy of both forelimb deep digital flexor

iii

tendons (DDFTs) was induced with collagenase under ultrasonographic guidance. One randomly assigned limb was treated with intra-lesional mesenchymal stem cell (MSC) injection with the opposite limb serving as an untreated control. Horses were placed into a controlled exercise program with elastographic evaluations performed baseline (0) and 14, 60, 90, and 214 days post treatment. Post-mortem biochemical analysis was performed. Elastographic outcome parameters were found to be weak predictors of biochemical tissue analysis, with all R^2 values ≤0.50. Additionally, within this range of differences in glycosaminoglycan content between treatment groups, elastography outcomes did not predict biochemical differences. Tissue-specific differences between DDFTs treated with MSCs compared to untreated controls were apparent biochemically, but not predicted by elastography.

Thirdly, the therapeutic benefits of various exercise protocols for mid-body Achilles tendinopathy with relationship to exercise capacity, morphology, and mechanical outcomes were explored using an established model of murine tendinopathy. Additionally, the relationship between exercise and the local and systemic levels of Collagen X (COLX), a marker of endochondral ossification, with respect to tendon zonal enthesis attachment and healing was investigated. Specifically, the objectives of this study were: 1) To advance the understanding of how alterations in exercise speed and grade (flat vs 17° incline or decline) affect the quality of tendon healing, and 2) To determine if a biomarker relationship exists between serum levels of ColX and animals exposed to treadmill running protocols. Tendinopathy was induced by two intra-tendinous TGFβ1 injections (performed on study days 0 and 2) followed by randomization into the following groups: 1) rest (normal cage activity); and exercise protocols of 2) slow (no grade), 3) fast (no grade), 4) slow-incline, 5) fast-incline, 6) slow-decline, and 7) fast-decline. Exercise capacity and objective gait analysis were measured weekly during the experimental

time-course up to the final 14-day timepoint. Mice were euthanized, and histopathologic analysis and evaluation of serum ColX levels were performed. Exercise initiated at a fast, flat speed (in absence of incline or decline, and in comparison to all other exercise groups) demonstrated inferior tendinopathic healing at the cellular level; and impaired stance braking abilities, which were compensated for by increased propulsion. Mice exposed to exercise (at any speed or grade) demonstrated higher systemic levels of COLX than those that were cage rested, and mice exposed to fast exercise had the highest levels of articular COLX in comparison to slow exercise groups.

Lastly, the final chapters herein describe both the safety and musculoskeletal effects of BFR in horses. From a safety perspective, exposure to BFR did not result in forelimb biomechanical dysfunction. Applied pressures of 75-151 mm Hg simulated a range of 50-80% vascular occlusion in horses. In the series of musculoskeletal investigations comparing BFR and sham cuff exposure over a 56-day study period in 8 healthy horses, BFR resulted in intra-horse differences in SDFT stiffness, with tendons exposed to BFR demonstrating increased stiffness relative to contralateral counterparts. This was associated with a trend in increased CSA, but no differences in elastic modulus. Similarly, BFR exposure did not significantly affect bone density as assessed on CT evaluation, and no differences in gross, histologic or biochemical articular cartilage properties as a result of BFR exposure were appreciated. Cumulatively, this initial investigation determined that no detrimental effects related to BFR use occurred in normal (healthy) equine tissues, and there's now evidence to suggest that BFR may beneficially improve (normal) tendon stiffness. These findings are exciting and warrant further investigation into BFR's application for a variety of equine orthopedic injuries.

In conclusion, incorporation of various experimental tendinopathic models as described herein has helped provide insight into the diagnostic capabilities of advanced imaging methods pertinent to tendon injury. In the author's opinion, the surgical tendinopathy model is currently the most similar experimental model to that of naturally occurring injury. Within the realm of tendon diagnostics, non contrast-enhanced CT evaluation shows significant promise due to its correlation to aggrecan deposition. Rehabilitative modalities of controlled exercise variables and BFR were also investigated, with musculoskeletal effects of BFR in healthy horses providing promising (non-detrimental) results that may inspire future translational research. Specifically, exercise initiated at a fast, flat speed appears most detrimental for tendon healing, and BFR exposure appears to increase tendon stiffness. These findings are exciting and will inspire subsequent investigations exploring exercise and BFR as bio-hack solutions to expedite orthopedic healing. Further work within the field of BFR utilizing experimental injury models and clinical trial study designs will be expected to further guide injury-specific usage in both horses and humans.

ACKNOWLEDGEMENTS

TABLE OF CONTENTS

CHAPTER 1 – Literature Review of Naturally Occurring Equine Tendinopathy and Experimental Tendinopathic Models

1.1 Introduction

For decades, tendon injuries have been a source of debilitating morbidity and economic loss for the equine industry [1]. When managing an equine athlete with tendon injury, the clinician must consider several factors that will ultimately affect each horse's rehabilitation and subsequent prognosis including: 1) Affected tendon, 2) Intra-thecal vs. extra-thecal nature of the injury, 3) Lesion configuration (core vs. peripheral margin tear vs. spiraling), 4) Anatomic lesion length and extent (peritendinous tissue and involvement of the enthesis vs. discrete lesion confinement), and 5) Chronicity. Adding to the complexity of injury considerations are the inherent structural differences in superficial digital flexor tendon (SDFT) and deep digital flexor tendon (DDFT) anatomic configurations. While broad-sweeping conclusions regarding each tendon injury type are yet to be defined, numerous investigations to-date have helped refine injury patterns, risk factors and proposed etiologies. With few therapeutic interventions having been shown to be consistently superior to that of controlled exercise alone, the translational orthopedic community still relies on various experimental tendon injury models to further investigate this frustrating source of soft tissue injury. This chapter serves to outline the most pertinent investigations to this extent, while also highlighting opportunities for future (expected) advancements into tendinopathic repair.

1.2 Anatomic and Functional Overview of the Equine Superficial Digital Flexor and Deep Digital Flexor Units

The equine superficial digital flexor (SDF) muscle originates from the medial epicondyle of the humerus and courses along the palmar-medial aspect of the antebrachium before entering the carpal canal at the myotendinous junction [2,3]. At the distal extent of the carpal canal, it becomes extra-thecal within the mid metacarpal region before entering the tendon sheath and eventually inserting on the distal lateral aspects of the proximal phalanx and the proximal palmar aspect of the middle phalanx [2,3]. The SDF muscle is known for being highly pennate and small in volume with a long tendon relative to its contractile fibre length [4]. With this anatomic architecture, it is suggested that smaller distal muscles such as the SDF help stabilize the forelimb in early stance phase in preparation for the corresponding tendons (passive structures) to be stretched, thereby promoting efficient locomotion [5]. Coordinated muscle co-contraction with simultaneous stretching of the accessory ligaments of the SDF and deep digital flexor (DDF) help promote further positional control of the limb [5]. The SDF muscle specifically is known for attenuating high-frequency vibrations of the forelimb [6], aiding in carpal/digit flexion and elbow extension [3] and enhancing elastic energy storage [5, 7-8]. Cumulatively, these features suggest that the SDF muscle-tendon unit comprises a biomechanically critical limb-spring system that reduces the metabolic cost of locomotion [5, 7-8].

Perhaps the most complex tendon in the equine body, the forelimb deep digital flexor (DDF) originates as three individual muscle bellies from: 1) Medial epicondyle of the humerus (humeral head), 2) Middle caudal radius (radial head) and 3) Medial olecranon of the ulna (ulnar head) [2,3]. At the myotendinous junction, the DDFT traverses through the carpal canal and emerges extra-thecally within the mid-metacarpal region before coursing into the tendon sheath. At the level of the proximal sesamoid bones and middle scutum it assumes a fibrocartilaginous (thick, pad-like) composition, then courses through the pastern as a bi-lobed, intra-thecal tendon,

navigating eventually through the navicular bursa where it again becomes fibrocartilaginous at the level of the flexor surface of the navicular bone (distal scutum). The DDFT then inserts as an enthesis on the palmar aspect of the distal phalanx [2,3]. Similar to the structure and function of the SDF, the DDF muscle is highly pennate, small in volume and has a long tendon relative to its contractile fibre length [4]. Biomechanically, it is activated just prior to hoof-strike and deactivated during stance phase (just as that of the SDFT) [5] and serves to flex the carpus/digit, extend the elbow and aid in weight-bearing [3].

1.3 Prevalence of Tendon Injuries in the Equine Athlete:

Across all equine disciplines, the Thoroughbred racehorse has become one of the most frequently reported athletes suffering from SDFT overuse injuries [9-11]. Superficial digital flexor tendon injury specifically was implicated as the primary reason for retirement of Thoroughbred racehorses over a 12-year epidemiologic study period [12], with re-injury rates reported to be as high as 82% in slight, moderate, or severe injuries [13]. Pursuant to the New Zealand racehorse, risk factors for injury to the SDFT were found to be higher in males, older horses and in horses in active training but without any starts [14]. Similarly, superficial digital flexor (SDF) tendinopathy was documented in 24% of National Hunt racehorses, with older horses having a significantly higher prevalence of SDFT pathologic change compared to younger horses [15]. With a reported prevalence of 11.1%, forelimb SDFT injuries were also associated with a horse's age and sex in Japanese Thoroughbred flat racehorses [11]. Also noteworthy, authors investigating association of type of sport and performance level with the anatomic site of orthopedic injury found a high risk of forelimb SDFT injury in elite Eventing and elite show-jumping horses [16]. Likewise, various breed-specific differences in mechanical properties of the SDFT have been recently described, leading authors to suspect that selection for high-speed (race horses) vs. extravagant elastic gait

(sport horses) to maximize performance ability has led to dichotomous differences in inherent elastic modulus [17].

In contrast to classic SDFT mid-metacarpal lesions, intrathecal DDFT injuries are a common source of distal limb lameness in athletic horses [18-21], being documented in 83% of cases evaluated with high-field magnetic resonance imaging (MRI) [20]. The physiologic complexity of distal limb DDFT injuries has been attributed to structural and biomechanical differences that occur in the proximal to distal and dorsal to palmar directions, with 50% of lesions occurring within the pastern region [22] and 96% of those configured as core lesions [22]. Most recently, the prevalence and character of DDF tendinopathy in the pastern and its association with concurrent DDFT injury within the foot was investigated [23]. Authors documented core lesions in the pastern to be significantly more likely to be associated with injury in the foot, with 97% of core pastern lesions also demonstrating distal tendinopathy [23]. Prognosis for athletic soundness in horses with distal limb DDFT injuries is considered guarded to poor, with only 41% of horses with core lesions returning to some level of activity [24]. Interestingly, in the author's experience for both SDFT and DDFT injuries, lesion configuration extending from intra-thecal to extra-thecal (or vice versa) is much less common than lesion confinement to solely one thecal region. For example, more rarely (and in absence of catastrophic breakdown) does an injury of the SDFT within the tendon sheath extend to the mid-metacarpal extra-thecal region (or vice versa).

With injury rates and lesion characteristics having been well-described for both SDFT and DDFT injuries, their early detection and appropriate management remains a central focus for the equine sports medicine community. While advanced imaging techniques have certainly improved lesion characterization, the looming question of pathophysiologic mechanisms of injury remain. Even after adequate healing is perceived based on diagnostic imaging and clinical impressions, the

risk for tendon re-injury remains high. For conciseness, the remainder of this chapter will focus on the SDFT in terms of proposed mechanisms of injury and experimental models of tendinopathy.

1.4 Proposed Pathophysiologic Mechanisms of Equine SDF Tendinopathy:

Compositionally, tendons are made of 50-60% water with the remaining dry matter (70-85%) being composed primarily of type I collagen [25-27]. Suspended in a non-collagenous matrix containing a small, yet critical population of tenocytes, collagen molecules are aligned in a hierarchical structure of fibrils [25]. Fibrils coalesce into fibres and ultimately fascicles [25, 28]. An interfascicular matrix (IFM) encases and links the fascicles and is made primarily of type III collagen, elastin and proteoglycans [29]. Historically noted to have poor vascular supply, low regenerative capability and in general slow and limited physiologic responses to injury, decades' worth of investigations into the predisposition of the equine SDFT to overstrain injury are reported with three main theories persisting in relevance: 1) biomechanical, 2) biothermal and 3) age-related alterations [25]. Through subsequent and ongoing investigations, most authors acknowledge that the true source of injury is likely multi-faceted, complex and still not fully understood.

As the principal energy-storing tendon of the equine forelimb, the SDFT undergoes constant stretch and recoil with active locomotion, conserving energetic costs by as much as 36% [25, 30-31]. Albeit efficient, this extreme loading environment makes tendons such as the equine SDFT prone to strain-induced injury [25]. Worth specific mention is the accumulation of microdamage in absence of adequate recovery time that fosters susceptibility to injury [25, 32-33]. Specific to the racehorse, a 72-hour time period following a race has been suggested to re-establish tendon homeostasis [33]. As matrix microdamage accumulates, the capacity of cells to repair micro-tears prior to further loading is diminished, leading to clinical injury that is believed to occur

as a result of continuous loading cycles (rather than one singular event) [25, 34]. While mechanistic focus has historically implicated the role of progressive microdamage of collagen fibrils, investigators have recently concluded that tendon injury may not be due exclusively to tendon weakness, but rather may be the result of functional deficiencies through the entire SDF muscle-tendon complex [7, 35-36]. This fatigue-predisposition compounds the SDF muscle's inability to accommodate large biomechanical forces during maximal exercise [7-8] leading to inherent, potentially catastrophic limitations of the SDF muscle-tendon unit. Despite the exact etiology of cumulative biomechanical strain, the deposition of subsequent scar tissue creates a persistently weakened tendon even more prone to re-injury.

Tendinopathic adaptations to biomechanical strains are complex and have been demonstrated to involve production of beneficial inflammatory agents that aide in the early stages of tendon healing [25, 37]. It has even been suggested that recurring, interval exposures to elevated intra-tendinous temperatures through exercise-induced hysteresis may protect tendon cells from further stresses [37], but this exact *in-vivo* threshold between beneficial and harmful exposure remains unknown. In the event of tendinopathy, temperature rises as a result of high-intensity exercise are proposed to initiate degenerative processes in the central core of the tendon, predisposing it to mechanical failure [37]. Explanted SDFT cells have demonstrated negatively correlated cell survival rates with rising temperatures and time of exposure to heat [38]. Additionally, methods to measure *in-vivo* core tendon temperatures that occur during exercise are invasive with ethical implications that have precluded their pursuit [25].

Lastly, previous studies have documented increased risks of SDFT injury with age [11, 15, 35, 39-40]. Potential explanations for this involve an increased stress relaxation with subsequently altered responses to loading leading to decreased fatigue resistance [39-40]. Other investigators

6

postulate that lower levels of fibromodulin and collagen III may impair tendinopathic healing and predispose to chronic tendinopathy [40-41]. It may also be as simple as a reduced ability to respond to general inflammation [27]. With a single etiology yet to prove biologically capable of encompassing tendon injury, efforts to corroborate multiple theories and how they may manifest are ongoing.

1.5 Historical Perspective on Tendinopathic Models in the Horse

Animal models of orthopedic injury offer researchers a venue through which controlled, homogenous experimentation can be performed [42]. Specific to the study of tendinopathy, it would prove extremely difficult, if not impossible, to enroll a study group with homogenous lesion characteristics for which therapeutics may be justly compared. With an inconsistent study population, subsequent high probabilities of false positive and false negative results would represent a significant source of inherent study limitation. This lesion variability would also require an exuberantly large number of subjects to sufficiently power statistical analysis, for which practicality must be considered. Additionally, enrolling patients into a control group carries its own obvious frustrations. For these reasons, superior and more efficient investigative alternatives are warranted to advance our understanding of tendon injury and repair. In comparison to human studies, animal models of disease facilitate multi-stage, longitudinal tissue sampling that remains crucial to investigating cellular etiologies of response to injury [42]. Optimized models of tendon injury seek to simulate the clinical, diagnostic, histopathological and functional (biomechanical) characteristics of naturally occurring disease. Several equine SDFT injury models via lesion induction have been described [43-52]. Investigated models of equine tendon injury are broadly characterized as mechanically or chemically induced.

Chemical induction of tendon injury most often involves the use of collagenase or collagenase gel to enzymatically degrade the normal cell matrix [49-51]. These chemical models have been praised for simulating the natural enzymatic degradative process that occurs with clinical tendinopathy, yet widely criticized for causing unnatural, widespread fiber disruption under a strong, exaggerated inflammatory response [47,53]. This model has also been disparaged for inconsistent lesion size, severity, and character of tendon and peritendon involvement [47,53-54]. It also fails to replicate the mechanical environment often attributed to the etiopathogenesis of clinical tendon strain [46]. While acknowledged in-vivo work using this model has been performed, longitudinal tracking has been limited to sixteen weeks following lesion induction [51], making longer-term assumptions of the chronic response to injury and overall healing process more difficult to ascertain.

Mechanical induction of tendon injury originated as a surgically-induced, full-thickness defect created in the superficial digital flexor tendon [43-44]. As surgical technique evolved, lesion creation became more refined with the use of a synovial resector to create lesions specifically within the core of the superficial digital flexor tendon [45-47]. This mechanical method proved a consistent means of inducing experimental tendon injury, and with technique refinement has been more accurately localized to the tensile region. Although improvements in lesion confinement have been realized with mechanical induction of tendon injury, this method (particularly in absence of post operative exercise) has been criticized for not replicating physiologic over-strain.

Initial proponents of the surgical tendinopathy model using a synovial resector validated its use based on short-term follow-up of clinical, diagnostic imaging, & histologic outcome parameters [45-47]. Our research group with the guidance of Gerco Bosch has since further investigated, refined and verified these outcome parameters in a more longitudinal fashion than

has previously been performed [52]. In brief, by longitudinally evaluating horses with surgically induced SDFT lesions over twelve months with multi-modality advanced imaging including high-field magnetic resonance imaging (MRI), contrast enhanced computed tomography (CT) and ultrasonography, the understanding of diagnostic imaging patterns of tendon healing that may correlate to superior healing and to naturally occurring disease has improved. At each imaging time point (seven evaluations over the twelve months), each horse was also clinically evaluated allowing us to monitor pain and any associated lameness. At the termination of the study, horses were humanely euthanized in accordance with IACUC protocol and biomechanical, immunohistochemical and histologic analysis was performed. The full manuscript comprises Chapter 2, but in summary, lesion isoattenuation on CT evaluation suggested scar tissue (aggrecan) deposition, while T2-weighted hyperintensity indicated hypercellular tendinopathy even in chronic stages of healing [52]. While one specific tendon injury model is yet to be unequivocally agreed upon, this proposed surgical model (in the author's experience and opinion) appears to embody many biologic characteristics of naturally occurring tendinopathy despite its inability to replicate physiologic overstrain.

1.6 Conclusions

In conclusion, equine tendinopathies remain prevalent and difficult to treat. The etiopathogenesis of equine SDF tendinopathy specifically remains incompletely understood, but the most popular theories are rooted in biomechanical, biothermal and age-related predispositions. While clinical trials remain necessary in many circumstances, initial equine tendinopathic experimentation with ensuing clinical trials may be the most standardized, expeditious way to investigate novel therapeutics specific to tendon healing. Early screening

tools and preventative strategies to minimize incidence and severity of SDFT injury represent

ongoing sources of investigation for sports medicine clinician-researchers.

References:

1. Ross MW et al. Equine Superficial Digital Flexor Tendonitis. Diagnosis & Management of Lameness in the Horse. 2011, St. Louis, MO: Elsevier Saunders.

2. Budras KD, Sack WO, Rock S. Anatomy of the Horse. 2012 (6th ed). Schluetersche. https://doi.org/10.1201/9783842683686

3. Haussler KK. Thoracic limb muscle attachments. 2012.

4. Brown NAT, Kawcak CE, McIlwraith CW, et al. Architectural properties of distal forelimb muscles in horses, Equus caballus. *J Morphol* 2003;258: 106-114.

5. Harrison S, Whitton R, King M, et al. Function of the forelimb muscles of the horse during locomotion. *J Exper Biol* 2012;215:2980-91.

6. Wilson AM, McGuigan MP, Su A, et al. Horses damp the spring in their step. *Nature* 2001;414:895-899.

7. Butcher MT, Hermanson JW, Ducharme NG, et al. Contractile behavior of the forelimb digital flexors during steady-state locomotion in horses (Equus caballus): An initial test of muscle architectural hypotheses about in vivo function. *Comp Biochem Physiol, Part A* 2009:100-114.

8. Zarucco L, Taylor KT, Stover SM. Determination of muscle architecture and fiber characteristics of the superficial and deep digital flexor muscles in the forelimbs of adult horses. *Am J Vet Res* 2004;65(6):819-828.

9. Williams RB, Harkins LS, Hammond CJ, et al., Racehorse injuries, clinical problems and fatalities recorded on British racecourses from flat racing and National Hunt racing during 1996, 1997 and 1998. *Equine Vet J*, 2001;33(5): 478-86.

10. Davis CS, Ely ER, and Smith RKW, The effect of routine tendon scanning on the incidence of injury in National Hunt racehorses in training: preliminary findings. *Proc Ann Congress of British Equine Vet Assoc* 2005;44:125-126.

11. Kasashima Y, Takahashi T, Smith RK, et al. Prevalence of superficial digital flexor tendonitis and suspensory desmitis in Japanese Thoroughbred flat racehorses in 1999. *Equine Vet J* 2004;36:346-350.

12. Lam KH, Parkin TDH, Riggs CM, et al., Descriptive analysis of retirement of Thoroughbred racehorses due to tendon injuries at the Hong Kong Jockey Club (1992-2004). *Equine Vet J* 2007;39(2): 143-8.

13. Genovese R. Quantitative sonographic assessment in the clinical management of superficial digital flexor injuries in Thoroughbred racehorses. *Proc Am Assoc Equine Pract* 1997; 43(285).

14. Perkins NR, Reid SWJ, Morris RS. Risk factors for injury to the superficial digital flexor tendon and suspensory apparatus in Thoroughbred racehorses in New Zealand. *N Z Vet J* 2005;53:184-192.

15. Avella CS, Ely ER, Verheye KLP, et al. Ultrasonographic assessment of the superficial digital flexor tendons of National Hunt racehorses in training over two racing seasons. *Equine Vet J* 2009;41(5):449-454.

16. Murray RC, Dyson SJ, Tranquille C, et al. Association of type of sport and performance level with anatomical site of orthopaedic injury diagnosis. *Equine Exer Phys, Equine Vet J Suppl* 2006;36:411-416.

17. Verkade ME, Back W, Birch HL. Equine digital tendons show breed-specific differences in their mechanical properties that may relate to athletic abiliyt and predisposition to injury. *Equine Vet J* 2020;52:320-325.

18. Dyson S, Murray R, Schramme M, et al. Lameness in 46 horses associated with deep digital flexor tendonitis in the digit: diagnosis confirmed with magnetic resonance imaging. *Equine Vet J* 2003;35:681–90.

19. Dyson S, Murray R, Schramme M. Lameness associated with foot pain: results of MRI in 199 horses (January 2001-December 2003) and response to treatment. *Equine Vet J* 2005;37:113–21.

20. Dyson S, Murray R. Magnetic resonance imaging evaluation of 264 horses with foot pain: the podotrochlear apparatus, deep digital flexor tendon and collateral ligaments of the distal interphalangeal joint. *Equine Vet J* 2007;39:340–3.

21. Sampson SN, Schneider RK, Gavin PR, et al. Magnetic resonance imaging findings in horses with recent onset navicular syndrome but without radiographic abnormalities. *Vet Radiol Ultrasound* 2009;50:339–46.

22. Lutter J, Schneider R, Sampson S., et al. Medical treatment of horses with deep digital flexor tendon injuries diagnosed with high-field-strength magnetic resonance imaging: 118 cases (2000-2010). *J Am Vet Med Assoc* 2015;247:11;1309-1318.

23. Acutt EV, Contino EK, Frisbie DD, et al. Deep digital flexor tendon lesions in the pastern are associated with the presence of distal tendinopathy. *Equine Vet J* 2021;00:1-11.

24. Cillan-Garcia E, Milner P, Talbot A, et al. Deep digital flexor tendon injury within the hoof capsule; does lesion type or location predict prognosis? *Vet Rec* 2013;doi:10.1136/vr.101512.

25. O'Brien C, Marr N, Thorpe C, et al. Microdamage in the equine superficial digital flexor tendon. *Equine Vet J* 2020;00:1-14.

26. Herod TW, Chambers NC, Veres SP. Collagen fibrils in functionally distinct tendons have differing structural responses to tendon rupture and fatigue loading. *Acta Biomater* 2016;42:296-307.

27. Dakin SG. A review of the healing processes in equine superficial digital flexor tendinopathy. *Equine Vet Educ* 2016;doi:10.111/eve.12572.

28. Thorpe CT, Godinho MSC, Riley GP, et al. The interfascicular matrix enables fascicle sliding and recovery in tendon, and behaves more elastically in energy storing tendons. *J Mech Behav Biomed Mater* 2015;52:85-94.

29. Spiesz EM, Thorpe CT, Chaudhry S, et al. Tendon extracellular matrix damage, degradation and inflammation in response to in vitro overload exercise. J Orthop Res 2015;33:889-897.

30. Biewener AA. Muscle-tendon stresses and elastic energy storage during locomotion in the horse. *Comp Biochem Physiol Part B Biochem Mol Biol* 1998;120:73-87.

31. Lichtwark GA, Wilson AM. Is Achilles tendon compliance optimised for maximum muscle efficiency during locomotion? *J Biomech* 2007;40:1768-1775.

32. Thornton GM, Hart DA. The interface of mechanical loading and biological variables as they pertain to the development of tendinosis. *J Musculoskelet Neuronal Interact* 2011;11:94-105.

33. Docking SI, Daffy J, van Schie HTM, et al. Tendon structure changes after maximal exercise in the Thoroughbred horse: use of ultrasound tissue characterisation to detect in vivo tendon response. *Vet J* 2012;194:338-342.

34. Herod TW, Veres SP. Development of overuse tendinopathy: a new descriptive model for the initiation of tendon damage during cyclic loading. *J Orthop Res* 2018;36:467-476.

35. Patterson-Kane JC, Becker DL, Rich T. The pathogenesis of tendon microdamage in athletes: the horse as a natural model for basic cellular research. *J Comp Pathol* 2012;147:227–247.

36. Firshman AM, Borgia LA, Valberg SJ. Effects of training at a walk on conventional and underwater treadmills on fiber properties and metabolic responses of superficial digital flexor and gluteal muscles to high-speed exercise in horses. *Am J Vet Res* 2015;76:1058-1065.

37. Wilson AM, Goodship AE. Exercise-induced hyperthermia as a possible mechanism for tendon degeneration. *J Biomech* 1994;27(7):899-905.
38. Birch HL, Wilson AM, Goodship AE. The effect of exercise-induced localised hyperthermia on tendon cell survival. *J Exp Biol* 1997;200:1703-1708.

39. Thorpe CT, Riley GP, Birch HL, Clegg PD, Screen HRC. Fascicles and the interfascicular matrix show adaptation for fatigue resistance in energy storing tendons. Acta Biomater. 2016;42:308-315.

40. Thorpe CT, Peffers MJ, Simpson D, et al. Anatomical heterogeneity of tendon: Fascicular and interfascicular tendon compartments have distinct proteomic composition. *Sci Rep* 2016;6.

41. de Cássia Marqueti R, Almeida JA, Nakagaki WR, et al. Resistance training minimizes the biomechanical effects of aging in three different rat tendons. *J Biomech* 2017;53:29-35.

42. Lui P. What are the validated animal models for tendinopathy. *Scand J Med Sci Sports* 2011. 21(3-17).

43. Watkins JP, Auer JA, Gay S, et al. Healing of surgically created defects in the equine superficial digital flexor tendon: collagen-type transformation and tissue morphologic reorganization. *Am J Vet Res* 1985;46:2091-2096.

44. Watkins JP, Auer JA, Morgan SJ. Healing of surgically created defects in the equine superficial digital flexor tendon: effects of pulsing electromagnetic field therapy on collagen-type transformation and tissue morphologic reorganization. *Am J Vet Res* 1985; 46:2097-2103.

45. Little C, Schramme M. Ultrasonographic and MRI evaluation of a novel tendonitis model in the horse. *Vet Surg* 2006;35:E15.

46. Schramme M, Hunter S, Campbell N et al., A surgical tendonitis model in horses: technique, clinical, ultrasonographic and histological characterisation. *Vet Comp Orthop Traumatol* 2010; 23(4):231-9.

47. Cadby JA, David F, van de Lest C, et al., Further characterisation of an experimental model of tendinopathy in the horse. *Equine Vet J* 2013;45(5):642-8.

48. Zedler S, Schaer T, Ebling A, et al. Evaluation of a novel model of equine superficial digital flexor tendonitis in regenerative tendon research. *Vet Surg* 2008;37:E34.

49. Silver IA, Brown PN, Goodship AE, et al. A clinical and experimental study of tendon injury, healing and treatment in the horse. *Equine Vet J Suppl* 1983;1:1-43.

50. Williams IF, McCullagh KG, Goodship AE, et al. Studies on the pathogenesis of equine tendonitis following collagenase injury. *Res Vet Sci* 1984;36:326-338.
51. Watts AE, Nixon AJ, Yeager AE, et al., A collagenase gel/physical defect model for controlled induction of superficial digital flexor tendonitis. *Equine Vet J* 2012;44(5):576-86.

52. Johnson SA, Valdez-Martinez A, Turk P, et al. Longitudinal tendon healing as assessed with multi-modality advanced imaging and tissue analysis. *Equine Vet J* 2021;00:1-16.

53. Dahlgren LA, Mohammed HO, Nixon AJ, et al. Temporal expression of growth factors and matrix molecules in healing tendon lesions. *J Orthop Res* 2005;23:84-92.

54. Birch HL, AJ Bailey, Goodship, AE. Macroscopic 'degeneration' of equine superficial digital flexor tendon is accompanied by a change in extracellular matrix composition. *Equine Vet J* 1998;30(6):534-9.

CHAPTER 2: Longitudinal Tendon Healing Assessed with Multi-Modality Advanced Imaging and Tissue Analysis[1]

2.1 Overview

The range of diagnostic modalities available to evaluate superficial digital flexor tendon (SDFT) injury includes magnetic resonance imaging (MRI), computed tomography (CT) and ultrasound (US). Direct, comprehensive comparison of multi-modality imaging characteristics to end-point data has not previously been performed using a model of tendinopathy but is required to obtain a better understanding of each modality's diagnostic capabilities. The objective of this study was to compare CT, MRI, and US evaluation to outcome measures for histologic, biochemical and biomechanical parameters using an equine surgical model of tendinopathy. Lesions were surgically created in both forelimb SDFTs of eight horses and imaged using MRI, CT and US at seven time points over twelve months. Imaging characteristics were then correlated to end point histologic, biochemical and biomechanical data using lasso regression. Longitudinal lesion size was compared between imaging modalities. Lesion to tendon isoattenuation on CT evaluation correlated with the greatest levels of aggrecan deposition. A significant correlation between cellular density and percentage of tendon involvement on the T2-weighted sequence and signal intensity on the proton density fat saturated (PD FS) sequence was appreciated at the twelve-month time point ($P = 0.006$, $P = 0.02$, respectively). There was no significant correlation between end-point data and US or contrast imaging characteristics. Cross

---

[1] This chapter includes the complete published manuscript: Johnson SA, Valdez-Martinez A, Turk P, McIlwraith CW, Barrett MF, McGilvray KC, Frisbie DD. Longitudinal tendon healing as assessed with multi-modality advanced imaging and tissue analysis. *Equine Vet J.* 2021;00:1-16. This article is reproduced with permission from the Editor, Equine Veterinary Journal.

sectional area lesion to tendon measurements were significantly largest on CT evaluation, followed by MRI and then US ($P < 0.0001$). The main limitation of this study was the use of experimentally induced tendon injury with singular end-point data correlation. Lesion isoattenuation on CT evaluation suggested scar tissue deposition, while T2-weighted hyperintensity indicated hypercellular tendinopathy even in chronic stages of healing. Non contrast-enhanced MRI and CT evaluation correlated most closely to cellular characteristics of surgically damaged tendons assessed over a twelve month study period. Ultrasonographic evaluation underestimates true lesion size and should be interpreted with caution.

2.2 Introduction

Superficial digital flexor tendon (SDFT) injuries continue to plague the equine athletic world and represent a challenging disease process due to high rates of re-injury [1, 2] and reduced biomechanical fortitude despite long periods of rehabilitation [3]. SDFT injury specifically was implicated as the primary reason for retirement of Thoroughbred racehorses over a 12 year epidemiologic study period [4]. Regardless of the employed treatment protocol, clinicians are often required to define the crucial, yet indistinct physiologic benchmark of when a tendon can safely withstand biomechanical loading. This back-to-work determination often relies on the extent of the original injury, subjective clinical impression, and imaging characteristics. Although significant improvements in technology continue to optimize soft tissue diagnostic capabilities, an improved understanding of the intricacies that link multi-modal imaging characteristics and tendinopathic features would be invaluable to the sports medicine world.

The range of diagnostic modalities available to evaluate tendon injury includes magnetic resonance imaging (MRI), computed tomography (CT) and B (brightness) mode ultrasound

(US). While MRI is often considered the gold standard in advanced imaging [5], CT has also been used to evaluate soft tissue lesions within the equine distal limb [6-9]. Furthermore, contrast-enhanced computed tomography (CECT) evaluations have demonstrated correlation to tissue neovascularization and vascular permeability [6-7,9]. When compared to low-field MRI of the equine foot, CECT offered improved deep digital flexor tendon (DDFT) lesion visualization [10-11]. Similarly, the use of contrast-enhanced MRI (CE-MRI) has been investigated within the realm of equine orthopedic imaging [9,12-13]. Despite the investigation of these advanced imaging modalities, B mode US remains the most clinically utilized and economically practical modality for stall-side equine use.

Albeit popular, evaluation of the equine SDFT with B mode US has demonstrated wide operator-related variability, specifically in image interpretation [14], and has proven limited in the staging of tendinopathic healing [15-20]. Computerized analysis of B mode US with histologic correlation has been reported, but impressions were subjective and limited to 24 weeks post-injury [21]. Similarly, studies comparing B mode US and MRI in tendon injury are limited [22-23], and US has shown poor correlation to clinical features of tendinopathy [24]. Ultrasonographic image interpretation in superficial digital flexor (SDF) tendinopathy can also be affected by varying degrees of diffuse micro-damage at the tendon matrix level that subsequently alter the appearance of fiber alignment, echogenicity and cross-sectional area (CSA) and potentially lead to under-estimation of damage [25]. Despite these limitations, US is the most used stall-side modality and there is persistent interest concerning the correlation of B mode US to the more advanced imaging protocols of MRI and CT to confirm and subsequently refine the diagnostic scope of each modality. While several studies have compared a singular imaging modality to post-mortem data [21,23] or one modality to another [7,10-11,22-24], direct

comprehensive multi-modality comparison with tissue correlation has not been performed. An improved understanding of how advanced imaging modalities compare to one another and to physiologic tissue properties using an experimental model of tendinopathy may further cultivate monitoring strategies to assess healing.

Therefore, the objective of this prospective controlled experiment was to compare CT, CECT, MRI, CE-MRI and US evaluation to outcome measures for histologic, biochemical and biomechanical parameters using an equine surgical model of tendinopathy. Additionally, a goal of this study was to compare assessment of longitudinal lesion size between the three imaging modalities. It was hypothesized that contrast enhancement as assessed as hyperattenuation on CECT images and hyperintensity on CE-MR images would be correlated with inferior histologic, biochemical, and biomechanical properties. It was also hypothesized that lesion size would be similar between CT and MRI, but smallest on US evaluation.

2.3 Materials and Methods

This study was a prospective controlled experiment. All study methods were conducted in compliance with Institutional Animal Care and Use Committee (IACUC) standards (protocol #10-2201A). The experimental sample size (n = 8 horses) was calculated using GPower Version 3.1.1 (GPower, Brunsbuttel Germany). Values from a published study investigating lesion detection differences between CT and MRI were used for power calculation [11]. Specifically, an a priori power analysis was conducted. Using a two-sample t-test with expected group mean lesion identification difference of 20.3%, this power analysis resulted in an effect size of 2.03 and a power of 0.95 using a 95% confidence interval and a standard deviation of 10% between groups.

Experimental Animals: Eight healthy mixed breed horses (two geldings and six mares), aged two to four years that showed no clinical or ultrasonographic evidence of current or previous SDFT injury were purchased from an outside vendor for study enrollment. Horses weighed 336-409 kg and showed no evidence of lameness on baseline evaluation. A portion of the limbs in this study were treated with a biologic[2] which was taken into consideration for statistical evaluation (blocks) but not relevant to the study objectives described herein.

Surgical Procedure & Post-Operative Care: All eight horses underwent general anesthesia using isoflurane in oxygen. Surgical core lesions were created in the mid-metacarpal region of the SDFT of each forelimb using a synovial resector as previously described [21]. Briefly, a small skin incision was made in the palmar midline of the limb, just proximal to the digital tendon sheath. A small (1 cm) longitudinal incision was made into the core of the SDFT, through which an arthroscopic burr (Ø 3.5 mm, Linvatec, Largo, FL) was bluntly, and in inactivated state, inserted proximally over a length of 7–8 cm. The obturator position was digitally palpated and position subsequently determined and directed towards the center of the tendon in all limbs. Then, the burr was activated and slowly retracted in approximately 20 seconds [21]. The incisions in the paratenon and skin were sutured in a simple interrupted pattern with resorbable 2-0 polydioxanone (PDS, 2-0, Ethicon, Somerville, NJ) and non-resorbable nylon (Ethilon; Ethicon), respectively. Pre-operatively and three days post-operatively, all horses received 4.4 mg/kg phenylbutazone (Phenylbutazone, Aspen Veterinary Resources, Liberty, MO) and perioperative antimicrobials. Distal limb bandages were applied to all forelimbs for 14 days

---

[2] Eight limbs received an intra-lesion injection of 10×10^6 autologous bone-marrow derived mesenchymal stem cells 56-66 days post surgical lesion induction

post-operatively and sutures were removed in standard fashion. All horses were confined to stall rest for eight weeks post-operatively. The horses were then turned out into paddocks (20,000 square feet in size) for the remainder of the study period, except for one day before and after all anesthetic procedures during which horses were on stall rest for feed restriction and post-anesthetic monitoring.

Computed Tomographic Image Acquisition & Analysis: CT examinations were performed on both forelimbs of all horses at seven time points in reference to surgical lesion induction (Fig 2.1). Evaluations were performed by one of the authors (AVM) using a dynamic CECT method adapted from a previously described technique [6]. Briefly, following standard (pre-contrast) image acquisition, 10.5grams (30cc of 350mg/ml solution) of Iohexol (Omnipaque, GE Healthcare, Princeton, NJ) diluted in 30mL of sterile saline was injected into the medial palmar artery under ultrasonographic guidance. Arterial, venous and delayed post-contrast CT images were then acquired, with arterial phase acquisition beginning five seconds post contrast injection. Venous phase images were acquired approximately ten seconds following completion of arterial phase images, and delayed phase images were obtained three minutes post-injection. Image acquisition parameters are listed in Table 2.1.

Quantitative measurements of lesion and total tendon CSA were made using the free-hand region of interest (ROI) tool on the standard (pre-contrast) phases (Table 2.2). Measurements were made by one observer (S.A.J.) three times and then the average (mean) was used for statistical analysis. If the tendon appeared homogenous in attenuation compared to the lesion (no lesion could be identified), the CSA of the lesion was considered zero. Lesion to

tendon CSA's were statistically analyzed as ratios, with values approaching 1 indicating large

lesion CSA and smaller values representing small lesion CSA.

Table 2.1 Table Summarizing Pre and Post-Contrast Computed Tomographic (CT) Image Acquisition Parameters for Evaluation of Surgically Induced Superficial Digital Flexor Tendon (SDFT) Lesions

	Standard CT (Pre-Contrast Phase)	**Arterial, Venous & Delayed CT Phases**
KVP	120	120
mAs	200	200
Slice Thickness (mm)	2 x 2, contiguous	1 x 0.5, overlapping
FOV (cm)	25	20 (based on patient size)
Algorithm	Standard (Filter B)	Sharp (Filter C)
Matrix (pixels)	1024x1024	768x768

KVP, peak kilovoltage; mAs, milliamperage; FOV, field of view.
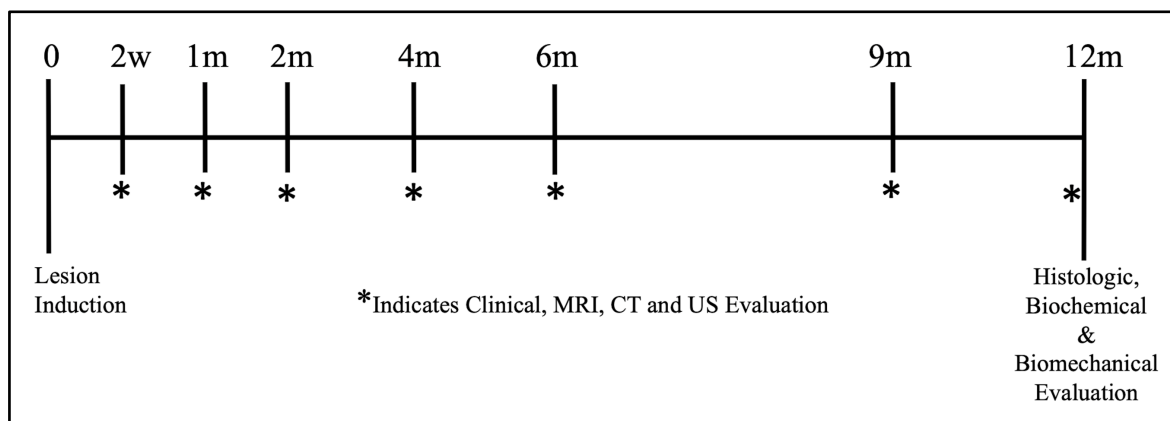
Fig 2.1 Experimental timeline, beginning with lesion induction (0) and ending with study termination twelve months later (12m). Baseline lameness evaluations were performed prior to lesion induction. Serial lameness and magnetic resonance imaging (MRI), computed tomography (CT) and B-mode ultrasound (US) evaluations were performed at seven time points post lesion creation, followed by end point data collection of histologic, biochemical and biomechanical outcome parameters. Imaging evaluations were performed over a period of 5-7 days for each time point.

Quantitative measurements of Hounsfield Units (HU) of both the lesion and the adjacent

tendon were made by one observer (S.A.J.) on the standard (pre-contrast), arterial, venous and

delayed phases. Lesional HU measurements were made using the free-hand region of interest

(ROI) tool to outline lesional boundaries. HU measurements were made for the adjacent tendon

using a uniformly-sized ellipse ROI tool (Table 2.2). Measurements were made three times by a

single operator and then the average (mean) was used for statistical analysis. Lesion to tendon

HU's were analyzed as ratios, with a ratio of one representing lesion to tendon isoattenuation,

values <1 representing lesion hypoattenuation, and values >1 representing lesion

hyperattenuation.

Lesion attenuation was also subjectively graded by one observer (S.A.J.) as

isoattenuating, hypoattenuating or hyperattenuating in comparison to the adjacent tendon on all

phases (Table 2.2). Additionally, the subjective degree of contrast enhancement was graded for

all contrast phases based on a 0-4 scale (0 = no contrast enhancement; 1 = very mild; 2 = mild; 3

= moderate; 4 = severe; Supplementary Figure 9.1). All objective imaging data collected is

summarized in Table 2.2.

Table 2.2: Objective and subjective imaging outcome parameters measured for surgically
induced superficial digital flexor tendon (SDFT) lesions at all evaluation time points.

Imaging Modality	Measurement	Sequence Used for Analysis	Unit of Measure or Scale
	CSA lesion	T1 FSE, PD, T2, STIR	cm^2
	CSA tendon	PD	cm^2
	Subjective Percent of Tendon Involvement	T1 FSE, PD, T2, STIR	0 to 4 scale 0 = no lesion visible

			1 = 1-25%
MRI			2 = 26-50%
			3 = 51-75%
			4 = 76-100%
	Presence of Contrast Enhancement	T1 FSE	Present or Absent
	Character of Lesion Signal Attenuation	PD, PD-FS, T2, STIR, 3D SPGR, 3D SPGR FS, T1 FSE, T1 FSE Post Contrast	Isointense or Hyperintense
CT	CSA lesion	Standard Phase	cm^2
	CSA tendon	Standard Phase	cm^2
	HU lesion / HU adjacent tendon	Standard, Arterial, Venous, Delayed	HU
	Character of Contrast Enhancement	Standard, Arterial, Venous, Delayed	Isoattenuating Hypoattenuating Hyperattenuating
	Degree of Contrast Enhancement	Standard, Arterial, Venous, Delayed	0 to 4 scale (0 = none; 4 = marked)
US	CSA lesion	Transverse	cm^2
	CSA tendon	Transverse	cm^2

CT, MRI, US	CSA lesion / CSA tendon	Standard, T1 FSE, Transverse (respectively)	cm^2

MRI, magnetic resonance imaging; CT, computed tomography; US, ultrasound; CSA, cross sectional area; HU, Hounsfield units; PD FSE, proton density fast spin echo sequence; PD-FS, proton density fat saturated; STIR, short τ inversion recovery; 3D SPGR, spoiled gradient echo; 3D SPGR-FS, spoiled gradient echo fat saturated; FSE, fast spin echo.

Magnetic Resonance Image Acquisition & Analysis: Two dimensional magnetic resonance transverse images (3mm, no gap) were acquired by one of the authors (AVM) for both forelimbs at all imaging time points (Fig 2.1) with a 1.0 Tesla MRI Unit (OrthoOne, ONI, Wilmington, MA). Sequences obtained included proton density fast spine echo (PD FSE), PD fat saturated (PD-FS), T2-weighted FSE, short τ inversion recovery (STIR), three dimensional (3D) spoiled gradient echo (SPGR), 3D SPGR-FS and T1-weighted FSE. Following acquisition of standard MRI images, 50 mL/horse of gadopentate dimeglumine (Magnevist, Bayer Healthcare, Shawnee Mission, KS) was administered intravenously (IV) using a previously described protocol [13]. Post contrast administration, T1-weighted FSE images were obtained. All images were acquired from the distal row of carpal bones to the level of the proximal sesamoid bones using a 15 cm field of view. All MRI studies were performed within 5-7 days of CT evaluation. Additional sequence parameters are listed in Table 2.3.

Table 2.3: Parameters Used in Pulse Sequences for Evaluation of Surgically Induced Superficial Digital Flexor Tendon (SDFT) Lesions with a 1.0 Tesla MRI Unit (OrthoOne ONI).

Image Orientation	Pulse Sequence	TR (ms)	TE (ms)	Slice Thickness (mm)	Matrix Size	FOV (cm)
Transverse	PD FSE	3789	25	3	320 x 192	15
Transverse	PD-FS	4000	45	3	320 x 192	15
Transverse	T2 FSE	6714	99.9	3	288 x 192	15
Transverse	STIR	9352	14.1	3	288 x 192	15
Transverse	3D SPGR	35	18	3	320 x 192	15
Transverse	3D SPGR-FS	63	14.8	3	320 x 192	15
Transverse	T1 FSE (no contrast	550	11.7	3	320 x 192	15
Transverse	T1 FSE (post contrast)	550	11.7	3	320 x 192	15

TE, echo time; TR, repetition time; FOV, field of view; PD FSE, two-dimensional proton density fast spin echo sequence; PD-FS, proton density fat saturated; STIR, short τ inversion recovery; 3D SPGR, spoiled gradient echo; 3D SPGR-FS, spoiled gradient echo fat saturated; FSE, fast spin echo.

Quantitative measurements of lesion CSA were made using the free-hand ROI tool on the PD, T2, STIR and T1-weighted FSE sequences (Table 2.2). If lesional borders could not be well defined from the adjacent tendon, the CSA of the lesion was considered zero. Tendon CSA was measured using the free-hand ROI tool on the PD sequence. Measurements were made three times and then the average (mean) was used for statistical analysis. The subjective percentage of

affected tendon was evaluated on the PD, T2, STIR and T1 FSE sequences using a 0 to 4 scale

(Table 2.2.). The presence of T1 FSE post-contrast enhancement was recorded as a binary

outcome (present or absent), and the character of lesion signal attenuation was evaluated on all

MRI sequences (Table 2.2).

Ultrasonographic Image Acquisition & Analysis: Ultrasound examination using the standard

ultrasound technique for both forelimbs of all horses was performed by one of the authors

(AVM) at all imaging time points (Fig 2.1). Images were obtained with all horses weight-

bearing, both in transverse and longitudinal planes beginning at the level of the accessory carpal

bone (zone 1) and extending to the level of the proximal sesamoid bones (zone 3C). Examination

was performed using a portable ultrasound machine (GE Logic E, Carlsbad, CA) with a 10 MHz

linear probe and flexible standoff. Quantitative measurements of lesion and tendon CSA were

made on transverse images (Table 2.2). Measurements were retrospectively performed by a

single operator. Specifically, measurements were made three times and then the average (mean)

was used for statistical analysis. All ultrasound images were obtained within 5-7 days of CT and

MRI evaluation.

Multi-Modality Image Analysis: All image analysis was performed on a diagnostic imaging

viewing station monitor; windowing and leveling was performed to optimize observation of the

lesions. All images were analyzed by a resident in Equine Sports Medicine and Rehabilitation

with a year of dedicated advanced imaging training (SAJ) under the guidance of board-certified

veterinary radiologists (AVM, MFB). All measurements were performed at the center of lesion

location in the transverse plane, and by modality. CSA lesion and tendon measurements were

directly compared between T1-weighted FSE MRI, standard phase CT and transverse US images (Table 2.2).

Tissue Harvest: Following the 12-month imaging examination, all horses were humanely euthanized according to IACUC standards. At post-mortem, all limbs underwent ultrasonographic, magnetic resonance (MR) computed tomographic (CT) evaluation. All images were evaluated by one of the authors (AVM) to identify the most affected site of SDFT injury. This location and its distance relative to the accessory carpal bone was then recorded and used as the center of evaluation for all subsequent multi-modality analysis. Following imaging evaluation, a longitudinal incision was made to remove the skin and subcutaneous tissue overlying the forelimb SDFTs from the level of the carpus to the proximal sesamoid bones. All SDFTs were visually evaluated, gross observations were recorded and limbs were photographed. Following evaluation, a suture was placed at the site of the most injured area of the SDFT based on advanced imaging evaluation and distance relative to the accessory carpal bone (Fig 2.1). The location of this suture and its distance relative to the accessory carpal bone was then recorded and used as the center of evaluation for future multi-modality analysis (Fig 2.2).
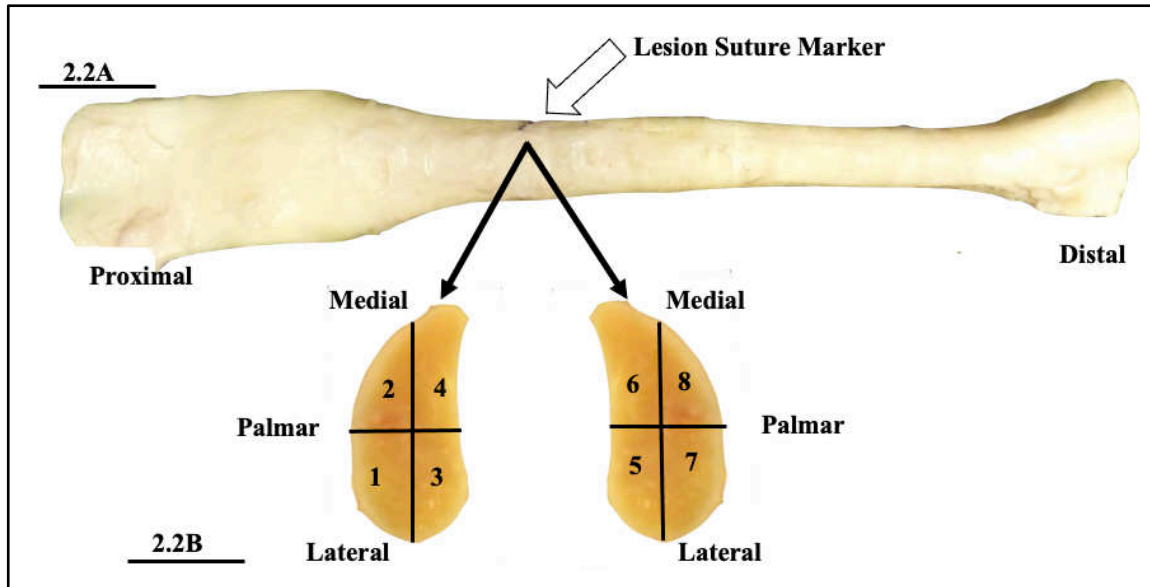
Fig 2.2. Post-mortem superficial digital flexor tendon (SDFT) tissue collection (Fig 2.2A). A suture was placed at the site of the most injured area of the SDFT based on advanced imaging analysis. The location of this suture and its distance relative to the accessory carpal bone was then recorded and used as the center of evaluation for future multi-modality analysis. Cut section of gross tendon specimen (Fig 2.2B) demonstrating 8 sites of tissue section analysis. Sections 1, 4, 5 & 8 were evaluated for cellular morphology, sections 2 and 6 were analyzed for glycosaminoglycan and sections 3 & 7 were evaluated for aggrecan and collagen content.

The forelimbs of all horses were then disarticulated at the level of the middle carpal joint and the SDFTs were carefully harvested from the proximal metacarpal region to the level of the proximal sesamoid bones using sharp dissection and Brown-Adson tissue forceps. Care was taken to minimize tissue handling when possible. Tendon samples were then immediately processed for non-destructive biomechanical testing.

Biomechanical Testing: All SDFT tissue was allowed to relax for five minutes prior to CSA data collection. The CSA of all tendons was measured at the three ROIs using an area micrometer and applied plunger pressure of 0.12 MPa as previously described [26]. These measurements were used to normalize load data to CSA thickening and later incorporated to

estimate tissue stress. To calculate localized tissue deformation and provide the ability to calculate tissue strain in the three ROIs, optical contrast tracking markers were then affixed to the tendon, using cyanoacrylate gel.

The proximal and distal aspects of each tendon were rigidly coupled to a materials testing machine (MTS 858, MiniBionix II, Eden Prairie, MN) using custom designed soft tissue clamps and consistent grip hold of 8.4 N-m. To ensure that biomechanical loading was representative of the physiological scenario, the testing apparatus was directed collinear to the long axis of the tendon fibers. A high-resolution force sensing transducer (5000N capacity, 0.01% resolution) was coupled to the actuator of the testing machine and used to measure the resultant force.

All tendons were pre-conditioned to normalize for viscoelastic effects and testing variability though the application of a static 10 N preload for 2 minutes, followed by the application of ten cyclic tensile loads, at 0.25 Hz, ranging from 12 to 25% of predicted failure stress under force control at a rate of 25N/sec. Predicted failure stress ranges (force at failure divided by CSA of the tendon) were calculated using previously reported failure force of equine digital flexor tendons (7.9±0.9kN, [27]), normalized to the sample's pre-testing CSA. Immediately following pre-conditioning, samples were quasi-statically ramped under force control at a rate of 25N/sec until failure or 40% of maximum stress was achieved. A force control testing protocol was used to ensure that the tendinous tissue was not mechanically damaged due to excessive tissue displacement. Using this value normalized to the CSA of each sample, the lowest intra-sample failure stress was calculated and used as set points for the sample's preconditioning protocols, consistent with previously reported failure force of equine digital flexor tendons (7.9±0.9kN, [27]). A high resolution digital camera and corresponding image capture software (Point Grey, FlyCapture, Canada) were used to measure localized tissue deformation (track relative

displacement of optical contrast tracking markers) during the quasi-static ramp for the three regions of interest. Force and localized optical marker tracking data were recorded at 15 Hz.

Stress, strain and resultant elastic modulus were then calculated. Stress values were calculated by normalizing force data measured from the MTS machine to CSA measurements at the three specific regions of interest (Supplementary Figure 9.2A). Localized tissue deformation was calculated from the high-resolution video data recorded during the quasi-static ramp period of testing. Optical tracking of the surface markers within the three regions of interest was performed using Matlab code, wherein the X-Y position of each marker was calculated and stored in an array. Strain was calculated as the instantaneous difference in the distance between two adjacent markers normalized to the initial (i.e. prior to quasi-static ramp) distance between the same two markers (Supplementary Figure 9.2B). Stress versus strain was plotted for the three regions of interest and the elastic engineering modulus was calculated from the resultant graph. The elastic modulus of the material was defined as the ratio of normal engineering stress over engineering strain in the portion of the stress-strain relationship that obeys Hooke's laws (i.e. linear response) (Supplementary Figure 9.2C). To ensure consistency across samples, elastic modulus was calculated between 1000-2000 N, which was the range for which all samples demonstrated linear behavior.

Specimen Preparation: Following non-destructive biomechanical testing, the site of the previously placed suture (central portion of the lesion) was transected and sections of the affected portion of the tendon were then divided equally for histologic, immunohistochemical and biochemical examination (Fig 2.2). Samples for histologic examination were fixed in 10% neutral buffered formalin solution for 48 hours, then stored at 4°C in sterile phosphate buffered

saline (PBS) until processing. Samples for immunohistochemical analysis were covered with

Optimal Cutting Temperature Compound (American Master*Tech Scientific Incorporated, Lodi,

CA), snap-frozen in liquid nitrogen and then stored at -80°C until processing. Samples obtained

for biochemical analysis were snap-frozen in liquid nitrogen until processing.

Histologic & Biochemical Preparation: Formalin fixed tissue sections were dehydrated, cleared

in xylene, embedded in paraffin, sectioned (5μm thick) and mounted on microscope slides.

Tissue morphology was examined with hematoxylin and eosin (H&E) staining and collagen

crimping was evaluated using picosirius red staining and polarized light microscopy. Scoring for

density, neovascularization, amount of inflammatory cellular infiltrate, linearity of collagen

fibers and crimping of collagen fibers was assessed using a previously described scale (1 =

normal; 4 = severe) [28-29] at four positions adjacent to the center of the lesion (Fig 2.2, Table

2.4).

Table 2.4: Table Summarizing Grading Criteria, Grading Scale and Site of Tissue Section
Sampled for Histologic, Immunohistochemical and Biochemical Analysis. Grading Criteria With
a '*' Superscript Indicate Examination of Both Normal and Abnormal Cells.

	Grading Criteria	Scale Used	Tissue Section Sampled
Cellular Morphology	Density*, Neovascularization*, Inflammatory Infiltrate*	1 = Normal 2 = Slight 3 = Moderate 4 = Marked	1, 4, 5 & 8

Collagen	Linearity	1 = Linear 2 = > 50% linear 3 = 20% to 50% linear 4 = No linear areas	1, 4, 5 & 8
	Crimping	1 = Coarse, even crimp 2 = Predominantly fine, even crimp 3 = <50% with crimp formation 4 = No crimp formation; complete disarray	1, 4, 5 & 8
Toluidine Blue	Amount of Uptake	0= None 1= Slight 2= Moderate 3= Normal	1, 4, 5 & 8
Collagen Type I	Presence of Type I Collagen	1 = > 90% type I 2 = > 50% to 90% type I 3 = 10% to 50% type I 4 = <10% type I	3 & 7
Collagen Type III	Presence of Type III Collagen	1 = <10% type III 2 = 10% to 50% type III 3 = > 50% to 90% type III 4 = > 90% type III	3 & 7
Aggrecan	Region of Interest Overall Presence	Percentage Percentage	3 & 7 3 & 7
Hoescht Concentration	Amount of total DNA	ng/mL	2 & 6
Glycosaminoglycan (GAG)	Total GAG / Total DNA Total GAG/ Dry Weight	µg mg	2 & 6 2 & 6

Immunohistochemical analysis was used to investigate the distribution of aggrecan and collagen type I and III proteins in two tissue sections (Fig 2.2, Table 2.4) using a manner similar to that previously described [28]. Briefly, fresh frozen tissues were embedded in OCT medium, sectioned (8μm thick) and probed with antibodies for collagen type I (Accurate Chemical & Scientific Company, Westbury, NY), collagen type III (BioGenex, Fremont, CA) and aggrecan (Acris Antibodies, Rockville, MD). Blocking serum that was protein matched to the primary antibody protein concentration was used for the negative control sections. For detection, all samples were treated with a horseradish peroxidase conjugated secondary antibody (Jackson ImmunoResearch Laboratories, West Grove, PA) followed by detection using NovaRED peroxidase substrate kit (Vector Laboratories Inc, Burlingame, CA). Immunoreactivity was graded on a scale of 1-to-4 as previously described (Table 2.4) [28-29].

Glycosaminoglycan and DNA were quantified in frozen tendon specimens from two tissue sections (Fig 2.2) by lyophilizing the specimen and digesting with 8U papain/mL using a protocol previously described [30]. A spectrophotometric dimethylmethylene blue dye binding (DMMB) assay quantified the glycosaminoglycan content following digestion for 18 hours at 60°C. in .5% papain. DNA quantification was assessed using the Hoescht assay as previously described [29]. Soluble collagen levels were measured using the sirius red-dye binding method (Sircol Soluble Collagen Kit, Bicolor LTD, County Antrim, UK) in a manner similar to that previously reported [28]. All values were normalized to original tissue dry weight and DNA content (Table 2.4).

Statistical analyses: Statistical analysis was performed using commercial software (R software (R-project®, R Foundation for Statistical Computing Vienna, Austria, v3.3.0 with packages car

and glmmLasso v1.5.1) and SAS v9.0401 (SAS Institute Inc., Cary, NC). Due to the complexity

of the study design, statistical analysis was considered in three phases including: 1) Imaging

modalities compared to 12-month end-point data (specific outcomes of interest listed in Table

2.2 and 2.4); 2) Longitudinal imaging outcome parameters assessed over time; 3) Analysis of

CSA lesion/tendon size across all imaging modalities. The statistical significance level was set to

0.05 for all phases of analyses.

Phase One Statistical Analysis: Imaging Modalities vs. End-Point Data: Response variables

are listed in Table 2.4, while predictor variables are listed in Table 2.2. Linear correlation among

the predictor variables and factors (multi-collinearity) was determined to be present using

generalized variance inflation factors [31]. Due to the presence of multi-collinearity, lasso

regression adapted for a generalized linear mixed model (GLMM) was used to fit the model.

A standard approach of specifying a cumulative logit link function (proportional odds)

GLMM was fit because most of the responses in this phase were ordinal in nature [32]. Aggrecan

and glycosaminoglycan responses were reported as derived percentages. Therefore, the logit of

these percentages was used to normalize the data [33]. Keeping with the framework of a

multilevel model, the resultant model had three levels of hierarchy which contained the fixed and

random effects. Level three contained random horse intercepts and the blocking variable. Level

two contained random limb intercepts, random tissue harvest location slopes, and modality-

specific predictor variables (Table 2.2). Level one corresponded to tissue harvest locations. To

determine the penalty parameter used in lasso regression, the model was iteratively fit using a

sequence of penalty parameter values, and Akaike's Information Criterion (AIC) was computed

to facilitate model selection [34]. Trace plots were then examined to assess selected variables and subsequent *F*-tests were computed from a standard GLMM.

Phase Two Statistical Analysis: Longitudinal Imaging Outcome Parameters Assessed Over Time: Imaging outcome measures for CT, MRI and US were treated as response variables in a three-level linear mixed model (LMM). Specifically, CT response variables for this phase of analysis were: 1) lesion CSA/tendon CSA on standard phase, 2) lesion/tendon attenuation on standard phase, 3) lesion/tendon attenuation on arterial phase, 4) lesion/tendon attenuation on the venous phase, and 5) lesion/tendon attenuation on the delayed phase. MRI response variables considered were: 1) Lesion CSA on T1-weighted sequence (pre-contrast), 2) Lesion CSA on PD-weighted sequence, 3) Lesion CSA on T2-weighted sequence and 4) Lesion CSA on STIR sequence. The only considered US response variable was lesion CSA. The hierarchical specification of the LMM with respect to fixed and random effects was similar to the phase one statistical analysis. Level three contained random horse intercepts, time (and time^2) slopes and the factor block. Level two contained random limb intercepts, time (and time^2) slopes, and level one corresponded to time (and time^2).

A first-order LMM was fit containing fixed effects of block, time and block *time. Random intercepts and time slopes for each horse and each limb within each horse were allowed. Each limb had its own error covariance structure that was modeled to allow for temporal correlation. In addition to looking at the linear component of tendon healing, curvature was also assessed by fitting a second-order (quadratic) LMM, augmenting the first-order model with additional fixed effects time^2 and time2*block and additional time^2 slopes for each horse and each limb within horse. For each response, a longitudinal limb profile plots, *F*-tests of fixed

effects and a fixed effects R^2 value [35] was generated along with an AIC value. The best fitting model of the two LMMs, linear or quadratic, was then selected.

Phase Three Statistical Analysis: Analysis of CSA Lesion Size Across All Imaging Modalities:
The model utilized in phase three was a generalization of the LMM used in phase two, allowing for the three imaging modalities. A four-level linear mixed model for only the response variable CSA lesion / CSA tendon (cm^2) was utilized for the three imaging modalities. Level four contained random horse intercepts, time (and $time^2$) slopes and the blocking variable. Level three contained random limb intercepts and time (and $time^2$) slopes. Level two contained random modality*limb intercepts, and time (and $time^2$). Level one corresponded to time (and $time^2$).

A first-order LMM containing fixed effects for block, time, imaging modality, block *time, modality*time and modality* block was utilized. Random intercepts and time slopes for each horse, each limb within each horse, and each modality*limb combination were allowed. Additionally, each modality*limb combination had its own error covariance structure in an effort to allow for temporal correlation. A second-order LMM augmenting the first-order LMM with additional fixed effects $time^2$, $time^2$* block, $time^2$*modality and additional $time^2$ slopes for each horse, each limb within each horse and each modality*limb combination was fitted. The best fitting LMM between the first and second-order candidates was utilized using the same approach as in the phase two analysis.

For LMMs, residuals were assessed for normality, constant variance, and outliers [36]. For the proportional odds GLMMs, the covariate effects were assumed to be the same across the levels of the ordinal outcome [37].

2.4 Results

Histologic, Immunohistochemical & Biochemical Outcomes:

A significant, moderate positive correlation between overall aggrecan present measured via immunohistochemistry and lesion to tendon attenuation as assessed on pre contrast (standard phase) CT images was appreciated at the twelve month time point ($z = 2.52$, $P = 0.01$). For all tendons, lesion to tendon isoattenuation correlated with the greatest levels of aggrecan deposition ($r=0.6$). Glycosaminoglycan and aggrecan values are presented in Table 2.5 while histologic and IHC values are presented in Table 2.6.

Table 2.5: Table summarizing mean glycosaminoglycan (GAG) and aggrecan biochemical analysis of surgically induced superficial digital flexor tendon (SDFT) lesions for all limbs of all horses at the twelve month evaluation timepoint. Site of tissue analysis corresponded to that described in Figure 2.2B (sections 2 and 6 for GAG and sections 3 and 7 for aggrecan). Mean corresponding Hounsfield Unit (HU) measurements on standard phase computed tomography (CT) are also presented. Lesion to tendon isoattenuation was significantly associated with greater levels of aggrecan deposition ($P = 0.01$, r = 0.6) based on lasso regression for the generalized linear mixed model fitted.

Horse	Mean Amount of total DNA (ng/mL)	Mean Total GAG/Total DNA (μg)	Mean Total GAG/dry weight (mg)	Mean Percentage of Aggrecan Present at Center of Lesion	Mean Percentage of Aggrecan Present Overall	Mean HU Lesion Standard Phase CT	Mean HU Tendon Standard Phase CT
1	9104.7	8.0	7.5	50	30	66.6	83.6
2	9203.1	11.3	10.8	77.5	70	73.3	73.3
4	8935.1	9.1	8.4	35	32.5	68.8	83.7

5	8801.6	12.3	11.3	83.8	62.5	72.0	72.0
6	8240.0	14.9	12.6	55	51.3	63.8	68.0
7	8879.3	9.4	8.7	62.5	51.3	71.08	71.1
8	8128.6	14.0	11.8	70	71.3	73.0	73.0
9	8191.2	13.4	11.4	55	51.3	60.9	60.9

Table 2.6: Table summarizing median and median absolute deviation (MAD) values for all histologic, immunohistochemical (IHC) and biochemical analyses.

	Tissue Analysis	**Median**	**Median Absolute Deviation (MAD) About The Median**
Cellular Morphology	Cellular Density (normal, 1 - 4)	2.00	0.00
	Cellular Density (abnormal, 1 – 4)	2.00	0.00
	Neovascularization (normal, 1- 4)	1.00	0.00
	Neovascularization (abnormal, 1 - 4)	2.00	0.00
	Inflammatory Infiltrate (normal, 1 - 4)	1.00	1.00
	Inflammatory Infiltrate (abnormal, 1 - 4)	1.05	1.00
Collagen	Linearity of Collagen Fibers (1- 4)	2.00	1.00
	Crimping of Collagen Fibers (1 – 4)	2.00	1.00
Toluidine Blue	Toluidine Blue (0 – 3)	2.00	1.00
Collagen Type I	Percent of Collagen Type 1 (0 – 4)	1.00	0.00
Collagen Type III	Percent of Collagen Type 3 (0 – 4)	3.00	1.00
Aggrecan	Percent Presence of Aggrecan (region of interest)	67.50	17.50
	Percent Presence of Aggrecan (overall presence)	50.00	15.00

Hoescht Concentration	Hoescht Concentration (ng/mL)	8693.3	412.7
Glycosaminoglycan (GAG)	Total GAG / Total DNA (µg)	11.79	2.5
	Total GAG / Dry Weight (mg)	10.57	1.8

For CT readings, the dorsomedial portion of all tendons tended towards less cellular density (hypocellularity) in comparison to dorsolateral (Odds Ratio (OR) = 7.3, 95% Confidence Interval (95%CI): [1.3, 41.8]; z = 2.2, P = 0.03) and palmaromedial (OR = 6.1, 95%CI: [1.0, 36.5]; z = 2.0, P = 0.05) tendon regions. Similarly, for MRI readings, the dorsomedial portion of tendons tended towards less cellular density (hypocellularity) in comparison to dorsolateral (OR = 26.3, 95%CI: [2.0, 338.3]; z = 2.5, P = 0.01) and palmaromedial (OR = 12.8, 95%CI: [1.3, 127.0]; z = 2.2, P = 0.03) tendon regions. A significant correlation between cellular density and percentage of tendon involvement on the T2-weighted sequence was appreciated (z = -2.7, P = 0.01). Specifically, cellular density increased as the percentage of tendon involvement on the T2 sequence increased (OR = 0.1, 95%CI: [0.0, 0.6]). Furthermore, a significant correlation between cellular density and signal intensity on the PD-FS sequence was appreciated (P = 0.02), for which hyperintensity on the PD sequence was associated with less cellular density (OR = 8.3, 95%CI: [1.4, 51.1]). There was no significant correlation between any other measured end-point data and imaging characteristics including contrast MRI sequences, contrast CT sequences or US.

Advanced, Multi-Modality Imaging Evaluation:

Cross sectional area lesion to tendon measurements significantly decreased over time across all imaging modalities ($f_{1,\ 6.15}$ = 75.82, P < 0.0001). Also, CSA lesion to tendon measurements were significantly largest on CT evaluation, followed by MRI and then US ($f_{2,\ 62.6}$

= 21.96, $P < 0.0001$) (Fig 2.3). Average lesion CSA obtained from the various MRI sequences over the 12-month study period are presented in Supplementary Figure 9.3.
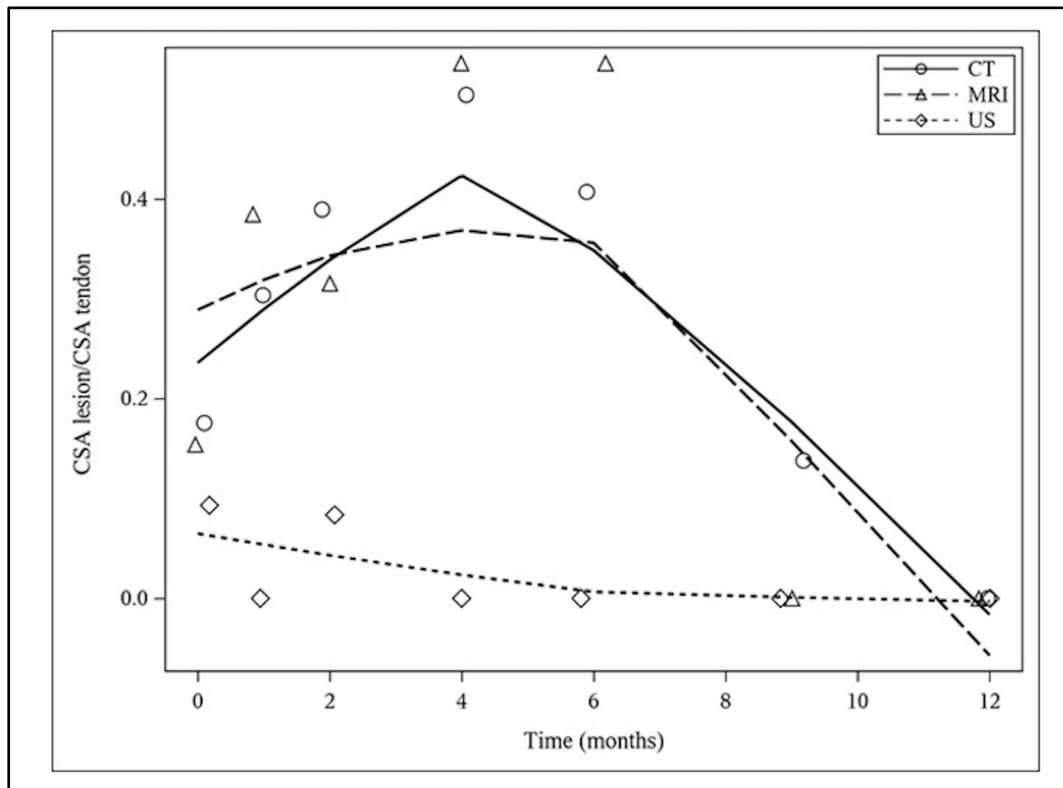
Fig 2.3. Mean cross sectional area (CSA) lesion to tendon ratios for all limbs recorded over the 12 month study period on standard phase computed tomography (CT), T1-weighted fast spin echo (FSE) magnetic resonance imaging (MRI) and transverse plane B-mode ultrasound (US) images. A larger CSA lesion/CSA tendon ratio represents larger lesional size in relation to the tendon. If lesion borders could not be well defined from the adjacent tendon, the CSA of the lesion was considered zero, and therefore the ratio was recorded as zero. Cross sectional area lesion to tendon measurements were significantly largest on CT evaluation, followed by MRI and US ($P < 0.0001$).

Biomechanical Analysis:

There was significant evidence of a positive association between biomechanically measured CSA and HU of lesion to tendon as assessed on the venous CECT phase ($t_{10.92} = 3.889$, $P = 0.03$). Similarly, there was significant evidence of a positive association between biomechanically measured CSA and lesion CSA on the T1 sequence ($t_{6.29} = 3.309$, $P = 0.02$).

41

Further statistical relationships between other imaging outcomes and biomechanical data were not statistically significant.

2.5 Discussion

This study compared the diagnostic utility of MRI, CT and US for the assessment of surgically induced SDFT lesions. The investigation further explored longitudinal imaging characteristics throughout various stages of tendinopathic healing and compared imaging characteristics to comprehensive end point data. Lesion to tendon isoattenuation on CT evaluation correlated with more aggrecan deposition. A significant correlation between cellular density and percentage of tendon involvement on the T2-weighted sequence and signal attenuation on the PD FS sequence was appreciated at the twelve-month time point. Cross sectional area lesion to tendon measurements were significantly largest on CT evaluation, followed by MRI and then US. The findings of this study have provided insight into multi-modal imaging characteristics and longitudinal tendinopathic features utilizing a surgical model of disease. Various MRI (T2 and PD-FS) sequences and standard phase CT evaluation correlated most closely to cellular characteristics of surgically damaged tendons assessed over the twelve month study period.

Clinical usage of CT in equine practice has increased in popularity due to advancements in hardware, software and availability. CT scanning utilizes x-ray beam attenuation for image formation and has therefore been best suited for evaluation of osseous anatomy [38]. Due to limitations of CT to differentiate tissues of similar density, the use of contrast media to perform CECT evaluations has been used to identify and characterize tendon lesions [7, 38]. Contrast administration has been documented to cause an increase in HU readings compared to baseline

values within the equine digit [6], and contrast enhancement was subsequently correlated with the presence of small blood vessels [7]. Contrast-enhanced CT has also been described as aiding in soft tissue lesion evaluation by highlighting the formation of small blood vessels that form as part of the tissue reparative process [7,39]. The significance of this angiogenesis has been reported as relevant to tendon healing, yet discrepancy exists on optimal configuration, appearance, and temporal existence in relation to tendon healing [7,21,38,40-43]. Specifically, persistent vascularization has been associated with pain and inadequate healing in human Achilles tendinopathy patients [40-41], while new vessel formation and increased vascular permeability have been described as important aspects of tendon repair, indicative of active healing [40-41].

There are a limited number of studies investigating the use of dynamic CECT evaluations for tendon assessment in the horse [6-7]. These studies evaluated dynamically generated CT images following intra-arterial contrast administration, similar to the methodology described herein. Criteria used to describe contrast enhancement characteristics consisted of phase of enhancement (early vs. contrast-retention) and location in reference to the lesion (central vs. peripheral). Specifically, peripheral rims of contrast enhancement correlated to regions of tissue hyperemia, while lack of contrast enhancement indicated poor blood supply, and contrast retention correlated to vascular permeability [7]. The study herein is the first to longitudinally evaluate the attenuation and configuration of these angiogenic patterns and correlate their presence to end-point data in a model of tendon injury. Interestingly, neither phase of contrast retention, location of enhancement in reference to the lesion nor hyperattenutation were useful indicators of 12-month tendinopathic healing or biomechanical fortitude for tendons in this study. Furthermore, those tendons demonstrating persistent lack of contrast enhancement, and by

extension less vascularity, healed similarly (histologically and biomechanically) to those tendons demonstrating more consistent vascularization. These results were surprising and contrary to the authors' hypothesis that persistent vascularity assessed as hyperattenuation on dynamic CECT evaluation would be associated with inferior physiologic characteristics. The three overlapping phases of tendon healing have been hypothesized to be identifiable using CECT to gauge changes in tissue permeability and neovascularization [6], but it was the authors' subjective impression herein that phase and location of contrast enhancement for tendons in this study were not temporally predictable or consistent in nature (Figure 2.4). This may be a reflection of model of injury employed or capability of the CECT protocol utilized. It is also possible that further associations to end-point tissue analysis may have been made if evaluated earlier than 12 months although statistical analysis included evaluation of temporal changes in attenuation. The experimental study duration reported herein was unusually long in nature and reports only those vascular patterns associated with surgically induced tendon injury, making extrapolations to clinical disease less certain. It may be possible that a static, chronic tendinopathy stage of healing was reached by all tendons at the 12 month time point, so differences in the rate at which healing occurred may have been missed by singular tissue analysis. As CECT evaluations are further utilized, clinical significance to naturally occurring disease may become apparent.
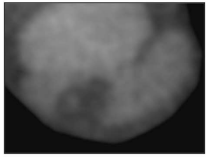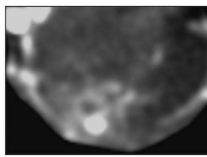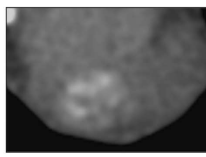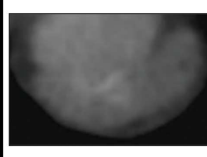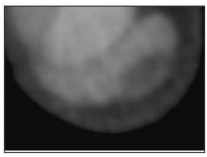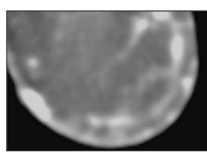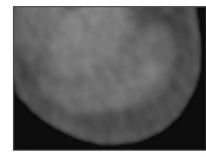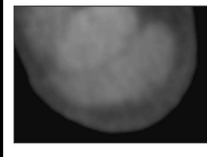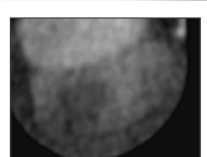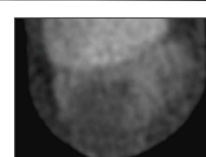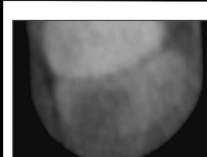
	Standard CT Phase	Arterial CECT Phase	Venous CECT Phase	Delayed CECT Phase
Horse 2 **Vascular** **Retention**				
Horse 6 **Peripheral** **Enhancement**				
Horse 8 **No Contrast** **Enhancement**				

Fig 2.4. Standard computed tomography (CT) and contrast-enhanced computed tomography (CECT) phases of three different limbs at the one-month evaluation time point. Vascular retention, peripheral enhancement and no contrast enhancement were observed angiogenic patterns at various time points across all limbs. Vascularity was not associated with end point histologic, biochemical or biomechanical properties.

Tendon lesions have been described as hypoattenuating in relation to more normal surrounding tendon on standard CT [8, 44], with tendinopathy specifically characterized by histologic abnormalities including collagen disruption, aggrecan deposition and altered cellular morphology [45-47] Similar to the above-mentioned reports [8, 44], surgically-created tendon lesions in this study were initially hypoattenuating with end-point histologic characteristics of aggrecan deposition, hypercellularity and fiber disruption (Fig 2.5A, Fig 2.5B). All surgically induced tendon lesions in this study were subjectively consistent in location, size, extent and severity. Histopathologically and biomechanically, all tendons demonstrated similar healing with no major outliers noted. Interestingly, all SDFTs in this study demonstrated less cellular density along the dorsomedial aspect of the tendon. A retrospective review of clinical SDFT

injury in a population of cutting horses ultrasonographically diagnosed injury consistently along

the dorsolateral aspect compared to the dorsomedial tendon region [48]. It remains unclear as to

why the dorsomedial aspect of the tendon appears to be less predisposed to clinical injury and

demonstrate improved healing in this experimental model. Potential explanations include

inherent biomechanical loading differences or asymmetric surgical disruption despite perceived

standardization.
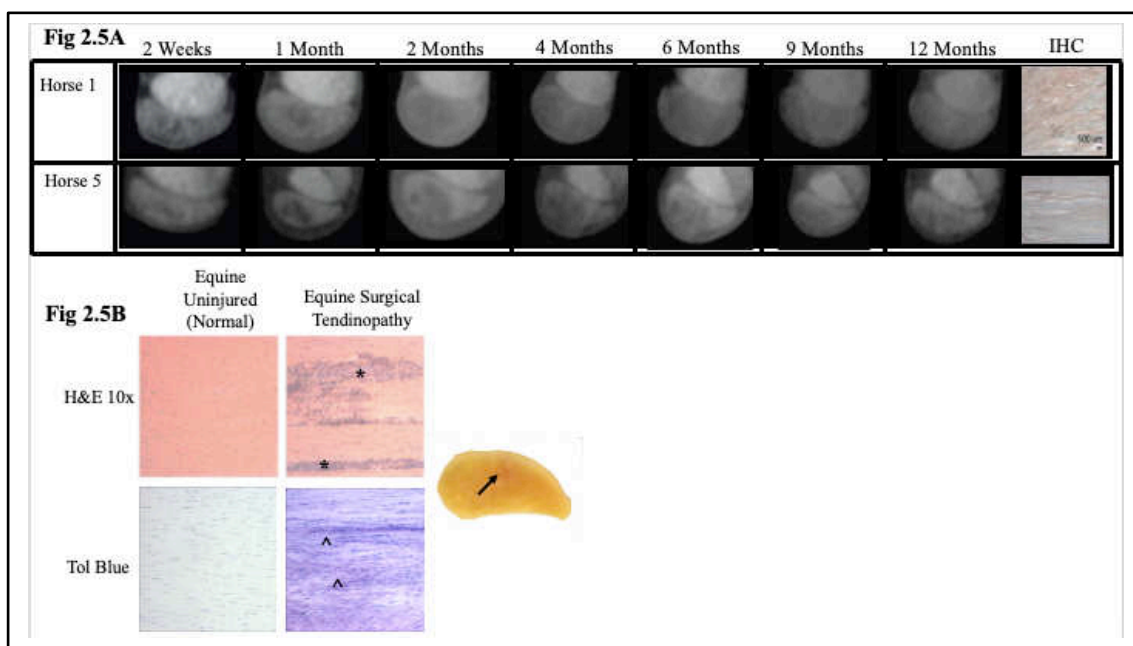
Fig 2.5A. Standard (pre-contrast) computed tomography (CT) phase at seven study time points demonstrating longitudinal lesion attenuation for two different tendons. Isoattenuation at the 12 month time point correlated with greatest amounts of aggrecan deposition (top, horse 1) whereas lesion hypoattenuation corresponded with less aggrecan deposition (bottom, horse 5). Fig 2.5B. Stained sections (Hematoxylin and eosin (H&E) and Toluidine Blue (Tol Blue) of an uninjured (normal) superficial digital flexor tendon and a surgically induced tendinopathic equine specimen. Fiber disruption (^) and hypercellularity (*) were appreciated at the 12 month evaluation time point in surgically damaged tendons. Gross specimen corresponds to surgically induced histopathologic examples.

Over time, all tendon lesions in this study became less visible, or more isoattenuating, on standard phase CT images. Interestingly, this isoattenuation was significantly associated with increased aggrecan deposition ($P = 0.01$, r = 0.6, Table 2.5) at the 12 month timepoint based on lasso regression for the generalized linear mixed model fitted, suggesting that decreased lesion conspicuity on standard phase CT images may indicate the presence of this scar tissue protein. Aggrecan specifically has been demonstrated to be related to decreased tendinous biomechanical strength [45, 49-50] and is therefore considered detrimental to optimal healing. Furthermore, mitigating aggrecan deposition as a therapeutic for tendinopathy is an area of active research [45]. This relationship of standard phase CT to aggrecan deposition in a surgically damaged tendon was an unexpected finding and may be a spurious finding, but it warrants careful consideration, nonetheless. As clinicians often consider a less visible lesion an indicator of healing, the results of this study suggest that longitudinal lesion isoattenuation on standard CT phases may indicate the presence of biomechanically inferior scar tissue instead of adequate healing. Further studies investigating the relevance of this finding and its relationship to clinical outcome are warranted.

In addition to aggrecan deposition, tendinopathy is classically characterized by hypercellular inflammatory infiltrates [45,50], in contrast to the normal, hypocellular tendon matrix. Imaging outcome parameters associated with hypercellularity were limited to the percentage of involvement on the T2-weighted sequence and isointensity on the PD-FS sequence. More specifically, as the percentage of T2-weighted involvement increased, so did histologically appreciated hypercellularity. This was in contrast to the PD-FS sequence for which less cellularity was associated with signal hyperintensity.

It has been suggested that hyperintensity on the T2 sequence is indicative of an acute or active lesion [23, 51-53], but the results of this study suggest that 37.5% (6/16) of tendon lesions twelve months in chronicity may also be hyperintense. Furthermore, the proportion of tendon demonstrating T2-weighted hyperintensity may indicate the specific presence of increased cellularity and therefore chronic tissue remodeling. Previous authors have also observed this relationship grossly seven weeks following initial injury, describing hyperintensity on both T1 and T2-weighted images to be correlated with hypercellularity [22]. Within the equine digit, T2 hyperintensity has been correlated with the most severe areas of fiber disruption [54-55]. Similarly, in a similar surgical model of tendinopathy, lack of T2 hyperintensity 8 and 12 weeks post lesion induction was associated with less inflammatory infiltrate [23]. The results of this study complement the existing body of knowledge and add to the longitudinal breadth of data available regarding the temporal existence of T2 signal hyperintensity in tendon injury. MRI sequence selection to fully evaluate type of tissue present requires not only a battery of protocols, but strategic incorporation of fluid-sensitive sequences as well.

Fluid-sensitive sequences such as PD-FS and STIR are traditionally utilized for the most robust evaluation of fat and fluid presence [52] and are often compared to other sequences within the same imaging plane [52]. Based on the results of this study, hyperintensity on the PD-FS sequence at 12 months post lesion induction was found in 37.5% (6/16) of limbs and was associated with tendinous hypocellularity, which was not an expected finding. Hyperintensity on the PD-FS sequence has classically been associated with acute tendon injury and therefore increased fluid content [56]. The herein reported results are contrary and difficult to explain. It is possible that scarred, hypercellular tendinous tissue is less fluid-sensitive due to chronically altered physiologic properties of the tissue itself compared to more naïve, hypocellular tendon

48

that can still retain fluid signal. Other potential explanations as to why PD-FS hyperintensity may indicate the presence of hypocellular tendon matrix remain unknown and may simply reflect a progression of healing. The MRI characteristics in this study were longitudinally compared to the other imaging modalities and end-point data, but were not evaluated in relation to each other, which may provide further insight on how the sequences may be best strategized for interpretation. Further investigation into mechanistic explanations are warranted.

It has been reported that longitudinal assessment and monitoring of lesion size remains a relevant predictor of future tendon function as prognosis worsens with increasing lesion severity [57]. In a recent study evaluating US factors to predict a successful return to racing, tendon CSA and fiber disruption were the two most predictive outcomes, with racing prognosis worsening with increased severity, respectively [25]. Through longitudinal assessment of lesion to tendon CSA across all three imaging modalities, the results of this study demonstrated that lesional proportion was largest when measured on CT, followed by MRI and lastly US evaluation ($P <$ 0.0001, Fig 2.3, 2.6). Inherent inaccuracy exists with making free-hand ROI measurements, and in the later phases of healing lesion boundaries were especially difficult to discern on US evaluation, obviating explanations for why measurements were more visible (and therefore larger) on CT and MRI evaluation (Fig 2.6), and similarly not appreciated as increases in lesion CSA on US as one might expect (Fig 2.3). Several methods of objectively assessing lesion and tendon size ultrasonographically have been reported [15-18, 20-21], and while they remain relevant to stall-side longitudinal assessment, the clinician should also be aware that based on the results of this study and consistent with previous reports [23], ultrasonographically assessed boundaries between healthy and injured tissue can be ill-defined and subsequent lesion size likely significantly underestimated in comparison to both MRI and CT evaluation.
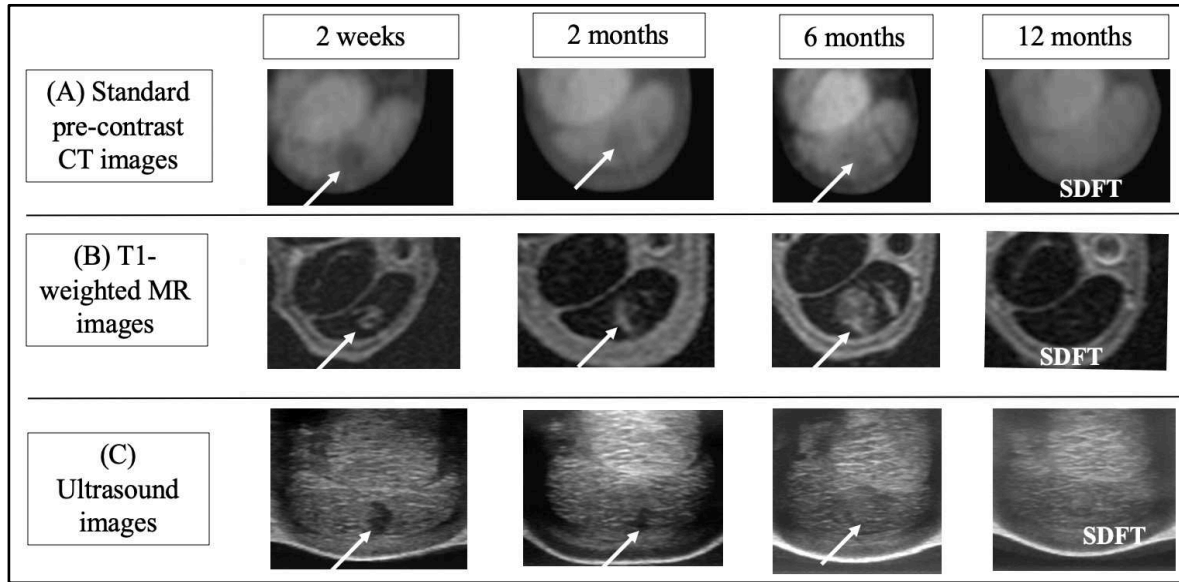
Fig 2.6. Standard, pre-contrast computed tomographic (CT) showing surgically induced lesion (arrows) progression over time (A). The lesion is initially hypoattenuating (dark) at the two week and two month time points, and gradually fills in with isoattenuating tissue by 12 months. T1-weighted, post-contrast magnetic resonance (MR) images (B) of the same lesion, demonstrating early lesion demarcation with progressive lesion expansion and subsequent signal resolution by 12 months. Ultrasonographic evaluation (C) of the same lesion is presented for comparison.

Interestingly, statistical relationships between biomechanical properties (stress, strain and elastic modulus) and imaging characteristics were not observed. The relevance of positive associations between biomechanically measured CSA and venous phase CECT HU readings and lesion CSA on the T1 sequence, respectively, remains uncertain and were unexpected findings. It is possible that gross tendon CSA as assessed through biomechanical data gathering has some relationship to increased HU readings on the venous CECT phase, but further investigation would be required to fully elucidate this interplay. It is also possible that lesion CSA on the T1 sequence is associated with subsequent tendon enlargement and therefore grossly measured CSA.

Study limitations the authors would like to acknowledge include the use of experimentally induced tendon injury, and limited end-point data correlation opportunities, making data extrapolation to earlier imaging time points less certain. Despite these limitations, a controlled, homogenous population of horses with disease consistent in size, severity and location was longitudinally evaluated under three advanced imaging modalities including contrast enhancement. It must also be recognized that the age and other signalment characteristics of the horses in this study are likely not representative of cases with naturally occurring tendon injuries, so care must be taken as to not extrapolate results directly to spontaneous disease. Tissue analysis at more time points utilizing more horses may have been ideal, but such a study would present difficult financial and ethical barriers to overcome. Additionally, extreme care was taken to ensure that site of tissue evaluation remained consistent across all aspects of analysis. Cross-sectional area and lesion measurements on imaging evaluation were repeated three times to reduce inaccuracy, but inherent operator-dependent inexactitude still exists. Subjective impressions of being unable to clearly define a lesion from the adjacent tendon may have also led to measurement inaccuracies. Repeatability studies are also needed for several of the measurements utilized in this work. Further incorporation of additional imaging modalities such as Doppler US and elastography may also have provided insight into stall-side tendinopathic diagnostic evaluation. Investigation of such techniques compared to MRI and CT are warranted. Lastly, a controlled exercise protocol was not utilized herein. A uniform exercise regimen may have more closely mimicked the usual clinical scenario and represents an additional consideration for further tendinopathic studies to consider incorporating into study design.

In summary, the interplay of advanced imaging modalities and tendinopathic healing remains a complex relationship. Imaging features most relevant to tendinopathic properties were appreciated on standard phase CT and T2 and PD-FS sequences. Lesion to tendon isoattenuation on CT evaluation correlated with the presence of aggrecan. Therefore, conversion of a lesion from hypoattenuating to isoattenuating on standard phase CT images should be interpreted as scar tissue deposition and consistent with suboptimal healing. A significant correlation between cellular density and percentage of tendon involvement on the T2-weighted sequence and signal attenuation on the PD FS sequence was appreciated at the twelve month time point. T2-weighted hyperintensity within the realm of tendon imaging should therefore be interpreted as an indicator of increased cellular density and chronic tissue remodeling. The use of contrast for CT and MRI evaluation was not relevant to end-point tissue analysis as described herein and was not useful to predict ongoing physiologic events for longitudinal tendinopathic evaluation. Cross sectional area lesion to tendon measurements were significantly largest on CT evaluation, followed by MRI and US. While US is still considered the first-line imaging modality, clinicians should be aware that distinctions between healthy and injured tissue may be difficult to define, resulting in underestimation of true lesion size. Ultrasonographic appearance should therefore be interpreted with caution when using it to accurately diagnose and prognose tendinopathy in the field.

References

1. Marr, C.M., McMillan, I., Boyd, J.S., Wright, N.G., Murray, M. (1993) Ultrasonographic and histopathological findings in equine superficial digital flexor tendon injury. *Equine Vet. J.* **25**, 23-29.

2. Dyson, S.J. (2004) Medical management of superficial digital flexor tendonitis: a comparative study in 219 horses (1992–2000). *Equine Vet. J.* **36**, 415-419.

3. Crevier-Denoix, N., Collobert, C., Pourcelot, P., Denoix, J.M., Sanaa, M., Geiger, D., Bernard, N., Ribot, X., Bortolussi, C., Bousseau, B. (1997) Mechanical properties of pathological equine superficial digital flexor tendons. *Equine Vet. J.* Suppl **23**, 23-6.

4. Lam, K.H., Parkin, T.D., Riggs, C.M., Morgan, K.L. (2007) Descriptive analysis of retirement of Thoroughbred racehorses due to tendon injuries at the Hong Kong Jockey Club (1992-2004). *Equine Vet. J.* **39**(2), 143-148.

5. Whitton, R., Buckley, C., Donovan, T., Wales, A., Dennis, R. (1998) The diagnosis of lameness associated with distal limb pathology in a horse: a comparison of radiology, computed tomography and magnetic resonance imaging. *Vet. J.* **155**, 223-229.

6. Puchalski, S.M., Galuppo, L.D., Hornof, W.J., Wisner, E.R. (2007) Intraarterial contrast-enhanced computed tomography of the equine distal extremity. *Vet. Radiol.* **48**, 21-29.

7. Puchalski, S.M., Galuppo, L.D., Clifton, D.P., Wisner, E.R. (2009) Use of contrast-enhanced computed tomography to assess angiogenesis in deep digital flexor tendonopathy in a horse. *Vet. Radiol.* 50, 292-297.

8. Jones, A.R.E., Ragle, C.A., Mattoon, J.S., Sanz, M.G. (2019) Use of non-contrast-enhanced computed tomography to identify deep digital flexor tendinopathy in horses with lameness: 28 cases (2014-2016). *J. Am. Vet. Med. Assoc.* **254**(7), 852-858.

9. Judy, C.E., Saveraid, T.C., Rodgers, E.H., Rick, M.C., Herthel, D.J. (2008) Characterization of foot lesions using contrast enhanced equine orthopedic magnetic resonance imaging. In: *Proceedings Am. Assoc. Eq. Pract. 2008 Annual Convention*, 6-10 December 2008, San Diego, CA.

10. Vallance, S.A., Bell, R.J., Spriet, M. Kass, P.H., Puchalski, S.M. (2012) Comparisons of computed tomography, contrast enhanced computed tomography and standing low-field magnetic resonance imaging in horses with lameness localized to the foot. Part 1: anatomic visualization scores. *Equine Vet. J.* **44**, 51-56.

11. Vallance, S.A., Bell, R.J.W., Spriet, M., Kass, P.H., Puchalski, S.M. (2012) Comparisons of computed tomography, contrast-enhanced computed tomography and standing low-field magnetic resonance imaging in horses with lameness localised to the foot. Part 2: Lesion identification. *Equine Vet. J.* **44**, 149-156.

12. Asperio, R.M., Marzola, P., Sbarbati, A., Osculati, F., Addis, F. (2000) Comparison of results of scanning electron microscopy and magnetic resonance imaging before and after administration of a radiographic contrast agent in the tendon of the deep digital flexor muscle obtained from horse cadavers. *Am. J. Vet. Res.* **61**(3), 321-325.

13. Saveraid, T.C., Judy, C.E. (2012) Use of intravenous gadolinium contrast in equine magnetic resonance imaging. *Vet. Clin. Equine* **28**, 617-636.

14. Pickersgill, C.H., Marr, C.M., Reid, S.W.J. (2001) Repeatability of diagnostic ultrasonography in the assessment of the equine superficial digital flexor tendon. *Equine Vet. J.* **33**(1), 33-37.

15. van Schie, J.T.M., Bakker, E.M., van Weeren, P.R. (1999) Ultrasonographic evaluation of equine tendons: a quantitative in vitro study of the effects of amplifier gain level, transducer-tilt, and transducer-displacement. *Vet. Radiol.* **39**(5), 151–160.

16. van Schie, H.T., Bakker, E.M. (2000) Structure-related echoes in ultrasonographic images of equine superficial digital flexor tendons. *Am. J. Vet. Res.* **61**, 202–209.

17. van Schie, H.T., Bakker, E.M., Jonker, A.M., van Weeren, P.R. (2000) Ultrasonographic tissue characterization of equine superficial digital flexor tendons by means of gray level statistics. *Am. J. Vet. Res.* **61**, 210–219.

18. van Schie, H.T., Bakker, E.M., Jonker, A.M., van Weeren, P.R. (2001) Efficacy of computerized discrimination between structure-related and non-structure- related echoes in ultrasonographic images for the quantitative evaluation of the structural integrity of superficial digital flexor tendons in horses. *Am. J. Vet. Res.* **62**, 1159–1166.

19. van Schie, H.T., Bakker, E.M., Jonker, A.M., van Weeren, P.R. (2003) Computerized ultrasonographic tissue characterization of equine superficial digital flexor tendons by means of stability quantification of echo patterns in contiguous transverse ultrasonographic images. *Am. J. Vet. Res.* **64**, 366–375.

20. van Schie, H.T, Bakker, E.M, Cherdchutham, W., Jonker, A.M., van de Lest C.H.A., van Weeren, P.R. (2009) Monitoring of the repair process of surgically created lesions in equine superficial digital flexor tendons by computerized ultrasonography. *Am. J. Vet. Res.* **70**, 37–48.

21. Bosch, G., van Schie, H.T.M., de Groot M.W., Cadby J.A., van de Lest C.H., Barnevald A., van Weeren P.R. (2010) Effects of platelet-rich plasma on the quality of repair of mechanically induced core lesions in equine superficial digital flexor tendons: A placebo-controlled experimental study. *J Orthop. Res.* **28**, 211-217.

22. Crass, J.R., Genovese, R.L., Render, J.A., Bellon, E.M. (1992) Magnetic resonance, ultrasound and histopathologic correlation of acute and healing equine tendon injuries. *Vet. Radiol.* **33**(4), 206-216.

23. Schramme, M., Kerekes, Z., Hunter, S., Labens, R. (2010) MR imaging features of surgically induced core lesions in the equine superficial digital flexor tendon. *Vet. Radiol.* **51**(3), 280-287.

24. Moller, M., Kalebo, P., Tidebrant, G., Movin, T., Karlsson, J. (2002) The ultrasonographic appearance of the ruptured Achilles tendon during healing: a longitudinal evaluation of surgical and nonsurgical treatment, with comparisons to MRI appearance. *Knee Surg. Sports Traumatol. Arthrosc.* **10**, 49-56.

25. Alzola, R., Easter, C., Riggs, C.M., Gardner, D.S., Freeman, S.L. (2018) Ultrasonographic-based predictive factors influencing successful return to racing after superficial digital flexor tendon injuries in flat racehorses: a retrospective cohort study in 469 Thoroughbred racehorses in Hong Kong. *Eq. Vet. J.* **50**, 602-608.

26. McGilvray, K.C., Santoni, B.G., Turner, A.S., Bogdansky, S., Wheeler, D.L., Puttlitz, C.M. (2010) Effects of ^{60}Co gamma radiation dose on initial structural biomechanical properties of ovine bone-patellar tendon-bone allografts. *Cell Tissue Bank.* **12**, 89-98.

27. Dowling, B.A., Dart, A.J. (2005) Mechanical and functional properties of the equine superficial digital flexor tendon. *Vet. J.* **170**(2), 184-192.

28. Marsh, C., Schneider, R.K., Frisbie, D.D., Roberts, G.D., Neelis, D., Yiannikouris, S., Sampson, S. (2012) Evaluation of bone marrow-derived mesenchymal stem cells as a treatment for collagenase-induced desmitis of the proximal suspensory ligament in horses. In: *Proceedings Am. Assoc. Equine Pract. 2012 Annual Convention*, 1-5 December 2012, Anaheim, CA.

29. Nixon, A.J., Dahlgren, L.A., Haupt, J.L., Yeager, A.E., Ward, D.L. (2008) Effect of adipose-derived nucleated cell fractions on tendon repair in horses with collagenase-induced tendinitis. *Am. J. Vet. Res.* **69**(7), 928-937.

30. Kim, Y.J., Sah, R.L.Y., Doong, J.Y.H., Grodzinsky, A.J. (1988) Fluorometric assay of DNA in cartilage explants using Hoescht 33258. *Anal. Biochem.* **174**, 168-176.

31. Fox, J., Monette, G. (1992) Generalized collinearity diagnostics. *J. Am. Stat. Assoc.* **87**, 178-183.

32. Groll, A., Tutz, G. (2014) Variable selection for generalized linear mixed models by L_1-penalization. *Stat. Comp.* **24**, 137-154.

33. Warton, D.I., Hui F.K.C. (2011) The arcsine is asinine: the analysis of proportions in ecology. *Ecology* **92**, 3-10.

34. Akaike, H. (1973) Information theory and an extension of the maximum likelihood principle. In: *Proceedings Int. Symp. Info. Theory* 1973 2-8 September 1971, Tsahkadsor, Armenia.

35. Edwards, L., Muller, K., Wolfinger, R., Qaqish, B.F., Schabenberger, O. (2008) An R^2 statistic for fixed effects in the linear mixed model. *Stat. Med.* **27**, 6137-6157.

36. West, B.T., Welch, K.B., Galecki, A.T., Gillespie, B.W. (2015) Linear mixed models: An Overview. In: *Linear mixed models: a practical guide using statistical software*, 2nd ed., Ed: West, B.T., Welch, K.B., Galecki, A.T, CRC Press Taylor & Francis Group Boca Raton, FL., 9-58.

37. Hedecker, D. (2015) Methods for multi-level ordinal data in prevention research. *Prev. Science.* **16**, 997-1006.

38. Puchalski, S. (2012) Advances in equine computed tomography and use of contrast media. *Vet. Clin. North Am.* **28**,563-581.

39. Dawson, P. (2006) Functional imaging in CT. *Eur. J. Radiol.* **60**, 331-340.

40. Kristoffersen, M., Öhberg, L., Johnston, C., Alfredson, H. (2005) Neovascularisation in chronic tendon injuries detected with colour doppler ultrasound in horse and man: implications for research and treatment. *Knee Surg. Sports Traumatol. Arthrosc.* **13**, 505-508.

41. Sharma, P., Maffuli, N. (2005) Tendon injury and tendinopathy: healing and repair. *J Bone Jt. Surg.* **87**,187-202.

42. Murata, D., Misumi, K., Fujiki, M. (2012) A preliminary study of diagnostic color doppler ultrasonography in equine superficial digital flexor tendonitis. *J. Vet. Med Sci.* **74**(12), 1639-1642.

43. Smith, R.K.W. (2009) Mesenchymal stem cell therapy for equine tendinopathy. *Disabil. Rehabil.* **30**(20), 1752-1758.

44. Nowack, M. (2002) The role of DDFT tendinitis in navicular syndrome – a CT perspective. In: *Proceedings World Orthop. Vet. Congress 2002.* 5-8 September 2002, Munich, Germany.

45. Bell, R., Li, J., Gorski, D.J., Bartels, A.K., Shewman, E.F., Wysocki, R.W., Cole, B.J., Bach, B.R., Mikecz, K., Sandy, J.D., Plaas, A.H., Wang, V.M. (2013) Controlled treadmill exercise eliminates chondroid deposits and restores tensile properties in a new murine tendinopathy model. *J. Biomech.* **46**(3), 498-505.

46. Corps, A.N., Robinson, A.H., Movin, T., Costa, M.L., Hazleman, B.L., Riley, G.P. (2006) Increased expression of aggrecan and biglycan mRNA in Achilles tendinopathy. *Rheumatol.* **45**, 291–294.

47. de Mos, M., Koevoet, W., van Schie, H.T., Kops, N., Jahr, H., Verhaar, J.A.N., van Osch, J.V.M. (2009) In vitro model to study chondrogenic differentiation in tendinopathy. *Am J Sports Med* **37**, 1214–1222.

48. Tipton TE, Ray CS, Hand RD. (2013) Superficial digital flexor tendonitis in cutting horses: 19 cases (2007-2011). *J. Am. Vet. Med. Assoc.* **243**,1162-1165.

49. Jarvinen, M., Jozsa, L., Kannus, P., Jarvinen, T.L.N., Kvist, M., Leadbetter, W. (1997) Histopathological findings in chronic tendon disorders. *Scand. J. Med. Sci. Sports* **7**(2), 86-95.

50. Kannus, P., Jozsa, L. (1991) Histopathological changes preceding spontaneous rupture of a tendon. A controlled study of 891 patients. *J. Bone Joint Surg. Am.* **73**, 1507-1525.

51. Murray, R.C., Dyson, S.J. (2007) Image interpretation and artifacts. *Clin. Tech. Eq. Pract.* **6**, 16-25.

52. Winter, M.D. (2012) The basics of musculoskeletal magnetic resonance imaging. *Vet. Clin. Equine* **28**, 599-616.

53. Werpy, N.M. (2004) Magnetic resonance imaging for diagnosis of soft tissue and osseous injuries in the horse. *Clin. Tech. Eq. Pract.* **3**, 389-398.

54. Blunden, A., Murray, R., Dyson, S. (2009) Lesions of the deep digital flexor tendon in the digit: a correlative MRI and post mortem study in control and lame horses. *Equine Vet. J.* **41**, 25–33.

55. Busoni, V., Heimann, M., Trenteseaux, J., Snaps, F., Dondelinger, R.F. (2005) Magnetic resonance imaging findings in the equine deep digital flexor tendon and distal sesamoid bone in advanced navicular disease—an ex vivo study. *Vet. Radiol.* 46, 279–286.

56. Zubrod, C.J., Barrett, M.F. (2007) Magnetic resonance imaging of tendon and ligament injuries. *Clin. Tech. Eq. Prac.* **6**, 217-229.

57. Genovese, R., Longo, K., Berthold, B., Jorgenson, J. (1997) Quantitative sonographic assessment in the clinical management of superficial digital flexor injuries in Thoroughbred racehorses. In: *Proceedings Am. Assoc. Eq. Pract. 1997 Annual Convention*, 7-10 December 1997, Phoenix, AZ.

CHAPTER 3: Surgical Lesion Induction Increases Global Elastic Modulus in Equine Superficial Digital Flexor Tendons

3.1 Overview

Spontaneous tendon injury is the most ideal avenue through which tendinopathy is studied, but inconsistencies in extent, severity and treatment prohibit it from being a reliable mechanism through which experimental trials can be performed. A model of disease that induces chronic structural weakness compared to an uninjured state would represent an avenue to standardize the study of tendinopathy. The objective of this study was to determine the long-term (twelve month) biomechanical properties of equine superficial digital flexor tendons (SDFTs) with surgically induced lesions compared to uninjured equine SDFTs. SDFT lesions were surgically created in both forelimbs of four horses (n = 8 limbs) using a modified synovial resector technique. Twelve months post lesion induction, SDFTs underwent non-destructive biomechanical testing. Elastic modulus and tendon cross-sectional area (CSA) values at three regions of interest (ROI) were compared to those of forelimb SDFTs collected from four uninjured horses (n = 8 limbs). Significant differences in mean elastic modulus and tendon CSA were appreciated at all three ROIs when comparing uninjured and surgically damaged tendons ($P < 0.001$). Increases in elastic modulus and CSA were increased not only at the site of lesion creation, but also proximal and distal to the site of surgical lesion induction, suggestive of global tendinopathic change. While these findings cannot be directly extrapolated to spontaneous injury, the results described herein may serve as a basis for further model development and comparison to naturally occurring tendon injury. Equine SDFT injuries remain prevalent and difficult to treat, with several extrinsic factors limiting the ability to reliably study natural disease. Long-term biomechanical analysis of surgically induced lesions herein suggests that

chronic structural weakness occurs and is similar to that described for naturally occurring disease. The main limitation of this study was the use of non-destructive biomechanical analysis utilizing a low applied strain.

3.2 Introduction

The quest for improved diagnostic and therapeutic approaches to optimize tendon healing and rehabilitation remains a central focus of equine practitioners. Specific to the horse, superficial digital flexor tendon (SDFT) overuse injuries are a frequent and frustrating cause of morbidity in athletic horses [1-4]. Tendon injury was implicated as the primary reason for retirement of Thoroughbred racehorses over a twelve year epidemiologic study period in Hong Kong [5]. Similarly, event horses were most commonly unable to compete due to tendon or ligament injury in the United Kingdom [6]. Naturally occurring tendon injury remains the most ideal avenue through which tendinopathy is studied, but inconsistencies in extent, severity, duration and treatment prohibit it from being a reliable mechanism through which experimental trials can be performed. Additionally, clinical tendon injury does not commonly result in euthanasia, making tissue samples difficult to obtain. Therefore, an improved understanding of tendon healing using a model of disease that induces chronic structural weakness compared to an uninjured state would represent an avenue to standardize the study of tendinopathy.

Biomechanical properties of healthy and naturally injured equine SDFTs have been investigated *in vitro* [7-14]. Compared to uninjured tendons, those with naturally occurring injury demonstrated increases in cross-sectional area (CSA), reduced ultimate stress and lower strain [7,8,13]. The segments of tendon adjacent to the discrete regions of injury demonstrated evidence of compensatory overstrain, leading authors to conclude that junctions between normal and

59

abnormal tendon are most prone to re-injury due to their altered mechanical state [8]. To be considered biologically relevant, an optimized model of tendon injury would therefore need to replicate altered biomechanical loading not only at the site of injury, but in adjacent regions as well.

Several equine tendon injury models via lesion induction have been reported previously [15-25]. Physical induction of tendon injury was first described as a surgically-induced, full-thickness defect created in the superficial digital flexor tendon [15-16]. As surgical technique evolved, lesion creation became more refined with the use of a synovial resector to create lesions specifically within the core of the superficial digital flexor tendon [17-19, 26]. Despite its growing popularity as a relevant tendinopathic model, however, earlier studies utilizing the synovial resector technique are based on relatively short-term follow-up and limited material analysis, with no study investigating long-term biomechanical properties [17-19, 26]. Therefore, the objective of this prospective study was to determine the long-term (twelve month) biomechanical properties of equine SDFTs with surgically induced lesions compared to uninjured equine SDFTs. It was hypothesized that surgically damaged SDFTs would demonstrate increases in cross sectional area (CSA) and elastic modulus compared to normal SDFTs.

3.3 Materials and Methods

This study was a prospective experiment. All study methods were conducted in compliance with Institutional Animal Care and Use Committee (IACUC) standards. The experimental sample size (n = 8 limbs in each group) was calculated using GPower Version 3.1.1 (GPower, Brunsbuttel, Germany). Values from a published study investigating biomechanical differences between normal and naturally injured SDFTs were used for power calculation [7-8].

Specifically, an a priori power analysis was conducted. Using a two-sample-t-test with an expected group mean strain difference of 2.7%, this power analysis resulted in an effect size of 2.077 and a power of 0.95 using a 95% confidence interval and standard deviation of 1.3% between groups.

Experimental Animals:

Four healthy mixed breed horses (two geldings and two mares), aged two to four years that showed no clinical or ultrasonographic evidence of current or previous SDFT injury were purchased from an outside vendor for study enrollment into the surgical tendinopathy group (n = 8 limbs). Horses weighed 336-409 kg and showed no evidence of lameness on baseline evaluation.

Eight healthy mixed breed horses (three geldings, three mares and two stallions), ages two to three years that showed no clinical evidence of current or previous SDFT injury were purchased from an outside vendor for enrollment in an unrelated study, and to serve as control SDFTs (n = 8 limbs) for the study herein. Horses weighed 412-481 kg and showed no evidence of current or previous SDFT injury based on clinical and ultrasonographic examination.

Surgical Procedure & Post-Operative Care:

Surgical Tendinopathy Limbs:

The four horses designated for surgical tendinopathy underwent general anesthesia using isoflurane in oxygen. Surgical core lesions were created in the mid-metacarpal region of the SDFT of each forelimb (n = 8 forelimbs) using a synovial resector as previously described [26-27]. Briefly, a small skin incision was made in the palmar midline of the limb, just proximal to

the digital tendon sheath. A small (1 cm) longitudinal incision was made into the core of the SDFT, through which an arthroscopic burr (Ø 3.5 mm, Linvatec, Largo, FL) was bluntly, and in inactivated state, inserted proximally over a length of 7–8 cm. The obturator position was digitally palpated and position subsequently determined and directed towards the center of the tendon in all limbs. Then, the burr was activated and slowly retracted in approximately 20 seconds [26, 27]. The incisions in the paratenon and skin were sutured in a simple interrupted pattern with resorbable 2-0 polydioxanone (PDS, 2-0, Ethicon, Somerville, NJ) and unresorbable nylon (Ethilon; Ethicon), respectively. Pre-operatively and three days post-operatively, all horses received 4.4 mg/kg phenylbutazone (Phenylbutazone, Aspen Veterinary Resources, Liberty, MO) and perioperative antimicrobials. Distal limb bandages were applied to all forelimbs for 14 days post-operatively and sutures were removed in standard fashion. All horses were confined to stall rest for eight weeks post-operatively. The horses were then turned out into paddocks (20,000 square feet in size) for the remainder of the study period, with the exception of one day before and after all anesthetic procedures during which horses were on stall rest for feed restriction and post-anesthetic monitoring.

Control Limbs:

The limbs belonging to the control group were enrolled in a 78-week, unrelated study [Frisbie et al unpublished data] that underwent the exercise protocol described in Table 3.1. Limbs belonging to control horses were not surgically damaged and housed in stalls (12x12) while not being exercised.

Table 3.1: Table describing the 78-week exercise protocol for control limbs.

Study Week	Exercise Protocol Performed Per Day, Five Days Per Week
Weeks 1-4	Stall rest
Week 5	Handwalk 5 minutes
Week 6	Handwalk 10 minutes
Week 7	Handwalk 15 minutes
Week 8	Handwalk 20 minutes
Week 9	Treadmill trot 2 minutes
Week 10	Treadmill trot 5 minutes
Week 11	Treadmill trot 8 minutes
Week 12	Treadmill trot 10 minutes
Weeks 13-14	Stall rest
Week 15	Treadmill trot 5 minutes
Week 16	Treadmill trot 8 minutes
Weeks 17-18	Treadmill trot 10 minutes
Week 19	Treadmill trot 15 minutes
Week 20	Treadmill trot 20 minutes
Weeks 21-25	Trot-gallop-trot 6 minutes
Weeks 26-27	Stall rest
Week 28	Handwalk 10 minutes
Week 29	Handwalk 15 minutes
Week 30	Treadmill trot 2 minutes

Weeks 31-32	Treadmill trot 5 minutes
Weeks 33-34	Treadmill trot 8 minutes
Week 35	Treadmill trot 10 minutes
Week 36	Treadmill trot 10 minutes
Weeks 37-42	Trot-gallop-trot 6 minutes
Weeks 43-51	Trot-gallop-trot fast 6 minutes
Weeks 52-53	Stall rest
Week 54	Hand walk 10 minutes
Week 55	Hand walk 15 minutes
Week 56	Treadmill trot 2 minutes
Weeks 57-58	Treadmill trot 5 minutes
Weeks 59-60	Treadmill trot 8 minutes
Week 61	Treadmill trot 10 minutes
Week 62	Treadmill trot 10 minutes
Week 63	Trot-gallop-trot 6 minutes
Weeks 64-78	Trot-gallop-trot 6 minutes

Tissue Harvest:

Surgical Tendinopathy Limbs:

At 12 months post lesion induction, all surgical tendinopathy horses were humanely euthanized according to IACUC standards. Post-mortem, a longitudinal incision was made to remove the skin and subcutaneous tissue overlying the forelimb SDFTs from the level of the carpus to the proximal sesamoid bones. All SDFTs were visually evaluated, gross observations

were recorded and limbs were photographed. Following evaluation, a suture was placed at the

site of the most injured area of the SDFT based on advanced imaging (magnetic resonance

imaging (MRI)) evaluation and distance relative to the accessory carpal bone (Figure 3.1). The

location of this suture (site of surgical defect) in addition to 3cm proximal (proximal to defect)

and 3cm distal (distal to defect) made up the three regions of interest (ROI) for subsequent non-

destructive biomechanical analysis.

Lesion Suture Marker
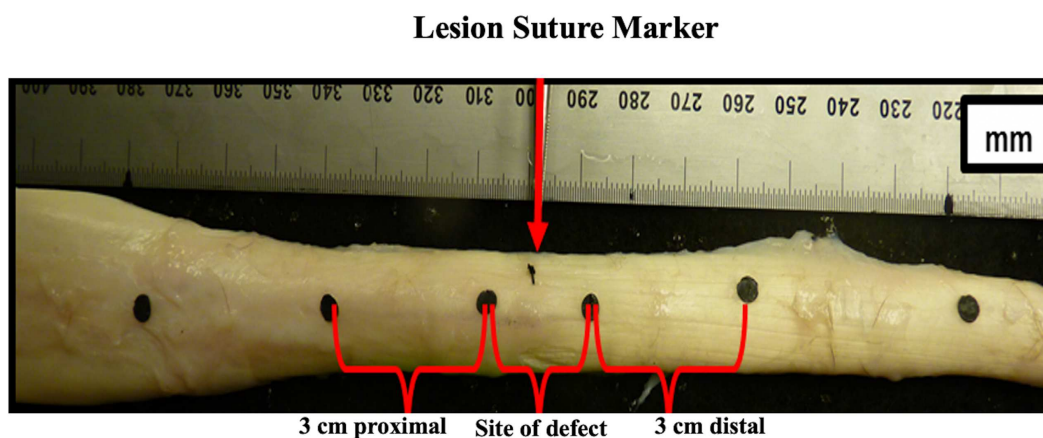
Fig 3.1. Suture placement indicating the site of the most grossly injured region of the equine superficial digital flexor tendon (SDFT). The location of this suture was used as the center of biomechanical evaluation (defect site), with subsequent analysis also including 3cm proximal and 3cm distal to this area. Optical contrast tracking markers were affixed to each tendon at these sites in order to calculate localized tissue strain.

Control Limbs:

Forelimb SDFTs were also collected from 8 uninjured horses (n = 8 limbs) following

their inclusion in an unrelated 78-week study. Three extra-thecal regions of interest were

similarly identified on uninjured tendons for subsequent biomechanical analysis.

The forelimbs of all horses were then disarticulated at the level of the middle carpal joint

and the SDFTs were carefully harvested from the proximal metacarpal region to the level of the

proximal sesamoid bones using sharp dissection and Brown-Adson tissue forceps. Care was

taken to minimize tissue handling when possible. Upon harvest, tendons were wrapped in saline-soaked gauze and transported to the adjacent laboratory for biomechanical testing. Tissue hydration was continually maintained with saline spray at 15-minute intervals throughout dissection and non-destructive biomechanical testing.

Biomechanical Testing:

All superficial digital flexor tendon tissue were allowed to relax for five minutes prior to cross-sectional area (CSA) data collection. The CSA of all tendons was measured at the three ROIs using an area micrometer and applied plunger pressure of 0.12 MPa as previously described [28] (Figure 3.2). These measurements were used to normalize load data to CSA thickening and later incorporated to estimate tissue stress. To calculate localized tissue deformation and provide the ability to calculate tissue strain in the three ROIs (Figure 3.1), optical contrast tracking markers were then affixed to the tendon, using cyanoacrylate gel.
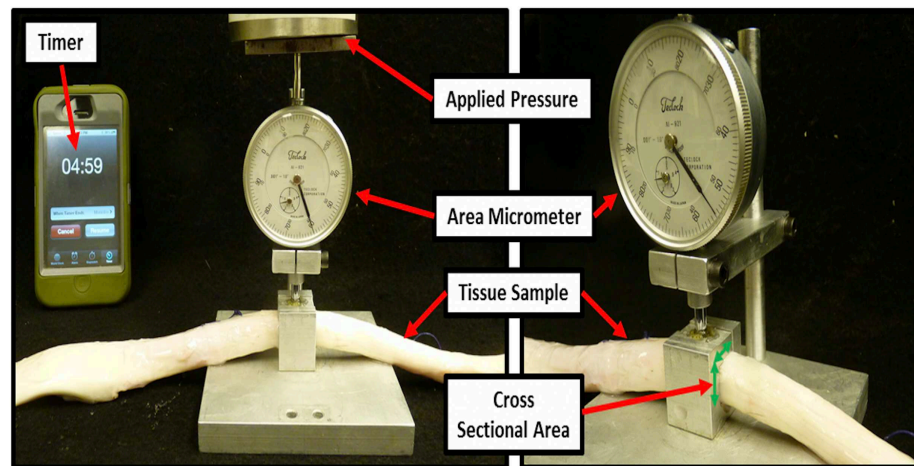
Fig 3.2. The cross-sectional area (CSA) for all tendons was measured for the three regions of interest (ROI). The CSA measurements were subsequently used in tissue stress calculations.

The proximal and distal aspects of each tendon were rigidly coupled to a materials testing machine (MTS 858, MiniBionix II, Eden Prairie, MN) using custom designed soft tissue clamps and consistent grip hold of 8.4 N-m. (Figure 3.3). To ensure that biomechanical loading was representative of the physiological scenario, the testing apparatus was directed collinear to the long axis of the tendon fibers. A high-resolution force sensing transducer (5000N capacity, 0.01% resolution) was coupled to the actuator of the testing machine and used to measure the resultant force.
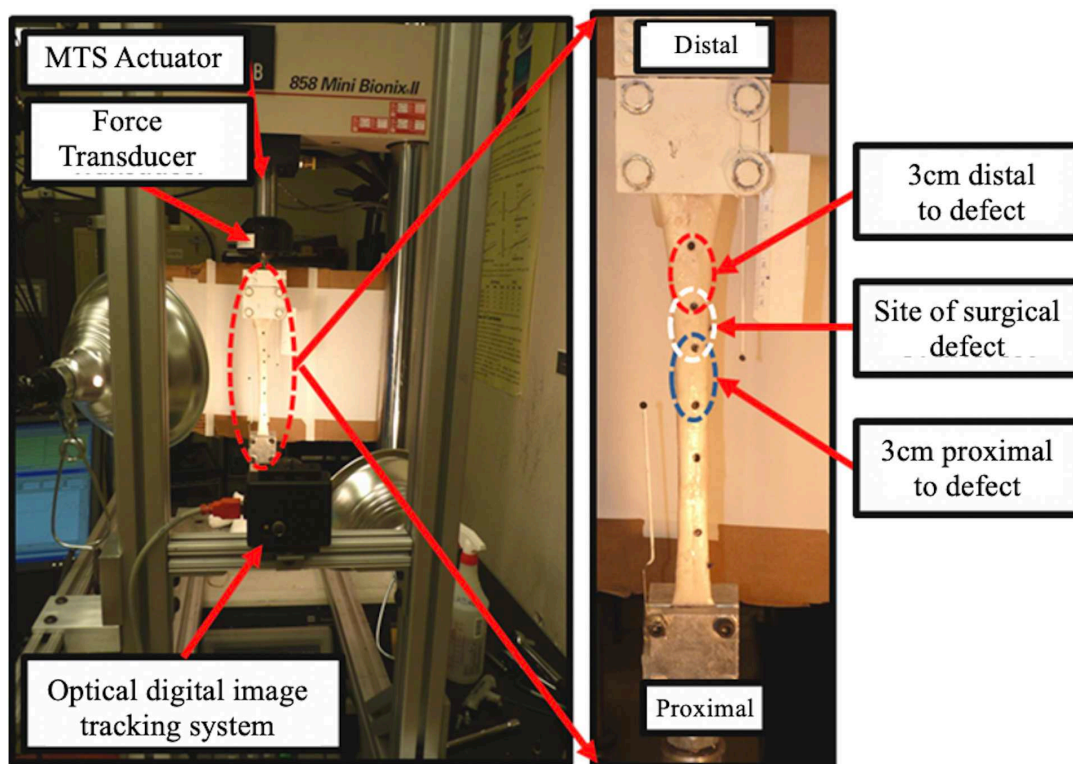
Fig 3.3. The biomechanical testing apparatus utilized with a sample mounted. The key components of the mechanical testing and image tracking systems have been highlighted. The areas of interest within the tissue are outlined.

All tendons were pre-conditioned to normalize for viscoelastic effects and testing variability though the application of a static 10 N preload for 2 minutes, followed by the application of ten cyclic tensile loads, at 0.25 Hz, ranging from 12 to 25% of predicted failure stress under

force control at a rate of 25N/sec. Predicted failure stress ranges (force at failure divided by CSA of the tendon) were calculated using previously reported failure force of equine digital flexor tendons (7.9±0.9kN, [13]), normalized to the sample's pre-testing CSA. Immediately following pre-conditioning, samples were quasi-statically ramped under force control at a rate of 25N/sec until failure or 40% of maximum stress was achieved. A force control testing protocol was used to ensure that the tendinous tissue was not mechanically damaged due to excessive tissue displacement. Using this value normalized to the CSA of each sample, the lowest intra-sample failure stress was calculated and used as set points for the sample's preconditioning protocols, consistent with previously reported failure force of equine digital flexor tendons (7.9±0.9kN, [13]). A high resolution digital camera and corresponding image capture software (Point Grey, FlyCapture, Canada) were used to measure localized tissue deformation (track relative displacement of optical contrast tracking markers) during the quasi-static ramp for the three regions of interest. Force and localized optical marker tracking data were recorded at 15 Hz.

Biomechanical Data Analysis:

Stress, strain and resultant elastic modulus were calculated. Stress values were calculated by normalizing force data measured from the MTS machine to CSA measurements at the three specific regions of interest (Figure 3.4A). Localized tissue deformation was calculated from the high-resolution video data recorded during the quasi-static ramp period of testing. Optical tracking of the surface markers within the three regions of interest was performed using Matlab code, wherein the X-Y position of each marker was calculated and stored in an array. Strain was calculated as the instantaneous difference in the distance between two adjacent markers normalized to the initial (i.e. prior to quasi-static ramp) distance between the same two markers

(Figure 3.4B). Stress versus strain was plotted for the three regions of interest and the elastic

engineering modulus was calculated from the resultant graph. The elastic modulus of the material

was defined as the ratio of normal engineering stress over engineering strain in the portion of the

stress-strain relationship that obeys Hooke's laws (i.e. linear response) (Figure 3.4C). To ensure

consistency across samples, elastic modulus was calculated between 1000-2000 N, which was the

range for which all samples demonstrated linear behavior.

$$\boxed{\text{Fig 3.4A}} \qquad \text{Stress (MPa)} = \frac{\text{Force}_{\text{MTS}}(\text{N})}{\text{Cross Sectional Area}_{\text{AOI Specific}}(\text{mm}^2)}$$

$$\boxed{\text{Fig 3.4B}} \qquad \text{Strain} \left(\frac{\text{mm}}{\text{mm}}\right) = \frac{\text{Length}_{\text{Initial}} - \text{Length}_{\text{Instantaneous}}}{\text{Length}_{\text{Initial}}}$$

$$\boxed{\text{Fig 3.4C}} \qquad \text{Modulus}_{\text{Elastic}} = \frac{\text{Stress}_{\text{Linear Region}}}{\text{Strain}_{\text{Linear Region}}}$$

Fig 3.4. Equations and associated units of measurement used to calculate stress (A), strain (B)
and elastic modulus (C) for each superficial digital flexor tendon (SDFT) region of interest
(ROI).

Statistical analyses:

Statistical analysis was performed using the statistical software package R (version 4.0.3,

R-project®, R Foundation for Statistical Computing Vienna, Austria). A Shapiro-Wilk test was

used to confirm non-normality of the data. A non-parametric analysis was performed. Elastic

modulus and CSA data for surgical and control limbs were compared at the three ROI's using a

Wilcoxon rank sum analysis with clustering by limb for each horse using the clusrank pancake

package in RStudio. Statistical significance was considered $P < 0.05$ for all statistical analysis.

3.4 Results

Median and standard deviation elastic modulus values for surgically damaged tendons distal to the defect, at the defect and proximal to the defect were 546.9 (+/- 158.5), 585.9 (+/- 78.7) and 653.5 (+/- 235.3) MPa, respectively. This contrasted with median elastic modulus values for control tendons in the same locations of 263.1 (+/- 117.0), 199.2 (+/- 57.7) and 290.0 (+/- 116.9) MPa. Statistically significant differences in median elastic modulus were appreciated at all three ROIs when comparing uninjured and surgically damaged tendons ($P < 0.01$). Similarly, median CSA measurements (mm^2) for surgically damaged tendons were found to be 116.2 +/- 21.6 (distal to defect), 163.1 +/- 16.3 (defect) and 171.4 +/- 26.5 (proximal to defect). Median CSA measurements for control tendons in the same locations were found to be 86.9 +/- 8.2, 90.0 +/- 4.1 and 87.1 +/-8.1 mm^2. Significant differences in tendon CSA were appreciated at all three ROIs between the two groups ($P < 0.01$). The median and standard deviation elastic modulus and CSA data calculated from the non-destructive biomechanical testing are summarized in Figure 3.5.

	Distal to Defect	Defect Site	Proximal to Defect
Surgical Lesion Induction	546.89	585.94	653.50
Uninjured Tendon	263.11	199.22	289.96

☑ Surgical Lesion Induction ☐ Uninjured Tendon

Fig 3.5A

	Distal to Defect	Defect Site	Proximal to Defect
Surgical Lesion Induction	116.21	163.07	171.36
Uninjured Tendon	86.85	90.03	87.14

☑ Surgical Lesion Induction ☐ Uninjured Tendon
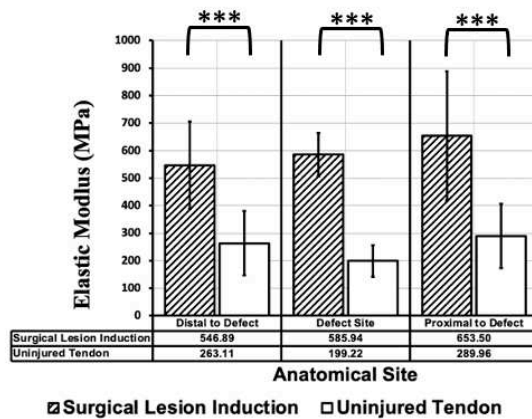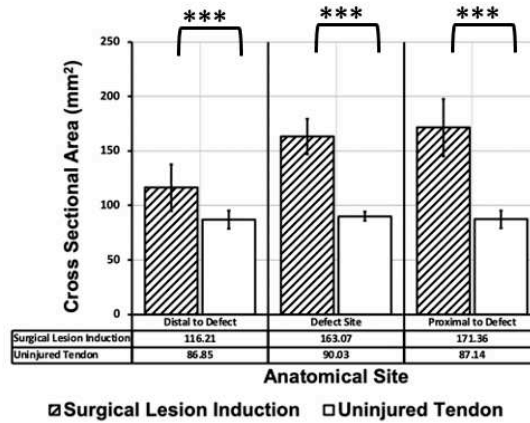
Fig 3.5B

Fig 3.5. Median elastic modulus (Fig 3.5A) and median cross-sectional area (CSA, Fig 3.5B) of tendons with surgically created lesions compared to normal, uninjured (control) tendons. Tendons with surgically created lesions demonstrated significantly larger values elastic modulus and CSA based on results of the Wilcoxon rank sum analysis with clustering by limb for each horse (*** indicates $P < 0.01$). Data medians are shown with standard deviation bars.

3.5 Discussion

This study compared the long-term (twelve month) material properties of SDFTs with surgically induced tendon lesions to those of healthy, uninjured SDFTs utilizing non-destructive biomechanical analysis. Statistically significant increases in CSA and elastic modulus were appreciated at all three sites of tissue analysis, consistent with hypertrophy and increased material stiffness, respectively.

Various equine SDFT surgical models of tendinopathy have been evaluated at several different investigative levels including imaging characteristics [18-19], cellular analysis [15, 18-19] and biomechanical testing [29-30]. When SDFTs were hemi-transected and subsequently biomechanically tested six weeks after lesion induction, significant changes in elastic modulus and ultimate tensile strength compared to healthy tendons were appreciated [29]. An *ex vivo* study investigating the effect of cyclic loading on the propagation of enzymatically and

physically induced tendon lesions reported that a combination of enzymatic and mechanical stimulation caused lesions to significantly propagate [30]. The results of the study herein have provided insight into the long-term (twelve month) biomechanical effects of lesions created using the modified synovial resector technique [17, 26-27]. Horses in this study were stall-rested for eight weeks following lesion induction and then housed in paddocks for the remainder of the study period. It's possible that a different exercise regimen may have altered terminal biomechanical findings, but even in absence of mechanical stimulation all surgically damaged tendons demonstrated an approximate 31% decrease in material strength and 57% increase in CSA at the defect site (Figure 3.5).

The effect of exercise on tendon remodeling has been an area of active research, yet direct causal relationships between tendon strength and training regime are still undetermined [13, 31-33]. An early investigation demonstrated that SDFT CSA following 4 months of race training increased, which was interpreted as an adaptation to training [34]. This contrasts with an investigation that documented unchanged SDFT CSAs in response to training [31]. The effect of exercise regimens on SDFT properties in three groups of foals revealed a persistent positive effect of free pasture exercise on tendon elasticity [35]. Subsequent studies have described the role of galloping and its relation to micro-trauma that may eventually result in tendinopathic injury [36-37]. It is currently believed that exercise may influence the structure, chemical composition and/or mechanical properties of tendon [32], but study design inconsistencies and wide variation in clinical application of exercise regimes makes it difficult to directly compare studies or develop definitive conclusions [38]. It is important to acknowledge that the two study groups described herein were exposed to different exercise regimes. The surgically damaged tendons were stall-rested for eight weeks following lesion induction and then housed in paddocks

for the remainder of the study period. The control tendons were exposed to the exercise regime as described in Table 3.1, which more closely resembled a normal exercise routine. Although identical exercise regimes between the two treatment groups would have facilitated a more direct experimental comparison, it would not have reflected the clinical scenario of comparing biomechanical strength of an injured SDFT restricted to stall rest, then pasture exercise to that of a healthy tendon exposed to routine exercise, which more closely aligned with the study objective described herein. While this difference in exercise exposure is indeed a study limitation, the authors have provided two study groups otherwise exposed to similar environment, housing and nutrition while maximizing tissue usage. Additionally, optimal controlled exercise conditions for experimental tendinopathic investigations are still undetermined. Lastly, a comparable 18-month (72-week) treadmill-training program involving galloping did not change collagen fibril diameter in the deep digital flexor tendon [39], substantiating that the 78-week treadmill regime utilized herein for control tendons was unlikely to alter chemical composition to the extent of having a biomechanical effect.

The high rate of equine tendon re-injury is believed to be due to the inferior biomechanical properties of the damaged tendon and the higher compensatory stresses and strains of the adjacent transitional areas between healthy and pathologic tissues [8]. Normal and tendinopathic biomechanical profiles have been evaluated *in-vitro* for healthy and variably diseased equine SDFTs [7-12, 14]. SDFTs with natural injury demonstrated significant increases in tendon CSA, lower ultimate tensile strain and lower ultimate tensile stress across seven evaluated segments [8] when compared to homologous data from uninjured SDFTs [7]. Lesion chronicity in the aforementioned study varied from several months to several years [8] but was mainly chronic in nature (minimum of one year from first injury except for one tendon).

Other investigations utilizing the surgical model of tendinopathy have reported experimental timelines of 6 weeks [19], 12 weeks [17], 12 weeks [18] and 24 weeks [15, 26, 41]. The study timeline described herein was unusually long in experimental nature (52 weeks) and is the first to report such long-term outcomes that facilitate the most clinically relevant comparisons. With characterization of the long-term injury model effects now reported, future studies can be more efficiently designed to facilitate clinical comparisons of interest. Specifically, the elastic modulus and cross-sectional area of tendons with surgically created lesions herein were significantly higher than those values of normal, uninjured tendons ($P =$ <0.01, respectively, Fig 3.5). The increases in elastic modulus and CSA were increased not only at the site of lesion creation, but also proximal and distal to the lesion, suggestive of global tendinopathic change. These observed biomechanical differences are consistent with the changes described for naturally occurring tendinopathy where rigid, less functional scar tissue has replaced naïve tendon tissue [8]. Median elastic modulus and CSA values proximal to the defect were slightly higher than at the defect site (Figure 3.5) likely because of regional tendinopathic weakness and potential inaccuracy in locating the most affected site on gross evaluation. While these findings cannot be directly extrapolated to spontaneous injury, the results described herein may serve as a basis for further model development and comparison to naturally occurring tendon injury.

Although the focus of the study was to investigate biomechanical features of surgical tendinopathic lesion induction, there is persistent interest in how this method of injury creation may relate to naturally occurring lesions. Specifically, clinical diagnostic imaging features and histopathologic analysis are of interest if this model is to be further utilized and are reported in detail in a separate investigation [27]. Briefly, surgical lesion induction in this study induced

mild (transient) metacarpal soft tissue thickening along with mild (grades 1-2) clinical lameness (assessed subjectively on the 0 to 5 American Association of Equine Practitioners scale). No horses in this study exhibited severe or long-term lameness as a result of lesion creation. Ultrasonographic evaluation revealed generalized tendon enlargement, hypoechoic core lesion formation and peritendinous soft tissue thickening (Figure 6), for which a longitudinal comparison to naturally occurring tendinopathy is presented.
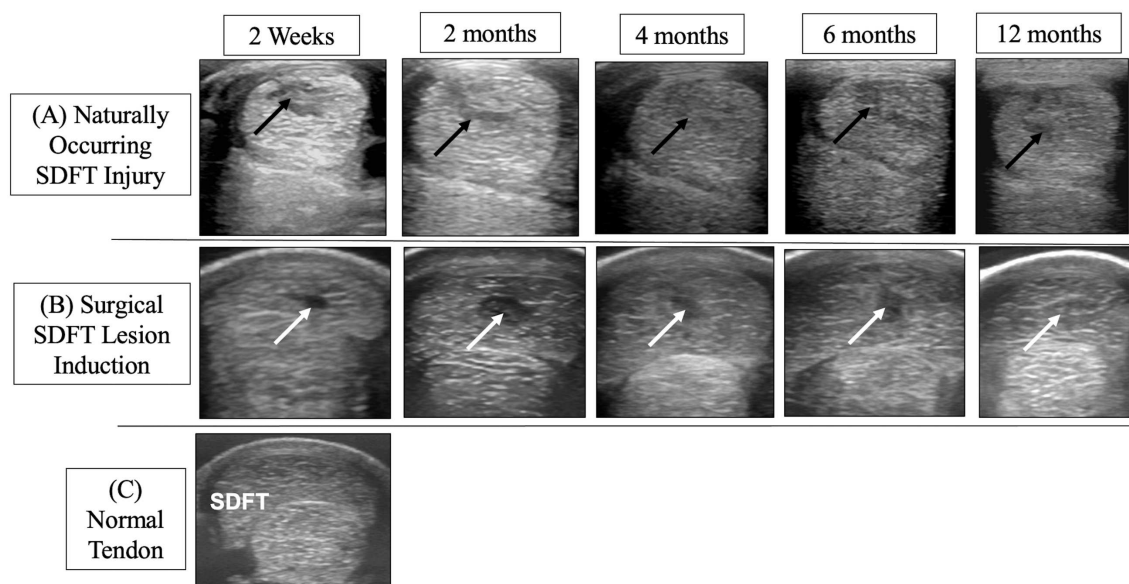
Fig 3.6. Longitudinal ultrasonographic evaluation of naturally occurring SDF tendinopathy (A) and surgically induced tendinopathy (B) at various stages post-injury (2 weeks to 12 months). Normal, uninjured tendon for comparison (C). Note the diffuse enlargement of the SDFT with dark core-like lesions (arrows) in both types of injury. In both naturally and experimentally induced disease, the hypoechoic, core lesion expands in size from 0-2 months, then gradually becomes isoechoic in the latter phases.

Histologically, naturally damaged equine SDFTs display significant disruption of tissue architecture characterized by collagen disorganization, hypercellularity, proteoglycan accumulation, and hemorrhage [41-42]. More specifically, human and murine tendinopathic changes have been further characterized by elevated levels of sulfated glycosaminoglycans [43-

45], aggrecan [43], and hyaluronan [46]. Variations of this abnormal protein deposition have also been confirmed in equine surgically induced tendinopathy lesions [40, 47]. The horses in this longitudinal study demonstrated these abnormal protein characteristics as well, most notably increased deposition of aggrecan and its glycosaminoglycan components. Additionally, toluidine blue (Tol Blue) staining revealed hypercellularity, collagen disorganization, and increased deposition of polysaccharides in tendinopathic samples (relative to normal un-injured) (Figure 3.7). More detailed histologic analysis is reported elsewhere [27].
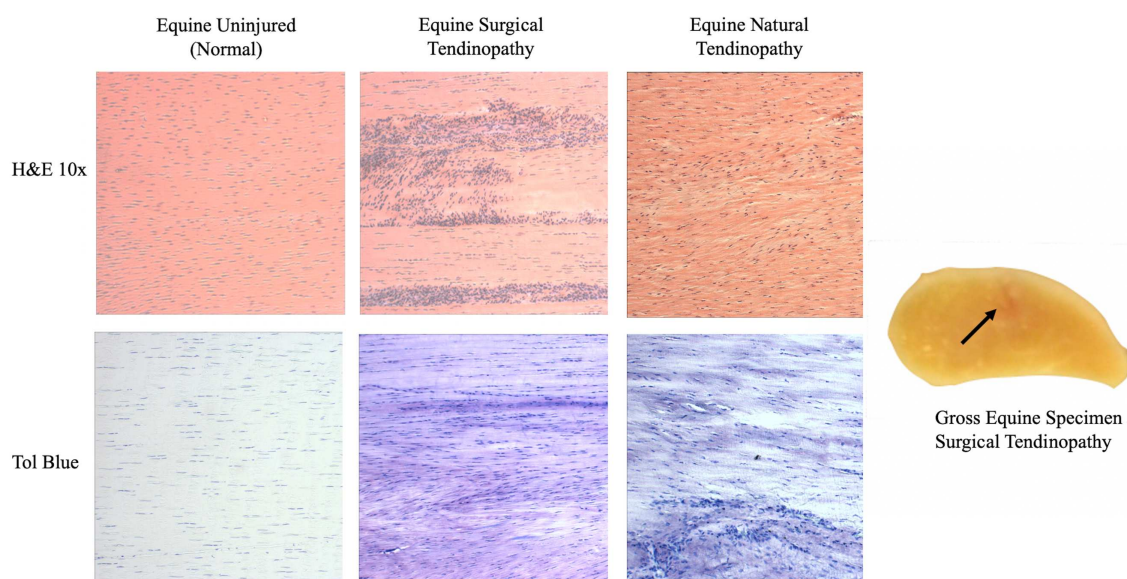
Fig 3.7. Stained sections (H&E and Toluidine Blue (Tol Blue) of the SDFT body of normal, surgically induced and naturally occurring tendinopathic equine specimens. Gross specimen corresponds to surgically induced histopathologic examples.

Study limitations the authors would like to acknowledge include the use of non-destructive biomechanical testing to avoid tissue damage. Subsequently, a low applied strain (3-4% maximum strain magnitude) was utilized, which makes it difficult to ensure that the calculated elastic modulus value was taken from the linear portion of the stress-strain curve. Previous work has demonstrated the linear range to be 3.6-10.6% [13], but caution should be

utilized when interpreting the reported elastic modulus values herein as absolute magnitude values. Additionally, the study described herein utilized a small sample population (n = 8 limbs for each group), and although our aforementioned power analysis insinuates statistical robustness, limbs for the performed power calculation were considered independent and not clustered as the statistical analysis was actually performed. Comparable studies assessing biomechanical strength of surgically induced SDFT lesions to assess treatment differences have also considered limbs independent and been powered similarly (n = 9 limbs per group) [40]. Lastly, significant exercise differences and differing study timelines obviate study design imperfections that limit direct comparisons. Despite these limitations, however, long-term biomechanical properties of tendons from a controlled, homogenous population of horses with surgically induced tendon injury consistent in size, severity and location was evaluated and compared to uninjured tendons. It is also the authors' belief that maximizing tissue usage to report reasonable comparison investigations for reader interpretation supersedes the ethical concerns that surround repeating experiments to obtain normal tissue as acknowledge by others [38]. Although imperfect in methodology, this report broadens the information available about the long-term biomechanical effects of surgical lesion creation.

In summary, equine SDFT injuries remain prevalent and difficult to treat, with several extrinsic factors limiting the ability to reliably study natural disease. Long-term biomechanical analysis of surgically induced lesions herein suggests that chronic structural weakness occurs and is similar to that described for naturally occurring disease. Future investigations directly comparing biomechanical properties of surgically induced lesions to those of natural tendon injury will be pivotal for further model consideration.

References

1. Williams, R.B., Harkins, L.S., Hammond, C.J. and Wood, J.L.N. (2001) Racehorse injuries, clinical problems and fatalities recorded on British racecourses from flat racing and National Hunt racing during 1996, 1997 and 1998. *Equine Vet. J.* **33**(5), 478-86.

2. Godwin, E.E., Young, N.J., Dudhia, J., Beamish, I.C., Smith, R.K.W. (2012) Implantation of bone-marrow derived mesenchymal stem cells demonstrates improved outcome in horses with overstrain injury of the superficial digital flexor tendon. *Equine Vet. J.* **44**, 25-32.

3. Palmer, S., Genovese, R., Longo, L., Goodman, N. and Dyson, S. (1994) Practical management of superficial digital flexor tendonitis in the performance horse. *Vet. Clin. N. Am.: Equine Pract.* **10**, 425-482.

4. Sarrafian, T.L., Case, J.T., Kinde H., Daft, B.M., Read, D.H., Moore, J.D., Uzal F.A., Stover, S.A. (2012) Fatal musculoskeletal injuries of Quarter Horse racehorses: 314 cases (1990-2007). *J. Am. Vet. Med. Assoc.* **241**(7), 935-942.

5. Lam, K.H., Parkin, T.D.H., Riggs, C.M. and Morgan, K.L. (2007) Descriptive analysis of retirement of Thoroughbred racehorses due to tendon injuries at the Hong Kong Jockey Club (1992-2004). *Equine Vet. J.* **39**(2), 143-148.

6. Singer, E.R., Barnes, J., Saxby, F., Murray, J.K. (2008) Injuries in the event horse: Training versus competition. *Vet. J.* **175**(1), 76-81.

7. Crevier-Denoix, N., Denoix, J.M., Geiger, D., Bortolussi, C., Ribot, X., Sanaa, M. (1996) Segmental variations of in vitro mechanical properties in equine superficial digital flexor tendons. *Am. J. Vet Res.* **57**(8), 1111-1117.

8. Crevier-Denoix, N., Collobert, C., Pourcelot, P., Denoix, J.M., Sanaa, M., Geiger, D., Bernard, N., Ribot, X., Bortolussi, C. and Bousseau, B. (1997) Mechanical properties of pahological equine superficial digital flexor tendons. *Equine Vet. J. Suppl.* **23**, 23-26.

9. Smith, R.K.W., Gerard, M., Dowling, B., Dart, A.J., Birch, H.L., Goodship, A.E. (2002) Correlation of cartilage oligomeric matrix protein (COMP) levels in equine tendon with mechanical properties: a proposed role for COMP in determining function-specific mechanical characteristics of locomotor tendons. *Equine Ex. Phys, Equine Vet. J.* **34**(6), 241-244.

10. Thorpe, C.T., Stark, R.J.F., Goodship, A.E., Birch, H.L. (2010) Mechanical properties of the equine superficial digital flexor tendon relate to specific collagen cross-link levels. *Equine Vet. J.* **42**(38), 538-543.

11. Gillis, C., Pool, R.R., Meagher, D.M., Stover, S.M., Reiser, K., Willits, N. (1997) Effect of maturation and aging on the histomorphometric and biochemical characteristics of equine superficial digital flexor tendon. *Am. J. Vet Res* **58**(4), 425-430.

12. Dowling, B.A., Dart, A.J., Hodgson, D.R., Rose, R.J., Walsh, W.R. (2002) Recombinant equine growth hormone does not affect the in vitro biomechanical properties of equine superficial digital flexor tendon. *Vet. Surg.* **31**, 325-330.

13. Dowling, B.A., Dart, A.J. (2005) Mechanical and functional properties of the equine superficial digital flexor tendon. *Vet. J.* **170**(2), 184-192.

14. Gerard, M.P., Hodgson, D.R., Rose, R.J. Walsh, W.R. (2005) Effects of recombinant equine growth hormone on in vitro biomechanical properties of the superficial digital flexor tendon of standardbred yearlings in training. *Vet. Surg.* **34**, 253-259.

15. Watkins, J.P., Auer, J.A., Gay, S. and Morgan, S.J. (1985) Healing of surgically created defects in the equine superficial digital flexor tendon: collagen-type transformation and tissue morphologic reorganization. *Am. J. Vet. Res.* **46**, 2091-2096.

16. Watkins, J.P., Auer, J.A., Gay, S. and Morgan, S.J. (1985) Healing of surgically created defects in the equine superficial digital flexor tendon: effects of pulsing electromagnetic field therapy on collagen-type transformation and tissue morphologic reorganization. *Am. J. Vet. Res*. **46**, 2097-2103.

17. Little, C. and Schramme, M.C. (2006) Ultrasonographic and MRI evaluation of a novel tendonitis model in the horse. *Vet. Surg*. **35**, E15.

18. Schramme, M., Hunter, S., Campbell, N., Blikslager, A. and Smith, R. (2010) A surgical tendonitis model in horses: technique, clinical, ultrasonographic and histological characterisation. *Vet. Comp. Orthop. Traumatol.* **23**(4), 231-9.

19. Cadby, J.A., David, F., van de Lest, C., Bosch, G., van Weeren, P.R., Snedeker, J.G. and van Schie, H.T.M. (2013) Further characterisation of an experimental model of tendinopathy in the horse. *Equine Vet. J.* **45**(5), 642-8.

20. Zedler, S., Schae, T., Ebling, A. and Richardson, D. (2008) Evaluation of a novel model of equine superficial digital flexor tendonitis in regenerative tendon research. *Vet. Surg.* **37**, E34.

21. Silver, I.A., Brown, P.N., Goodship, A.E., Lanyon, A.E., McCullagh, K.G., Perry, G.C. and Williams, I.F. (1983) A clinical and experimental study of tendon injury, healing and treatment in the horse. *Equine Vet. J. Suppl.* **1**, 1-43.

22. Williams, I.F. and Goodship, A.E. (1984) Studies on the pathogenesis of equine tendonitis following collagenase injury. *Res. Vet. Sci*. **36**, 326-338.

23. Watts, A.E., Nixon, A.J., Yeager, A.E. and Mohammed, H.O. (2012) A collagenase gel/physical defect model for controlled induction of superficial digital flexor tendonitis. *Equine Vet. J*. **44**(5), 576-86.

24. Dahlgren, L.A., Mohammed, H.O. and Nixon, A.J. (2005) Temporal expression of growth factors and matrix molecules in healing tendon lesions. *J. Orthop. Res*. **23**, 84-92.

25. Schnabel, L.V., Lynch, M.E., van der Meulen, M.C.H., Yeager, A.E., Kornatowski, M.A., Nixon, A.J. (2009) Mesenchymal stem cells and insulin-like growth factor-I gene-enhanced mesenchymal stem cells improve structural aspects of healing in equine flexor digitorum superficialis tendons. *J. Orthop. Res.* **27**, 1392-1398.

26. Bosch, G., van Weeren, P.R., Barneveld, A., van Schie, H.T.M. (2011) Computerised analysis of standardized ultrasonographic images to monitor the repair of surgically created core lesions in equine superficial digital flexor tendons following treatment with intratendinous platelet rich plasma or placebo. *The Vet. J*. **87**, 92-98.

27. Johnson, S.J., Valdes-Martinez, A., Turk, P.J., McIlwraith C.W., Barrett, M.F., McGilvray, K.C., Frisbie, D.D. (2021) Longitudinal tendon healing assessed with mult-modality advance dimaging and tissue analysis. *Equine Vet J* **00**:1-16.

28. McGilvray, K.C., Santoni, B.G., Turner, A.S., Bogdansky, S., Wheeler, D.L., Puttlitz, C.M. (2010) Effects of ^{60}Co gamma radiation dose on initial structural biomechanical properties of ovine bone-patellar tendon-bone allografts. *Cell Tissue Bank.* **12**, 89-98.

29. Choi, R.K., Smith, M.M., Martin, J.H., Clarke, J.L., Dart, A.J., Little, C.B., Clarke, E.C. (2016) Chondroitin sulphate glycosaminoglycans contribute to widespread inferior biomechanics in tendon after focal injury. *J. Biomech.* **49**, 2694-2701.

30. Bosch, G., Lameris, M.C., van den Belt, J.M., Barneveld, A., van Weeren, P.R. (2010) The propagation of induced tendon lesions in the equine superficial digital flexor tendon: an ex vivo study. *Eq. Vet. J.* **42**(5), 407-411.

31. Birch, H.L., McLaughlin L., Smith, R.K.W., Goodship, A.E. (1999) Treadmill exercise-induced tendon hypertrophy: assessment of tendons with different mechanical functions. *Equine Ex. Phys.* **30**, 222-226.

32. Buchanan, C.I., Marsh, R.L. (2002) Effects of exercise on the biomechanical, biochemical and structural properties of tendons. *Compar. Biochem. Phys*. **133**, 1101-1107.

33. Moffat, P.A., Firth, E.C., Rogers, C.W., Smith, R.K.W., Barneveld, A., Goodship, A.E., Kawcak, C.E., McIlwraith, C.W., van Weeren, P.R. (2008) The influence of exercise during growth on ultrasonographic parameters of the superficial digital flexor tendon of young Thoroughbred horses. *Equine Vet. J.* **40**(2), 136-140.

34. Gillis, C.L., Meagher, D.M., Pool, R.R., Stover, S.M., Craychee, T.J. and Willits, N. (1993) Ultrasonographically detected changes in equine superficial digital flexor tendons during the first months of race training. *Am. J. vet. Res.* **54**, 1797-1802.

35. Cherdchutham, W., Meershoek, L.S., van Weeren, P.R. and Barneveld, A. (2001) Effects of exercise on biomechanical properties of the superficial digital flexor tendon in foals. *Am. J. vet. Res.* **62**, 1859-1864.

36. Patterson, J.C., Wilson, A.M., Firth, E.C., Parry, A.D., Goodship, A.E. (1997) Comparison of collagen fibril populations in the superficial digital flexor tendons of exercise and nonexercised Thoroughbreds. *Equine Vet. J.* **29**(2), 121-125.

37. Patterson, J.C., Wilson, A.M., Firth, E.C., Parry, A.D., Goodship, A.E. (1998) Exercise-related alterations in crimp morphology in the central regions of superficial digital flexor tendons from young Thoroughbreds: a controlled study. *Equine Vet. J.* **30**(1), 61-64.

38. O'Brien, C., Marr, N., Thorpe, C. (2020) Microdamage in the equine superficial digital flexor tendon. *Equine Vet. J.* **00**, 1-14.

39. Patterson-Kane, J.C., Firth, E.C., Parry, D.A., Wilson, A.M., Goodship, A.E. (1997) Effects of training on collagen fibril populations in the suspensory ligament and deep digital flexor tendon of young Thoroughbreds. *Am. J. Vet Res.* **59**(1), 64-68.

40. Geburek, F., Roggel, F., van Schie, H.T.M., Beineke, A., Estrada, R., Weber, K, Hellige, M., Rohn, K., Jagodzinksi, M., Welke, B., Hurschler, C., Conrad, S., Skutella, T., van de Lest, C., van Weeren, R., Stadler, P.M. (2017) Effect of single intralesional treatment of surgically induced equine superficial digital flexor tendon core lesions with adipose-derived mesenchymal stromal cells: a controlled experimental trial. *Stem Cell Res. Ther.* **8**(129), 1-21.

41. Smith, R., Little, C., Frisbie, D., Kjaer, M. and van Weeren, R. (2014) Advances in the understanding of tendinopathies: a report on the Second Havemeyer Workshop on equine tendon disease. *Equine Vet. J.* **46**(1), 4-9.

42. Goodship, A.E., Birch, H.L. and Wilson, A.M. (1994) The pathobiology and repair of tendon and ligament injury. *Vet. Clin. North Am. Equine Pract.* **10**(2), 323-49.

43. Bell, R., Li, J., Gorski, D.J., Bartels, A.K., Shewman, E.F., Wysocki, R.W., Cole, B.J., Bach, B.R., Mikecz, K., Sandy, J.D., Plaas, A.H. and Wang, V.M. (2013) Controlled treadmill exercise eliminates chondroid deposits and restores tensile properties in a new murine tendinopathy model. *J. Biomech.* **46**(3), 498-505.

44. Jarvinen, M., Kannus, P., Jarvinen, T.L.N., Kvist, M., Leadbetter and W. (1997) Histopathological findings in chronic tendon disorders. *Scand. J. Med. Sci. Sports*. **7**(2), 86-95.

45. Kannus, P., and Jozsa, L. (1991) Histopathological changes preceding spontaneous rupture of a tendon. A controlled study of 891 patients. *J. Bone Joint Surg. Am.***73**, 1507-1525.

46. Trella, K.J., Li, J., Galante, J., Wysocki, R., Sandy, J.D., Plaas, A. and Wang, V.M. (2015) Treadmill Running Mitigates the Post-Injury Hypoxic Response in a Murine Model of Tendinopathy. *Trans. Biom. Eng. Soc*. Tampa, FL.

47. Jacobson, E., Dart, A.J., Mondori, T., Horadogoda, N., Jeffcott L.B., Little, C.B., Smith, M.M. (2015) Focal experimental injury leads to widespread gene expression and histologic changes in equine flexor tendons. *Plos* **10**, 1-25.

CHAPTER 4: Tissue Predictability of Elastography is Low in Collagenase Induced Deep Digital Flexor Tendinopathy[3]

4.1 Overview

Elastography is an emerging imaging modality to diagnose and monitor tendon injury in horses, but its ability to differentiate tissue deformability characteristics associated with treatment and biochemical properties using a prospective, experimental study design is unknown. Study objectives included: 1) To investigate differences in glycosaminoglycan, DNA and soluble collagen levels in mesenchymal stem cell (MSC) treated limbs compared to untreated control limbs utilizing a collagenase model of tendinopathy; 2) Compare elastographic features between treatment groups; 3) Determine tissue-level predictive capabilities of elastography in relation to biochemical outcomes. Bone marrow was collected for MSC culture and expansion. Tendinopathy of both forelimb deep digital flexor tendons (DDFTs) was induced with collagenase under ultrasonographic guidance. One randomly assigned limb was treated with intra-lesional MSC injection with the opposite limb serving as an untreated control. Horses were placed into a controlled exercise program with elastographic evaluations performed baseline (0) and 14, 60, 90, and 214 days post treatment. Post-mortem biochemical analysis was performed. MSC-treated

---

[3] This is the peer reviewed version of the following article: Johnson SA, Biscoe EW, Eilertson KE, Lutter JD, Schneider RK, Roberts GD, Cary JA, Frisbie DD. Tissue predictability of elastography is low in collagenase induced deep digital flexor tendinopathy. *Vet Radiol Ultrasound.* 2021;1-13, which has been published in final form at https://doi.org/10.1111/vru.13026. This article may be used for non-commercial purposes in accordance with Wiley Terms and Conditions for Use of Self-Archived Versions. This article may not be enhanced, enriched or otherwise transformed into a derivative work, without express permission from Wiley or by statutory rights under applicable legislation. Copyright notices must not be removed, obscured or modified. The article must be linked to Wiley's version of record on Wiley Online Library and any embedding, framing or otherwise making available the article or pages thereof by third parties from platforms, services and websites other than Wiley Online Library must be prohibited.

limbs demonstrated statistically significantly less (42%) glycosaminoglycan ($P = 0.006$). Statistically significant differences in elastographic region of interest (ROI) percent hardness, ROI color histogram and subjective lesion stiffness were appreciated between treatment groups at various study time points. Elastographic outcome parameters were weak predictors of biochemical tissue analysis, with all R^2 values ≤ 0.50. Within this range of differences in glycosaminoglycan content between treatment groups, elastography outcomes did not predict biochemical differences. Tissue-specific differences between DDFTs treated with MSCs compared to untreated controls were apparent biochemically, but not predicted by elastography.

4.2 Introduction

Elastography is an emerging imaging modality to diagnose and monitor tendon injuries in horses. Elastography is utilized to estimate tissue stiffness properties by comparing echo signals before and after manual compression of the tissues with the ultrasound transducer [1]. Through these means, elastography has been promoted as a way to assess mechanical properties longitudinally to further assess stage and quality of healing [2,3]. The feasibility, reproducibility and repeatability of elastography of metacarpal tendons in sound horses has been previously reported with similar stiffness appreciated between the superficial digital flexor tendon (SDFT) and the deep digital flexor tendon (DDFT) [1]. Elastographic appearance of naturally occurring tendon and ligament injuries within the equine metacarpus have also been compared to grey-scale ultrasound and magnetic resonance imaging (MRI), for which significant correlations were appreciated [2]. While these initial reports are promising, equine elastographic investigators have noted that longitudinal studies and the use of tendinopathic models with tissue analysis are needed to ultimately determine the accuracy of elastography [1].

Deep digital flexor tendon injuries within the digital sheath (intra-thecal) are a common source of distal limb lameness in athletic horses, with 96% of those configured as core lesions [4]. Prognosis for athletic soundness in horses with distal limb DDFT injuries is considered guarded to poor, with only 41% of horses with core lesions returning to some level of activity [5]. Experimental replication of spontaneous DDFT injury is difficult, but collagenase (enzymatic) models have demonstrated characteristics consistent with clinical disease [6], and the intrathecal DDFT within the pastern region is anatomically accessible. Tendons treated with mesenchymal stem cells (MSCs) have consistently demonstrated significantly improved healing at the clinical (re-injury rate) and tissue quality level in both naturally occurring disease [7,8] and various models of tendinopathy [9,10]. Intra-lesional MSC therapy has specifically been shown to reduce deposition of the biomechanically inferior scar tissue protein glycosaminoglycan in naturally occurring tendinopathy [7], making this an attractive therapeutic mechanism for improved tendon healing [7,11-12]. Their strategic use alongside professional rehabilitation programs represents one of the most currently utilized avenues to augment recovery and reduce re-injury rate following significant tendinopathy [7]. An imaging modality such as elastography that could be used to non-invasively assess tissue stiffness properties following the incorporation of MSCs and graduated controlled exercise would be valuable for the equine athlete, but its use to assess the intrathecal equine DDFT following treatment in experimental tendinopathy has not been evaluated.

The objectives of this study were three-fold: 1) To investigate differences in biochemical tissue analysis for glycosaminoglycan (GAG), DNA and soluble collagen levels in MSC-treated limbs compared to untreated control limbs utilizing a collagenase model of deep digital flexor (DDF) tendinopathy; 2) To compare elastographic features of collagenase-induced DDFT injuries treated with intra-lesional MSCs compared to untreated control limbs; 3) To determine tissue-level

predictive capabilities of elastographic measures in relation to biochemical outcomes. It was hypothesized that there would be biochemical and elastographic differences between MSC-treated and untreated control limbs, and that elastography would be correlated to these biochemical changes related to treatment group.

4.3 Materials and Methods

This investigation was a prospective, experimental study. All study methods were conducted in compliance with Washington State University's Institutional Animal Care and Use Committee (IACUC) standards. The experimental sample size (six limbs) was calculated using GPower Version 3.1.1 (GPower, Brunsbuttel Germany). Values from a published study investigating GAG content of stem cell intra-lesional therapy over six months were used for power calculation [7]. Specifically, an a priori power analysis was conducted. Using a two-sample t-test with expected group mean difference of 18, this power analysis resulted in an effect size of 2.571 and a power of 0.95 using a 95% confidence interval and a standard deviation of 8 μg/mg GAG content between groups.

Experimental Animals:

Six adult horses purchased from an outside vendor were enrolled. The horses were of various breeds (two American Quarter Horses, one American Paint Horse and three Arabians), ages two to eight years, and showed no clinical or MRI evidence of current or previous forelimb DDFT injury based on assessment by a board-certified veterinary surgeon (DACVS) and resident in equine surgery.

Tendinopathy Induction & Post-Operative Care:

All horses were placed under general anesthesia and deep digital flexor (DDF) tendinopathy was induced using ultrasound guidance in a manner similar to that previously described by a board-certified veterinary surgeon (DACVS) and resident in equine surgery [13]. Briefly, 500 units of filter-sterilized bacterial collagenase (c0130 Sigma Aldrich Co., St. Louis, MO) diluted in 0.1mL of sterile water was injected into the medial DDFT lobes of both forelimbs at the level of the distal one-third of the proximal phalanx. Following injections, both forelimbs were bandaged routinely for 24 hours and all horses were administered two grams of phenylbutazone (4.4 mg/kg) orally every 24 hours for three days.

Following collagenase injection, horses were housed in stalls (4m x 4m) for 28 days, transitioned to 9m x 9m paddocks until 90 days, then housed in a pasture until day 214. Horses were incrementally hand-walked twice daily beginning 14 days after tendinopathy induction (5 minutes twice/day for two weeks, then 10 minutes twice/day for four weeks, lastly 20 minutes twice/day for four weeks). Hand-walking was discontinued when pasture turnout was commenced.

Mesenchymal Stem Cell Harvest, Processing & Injection:

One day prior to surgical DDFT lesion induction, bone marrow was harvested from each horse by a board-certified veterinary surgeon (DACVS) and resident in equine surgery with subsequent processing performed at Advanced Regenerative Therapies (Fort Collins, CO). Colony-forming cultures were developed using low glucose Dulbecco's Modified Eagle's Medium (DMEM, Thermo Fisher Scientific, Waltham, MA) with 10% fetal bovine serum (FBS, Atlas Biologicals, Fort Collins, CO). Mesenchymal stem cell colony-forming units were reseeded at 1.5×10^4 cells/cm^2 in minimum essential media (AMEM, Thermo-Fisher Scientific,

Waltham, MA) with 10% FBS and 2 ng/ml fibroblastic growth factor-2 (FGF2, Peprotech,

Rocky Hill, NJ), then culture-expanded through eight population doublings to ~80% confluence.

Culture-expanded MSCs were cryopreserved in 1mL of 95% autologous serum plus 5% dimethyl

sulfoxide.

Forelimbs in this study were then randomized into two treatment groups via coin flip.

One randomly assigned forelimb (n = 6 forelimbs) received an intra-lesional MSC injection,

while the opposite forelimb of each horse served as an untreated control (n = 6 forelimbs).

Specifically, $10x10^6$ MSCs that were suspended in 1mL of 95% autologous serum plus 5%

dimethyl sulfoxide, were thawed by gently swirling each vial in a 36°C water bath, then injected

as 0.2mL aliquots at five sites approximately every 10mm under ultrasound guidance 14 days

following lesion induction by a board-certified veterinary surgeon (DACVS) and resident in

equine surgery. Following MSC injection, the injected forelimbs were bandaged routinely for 24

hours. Limbs in Group 2 (n = 6 forelimbs, controls) did not receive any form of intra-lesional

injection.

Elastographic Image Acquisition:

Elastographic examination of the DDFT within the pastern region of all horses was

performed by two operators blinded to treatment group assignments; a board-certified veterinary

radiologist and a radiology resident experienced in equine ultrasound at all imaging time points

(Figure 4.1) using a 12.5 MHz 38mm linear array transducer (Biosound MyLab 70, Esaote North

America Inc., Indianapolis, IN) in a weight-bearing position as previously described [1,2].

Baseline elastographic evaluations on day 0 were performed prior to lesion induction. Hair of the

distal forelimb was clipped along the palmar aspect and the skin cleaned in standard fashion

prior to each elastographic evaluation. All forelimb DDFTs were examined in both transverse

and longitudinal planes utilizing a standoff pad at three levels using a palmar approach (3cm proximal to the proximal interphalangeal (PIP) joint, at the level of the PIP joint and 2cm distal to the PIP joint) by each observer. All elastographic images were obtained by applying gentle rhythmic pressure with the ultrasound probe in each area of interest [1]. Three separate images (replicates) in each scan plane at all three levels were recorded by each observer (n = 18 images per limb, per observer, per evaluation time point) when adequate, persistent displacement was achieved as indicated by the elastographic software (ElaXto, Biosound Easote Inc. Indianapolis, IN). All examinations were performed at the same time by each sonographer to ensure that each image was obtained at the same location under the same setting.
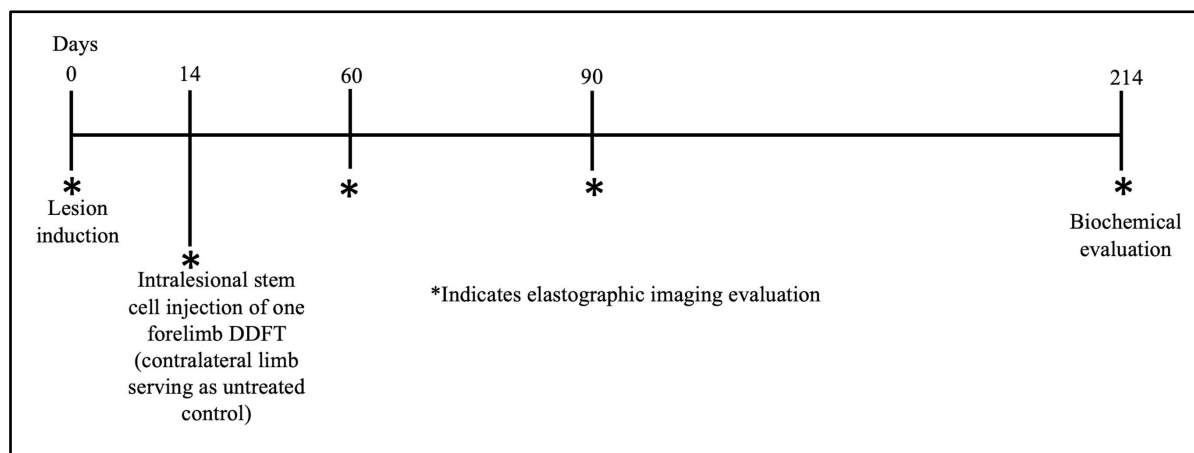
Fig 4.1. Experimental timeline, beginning with lesion induction (day 0) and ending with study termination 214 days later. Baseline elastographic imaging evaluations were performed prior to lesion induction (day 0). Serial elastographic evaluations were performed at four time points post lesion creation (days 14, 60, 90 & 214), followed by end point data collection of biochemical outcome parameters.

Elastographic Image Analysis:

Elastographic image analysis was performed on a diagnostic imaging viewing station monitor. Images with a high proportion of artifact or artifact superimposed over the region of interest were not included for subsequent evaluation. All images were assessed qualitatively and

quantitatively by a radiology resident experienced in equine ultrasound blinded to treatment

groups in independent fashion. Categorical qualitative analysis considered two measured

outcome parameters using a modified stiffness color scale of 1 to 4 (Table 4.1) for both the entire

DDF tendon (subjective stiffness tendon) and the lesion itself (subjective stiffness lesion) [1].

Table 4.1: Table summarizing qualitative grading scale utilized to assess the subjective stiffness
of both the lesion and entire deep digital flexor tendon (subjective stiffness tendon, subjective
stiffness lesion, respectively). This grading scale was adapted from that previously utilized by
Lustgarten et al 2013.

Grade	Color	Stiffness
1	>50% red	Mostly hard
1.5	50:50 red:yellow	Mostly hard
2.0	Mostly yellow or mostly red and yellow with small areas of violet	Intermediate
2.5	Mostly yellow with small areas of violet	Intermediate
3.0	Cyan, green and violet or 50:50 violet:green	Areas of softness
3.5	Mostly cyan and green	Areas of softness
4.0	Mostly green	Mostly soft

Quantitative analysis considered three measured outcome parameters: 1) region of

interest (ROI) strain ratio as an estimate of tissue stiffness [1], 2) ROI percent hardness, and 3)

ROI color histogram. Regions of interest were manually drawn over designated areas within the

elastography box and a designated algorithm optimized to differentiate the continuum of colors

and number of each pixel of each color within the image was utilized as previously described [1].

Specifically, the ROI strain ratio represented the color continuum differences appreciated

between the ROI of the lateral DDFT (normal) lobe compared to that of the sonographically

visible lesion in the medial lobe, with a value >1 indicating the medial (injured) lobe to be softer

than the lateral (uninjured) lobe, value <1 indicating the medial lobe to be stiffer than the lateral

lobe, and value = 1 indicating equivalent stiffness between the two DDFT lobes (Figure 4.2A).

The ROI percent hardness was calculated by the elastographic software and reflected the percentage of pixels within the manually drawn ROI that were within the hardest 15% of the designated color scale (Figure 4.2B), with a higher percentage indicating the presence of stiff tissue and a lower percentage consistent with softer tissue. The ROI color histogram was also calculated by the elastographic software and assigned a number from 0 (most firm, red) to 100 (softest, green) for the manually drawn ROI over each lesion (Figure 4.2C). Color means and standard deviations within the lesion ROI were subsequently recorded. The lesion ROI drawn for the strain ratio was the same as the ROI utilized for the color histogram.
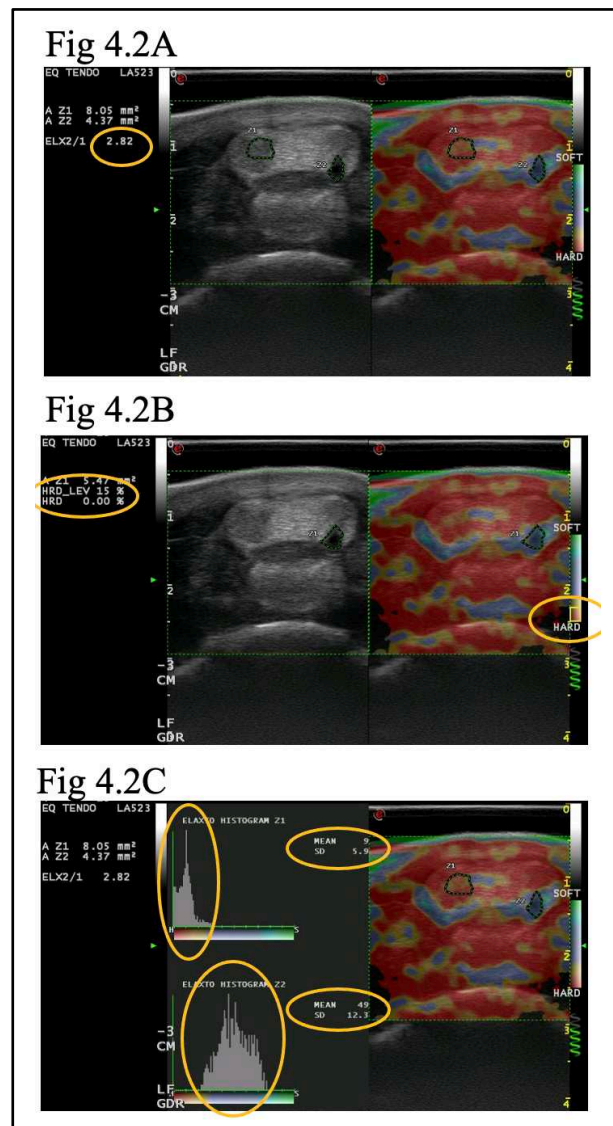
Fig 4.2. Quantitative elastographic analysis included measurement of region of interest (ROI) strain ratio (4.2A), ROI percent hardness (4.2B) and ROI color histogram (4.2C) with lateral to the left in each image. The ROI strain ratio represented tissue stiffness differences between the ROI of the lateral DDFT (normal) lobe compared to that of the sonographically visible lesion in the medial lobe, with a value >1 indicating the medial (injured) lobe to be softer than the lateral (uninjured) lobe, value <1 indicating the medial lobe to be stiffer than the lateral lobe, and value = 1 indicating equivalent stiffness between the two DDFT lobes. The ROI percent hardness measured the percentage of pixels within the manually drawn ROI that were within the hardest 15% of the designated color scale, with a higher percentage indicating the presence of stiff tissue and a lower percentage consistent with softer tissue. The ROI color histogram assigned a number from 0 (most firm, red) to 100 (softest, green) to the manually drawn ROI over each lesion (Figure 4.2C).

Tissue Harvest:

Following the 214 day imaging evaluation, all horses were humanely euthanized according to IACUC standards. Within one hour of euthanasia, all limbs underwent MRI evaluation with a 1.0 Tesla MRI Unit (Gyroscan, Philips Healthcare, Best, Netherlands) performed by a board-certified veterinary radiologist (Diplomat of the American College of Veterinary Radiologists, DACVR) and a resident in equine radiology. Sequences obtained included proton density turbo spin echo (PD TSE), T2-weighted TSE (T2 TSE) and short τ inversion recovery (STIR) with specific acquisition parameters listed in Table 4.2. All images were acquired from the level of the proximal sesamoid bones including the metacarpophalangeal joint distally using a 14-15 cm field of view. All magnetic resonance (MR) images were evaluated by a board-certified veterinary radiologist (DACVR) and a resident in equine surgery to identify the most affected site of DDFT injury. This location and its distance relative to the metacarpophalangeal joint at the most distal aspect of the third metacarpal bone (MC3) with the dorsal cortices of MC3, the proximal phalanx, middle phalanx and distal phalanx aligned was then recorded and used as the center of evaluation for subsequent biochemical analysis (Supplementary Figure 9.4). Following imaging evaluation, a longitudinal incision was made to

remove the skin and subcutaneous tissue overlying the forelimb DDFTs from the level of the

fetlock to the coronet band. All DDFTs were visually evaluated, gross observations were

recorded and limbs were photographed. Following evaluation, a suture was placed by a resident

in equine surgery at the site of the most injured area of the DDFT based on advanced imaging

evaluation and distance relative to the metacarpophalangeal joint using the previously described

anatomic landmarks.

The forelimbs of all horses were then disarticulated at the level of the middle carpal joint

and the DDFTs were carefully harvested from the fetlock region to the level of the coronet band

using sharp dissection and Brown-Adson tissue forceps. Care was taken to minimize tissue

handling when possible. Tendon samples were then immediately processed for biochemical

analysis.

Table 4.2 Table summarizing the magnetic resonance imaging (MRI) sequence parameters used
for imaging of the equine pastern region with the 1.0 Tesla at Washington State University.

Image Plane	Sequence	TR (ms)	TE (ms)	FOV (cm)	RFOV (cm)	Matrix	Slice Number	Slice Thickness (mm)	Gap (mm)
Transverse	T2 TSE	2116	100	15	10.5	256x512	30	4	0.5
Transverse	PD TSE	2116	11	15	10.5	256x512	30	4	0.5
Transverse	STIR	1725	35	15	10.5	192x256	30	3.5	1
Sagittal	T2 TSE	3395	110	14	10	256x512	22	4	0.5
Sagittal	PD TSE	3395	14	14	10	256x512	22	4	0.5
Sagittal	STIR	1500	35	14	10	192x256	22	3.5	0.5

TSE = turbo spin echo; T2 = T2 weighted sequence; PD = proton density; STIR = short tau
inversion recovery; TR = radiofrequency pulse repetition time; TE = echo sampling time; FOV =
field of view; RFOV = rectangular field of view; ms = microseconds; cm = centimeter; mm =
millimeter.

Specimen Preparation & Biochemical Evaluation:

Following tissue harvest, the site of the previously placed suture (central portion of the lesion) was transected and sections of the affected portion of the tendon were divided into sections for biochemical examination. Samples were covered with Optimal Cutting Temperature Compound (American Master*Tech Scientific Incorporated, Lodi, CA), snap-frozen in liquid nitrogen and then stored at -80°C until processing.

Glycosaminoglycan and DNA were quantified in frozen tendon specimens from two tissue sections by lyophilizing the specimen and digesting with 8U papain/mL using the protocol previously described [14]. A spectrophotometric dimethylmethylene blue dye binding (DMMB) assay quantified the GAG content following digestion for 18 hours at 60°C in .5% papain. DNA quantification was assessed using the Hoescht assay as previously described [15]. All values were normalized to original tissue dry weight and DNA content.

Soluble collagen levels were measured using the Sirius red dye-binding method (Sircol Collagen Assay, Biocolor Ltd., Carrickfergus, United Kingdom). Pulverized, lyophilized tissue samples were weighed, re-suspended in lysis buffer containing detergent, protease inhibitors (Complete Mini, Roche Molecular Biochemicals, Sigma Aldrich Co., Saint Louis, MO), and glycerol, homogenized, and centrifuged at 15,000 x g for 10 minutes. The pellet was acid-pepsin digested at 4°C overnight with stirring, centrifuged at 30,000 x g for 45 minutes, and the supernatant was utilized for the soluble collagen assay. All values were normalized to original tissue dry weight. All tissue analysis was performed by a board-certified veterinary surgeon (DACVS) with advanced training and experience in biochemical processing and assessment. This author was blinded to treatment groups for all tissue analysis.

Statistical analyses:

All statistical analysis was performed by an experienced statistician and a board-certified equine sports medicine specialist (Diplomat of the American College of Veterinary Sports Medicine and Rehabilitation, DACVSMR) under direct statistical supervision using the software package R (version 4.0.3, R-project®, R Foundation for Statistical Computing Vienna, Austria). Statistical analysis was performed by utilizing three approaches pertinent to evaluate the outlined study objectives of: 1) Biochemical differences between MSC-treated limbs and control limbs; 2) Elastographic feature differences between MSC-treated limbs and control limbs; 3) Longitudinal elastographic outcome parameters compared to biochemical tissue analysis. Statistical significance was considered $P < 0.05$ for all analysis.

To investigate the relationships between treatment condition and response variables of biochemical tissue analysis (GAG/tissue, DNA/tissue, GAG/DNA and soluble collagen), a linear mixed model was fit. To account for the design of data collection, the model included fixed effects of treatment and random effect of horse. Diagnostic plots were used to assess assumptions of equal variance and normality. Based on these plots, assumptions were met.

To investigate the relationships between treatment condition and elastographic outcomes (subjective stiffness tendon, subjective stiffness lesion, ROI strain ratio, ROI percent hardness and ROI color histogram), a linear mixed model at each evaluation time point was fit. To account for the design of data collection, the model included fixed effects of scan plane, scan level and random effects of horse and imager. Diagnostic plots were used to assess assumptions of equal variance and normality. Based on these plots, ROI strain ratio and ROI color histogram were square-root transformed. Following transformation, assumptions were met.

To investigate the predictive capability of a specific elastographic outcome at an individual time point with respect to the end-point biochemical analysis, a latent variable multilevel mixed model was utilized [16]. First, a multilevel mixed model was used to generate appropriately adjusted group level average values (the best linear unbiased estimates, or BLUPs) as estimates of the latent elastographic outcome at the horse-limb level [16]. This mixed model approach allowed us to appropriately pool values for each elastographic measurement across the two imagers, two imaging planes and all scan levels for our estimate of the latent horse-limb level elastographic outcome (the 36 measurements on each limb were summarized into one number). Next, these pooled elastographic estimates were used as predictors in a linear regression with the biochemical tissue analysis outcome as the response. The predictive ability of the elastographic outcomes was summarized using the coefficient of determination, R^2. For each elastographic outcome and each biochemical tissue analysis outcome, a total of five models was fit, one for each evaluation time point.

4.4 Results

Biochemical differences between MSC-treated limbs and control limbs

Statistically significant differences in GAG/DNA were found between treatment groups, with MSC-treated limbs demonstrating overall less GAG/DNA ($P = 0.006$, 95% confidence interval (95%CI) = -4.9 - -1.8). No statistically significant differences in the amount of GAG/tissue ($P = 0.12$, 95%CI = -7.75 - 0.49), DNA/tissue ($P = 0.19$, 95%CI = -.22 - 1.45), or soluble collagen between treatment groups were found ($P = 0.91$, 95%CI = -135.9 - 120.48) (Figure 4.3).
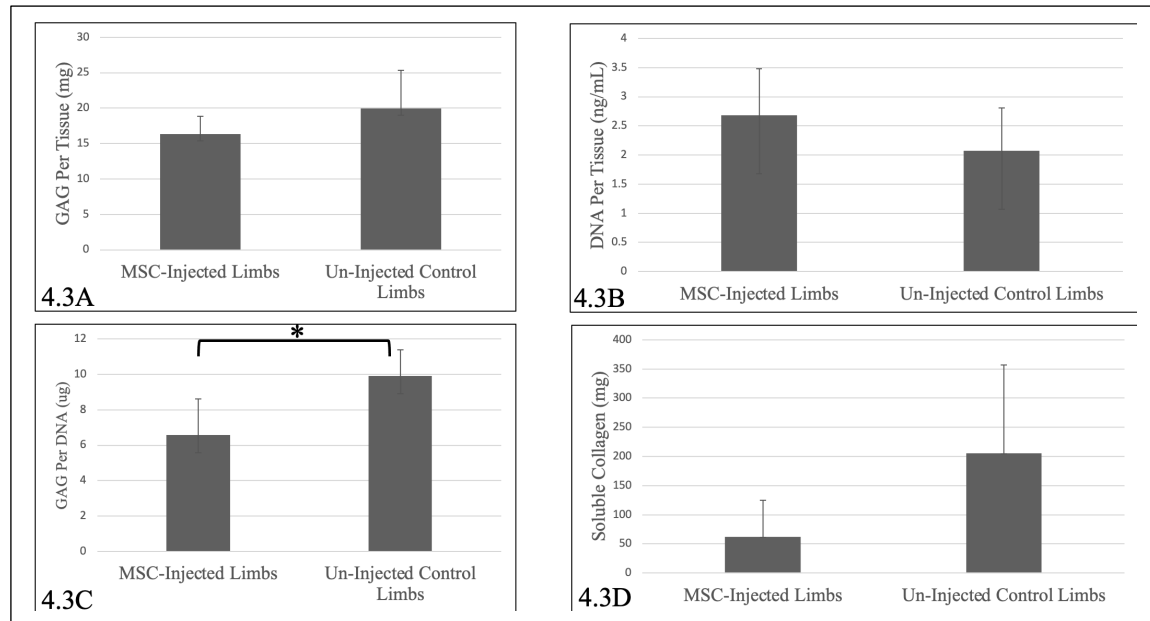
Fig 4.3. Mean biochemical outcome measures of glycosaminoglycan (GAG) per tissue (4.3A), DNA per tissue (4.3B), GAG per DNA (4.3C) and soluble collagen (4.3D) in deep digital flexor tendons (DDFTs) treated with mesenchymal stem cells (MSCs) compared to un-injected controls. Limbs injected with mesenchymal stem cells (MSCs) demonstrated significantly less GAG per DNA based on the results of a linear mixed model (* indicates $P < 0.05$). Data means are shown with standard deviation bars.

Elastographic feature differences between MSC-treated limbs and control limbs

After accounting for horse, imager, scan plane and scan level, no statistically significant association between ROI strain ratio and treatment was found at any evaluation time point (all linear mixed model relationships are listed in Table 4.3). All limbs demonstrated similar strain ratios of approximately 1.0 at day 0 with mean and standard deviation values for MSC-injected and untreated control limbs (pre-lesion induction) found to be 1.07 +/-0.33 and 1.05 +/- 0.30, respectively. Mean and standard deviation values for subsequent strain ratios on study days 14, 60, 90 and 214 were 2.17 +/-1.68, 1.59 +/-1.20, 1.53 +/-1.39, 1.38 +/-0.83 for MSC-injected limbs, respectively. Similarly, untreated control limbs' mean and standard deviation strain ratios on the corresponding study days were found to be 2.22 +/-1.63, 1.59 +/-0.97, 1.47 +/-0.72, 1.34 +/-0.62, respectively. Elastographically obtained ROI strain ratio values at all study time points

for both treatment groups are graphically depicted in Figure 4.4A with representative

elastographic images demonstrated in Figure 4.5.

Table 4.3 Summary of linear mixed model statistical relationships between all elastographic outcome measures and treatment (MSC-injected limbs vs. untreated control limbs) at all study time points.

Linear Mixed Model Relationships Between Elastographic Outcomes and Treatment at All Evaluated Study Time Points				
	Study Day	Estimate	Standard Error	*P* Value
Region of Interest (ROI) Strain Ratio	0	0.01	0.01	0.36
	14	-0.04	0.05	0.45
	60	-0.05	0.04	0.25
	90	-0.07	0.04	0.09
	214	-0.03	0.03	0.34
ROI Percent Hardness	0	-0.04	0.02	0.02*
	14	0.02	0.03	0.47
	60	0.02	0.03	0.50
	90	-0.10	0.02	<0.001***
	214	-0.02	0.02	0.4
ROI Color Histogram	0	0.32	0.11	0.005**
	14	-0.17	0.19	0.39
	60	0.46	0.16	0.005**
	90	-0.23	0.16	0.15
	214	-0.31	0.13	0.02*
Subjective Stiffness Tendon	0	0.07	0.04	0.08
	14	0.08	0.04	0.08
	60	0.03	0.05	0.45
	90	-0.03	0.04	0.38
	214	-0.05	0.04	0.23
Subjective Stiffness Lesion	0	-0.05	0.04	0.23
	14	-0.05	0.08	0.56
	60	-0.14	0.07	0.054
	90	-0.14	0.07	0.054
	214	-0.21	0.05	<0.001***

Statistically significant differences in ROI percent hardness between treatment groups

were appreciated on study days 0 (*P* = 0.02, 95%CI = -0.083 - -.007) and 90 (*P* < 0.001, 95%CI

= -0.15 - -0.05). Mean and standard deviation ROI percent hardness values for MSC-injected

limbs on sequential study days were found to be: 0.67 +/-0.26 (day 0), 0.36 +/-0.34 (day 14),

0.48 +/-0.32 (day 60), 0.50 +/-0.31 (day 90) and 0.60 +/-0.30 (day 214). These values were in

contrast to mean and standard deviation values for untreated control limbs across all study time

points of: 0.72 +/-0.23 (day 0), 0.34 +/-0.34 (day 14), 0.46 +/-0.32 (day 60), 0.60 +/-0.31 (day

90) and 0.62 +/-0.29 (day 214). Elastographically obtained ROI percent hardness values at all

study time points for both treatment groups are graphically depicted in Figure 4.4B.

Region of Interest (ROI) Strain Ratio at All Study Time Points

Fig 4.4A. Graphical representation of elastographically obtained region of interest (ROI) strain
ratios at all study time points in both mesenchymal stem cell (MSC)-injected and un-injected
control limbs. No significant association between ROI strain ratio and treatment was found at
any evaluation time point with all limbs demonstrating decreasing strain ratios over time.

Statistically significant differences in ROI color histogram between treatment groups

were appreciated on study days 0 ($P = 0.005$, 95%CI = 0.10 - 0.54) and 214 ($P < 0.001$, 95%CI =

-0.57 - -0.06). Mean and standard deviation ROI color histogram values for MSC-injected limbs

on sequential study days were found to be: 14.5 +/-12.8 (day 0), 27.7 +/-22.5 (day 14), 17.8 +/-

15.5 (day 60), 16.3 +/-13.8 (day 90) and 13.4 +/-10.0 (day 214). These values were in contrast to

mean and standard deviation values for untreated control limbs across all study time points of:

11.5 +/-9.18 (day 0), 28.8 +/-22.4 (day 14), 20.8 +/-15.2 (day 60), 16.9 +/-14.4 (day 90) and 15.7

+/-11.5 (day 214). Elastographically obtained ROI color histogram values at all study time points

for both treatment groups are graphically depicted in Figure 4.4C.
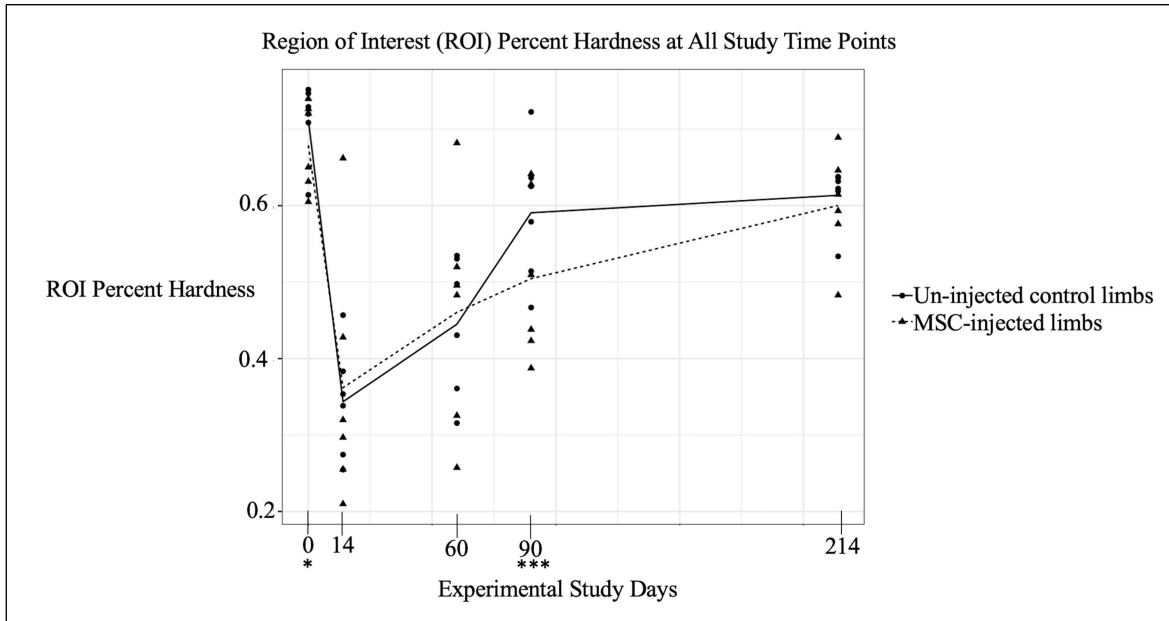
Fig 4.4B. Graphical representation of elastographically obtained region of interest (ROI) percent hardness at all study time points in both mesenchymal stem cell (MSC)-injected and un-injected control limbs. Significant differences between ROI percent hardness and treatment were found on days 0 and 90 (* denotes $P < 0.05$, *** denotes $P < 0.001$).

Statistically significant differences in subjective stiffness tendon between treatment

groups were not appreciated on any study days. Mean and standard deviation subjective stiffness

tendon values for MSC-injected limbs on sequential study days were found to be: 1.39 +/-0.60

(day 0), 1.34 +/-0.53 (day 14), 1.39 +/-0.57 (day 60), 1.27 +/-0.47 (day 90) and 1.29 +/-0.48 (day

214). These values were in contrast to mean and standard deviation values for untreated control

limbs across all study time points of: 1.31 +/-0.52 (day 0), 1.27 +/-0.49 (day 14), 1.36 +/-0.56

(day 60), 1.31 +/-0.50 (day 90) and 1.34 +/-0.49 (day 214). Subjective stiffness tendon values at

all study time points for both treatment groups are graphically depicted in Figure 4.4D.
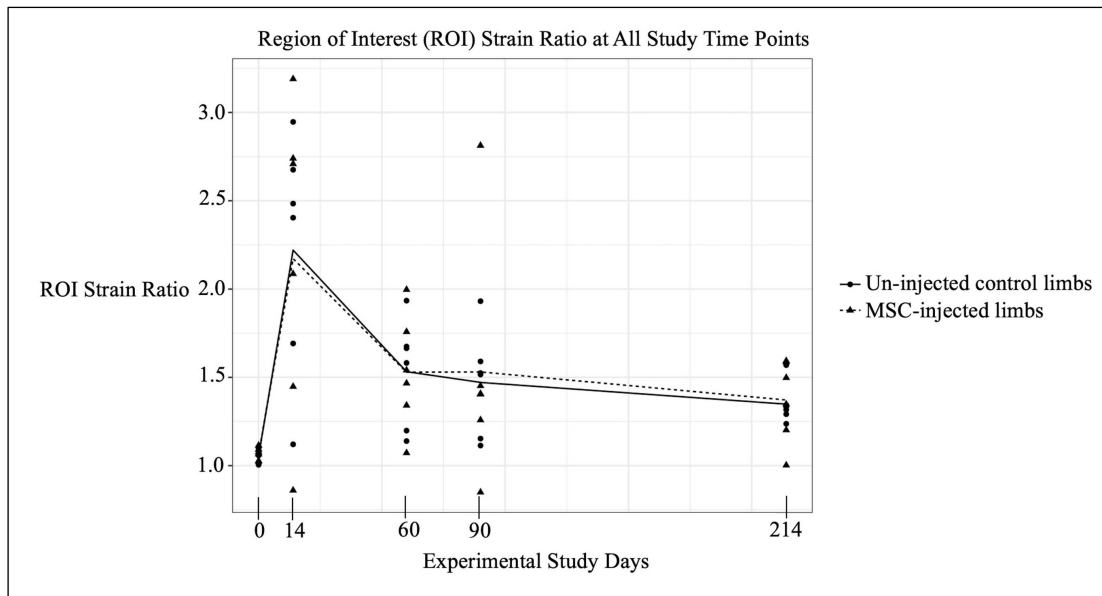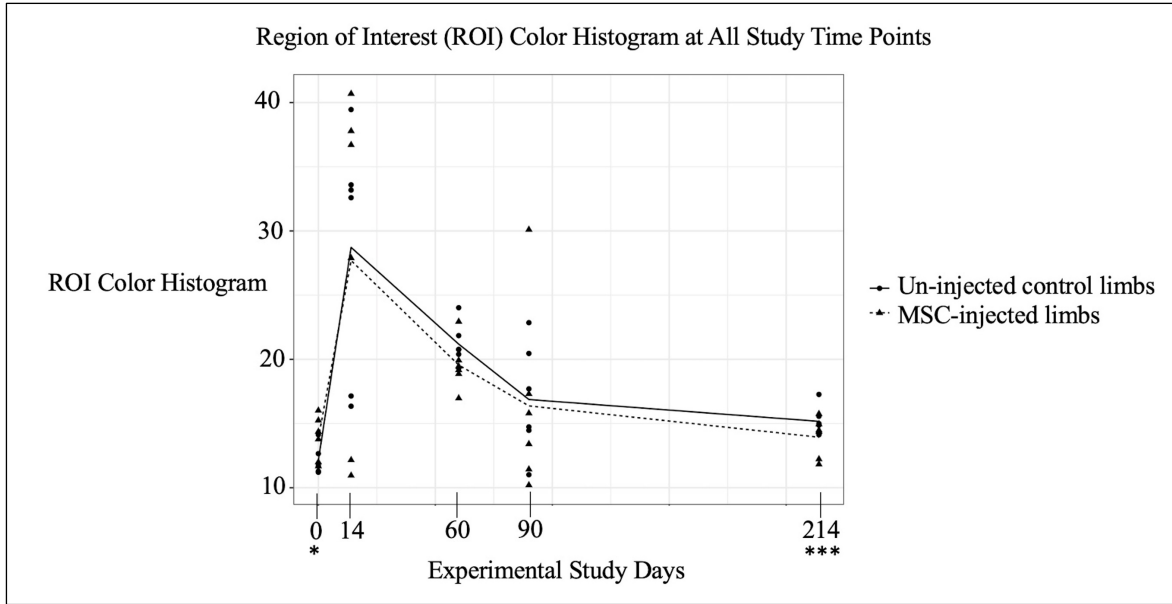
Fig 4.4C. Graphical representation of elastographically obtained region of interest (ROI) color histogram at all study time points in both mesenchymal stem cell (MSC)-injected and un-injected control limbs. Significant differences between ROI color histogram and treatment were found on days 0 and 214 (* denotes $P < 0.05$, *** denotes $P < 0.001$).
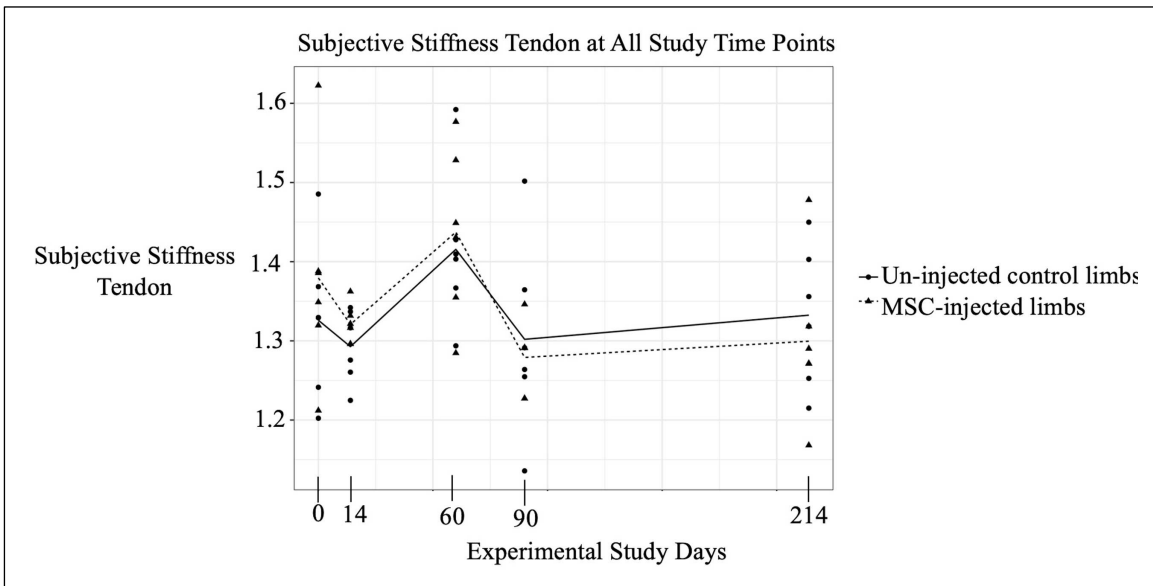
Fig 4.4D. Graphical representation of elastographically obtained subjective stiffness tendon at all study time points in both mesenchymal stem cell (MSC)-injected and un-injected control limbs. Significant differences between subjective stiffness tendon and treatment were not appreciated on any days.

Significant differences in subjective stiffness lesion between treatment groups were appreciated only at study day 214 ($P < 0.001$, 95%CI = -0.31 - -0.10). Mean and standard deviation subjective stiffness lesion values for MSC-injected limbs on sequential study days were found to be: 0 +/-0 (day 0, pre lesion induction), 2.09 +/-1.05 (day 14), 1.78 +/-0.91 (day 60), 1.63 +/-0.86 (day 90) and 1.59 +/-0.66 (day 214). These values were in contrast to mean and standard deviation values for untreated control limbs across all study time points of: 0 +/-0 (day 0, pre lesion induction), 2.13 +/-0.97 (day 14), 1.92 +/-0.85 (day 60), 1.77 +/-0.70 (day 90) and 1.79 +/-0.61 (day 214). Subjective stiffness lesion values at all study time points for both treatment groups are graphically depicted in Figure 4.4E.
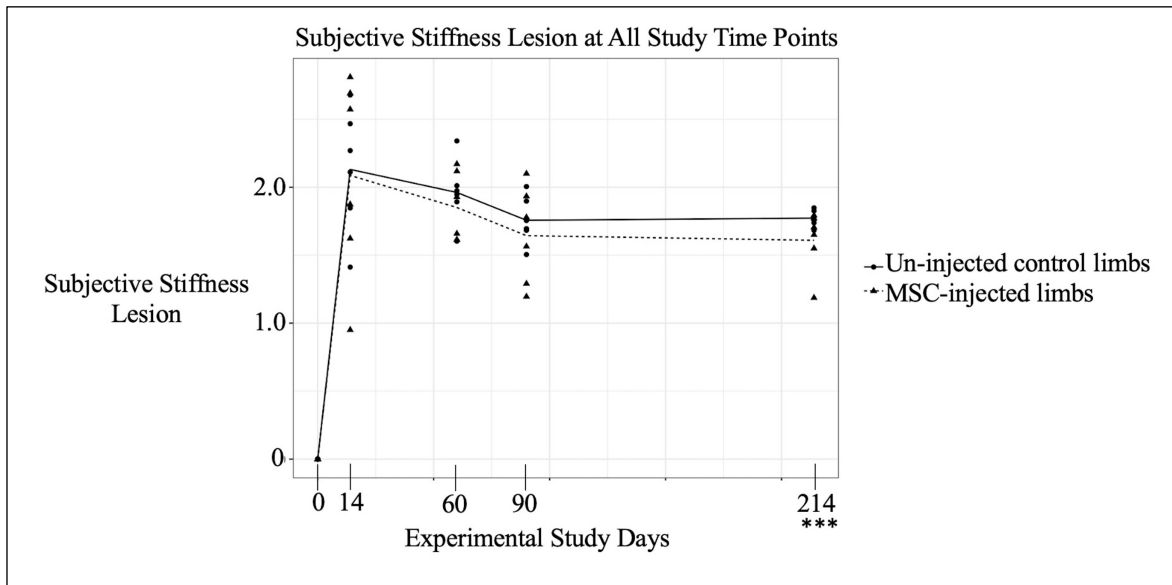
Fig 4.4E. Graphical representation of elastographically obtained subjective stiffness lesion at all study time points in both mesenchymal stem cell (MSC)-injected and un-injected control limbs. Significant differences between subjective stiffness lesion and treatment were only appreciated on study day 214 (*** denotes $P < 0.001$).

Longitudinal elastographic outcome parameters compared to biochemical tissue analysis

Coefficient of determination values (R^2 values) for each elastographic outcome parameter at each study date to explain the proportion of variance in each biochemical outcome measure

were all found to be ≤0.50. Specific R^2 values for strain ratio as a predictor of biochemical

outcome parameters GAG/DNA and GAG/tissue for each study date are listed in Table 4.4.

Table 4.4 Summary of coefficient of variation (R^2) values for glycosaminoglycan (GAG) per DNA (µg) and GAG/tissue (mg) calculated for region of interest (ROI) strain ratio at each study time point. Low R^2 values (≤0.50) across all five measured elastographic outcome parameters at each time point indicated that they were not useful predictors of any of the four end-point biochemical tissue analysis parameters.

Study Date	GAG/DNA (µg) & Region of Interest (ROI) Strain Ratio R^2 Value	GAG/Tissue (mg) & ROI Strain Ratio R^2 Value
0	0.023	0.031
14	0.024	0.50
60	0.47	0.12
90	0.00	0.01
214	0.001	0.10
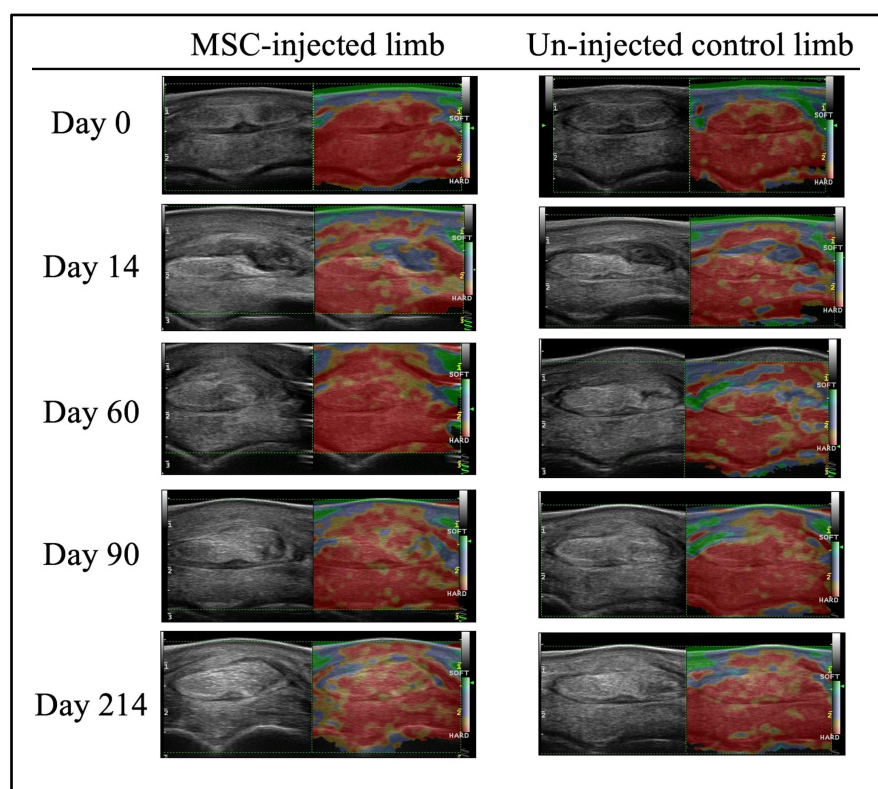
Fig 4.5. Representative grey-scale ultrasound and elastographic images of a limb injected with mesenchymal stem cells (MSCs) compared to the contralateral un-injected (control) limb. Both limbs are from the same horse at all evaluated study time points.

4.5 Discussion

The results of this study demonstrate that GAG levels were significantly lower in MSC-treated limbs compared to untreated control limbs. Additionally, significant differences in elastographic ROI percent hardness, ROI color histogram and subjective lesion stiffness were appreciated between treatment groups at various study time points. Despite these imaging findings, however, elastographic measurements were weak predictors of biochemical tissue analysis differences between groups. Specifically, variances in GAG levels between treatment groups were not reflected as elastographically-detectable differences.

Elastography and its ability to predict physiologic tissue characteristics has been a source of ongoing interest in human tendinopathic imaging [17-19]. Previous authors have noted that imaging modalities' diagnostic capability must be great enough to detect deformability differences between normal and diseased tissues [1,20]. Despite its increasing popularity due to consistent image reproducibility among observers [21], non-invasiveness and its potential to longitudinally monitor tendon healing through tissue stiffness estimation, elastographic measures have inconsistently demonstrated measurement distinctions between healthy and diseased soft tissues [17-19]. A meta-analysis revealed that no significant difference in elastographically estimated tendon elasticity or strain ratio could be identified between shoulders with and without rotator cuff tendinopathy [17]. Similarly, no significant difference in elasticity values were found between normal and torn supraspinatous tendons, despite authors noting that elasticity differences were significant according to whether symptoms were one year in duration or less [18]. When strain ratios and functional scores were compared in patients with subacromial impingement syndrome, no significant correlation was found [19]. These reports are in contrast to other investigations for which injured Achilles tendons assessed with elastography demonstrated superior agreement with

histologic assessment when compared to conventional ultrasonography [22]. Similarly, statistically significant differences in elastographic assessment between healthy volunteers and those with Achilles tendinopathy were associated with a considerable softening of intratendinous tissue [23]. In contrast, when utilizing this equine study model, all measured elastographic outcomes were found to be only weak predictors of GAG, DNA and collagen tissue analysis. Tendon GAGs act as molecular cross-links between collagen fibrils and also play a role in tendon elastic behavior [11], which ultimately inspired their targeted analysis in relation to elastography herein. It is possible that elastographic measurement differences correlate to tissue properties other than changes in GAG, DNA or collagen content that were not assessed. It's also possible that the scale of this data was too small to detect subtle differences or that the collagenase (enzymatic) model of tendinopathy resulted in altered tissue stiffness compared to that of naturally occurring tendon injury, for which elastography may be more useful. *In vitro* assessment of tendon strain with correlation to elastographic measures would help determine true mechanical properties. Nonetheless, this report is the first to investigate elastography's utility as a biochemical tissue predictor and serves as a basis for which future studies incorporating naturally occurring tendon injury can be compared, with correlative biomechanical analysis being warranted.

Elastography for use in horses has been previously reported [1-2,24-26]. The feasibility, reproducibility and repeatability of elastography of metacarpal tendons in sound horses demonstrated no difference between nor within operators [1]. Similar to human Achilles tendons, normal equine tendons were found to be predominantly hard with no significant difference in stiffness noted between the SDFT and the DDFT [1]. When the same research group elastographically evaluated naturally occurring tendon and ligament injuries in comparison to grey-scale ultrasound and MRI, significant correlations were appreciated [2]. Specifically,

hypoechoic and increased signal on short tau inversion recovery (STIR) and proton density (PD) sequences correlated with increased softness on elastography [2]. Naturally occurring SDFT injuries were then longitudinally evaluated with grey-scale ultrasound and elastography using echogenicity-grading and color-grading systems [26]. Authors reported that elastography was feasible and useful to evaluate injured SDFTs and to distinguish different phases of healing [26]. Despite these promising results, a study evaluating cadaveric SDFT lesions created with a biopsy punch demonstrated that elastography only inconsistently detected known lesions, with authors concluding that substantial improvements in quantitative ROI strain analysis were needed to make strain profile measurements diagnostically pertinent [25].

Methodology reported herein most closely mimics that of Lustgarten et. al for which similar analysis, grading scales and software utilization were employed [1,2]. Specifically, their previously reported qualitative grading scale was used to assess both the tendon and lesion, but with a different software-assigned color scheme (different colors were assigned to varying stiffness levels, but higher number still reflected the most soft reading). Quantitative analysis also utilized their previously reported ROI strain ratio assessment, with values close to 1 indicating equivalent stiffness between the two DDFT lobes (injured and uninjured). In the metacarpal SDFT and DDFTs of uninjured horses, mean strain ratios were reported to be 0.94 - 1.07 [1]. This study is the first analysis of elastography's diagnostic utility in experimental tendinopathy utilizing two treatment groups with comparison to equine tissue properties. No significant association between ROI strain ratio and treatment was found at any evaluation time point despite 42% differences in GAG levels between treatment groups. It is the authors' interpretation that 10-20% reductions in GAG are clinically significant for improved tendon healing, so it was disappointing that similar differences in strain ratio were not appreciated. Mean strain ratios were highest (>2.0 in both

treatment groups) at day 14 post lesion induction, then gradually decreased over time (Fig 4.4A) with mean values of 1.38 and 1.34 at day 214 for MSC-injected and untreated control limbs, respectively. This numeric value designated by the software to reflect the color continuum differences between the ROI of the lateral DDFT (normal) lobe compared to that of the medial (injected) lobe was utilized to estimate properties of tissue stiffness with values >1 indicating that the medial lobe was softer than the lateral lobe. Despite these temporal observations making biologic sense that a lesion would be initially soft, then gradually stiffen over time, the lack of statistical correlation with biochemical properties was surprising. The observed R^2 values in this study were all ≤0.50, a metric that explains at most 50% of the variation in the biochemical tissue analysis. Based on this finding, it is the authors' impression that elastography was not reliable and potentially a misleading diagnostic tool to predict GAG, DNA and collagen-related properties. It is possible that elastographically assessed ROI strain ratio might differentiate between a wider range of biochemical data, but our results suggest that more subtle tissue differences in GAG, DNA and collagen will not be reflected as changes in elastographic strain ratio, which is what would ultimately be useful to longitudinally assess tendon healing. Despite these findings, elastographic measurements were longitudinally consistent with expected biologic healing patterns, for example stiffness increased while ROI strain ratios decreased. Future studies that evaluate naturally occurring lesions with elastography and terminal tissue analysis will help confirm if these assumptions are valid.

In addition to strain ratio (the most commonly assessed outcome measure in both human and equine elastographic studies), this investigation also quantitatively measured the ROI percent hardness and the ROI color histogram as further measures to assess tissue stiffness properties. A higher ROI percent hardness value signified that the software detected more hard tissue in the

image, so as healing progressed the authors' expected this number to gradually increase over time, which is what was appreciated. What was surprising, however, was the wide variation in ROI percent hardness values across all limbs at all time points. A possible explanation is that elastographic software has not yet been adequately normalized for equine DDFT measurements or that earlier tissue sampling time points may have elucidated relationships not appreciated with day 214 sampling. In contrast to ROI percent hardness, ROI color histogram values were expected to gradually decrease with time, reflecting that higher values (green) indicated injured tissue and lower values (red) indicated more hard tissue. Values within each selected area were subsequently averaged by machine software to give the resultant recorded number used in statistical analysis. Manually drawing ROIs carry inherent potential for error, so it's possible that the selected ROIs drawn by the two observers blinded to treatment groups were not representative of true color differences. It's also possible that similar to ROI percent hardness, elastographic software has not yet been adequately optimized to differentiate color differences in equine intrathecal DDFT injuries.

Significant differences in ROI percent hardness were appreciated between treatment groups on days 0 and 90, while significant differences in ROI color histogram were appreciated on days 0 and 214. The relevance of these differences noted on day 0 (pre lesion induction) are difficult to explain as all DDFTs were assessed as normal on baseline MRI evaluation, but may have been attributable to subtle, inherent differences in hoof-pastern-axis conformation. Despite differences between treatment groups in these outcomes at 90 and 214 days, the correlation coefficients and wide prediction intervals to GAG, DNA and collagen analysis were weak, making their clinical usefulness still unknown. Qualitative analysis of both the lesion and tendon perceived stiffness revealed that across both treatment groups, lesions were in general graded subjectively

more soft (>2.0) than the entire tendon (<1.5). Significant treatment differences between subjective stiffness of the tendon were not appreciated at any evaluation time points while differences between subjective stiffness of the lesion were only appreciated on study day 214 (1.59/4 for (MSC-injected limbs vs 1.79/4 for untreated limbs. Despite this subjective difference in lesion stiffness between treatment groups, correlation to GAG, DNA and collagen remained low, indicating that this subjective impression is likely not a reflection of these specific tissue proteins, but rather overall lesion appearance. It is also possible that lesions were inherently different in biologic configuration despite standardizing as many lesion induction variables as possible (ultrasound guidance, location, operator inducing lesions, etc.).

The therapeutic use of MSCs in tendinopathic healing has been previously investigated in experimental models of tendinopathy [9-10,27-28] and naturally occurring SDFT injury [7-8,29], but has yielded a spectrum of results. Clinical usage of MSCs in superficial digital flexor (SDF) tendinopathy is supported by the ability to return to previous level of work [29], approximately 30% reduced re-injury rates in National Hunt horses [8], and beneficial effects at the cellular level as evidenced through improved histologic scoring, lower cellularity and reduced glycosaminoglycan content [7]. Similarly, collagenase models of SDFT injury have documented improved extracellular matrix ratios of collagen types I/III [28], histologic scores [10] and fiber orientation [28] following intra-lesional injections of MSCs. Pursuant to the findings of this investigation, elevated levels of glycosaminoglycans have been directly linked to decreased biomechanical strength [27,30-31], and mitigation of this scar tissue protein represents a promising therapeutic target for improved tendon healing [7,11-12]. The direct correlation of GAG content to that of biomechanical strength [27,30-31] and its significant role in tendon elastic behavior [11] inspired the targeted biochemical tissue analysis herein. Similar to naturally occurring SDFT injury

findings [7], limbs in this study receiving MSC therapy demonstrated significantly less GAG content (42%). This experiment ultimately provided a useful range of differences in GAG between treatment groups, but readers should be cautioned that these differences were appreciated when compared to untreated control limbs in an experimental tendinopathy model. Also noteworthy is that the focus of this investigation was not to exhaustively evaluate tissue-specific effects of intra-lesional MSC injection in collagenase induced tendinopathy that are reported elsewhere [Johnson et al, unpublished data], but rather to provide a spectrum of clinical disease for which elastographic outcome measures could be subsequently compared.

In contrast to enzymatically induced SDF tendinopathy, collagenase-induced equine DDFT injury investigations are considerably sparce, with only one study reporting effects of hyaluronic acid over a 6-week study period in a mid-metacarpal DDF tendinopathy model [32]. To the authors' knowledge, this is the first investigation of an intra-thecal DDFT collagenase tendinopathy model, and therefore inherent variability in lesion size, extent and severity despite the authors' homogenizing study-design factors is likely. While no model has been universally agreed upon to exactly replicate clinical disease, this study is a pilot investigation that attempted to standardize intrathecal DDFT lesions to assess the diagnostic utility of elastography and allow reasonable comparison to other published studies.

There are several study limitations the authors would like to acknowledge that include inherent biologic variability in lesion size, location and configuration associated with the experimental induction of tendinopathy using collagenase in a small sample population. One forelimb of each horse was treated with MSCs, while the contralateral limb of the same horse received no control injection. Injecting control lesions with 1mL of saline would have eliminated any healing responses associated with the volume utilized, but not allowed the more clinically

110

relevant comparison for when lesions are not injected with anything (untreated). Not utilizing a 1mL saline control allowed the MSC treatment to be compared to truly untreated tendons, which is often the most common clinical scenario. It does, however, set up an inherent study bias and increases the volume of tendon disruption that is not controlled for by study design. Secondly, the preferential timing, dosage and method of delivery for MSCs within the spectrum of tendon lesions remains unknown, so it is possible that further differences may have been appreciated had a different protocol, study timeline or rehabilitation regimen been used. The authors utilized MSCs as described herein to most closely mimic current clinical usage and provide a spectrum of disease for which elastographic outcome parameters could be compared. Thirdly, elastographic features of mid-metacarpal region DDFTs in both normal and injured horses have been previously reported [1,2], but this modality's use in the pastern region for DDFT assessment has not been previously investigated, so it is possible that software settings or measured outcomes were not adequately optimized. It is also possible that different elastographic values would have been obtained by using alternate ROIs within each DDFT lobe. Additionally, it may have been useful to compare elastographic findings to one another or to another imaging modality, but the authors statistical query herein was not elastography's relationship to other modalities that has been previously reported,[2] but rather direct tissue correlation of properties related to biomechanical strength. Formal lameness quantification may have also provided insight into further relationships not evaluated herein. The results of further inter-modality comparisons (MRI, ultrasound) utilizing this equine injury model are reported elsewhere [Johnson et al unpublished data]. Nonetheless, the study contributes to the breadth of information available on elastography's use in horses. Lastly, biomechanical testing of the injured tendons may have revealed functional strength differences able to be extrapolated to clinical or tissue-level differences. Further studies investigating these

tissue-specific differences with comparison to clinical outcomes in naturally occurring injury and advanced imaging will be useful.

In conclusion, the results of this study demonstrate that tissue-specific differences between DDFTs treated with MSCs compared to untreated controls were apparent, but longitudinal elastographic outcome measures did not predict corresponding intra-tendinous GAG, DNA or collagen content in a collagenase model of intra-thecal DDF tendinopathy. Several differences in elastographic outcome measures were appreciated at various time points between treatment groups, but their clinical relevance remains unknown. Specifically, statistically significant differences in ROI strain ratios were not appreciated between treatment groups at any evaluation time points. Significant differences in ROI percent hardness between treatment groups were found on study days 0 ($P < 0.05$) and 90 ($P < 0.001$), while significant differences in ROI color histogram were appreciated between treatment groups on study days 0 ($P < 0.05$) and 214 ($P < 0.001$).

References

1. Lustgarten M, Redding WR, Labens R, Morgan M, Davis W, Seiler GS. Elastographic characteristics of the metacarpal tendons in horses without clinical evidence of tendon injury. *Vet Radiol Ultrasound* 2013;55(1):92-101.

2. Lustgarten M, Redding WR, Labens R, Davis W, Daniel TM, Griffith E, Seiler GS. Elastographic evaluation of naturally occurring tendon and ligament injuries of the equine distal limb. *Vet Radiol Ultrasound* 2015;56(6):670-679.

3. Li Y, Snedeker JG. Elastography: modality-specific approaches, clinical applications, and research horizons. *Skeletal Radiol* 2011;40:389–397.

4. Lutter JD, Schneider RK, Sampson SN, Cary JA, Roberts GD, Vahl CI. Medical treatment of horses with deep digital flexor tendon injuries diagnosed with high-field-strength magnetic resonance imaging: 118 cases (2000-2010). *J. Am. Vet. Med. Assoc.* 2015;247(11);1309-1318.

5. Cillan-Garcia E, Milner PI, Talbot A, Tucker R, Hendey F, Boswell J, Reardon RJM, Taylor SE. Deep digital flexor tendon injury within the hoof capsule; does lesion type or location predict prognosis? *Vet. Rec.* 2013;doi:10.1136/vr.101512.

6. Lake S, Ansorge H, Soslowsky L. Animal models of tendinopathy. *Disabil. Rehab.* 2008; 30:20-22.

7. Smith R, Werling N, Dakin S, et al. Beneficial effects of autologous bone marrow-derived mesenchymal stem cells in naturally occurring tendinopathy. *PLOS* 2013;8:9;e75697.

8. Godwin EE, Young NJ, Dudhia J, Beamish IC, Smith RKW. Implantation of bone marrow-derived mesenchymal stem cells demonstrates improved outcome in horses with overstain injury of the superficial digital flexor tendon. *Equine Vet. J.* 2012;44:25-32.

9. Ahrberg AB, Horstmeier C, Berner D, Brehm W, Gittel C, Hillman A, Josten C, Rossi G, Schubert S, Winter K, Burk J. Effects of mesenchymal stromal cells versus serum on tendon healing in a controlled experimental trial in an equine model. *BMC M. Disorders* 2018;19:230.

10. Schnabel LV, Lynch ME, van der Meulen MCH, Yeager AE, Kornatowski MA, Nixon AJ. Mesenchymal stem cells and insulin-like growth factor-I gene-enhanced mesenchymal stem cells improve structural aspects of healing in equine flexor digitorum superficialis tendons. *J. Orthop. Res.* 2009;27:1392-1398.

11. Ryan NMC, Sorushanova A, Lomas AJ, Mullen AM, Pandit A, Zeugolis DI. Glycosaminoglycans in tendon physiology, pathophysiology, and therapy. *Bioconjugate Chem* 2015;26:1237-1251.

12. Smith R and McIlwraith W. Advances in the understanding of tendinopathies: a report on the second Havemeyer workshop on equine tendon disease. *Eq. Vet. J.* 2014;46:4-9.

13. Nixon AJ, Dahlgren LA, Haupt JL, Yeager AE, Ward DL. Effect of adipose-derived nucleated cell fractions on tendon repair in horses with collagenase-induced tendinitis. *Am. J. Vet. Res.* 2008;69:928-937.

14. Marsh C, Schneider RK, Frisbie DD, Roberts GD, Neelis D, Yiannikouris S, Sampson SN. Evaluation of bone marrow-derived mesenchymal stem cells as a treatment for collagenase-induced desmitis of the proximal suspensory ligament in horses. *Proc. Ann. Conv. Am. Assoc. Eq. Pract.* 2012;58:54-55.

15. Kim, Y.J., Sah, R.L.Y., Doong, J.Y.H., Grodzinsky, A.J. Fluorometric assay of DNA in cartilage explants using Hoescht 33258. *Anal. Biochem.* 1988;174:168-176.

16. Croon, Marcel A, and Marc JPM van Veldhoven. "Predicting Group-Level Outcome Variables from Variables Measured at the Individual Level: A Latent Variable Multilevel Model." *Psychological Methods* 2007;12(1):45.

17. Chiu YH, Chang KV, Chen IJ, Wu WT, Ozcakar L. Utility of sonoelastography for the evaluation of rotator cuff tendon and pertinent disorders: a systematic review and meta-analysis. *Eur Radiol* 2020;30:6663-6672.

18. Yoo SJ, Lee S, Song Y, Kim CK, Lee BG, Bae J. Elasticity of torn supraspinatous tendons measured by shear wave elastography: a potential surrogate marker of chronicity? *Ultrasonography* 2020;39:144-151.

19. Figen K, Kuyucu E, Kocyigit A, Herek DT, Savkin R, Aslan UB. Investigation of biomechanical characteristics of intact supraspinatus tendons in subacromial impingement syndrome: a cross sectional study with real-time sonoelastography. *Sports Med* 2016;95(8): doi: 10.1097/PHM.0000000000000450.

20. Murata D, Misumi K, Fujiki M. A preliminary study of diagnostic color doppler ultrasonography in equine superficial digital flexor tendonitis. *J Vet Med Sci* 2012;74:1639–1642.

21. Drakonaki EE, Allen GM, Wilson DJ. Real-time ultrasound elastography of the normal Achilles tendon: reproducibility and pattern description. *Clin Radiol* 2009;64(12):1196-1202.

22. Klauser AS, Miyamoto H, Tamegger M, Faschingbauer R, Moriggl B, Kima Guenther, Feuchtner GM, Kastlunger M, Jaschke WR. Achilles tendon assessed with sonoelastography: histologic agreement. *Radiol* 2013;267(3):837-842.

23. De Zordo T, Chhem R, Smekal V, Feuchtner G, Reindl M, Fink C, Faschingbauer R, Jaschke W, Klauser AS. Real-time sonoelastography: findings in patients with symptomatic achilles tendons and comparison to healthy volunteers. *Ultraschall in Med* 2010;31:394-400.

24. Bernardi NS, Feliciano MAR, Gravena K, Avante ML, Simoes APR, Uscategui RAR, Dias DPM, Lacerda Neto JC. Acoustic radiation force impulse (ARFI) elastography imaging of equine distal forelimb flexor structures. *Arq Bras Med Vet Zootec* 2020;72(4):1154-1162.

25. Buck AR, Verstraete N, Li Y, Schweizer A, Snedeker JG, Buck FM. Detection of small tendon lesions by sonoelastographic visualization of strain profile differences: initial experiences. *Skeletal Radiol* 2012;41:1073-1079.

26. Tamura N, Kuroda T, Ktoyori Y, Fukuda K, Nukada T, Kato T, Kuwano A, Kasashima Y. Application of sonoelastography for evaluating the stiffness of equine superficial digital flexor tendon during healing. *Vet Record* 2016;doi:10.1136/vr.103869.

27. Choi RK, Smith MM, Martin JH, Clark JL, Dart AJ, Little CB, Clarke EC. Chondroitin sulphate glycosaminoglycans contribute to widespread inferior biomechanics in tendon after focal injury. *J. Biomech.* 2016;49:2694-2701.

28. Crovace A, Lacitignola L, Rossi G, Francioso E. Histological and immunohistochemical evaluation of autologous cultured bone marrow mesenchymal stem cells and bone marrow mononucleated cells in collagenase-induced tendinitis of equine superficial digital flexor tendon. *Vet. Med. Int.* 2010;doi:10.40161/2010/250978.

29. Renzi S, Ricco S, Dotti S, Sesso L, Grolli S, Cornali M, Carlin S, Patruno M, Cinotti S, Ferrari M. Autologous bone marrow mesenchymal stromal cells for regeneration of injured equine ligaments and tendons: a clinical report. *Res. Vet. Sci.* 2013;95:272-277.

30. Bell R, Li J, Gorski DJ, Bartels AK, Shewman EF, Wysocki RW, Cole BJ, Bach BR, Mikecz K, Sandy JD, Plaas AH, Wang VM. Controlled treadmill exercise eliminates chondroid deposits and restores tensile properties in a new murine tendinopathy model. *J. Biomech.* 2013;46:3;498-505.

31. Attia M, Scott A, Carpentier G, Lian O, Van Kuppevelt T, Gossard C, Papy-Garcia D, Tassoni MC, Martelly I. Greater glycosaminoglycan content in human patellar tendon biopsies is associated with more pain and a lower VISA score. *Br J Sports Med* 2014;48:469-475.

32. Gift LJ, Gaughan EM, DeBowes JP, Douglass JP, Frank RK, Klemm RD. The influence of intratendinous sodium hyaluronate on tendon healing in horses. *Vet Comp Traumatol* 1992;05(04):151-157.

CHAPTER 5 – Fast, Non-Eccentrically Loaded Exercise Worsens Tendinopathic Healing Responses in a Murine Model

5.1 Overview

The therapeutic benefits of eccentric loading protocols for mid-body Achilles tendinopathy have been of recent interest; however, the optimum "dose" for therapeutic exercise and its relationship to exercise capacity, morphology, and mechanical outcomes are unknown. Additionally, the relationship between exercise and the local and systemic levels of Collagen X (COLX), a marker of endochondral ossification, with respect to tendon zonal enthesis attachment and healing are unknown. Using an established model of tendinopathy, the objectives of this study were: 1) To advance the understanding of how alterations in exercise speed and grade (flat vs 17° incline or decline) affect the quality of tendon healing, and 2) To determine if a biomarker relationship exists between serum levels of ColX and animals exposed to treadmill running protocols. Mice were preconditioned on a treadmill for 14 days. Tendinopathy was then induced by two intra-tendinous TGFβ1 injections followed by randomization into the following groups: 1) rest (normal cage activity); and exercise protocols of 2) slow (no grade), 3) fast (no grade), 4) slow-incline, 5) fast-incline, 6) slow-decline, and 7) fast-decline. Exercise capacity and objective gait analysis were measured weekly during the experimental time-course up to the final 14-day timepoint. Mice were euthanized, and histopathologic analysis and evaluation of serum ColX levels were performed. Exercise initiated at a fast, flat speed (in absence of eccentric loading) demonstrated inferior tendinopathic healing at the cellular level; and impaired stance braking abilities, which were compensated for by increased propulsion. Mice exposed to exercise (at any speed or grade) demonstrated higher systemic levels of COLX than those that were cage rested,

and mice exposed to fast exercise had the highest levels of articular COLX in comparison to slow exercise groups.

5.2 Introduction

Achilles tendinopathy remains a prevalent and frustrating sports injury for both athletes and aging populations [1-3]. Specific to top level runners, a 52% lifetime risk of developing Achilles tendinopathy has been reported [4]. Despite surgical and therapeutic advancements, few interventions have proven superior to controlled exercise alone. A clear explanation for the response of tendinopathy to exercise is lacking [5], but one proposed therapeutic mechanism of action includes the beneficial effects on collagen homeostasis [6]. Specifically, an increase in collagen synthesis measured via microdialysis was demonstrated following 12 weeks of eccentric exercise in Achilles tendinopathy [6]. Eccentric loading magnitudes [7] and intra-tendinous sinusoidal oscillations occurring specifically during the eccentric phase of therapeutic exercises have been proposed to stimulate tendon remodeling [8], consistent with other reports that collagen synthesis may be affected by exercise loading magnitude [9]. Despite these findings, the optimum "dose" and "type" of therapeutic exercise with respect to speed and grade of exercise remains unknown.

Murine studies have demonstrated that induction of tendinopathy via injection of TGF-β1 directly into the tendon body allows for the consistent reproduction of chronic tendinopathic change including hypercellularity, collagen disorganization, chondroid deposition, and decreased material properties [10]. Specifically, accumulation of a chondroid matrix in this model - characterized by elevated levels of sulfated glycosaminoglycans [10], aggrecan and hyaluronan [10-11] within the tendon body - replicates pathologic change appreciated in human

117

tendinopathic studies [10]. When a mechanical loading component was applied to this murine model via daily short-fast (32 cm/sec for 25 minutes) treadmill running, improved biomechanical properties and histopathology (lessened chondroid deposition and collagen disorganization) were evident at 2 weeks post-injury. However, long-term (4 weeks post-injury) continued treadmill running was detrimental [12]. Due to alterations in the tendinopathic response to varied exercise regimes, controlled studies investigating exercise variables such as speed, duration and incline are necessary to tease out parameters for clinical effectiveness of rehabilitative protocols.

Additionally, we were curious to determine whether ColX may be used to quantitatively assess tendon healing through serological assessments. COLX has been historically considered in context of cartilage, as its role in chondrogenic differentiation and chronic osteoarthritis has been previously described [13-14]. Specifically, an association between elevated levels of ColX and osteoarthritic cartilage has been demonstrated [13-17] but its role as it pertains to tendons is minimally described [18-19]. Specifically, expression of COLX in the enthesis of the rat Achilles tendon has been described as being produced by cells in transitional zones between calcified and non-calcified tissue (the interface between articular cartilage and subchondral bone) [18]. Similarly, another previous investigation describes identification of COLX at the insertion site of the bovine Achilles tendon, suggesting it may be a resident of mineralized fibrocartilaginous zones of tendon or enthesis junction that may aid in the anchoring of tendon or ligament to bone [19]. As hind limb exercise effects the entire calcaneous-Achilles-gastrocnemius (e.g. bone-tendon-muscle) unit, the study of COLX locally and systemically may assist in the evaluation of exercise protocol effectiveness on the ankle joint as it relates to tendon zonal enthesis attachment and healing.

Given this, the objective of this study was to advance the understanding of how alterations of speed and grade (incline vs. decline) of exercise-based rehabilitation affect 1) the quality of tendon healing using a translational murine model, and 2) local and systemic ColX levels using a translational murine model. It was hypothesized that gradual (slow) exercise at an incline (eccentric loading) following tendon injury would demonstrate superior kinematic and histopathologic healing compared to no activity, more intense (fast) exercise, or exercise at a decline. Overall, further understanding the relationship between exercise protocols and tendinopathic development is aimed to provide evidence-based recommendations for exercise regimes as a physiotherapeutic modality to augment currently used tendon therapies.

5.3 Materials and Methods

This study was a prospective, controlled, blinded experiment. All study methods were conducted in compliance with Colorado State University's Institutional Animal Care and Use Committee (IACUC) standards (Protocol #: 16-6927A). The proposed experimental sample size (5 mice per group) was calculated using GPower Version 3.1.1. Specifically, an a-priori power analysis utilized pilot gait data (min dA/dT). This power analysis resulted in an effect size of 1.25 and a power of 97.3%, using a standard deviation of 10 for all groups.

Murine Population:

Mice utilized for this study (C57/BI6) were males, 8 weeks of age and purchased from a commercial vendor (Jackson Laboratories). All mice were allowed to acclimate for 14 days prior to experimentation. Standard pre-conditional treadmill running was initiated during the acclimatization period (days -14 to 0; fast protocol; 32 cm/sec for 25 minutes) [10,12]. All mice

were weighed weekly, housed at 22–24 °C and maintained on a 12-h light/dark cycle with water

and food available ad libitum during the experiments. Thirty-five total animals were utilized for

this study with five mice in each exercise group (**Figure 5.1**).
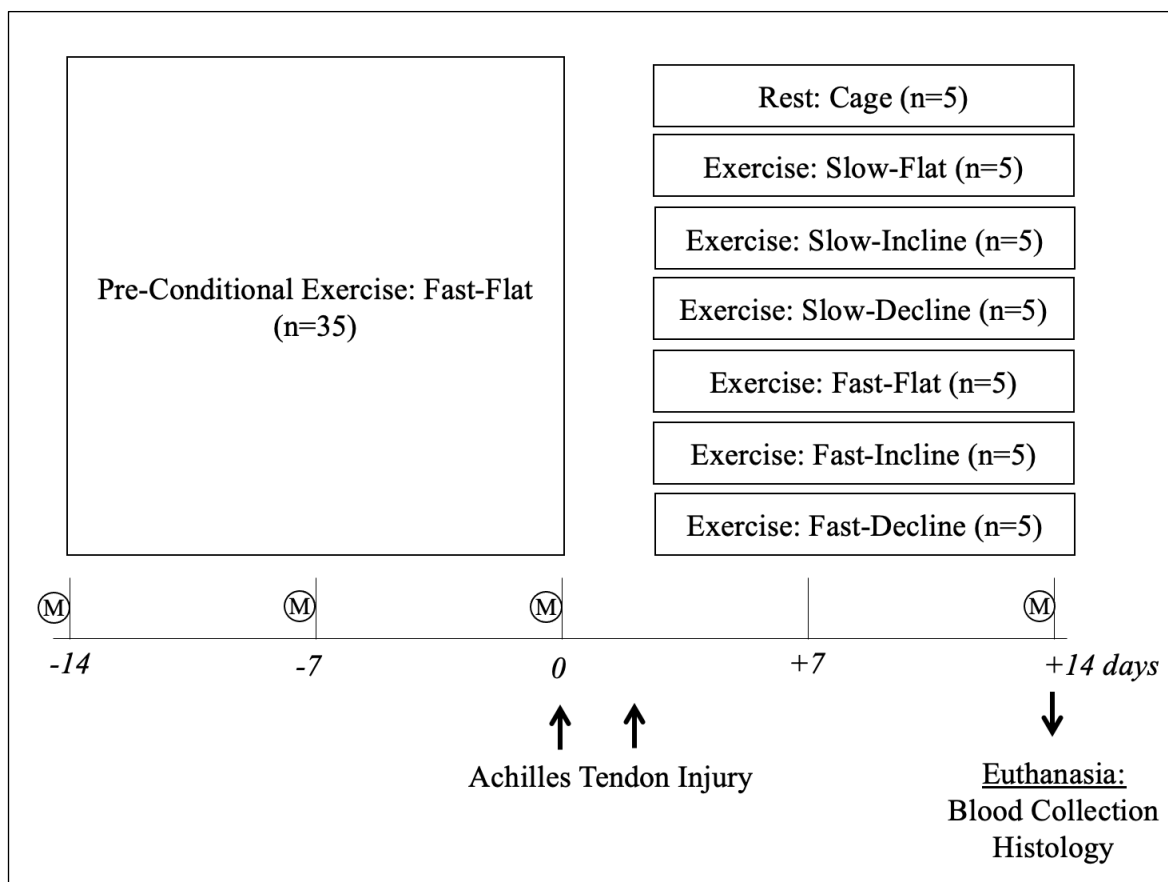
Figure 5.1. Experimental timeline and groups: Following pre-conditional treadmill running and induction of Achilles tendon injury via 2 injections (2 days apart) of TGF-β1, mice were randomized into seven treatment groups with the healing response assessed at 14 days post-injury. Gait analysis (M) was measured on days -15, -8, -1, and 13 with weekly maintenance in between measurements.

Murine Model of Tendinopathy & Exercise Groups:

To induce tendinopathy, 6uL of 100ng active human recombinent TGF-β1 was injected

into the body of the right Achilles tendon as previously described [12]. Two injections were

performed, two days apart using a 28G needle with mice under anesthesia with 2-3% isoflurane

[12]. Following injury, mice were randomized into the following groups: 1) rest (normal cage activity) and exercise protocols of 2) slow-flat (20 cm/sec with no incline), 3) fast-flat (32 cm/sec with no incline), 4) slow-incline (20 cm/sec at 17° incline), 5) fast-incline (32 cm/sec at 17° incline), 6) slow-decline (20 cm/sec at 17° decline) and 7) fast-decline (32 cm/sec at 17° decline). All animals underwent exercise protocols for 25 minutes per day starting on day 3 of the experimental protocol for 5 days per week with 2 days of rest each week [10,12]. All exercise protocols were performed on a 5-lane treadmill; and electrical stimulation (0.1-0.3mA) was utilized for compliance (PanLab, Barcelona, Spain).

Exercise Capacity:

To measure exercise capacity of animals undergoing treadmill running, the number of faults per animal were recorded during protocols, where a fault qualified as falling behind the treadmill onto the stimulation device. Exercise capacity was then expressed as the ratio of required stimulation after injury relative to pre-injury for comparison between exercise groups. The coefficient of variation was calculated for each animal and then averaged for each group to describe the spread as a representation of the animal-to-animal variability in completion of exercise protocols.

Gait:

Gait measurements were taken weekly prior to injury and prior to sacrifice at 14 days post-injury (**Figure 5.1**). Mice were acclimated to a treadmill-based gait analysis system (DigiGait™, Mouse Specifics, Boston, MA) over 1 week prior to data collection. Paw statistics, automatically calculated by associated software, were collected for all mice at 35 cm/sec on a flat

treadmill. Key gait parameters including stride length and swing speed were collected for all mice at each of the exercise protocols (all parameters measured can be seen in **Supplemental 1**).

COLX Serum Analysis:

Blood was collected via intracardiac stick while under general anesthesia (2-3% isoflurane) on day 14 of the experimental protocol (**Figure 5.1**). Blood serum concentrations of COLX for each experimental group were measured via ELISA as previously described [15].

Tissue Collection and Histopathology:

Mice were sacrificed on day 14 of the experimental protocol. Following intracardiac puncture for blood collection, euthanasia occurred via CO_2 asphyxia with cervical dislocation prior to tissue collection. Following euthanasia, both hind limbs were removed, fixed, embedded in paraffin, sectioned (5μm; sagittal) and stained with SafraninO/Fast Green and Hematoxylin and Eosin (H&E). Specimens were qualitatively interpreted by a board-certified clinical pathologist (KSS) based on the following criteria: 1) tissue swelling; 2) hyper-cellularity; 3) collagen disorganization; and 4) chondroid deposition. Additional parameters evaluated included peritenon 1) calcification, 2) edema, 3) neovascularization, and 4) inflammation, and modifications to the adjacent fat pad (mononuclear cell infiltration) and bursae (degree of synovial hyperplasia). Of note, samples were not quantitatively graded due to variable tissue sectioning which precluded full morphologic evaluation of all criteria.

Immunohistochemistry:

Given that only a subset was evaluated, a subjective impression of relative fluorescence of the distal hind-limb articular cartilage was provided (normalized to positive fluorescence for COLX in the growth plates).

Statistical analyses:

Statistical analysis was performed using commercial software (GraphPad Prism 7 (San Diego, CA 92108-2711). Exercise capacity was analyzed using a two-way analysis of variance (ANOVA) incorporating grade, speed and grade*speed interaction factors with Tukey's post-hoc comparisons. To evaluate two scenarios of changes in gait parameters [1) before and after preconditioning, and 2) following pre-conditioning compared to post-injury], paw statistics were analyzed using a one-way ANOVA with Tukey's post-hoc comparisons. Time-points for which various paw statistics were not able to be accurately calculated on the Digigait program were treated as missing data and omitted for statistical analysis. Statistical significance was considered $P < 0.05$.

5.4 Results

Exercise Capacity:

Exercise capacity expressed as the ratio of required stimulation after injury relative to pre-injury was not significantly different between groups for speed ($P = 0.07$), grade ($P = 0.28$) or speed*grade interaction ($P = 0.25$); however, trends and qualitative observations during exercise protocols suggest that animals required more simulation for maintenance over running for all fast exercise protocols **(Figure 5.2)**. Interestingly, this was animal specific as demonstrated via the coefficients of variations reported in **Figure 5.2**.
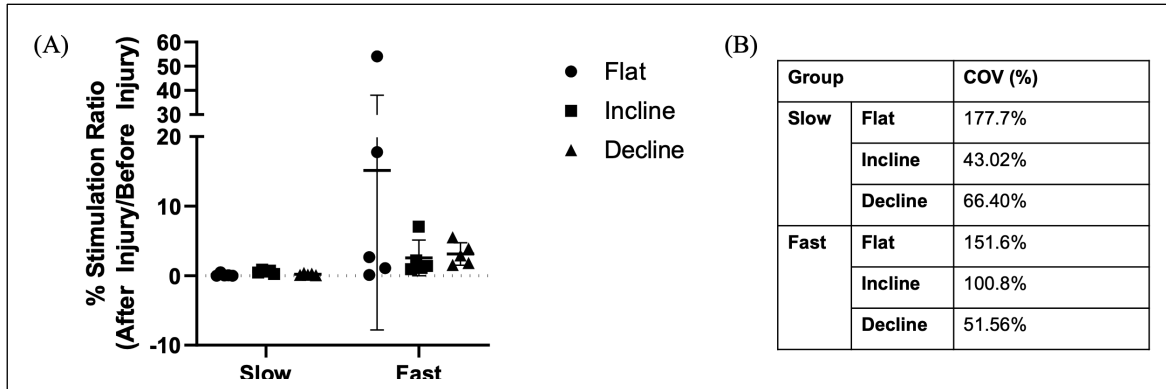
Figure 5.2. (A) Exercise capacity (% stimulation during running) of mice following injury relative to pre-conditioning levels (A). No significant differences were found between groups for speed (*P*=0.07), grade (*P*=0.28), and interaction (*P*=0.25) factors. (B) Coefficient of variation for exercise capacity following injury relative to pre-conditioning levels.

Gait:

Preconditioning Effects. All mice demonstrated a significant increase in max dA/dT when comparing day -15 to day -1 (before vs after the pre-conditioning period but prior to injury induction) ($P < 0.05$, **Figure 5.3A**). No significant differences in min dA/dT (**Figure 5.3B**), or any other gait parameters, were appreciated when comparing day -15 to day -1 (**Table 5.1**).

Exercise Protocol Effects. The mice in the fast-flat group demonstrated significantly increased max dA/dT (propel capacity) values compared to those in the slow-incline, slow-decline, fast-incline and fast-decline groups relative to pre-injury ($P < 0.0001$, **Figure 5.3C**). Mice in the fast-flat group also demonstrated a significantly decreased min dA/dT (braking capacity) compared to those in the slow-incline ($P < 0.05$), slow-decline ($P < 0.05$), fast-incline ($P < 0.05$) and fast-decline ($P < 0.01$) groups relative to pre-injury (**Figure 5.3D**). All evaluated gait parameters and statistical differences are reported in **Table 5.2**.
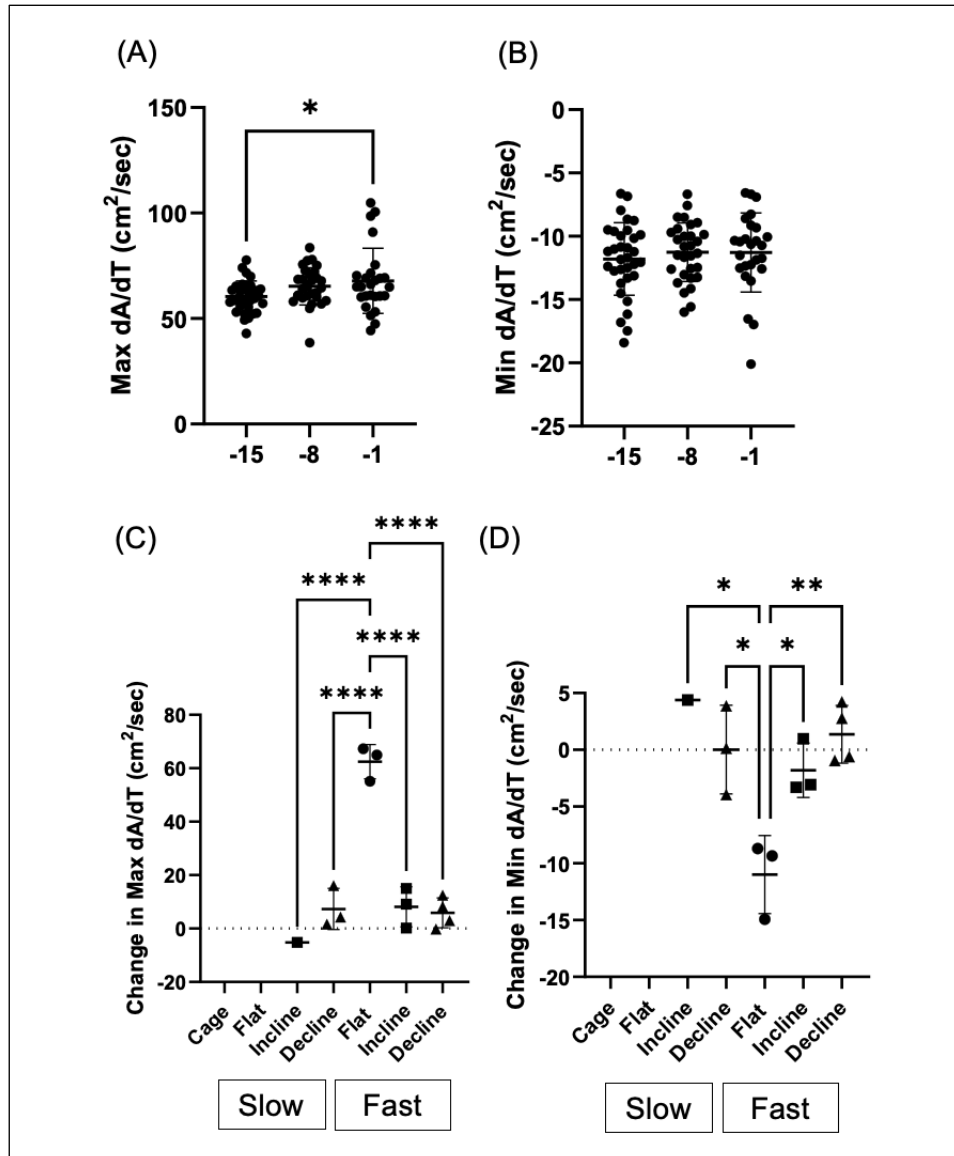
Figure 5.3. Effect of pre-conditioning on A) Max dA/dT and B) Min dA/dT gait parameters. Data represented as average +/- STD for all mice for each time-point. Significant p-values marked. Effect of injury and rehabilitation treatment on the change in C) Max dA/dt and D) Min dA/dT relative to pre-injury levels. Data represented as average +/- STD with individual animals marked. $*P<0.05$, $**P<0.01$, $***P<0.001$, $****P<0.0001$.

Table 5.1: Table summarizing statistical significance of all measured gait parameters for each exercise group (rest, slow-flat, fast-flat, slow-incline, fast-incline, slow-decline and fast-decline) before vs. after preconditioning. Arrow (up vs. down) indicates directionality of statistically significant change and number of arrows indicate statistical significance (↑ $P <0.05$, ↑↑ $P <0.01$, ↑↑↑ $P<0.001$, ↑↑↑↑ $P < 0.0001$ based on the results of a one-way ANOVA with Tukey's post-hoc comparisons. / indicates $P >0.05$.

Gait Parameter	Exercise Group						
	Rest	Slow-Flat	Fast-Flat	Slow-Incline	Fast-Incline	Slow-Decline	Fast-Decline
% Swing Stride	/	/	/	/	/	/	/
% Brake Stride	/	/	/	/	/	/	/
% Propel Stride	/	/	/	/	/	/	/
% Stance Stride	/	/	/	/	/	/	/
% Brake Stance	/	/	/	/	/	/	/
% Propel Stance	/	/	/	/	/	/	/
Stance/Swing (real number)	/	/	/	/	/	/	/
Stride Length	/	/	/	/	/	/	/
Stride Frequency	/	/	/	/	/	/	/
Absolute Paw Angle	/	/	/	/	/	/	/
Stance Width	/	/	/	/	/	/	/
Step Angle	/	/	/	/	/	/	/
Paw Area at Peak Stance	/	/	/	↑↑↑↑	/	/	/
Hindlimb Shared Stance Time	/	/	/	/	/	/	/
% Shared Stance	/	/	/	/	/	/	/
Stance Factor	/	/	/	/	/	/	/
Gait Symmetry	/	/	/	/	/	/	/
Max dA/dT	/	/	/	↑↑↑↑	/	/	/
Min dA/dT	/	/	/	↓↓↓	/	↑↑↑↑	/
Tau Propulsion	/	/	/	/	/	/	/
Overlap Distance	/	/	/	↑↑↑	/	/	/
Paw Placement Positioning	/	/	/	/	/	/	/

Ataxia Coefficient	/	/	/	/	/	/	/
Midline Distance	/	/	/	/	/	/	/
Axis Distance (absolute value)	/	/	/	/	/	/	↓↓↓
Paw Drag (real number)	/	/	/	/	/	/	/

Table 5.2: Table summarizing statistical significance of all measured gait parameters for each exercise group (rest, slow-flat, fast-flat, slow-incline, fast-incline, slow-decline and fast-decline) after pre-conditioning compared to post-injury. Arrow (up vs. down) indicates directionality of statistically significant change and number of arrows indicate statistical significance (↑ $P < 0.05$, ↑↑ $P < 0.01$, ↑↑↑ $P < 0.001$, ↑↑↑↑ $P < 0.0001$ based on the results of a one-way ANOVA with Tukey's post-hoc comparisons. / indicates $P > 0.05$.

Gait Parameter	Exercise Group						
	Rest	**Slow-Flat**	**Fast-Flat**	**Slow-Incline**	**Fast-Incline**	**Slow-Decline**	**Fast-Decline**
% Swing Stride	/	/	/	/	/	/	/
% Brake Stride	/	/	/	/	/	/	/
% Propel Stride	/	/	/	/	/	/	/
% Stance Stride	/	/	/	/	/	/	/
% Brake Stance	/	/	/	/	/	/	/
% Propel Stance	/	/	/	/	/	/	/
Stance/Swing (real number)	/	/	/	/	/	/	/
Stride Length	/	/	/	/	/	/	/
Stride Frequency	/	/	/	/	/	/	/
Absolute Paw Angle	/	/	/	/	/	/	/
Stance Width	/	/	/	/	/	/	/
Step Angle	/	/	/	/	/	/	/
Paw Area at Peak Stance	/	/	/	/	↑↑↑↑	/	/
Hindlimb Shared Stance Time	/	/	/	/	/	/	/
% Shared Stance	/	/	/	/	/	/	/
Stance Factor	/	/	/	/	/	/	/
Gait Symmetry	/	/	/	/	/		/

Max dA/dT	/	/	/	/	↑↑↑↑	/	/
Min dA/dT	/	/	/	/	↓↓↓↓	/	/
Tau Propulsion	/	/	/	/	/	/	/
Overlap Distance	/	/	/	/	↑↑↑↑	/	/
Paw Placement Positioning	/	/	/	/	/	/	/
Ataxia Coefficient	/	/	/	/	/	/	/
Midline Distance	/	/	/	/	/	/	/
Axis Distance (absolute value)	/	/	/	/	↑↑↑	/	/
Paw Drag (real number)	/	/	/	/	/	/	/

Histology:

Minimal histologic differences were seen in the Achilles tendons between the injured limb and contralateral limb **(Figure 5.4).** In the fast-flat group, the injured limb showed increased tendon mid-substance chondroid metaplasia **(Figure 5.4, marked by black arrows)** relative to the contralateral control limb. Specifically, chondroid metaplasia ranged from mild to moderate in the fast-flat group. Notably, some minor peritenon hyperplasia was evident in the injured limb of the cage active and fast-flat groups **(Figure 5.4, marked by * for the former).** Lastly, both the cage active and fast-flat exercise groups showed mild to moderate modifications to the adjacent fat pad and bursae in the right injured limb relative to the left contralateral control limb, with minor changes seen in all other groups. Specifically, these changes included bursal synovial hyperplasia and increased presence of perivascular mononuclear cells.
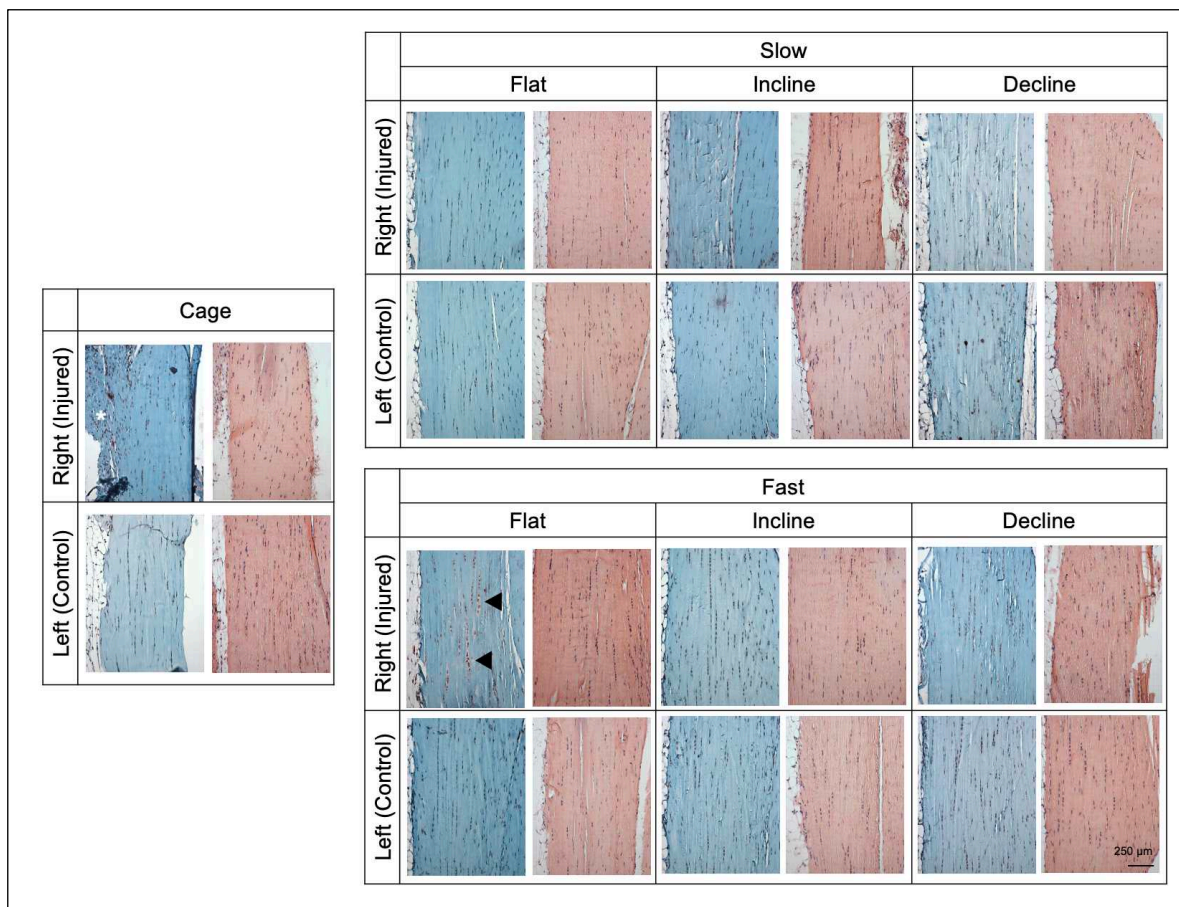
Figure 5.4. Representative SafraninO/Fast Green and Hematoxylin and Eosin (H&E) stained injured (right limb; top panels) and control (left limb; bottom panels) murine Achilles tendons for each experimental group. Each image is oriented as follows: top (proximal), bottom (distal), left (anterior), right (posterior). Arrows denote chondroid metaplasia and * denote peritenon hyperplasia.

COLX Serum Analysis:

All exercise groups showed significantly ($P<0.05$) less serum COLX than mice who did not receive exercise post-injury (cage activity, **Figure 5.5A**). Within the exercise groups, COLX was lowest in the slow-flat group, and highest in the decline groups irrespective of speed.
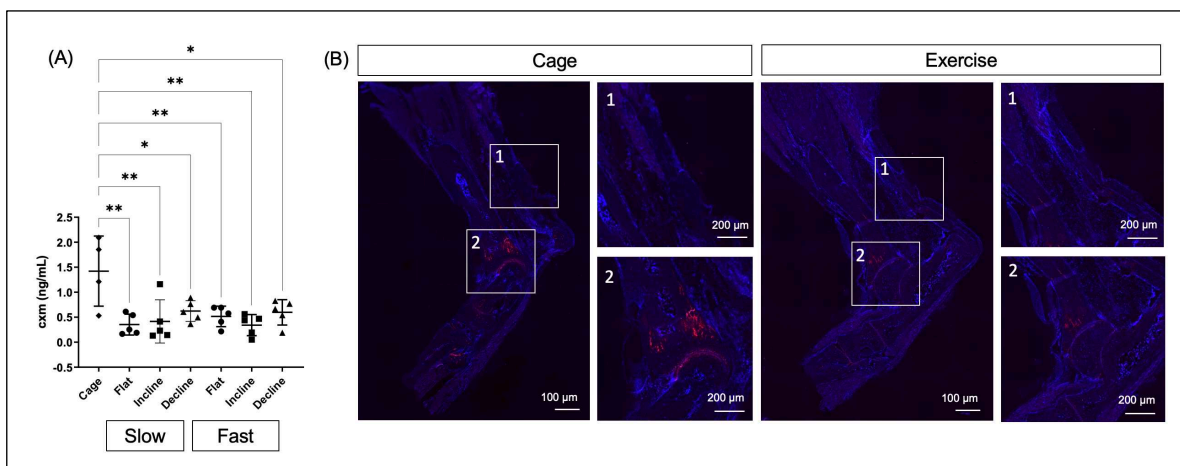
Figure 5.5: (A) Blood serum concentrations of collagen type X (COLX) for each experimental group. Data is presented as Mean +/- STD with individual data point marked. Statistically significance between groups is marked (*p<0.05, **p<0.01). (B) Representative COLX IHC stained mouse limbs for cage and exercise groups (blue: DAPI; red: COLX). Zoomed in areas represent (1) Achilles Tendon and (2) Tibiotarsal Joint.

COLX Immunohistochemistry:

For all groups, no positive COLX staining was observed in the Achilles tendon **(Figure 5.5B, callout 1)**, or calcaneal insertion. Notably, upon viewing joints within the distal hindlimb and foot, such as the tibial-tarso joint and interphalagal joints, subjective evaluation of fluorescence intensity for COLX IHC indicated that the highest fluorescence levels within the

articular cartilage tended to be in the cage active group **(Figure 5.5B, callout 2)**. Further, in other groups receiving exercise across all matched limb comparisons, the limb associated with tendon TGFβ1 injections (right hind) demonstrated higher COLX expression relative to contralateral limbs (left hind). Finally, fast exercise groups subjectively had higher levels of COLX within these joints compared to slow exercise groups.

5.5 Discussion

Given that few therapeutic interventions have proven superior to controlled exercise alone in the treatment of Achilles tendinopathy, the objective of this study was to advance the understanding of how alterations of speed and grade (flat vs. incline vs. decline) of exercise-based rehabilitation affect the quality of tendon healing using a translational murine model. Specifically, further understanding the relationship between exercise protocols and tendinopathic response would help provide evidence-based recommendations for exercise regimes as a physiotherapeutic modality to augment currently used tendon therapies.

The results of this study demonstrated that a fast-flat (non-eccentrically loaded) exercise protocol was the most detrimental to tendinopathic healing. This was substantiated by impaired braking (min dA/dT) and propelling (max dA/dT) gait abilities and histopathologic evidence of chondroid metaplasia. Additionally, serum (systemic) COLX levels were found to be highest in the cage-active group, while articular IHC COLX levels in articular joints were found to be highest in the fast exercise groups. Cumulatively, this study investigated exercise capacity, morphology, and functional outcomes to provide further insight into tendinopathic healing responses in relation to various exercise variables of exposure itself, speed and grade that are currently unknown.

131

An initial unexpected finding of this study was histopathologic evidence to suggest that pre-conditioning (exercise exposure itself prior to lesion induction) had a beneficial, protective effect in this murine model. Historically, a single injection of TGF-β1 into the body of the murine Achilles tendon has resulted in acute tendinopathic features of tendinous swelling, hyperplastic aggrecan-rich deposits and collagen disorganization accompanied by loss of tensile properties [10]. This early loss of biomechanical properties and matrix disorganization, however, was largely reversed by extended treadmill running, limiting its utility as an acute tendinopathic model only [10]. Subsequently, a two-injection lesion induction protocol (two injections of TGF-β1 performed two days apart, as used in the current study) was utilized that successfully simulated more severe injury, capturing acute, intermediate and chronic tendinopathic characteristics [12]. Previous histopathologic observations at day 14 post lesion induction demonstrated strong evidence of tendon swelling, collagen fiber disorganization, tendon mid-substance hypocellularity and peritendinous edema with hypercellularity [12]. This same two-injection TGF-β1 model was utilized herein, but interestingly, less chondroid metaplasia deposition, minor peritenon hyperplasia and less severe alterations in the adjacent fat pad and bursae in the injured limb compared to the uninjured contralateral limb were appreciated. In contrast to the previous investigation [12], the use of pre-conditioning as described herein prior to lesion induction may have subjectively reduced these more severe histologic findings. This finding, in conjunction with an increase in propelling capacity (max dA/dT) that was appreciated for day -15 to day -1 comparison (before vs after the pre-conditioning period but prior to injury induction) offers some evidence that preconditioning exercise to augment tendon 'fitness' may be protective against subsequent injury. This is not surprising given the extensive literature that has documented beneficial effects of exercise on tendon remodeling [5,7,20-22]. Specifically,

athletic loading has been documented to increase collagen turnover rates in naturally occurring Achilles tendinopathy as evidenced via serial microdialysis sampling [6]. Similarly, exercise has also been postulated to subsequently modify mechanical properties making tendons more load-resistant [20], and in a meta-analysis of exercise intervention studies on healthy adults, stiffness adaptation significantly depended on loading intensity [7]. Further work to delineate the mechanisms contributing to this protection is warranted, but similar to historic findings, the results described herein corroborate a beneficial, protective effect on tendinopathy when primed with exercise. This information is certainly worth noting as this tendinopathic model continues to be utilized in future studies.

When considering treatment regimens, mice exposed to fast-flat treadmill running demonstrated significantly decreased min dA/dT (braking capacity), increased max dA/dT (propelling capacity) and the most evidence of chondroid metaplasia compared to other exercise groups (rest/cage activity, slow-flat, fast-flat, slow-incline, fast-incline, slow-decline and fast-decline). When considered together, these findings suggest that the fast-flat exercise group has the most significantly impaired gait and deteriorated cellular qualities, respectively. Potential explanations for this include the absence of eccentric loading, the consistent exposure to fast speed itself, or a combination thereof. Given that similar findings were not appreciated in the other fast (fast-decline or fast-incline) or flat (slow-flat) exercise groups, authors speculate it is likely a combination of an impaired braking capacity (decreased min dA/dT) that resulted in compensatory propelling capacity (increased max dA/dT) due to the forced compulsory gait cycle that occurred with treadmill running post lesion induction. It may also be attributed to the fact that mice exposed to fast treadmill running in general had difficulty maintaining speed, which may have altered loading and potentially caused additional tendon micro-damage.

Biomechanical characteristics of *in-vivo* eccentric exercises in human Achilles tendons have been previously described, for which tendons were found to vibrate at higher frequencies during the eccentric phase than during the concentric phase [23]. Potential downstream effects that may subsequently reduce fortitude of tendons not exposed to eccentric exercise include incomplete activation of the motor neuron that occurs during concentric-only phases of exercise, or the lack of fibroblast stimulation amongst other various neural activation strategies that occurs with eccentric loading only [23]. Similarly, a systematic review concluded that tendon structural changes are not solely responsible for the positive effects of eccentric rehabilitation regimes, but rather neural, biochemical, and myogenic changes may be involved [5]. While the investigation herein did not focus on mechanistic explanations, the appreciated gait deficits and histopathologic characteristics of mice specifically exercised at a fast-flat speed highlight future potential avenues to assess interventional therapeutics.

In the present study, serum (systemic) COLX levels were found to be highest in the cage-active group. In contrast, articular IHC COLX levels were found to be highest in the fast exercise groups. It was noteworthy that no positive COLX staining was observed in the Achilles tendon or calcaneal insertion. These findings are intriguing because the relationship between COLX and exercise exposure specifically has not previously been reported but results herein suggest that cage activity alone (rest) leads to elevated systemic levels of COLX not appreciated in mice that were exercise-exposed. Given that cage activity mice demonstrated inferior morphologic and biomechanical gait patterns in comparison to those receiving exercise, and that rest in general is detrimental to tendinopathic healing [24-29], it would seem that longitudinal serum COLX levels may represent a future tendinopathic biomarker relationship to explore to non-invasively assess the quality or status of healing. It was also interesting to find that articular COLX levels were

highest in the fast exercise group, suggesting that chondrocyte stimulation through fast exercise exposure specifically results in increased COLX expression that was not similarly appreciated in slow or grade-related exercise. Overall, this suggests that further investigation into COLX expression patterns in relation to joint changes in the context of tendinopathy is warranted.

Acknowledged study limitations include the use of male mice, only; future work would consider both sexes. Further, consideration of age at time of injury would provide an interesting comparison. Of note, mice were 12 weeks old at the time of injury for historical comparison to previous studies utilizing this model. Finally, one predetermined timepoint was investigated based on outcomes utilized in previous studies. Inclusion of both earlier and later harvest days would allow longitudinal assessment of relevant outcomes.

In summary, mechanical loading through graduated, controlled exercise continues to be a fundamental aspect of tendon rehabilitation; however, there is a lack of studies investigating the specific thresholds of frequency, intensity, and duration in relation to the effect on healing. The major benefit of the proposed study design was the ability to relate exercise capacity, morphology, and functional outcomes to exercise using longitudinal tracking of individual animals. Through this investigation, exercise initiated at a fast speed and in absence of eccentric loading components demonstrated inferior tendinopathic healing at the cellular level and impaired braking abilities that were compensated for by increased propulsion. Mice exposed to exercise demonstrated higher systemic levels of COLX than those receiving cage rest, and mice exposed to fast exercise had the highest levels of articular COLX in comparison to slow exercise groups. These findings ultimately advance the understanding of how the intensity of exercise correlates to tendon injury and healing in a chronic tendon injury model, for which there currently is no peer-reviewed evidence to support.

References

1. Kvist M. Achilles tendon injuries in athletes. *Sports Medicine* 1994 18; 173-201.

2. Jarvinen M., Kannus P., Jarvinen TLN, et al. Histopathological findings in chronic tendon disorders. *Scand J Med Sci Sports* 2007; 7: 86-85.

3. Kannus P. Etiology and pathophysiology of chronic tendon disorders in sports. *Scand J Med Sci Sports* 1997; 7: 78-85.

4. Kujala UM, Sarna S, Kaprio J. Cumulative incidence of Achilles tendon rupture and tendinopathy in male former elite athletes. *Clin J Sport Med* 2005;15:133-135.

5. Drew BT, Smith TO, Littlewood C, et al. Do structural changes (eg, collagen/matrix) explain the response to therapeutic exercises in tendinopathy: a systematic review. *Br J Sports Med* 2014;48:966-972.

6. Langberg H, Ellingsgaard H, Madsen T, et al. Eccentric rehabilitation exercise increases peritendinous type I collagen synthesis in humans with Achilles tendinosis. *Scan J Med Sci Sports* 2007;17: 61-66.

7. Bohm S, Mersmann F, Arampatzis A. Human tendon adaptation in response to mechanical loading: a systematic review and meta-analysis of exercise intervention studies on healthy adults. *Sports Med* 2015; 1-7.

8. Rees JD, Lichtwark GA, Wolman RL, et al. The mechanism for efficacy of eccentric loading in Achilles injury; an in vivo study in humans. Rheumatology 2008;47:1493-1497.

9. Konsgaard M, Kovanen V, Aagaard P, et al. Corticosteroid injections, eccentric decline squat training and heavy slow resistance training in patellar tendinopathy. *Scand J Med Sci Sports* 2009;19:790–802.

10. Bell R, Li J, Gorski et al. Controlled treadmill exercise eliminates chondroid deposits and restores tensile properties in a new murine tendinopathy model. *J Biomech* 2013;46: 498-505.

11. Jacobson E, Dart A, Mondori T, et al. Focal experimental injury leads to widespread gene expression and histologic changes in equine flexor tendons. *PLoS ONE* 2015; 10(4): e0122220.doi:10.1371/journal.pone.0122220.

12. Trella KJ, Li J, Stylianou E, et al. Genome-wide analysis identifies differential promoter methylation of Leprel2, Foxf1, Mmp25, Ifgbp6, and Peg12 in murine tendinopathy. *J Orthop Res* 2017 35:947-955.

13. Bogin O, Kvansakul, Rom E, et al. Insight into Schmid metaphyseal chondrodysplasia from the crystal structure of the collagen X NC1 domain trimer. *Structure* 2002;10:165-173.

14. Shen G. The role of type X collagen in facilitating and regulating endochondral ossification of articular cartilage. *Orthod Craniofacial Res* 2005;8:11-17.

15. Coghlan RF, Oberdorf JA, Sienko S, et al. A degradation fragment of type X collagen is a real-time marker for bone growth velocity. *Sci Transl Med* 2017; 9: eaan4669.

16. Goldring MB, Berenbaum F. Emerging targets in osteoarthritis therapy. *Curr Opin Pharmacol* 2015;22:51-63.

17. He Y, Siebuhr AS, Brandt-Hansen NU, et al. Type X collagen levels are elevated in serum from human osteoarthritis patients and associated with biomarkers of cartilage degradation and inflammation. *BMC Musculoskelet Disord* 2014; 15:209.

18. Fujioka H, Wang JG, Mizuno K, et al. Changes in the expression of type-X collagen in the fibrocartilage of rat achilles tendon attachment during development. *J Orthop Res* 1997;15:675-681.

19. Fukuta S, Oyama M, Kavalkovich K, et al. Identification of types II, IX and X collagens at the insertion site of the bovine achilles tendon. *Matrix Biol* 1998;17(1):65-73.

20. Kjaer M, Magnusson P, Krogsgaard M, et al. Extracellular matrix adaptation of tendon and skeletal muscle to exercise. *J Anat* 2006;208: 445-450.

21. Spiesz EM, Thorpe CT, Chaudhry S, et al. Tendon extracellular matrix damage, degradation and inflammation in response to in vitro overload exercise. *J Orthop Res* 2015; 33:889-897.

22. Svensson RB, Heinemeier KM, Couppe C, et al. Effects of aging and exercise on tendon. *J Appl Physiol* 2016;121: 1353-1362.

23. Henricksen M, Aaboe J, Bliddal H, et al. Biomechanical characteristics of the eccentric Achilles tendon exercise. *J Biomech* 2009;42: 2702-2707.

24. Enwemeka CS. Functional loading augments the initial tensile strength and energy absorption capacity of regenerating rabbit achilles tendons. Am J Phys Med Rehabil 1992;71(1):31-38.

25. Enwemeka CS, Spielholz NI, Nelson AJ. The effect of early functional activities on experimentally tenotomized achilles tendons in rats. *Am J Phys Med Rehabil* 1988;67(6):264-269.

26. Andersson TP, Eliasson P, Aspenberg P. Tissue memory in healing tendons: short loading episodes stimulate healing. J Apply Physiol 2009;107(2): 417-421.

27. Palmes D, Spiegel HU, Schneider TO, et al. Achilles tendon healing: long-term biomechanical effects of postoperative mobilization and immobilization in a new mouse model. *J Orthop Res* 2002;20:939-946.

28. Murrell GAC, Lilly EG, Goldner RD, et al. Effects of immobilization on achilles tendon healing in a rat model. *J Orthop Res* 1994;12:582-591.

29. Virchenko O, Aspenberg P. How can one platelet injection after tendon injury lead to a stronger tendon after 4 weeks?: Interplay between early regeneration and mechanical stimulation. *Acta Orthop* 2006;77(5):806-812.

CHAPTER 6 - Novel Equine Rehabilitation Modalities: Safety Validation of Equine Blood Flow Restriction Training[4]

6.1 Overview

Background: Blood flow restriction (BFR) has become a key rehabilitative tool for human orthopedic conditions. With modernized technology and evolution of clinical application, patient-specific delivery of occlusion percentages is now considered the standard of care in human patients due to improved therapeutic outcomes and minimized safety risks. Safety validation and limb occlusion pressure (LOP) data for horses, however, is lacking.

Objective: The objectives of this study were: 1) To determine if BFR exposure resulted in forelimb biomechanical gait dysfunction and 2) To investigate inter-horse and inter-limb LOP differences.

Study Design: Prospective, controlled pilot experiment.

Methods: Daily unilateral forelimb BFR was performed in four horses over 56 days. Clinical examinations and objective gait analyses were performed on study days 0, 28 and 56. Daily LOP values were determined by Doppler evaluation to deliver 80% vascular occlusion at a walk. A linear mixed model was utilized to evaluate for differences in lameness, kinetic and kinematic gait parameters.

Results: There were no significant differences in forelimb lameness, kinematic or kinetic gait parameters over time or between BFR-exposed and control (contra-lateral) limbs ($P > 0.05$). Clinically apparent complications related to BFR such as thrombosis or dermatitis were not appreciated. Significant differences in mean LOP values between various horses ($P < 0.001$) and

---

[4] This chapter includes the submitted manuscript: Johnson SA, Frisbie DD, Griffenhagen GM, King MR. Equine Blood Flow Restriction Training: Part I Safety Validation. *Equine Vet J.* Minor revisions submitted 10/5/2022. This article is reproduced with permission from the Editor, Equine Veterinary Journal.

measured left (204.48mm Hg) and right (173.78mmHg) forelimbs ($P < 0.001$) were observed. Mean LOP and standard deviation across all readings was 189.1 ± 22.2mm Hg.

Main Limitations: Optimal BFR occlusion percentages and subsequent walk protocols with documented clinical efficacy are unknown. Small study population for pilot investigation.

Conclusions: Exposure to BFR did not result in forelimb biomechanical dysfunction in four horses. Applied pressures of 75-151 mm Hg would likely simulate a range of 50-80% vascular occlusion in horses, but inherent physiologic variation between horses and forelimbs warrants incorporation of individual pressures.

6.2 Introduction

Low load exercise training with blood flow restriction (BFR) involves application of a specialized tourniquet to temporarily reduce blood flow to an exercising limb. Human patients incorporating BFR into rehabilitative programs are able to increase strength and muscular hypertrophy using only light weights or low-intensity exercise (cycling or walking) while still getting the muscular response as if heavy loads were being used [1]. This technology has transformed traditional rehabilitative approaches for a variety of orthopedic injuries requiring greatly reduced workloads such as knee osteoarthritis [2], soft tissue injuries [3] and geriatric sarcopenia [4]. In essence, BFR is being used to increase strength via low intensity training to a level typically only achieved with mid to high intensity training. In a recent survey of human physical therapists, 46% were incorporating BFR into rehabilitative programs, with 80% of practitioners rating its use as very good to excellent [5]. With the ability to strengthen surrounding musculature without exposing healing tissue to damaging loads, physical therapists can more safely and efficiently prepare tissue to return to work [6]. Subsequently, BFR has

become a key rehabilitative tool for a variety of human orthopedic conditions and conditioning experts are using it to maintain peak muscular strength in absence of damaging loads. Its clinical use has significantly modernized traditional rehabilitative approaches previously limited by exercise restriction, with 33% of practitioners using it to increase muscle mass and 24% utilizing it to rehabilitate injuries [5].

While numerous studies have been performed validating human BFR use with compelling results [2,7-8], investigations to assess equine-specific application are considerably sparse [9-13]. An initial pilot study evaluated cuff application to a single equine forelimb (n = 6) using an occlusion pressure of 200mm Hg applied only at rest [9]. Following three sets of occlusion for five minutes, muscle thickness was assessed ultrasonographically. The authors noted that extensor and flexor muscle thickness was increased in the occluded limb, but not the control limb. Authors concluded that acute vascular occlusion may be safe and tolerable in horses [9]. Subsequently, the same research group confirmed that horses would tolerate BFR at a walk pace [10]. Specifically, six unfit Standardbred mares performed BFR of both forelimbs at a walk pace with 200-230mm Hg cuff pressure for 10 minutes, once per day, 6 days per week for a total of two weeks. Skeletal muscle thickness and tendon thickness were assessed ultrasonographically and serum growth hormone (GH) concentrations were determined 5, 15 and 60 minutes following BFR exercise sessions. Authors confirmed that similar to humans, BFR use in horses resulted in elevations in GH (at all three evaluated timepoints) and muscular hypertrophy [10].

With modernized technology and evolution of clinical application, patient-specific delivery of BFR occlusion percentages (instead of applying static predetermined pressures to all patients) is now considered the standard of care in human patients [14-15] due to improved

141

therapeutic outcomes, increased comfort, and minimized safety risks [14]. Specifically, the limb

occlusion pressure (LOP) is defined as the minimum amount of pressure required to occlude

vascular flow (pressure resulting in complete venous and arterial occlusion) [14-15]. Subsequent

clinician-prescribed occlusion percentages (usually in the 40-80% occlusion range) [14] are then

calculated from this LOP value to safely and effectively deliver BFR. In contrast to the use of

blanket occlusion methodology in the aforementioned equine investigations [9-10], only one

recent study describes short-term beneficial effects of BFR on equine superficial digital flexor

(SDF) muscle oxidative capacity over a 10-day study period utilizing patient-specific pressures

determined through machine prompts and confirmed with power doppler ultrasound [11-12].

Specifically, SDF muscle oxidative capacity increases were consistent with acute metabolic

adaptations of increased mitochondrial density and an improved ability to oxidize fuels [11-12].

While these initial findings are encouraging, safety validation for more long-term application of

patient-specific BFR for use in the horse is still lacking. Additionally, forelimb LOP values and

their inherent physiologic variation over time in the standing, un-sedated horse are currently

undetermined. Therefore, the objective of this study was two-fold: 1) To determine if BFR

exposure resulted in forelimb biomechanical gait dysfunction that would manifest as subjective

or objective lameness; 2) To determine inter-horse and inter-limb (left forelimbs compared to

right forelimbs) LOP value differences that are currently unknown. Providing this information to

clinicians is expected to help guide safe BFR clinical use in the horse.

6.3 Materials and Methods

Experimental Animals:

This study was a controlled prospective pilot experiment. All study methods were

conducted in compliance with the University's Institutional Animal Care and Use Committee

(IACUC, protocol #1013). Enrolled horses (n = 4) were purchased from an outside vendor and showed no evidence of current or previous osseous or soft tissue forelimb abnormalities on baseline lameness evaluation and ultrasonographic evaluation of the forelimb flexor tendons, accessory ligament of the deep digital flexor tendon and carpal canal.

Treadmill Acclimation:

All horses were acclimated to a treadmill through once daily exposures to an Equigym high-speed treadmill for 14 days. This exposure consisted of a 10-minute exercise period (brisk walk at a velocity of 3.5-3.7 mph), followed by a five-minute rest period. Horses were also acclimated to the application of a surcingle during this time.

Limb Occlusion Pressure Determination:

All forelimbs were circumferentially clipped with a #40 blade throughout the study period. Horses were randomly assigned to left or right forelimb BFR application using a random number generator. Each contralateral (unexposed) forelimb served as an internal control for further investigative purposes not reported herein. For all BFR sessions (n = 4 horses, 2 exposed right forelimbs and 2 exposed left forelimbs), limb occlusion pressures (LOP) of the BFR-exposed limbs were obtained immediately prior to each daily session by Doppler evaluation. The LOP was defined as the amount of pressure required to achieve 100% vascular occlusion. A standard human BFR cuff manufactured by Delfi Medical Innovations[5], Inc was utilized for all aspects of LOP assessment and BFR delivery for this study. Specifically, the Delfi Personalized Blow Flow Restriction Rehabilitation (PBFRR) blood pressure cuff was placed 6 inches distal to

---

[5] Delfi Medical Innovations, Inc. Vancouver, BC, Canada

the olecranon at the level of the mid to proximal antebrachium, at the same location as the cuff placement during BFR walk sessions (Figure 6.1A). The piezoelectric doppler probe was placed just distal to the blood pressure cuff and positioned so a clear distal pulse of the median artery was heard (Figure 6.1B). The blood pressure cuff was then inflated using the manual pressure regulator option on the Delfi system up to the pressure at which the distal pulse was no longer audible [16]. The value in mmHg for which the pulse of the median artery was no longer audible was then recorded as the LOP and utilized to calculate the specified 80% vascular occlusion. Resurgence of the median artery pulse with cuff deflation was confirmed for all successful Doppler readings to ensure probe placement remained accurate. All LOP determinations were measured by the same observer blinded to real-time numeric LOP measurements with horses in a standing, (un-sedated with the limb fully-weighted) square position within the same barn location.

Fig 6.1: Acquisition of Doppler limb occlusion pressure (LOP) reading in the standing, unsedated horse immediately prior to BFR walk exercise (6.1A). The blood pressure cuff was inflated using the manual pressure regulator option on the Delfi system up to the pressure at which the distal pulse was no longer heard. Once the Doppler LOP value was obtained, it was used to back-calculate 80% vascular occlusion pressure that was subsequently applied through the pressurized cuff. Note piezoelectric Doppler probe placement immediately distal to the cuff along the medial aspect of the limb to obtain the pulse of the median artery (6.1B).

Blood Flow Restriction Exercise:

The previously described blood pressure cuff was placed 6 inches distal to the olecranon within the mid to proximal antebrachium (Figure 6.1) during walk exercise. All BFR limbs were appropriately fitted to an Easi-Fit Tourniquet Cuff 24" in circumference as previously described (Figure 6.2) [11-12]. The personalized tourniquet system (PTS) matching limb protection sleeve was applied underneath each tourniquet and secured with elastic adhesive tape to circumvent any inadvertent dermatitis (Figure 6.2). A small bungee (elastic) cord was used to suspend the cuff to a surcingle ring to avoid any cuff slippage. Each BFR session was performed by the same

investigator who has clinical experience in the use of the PTS, completed the Owens Recovery

Science BFR certification course and initial pilot experimentation [11-12].
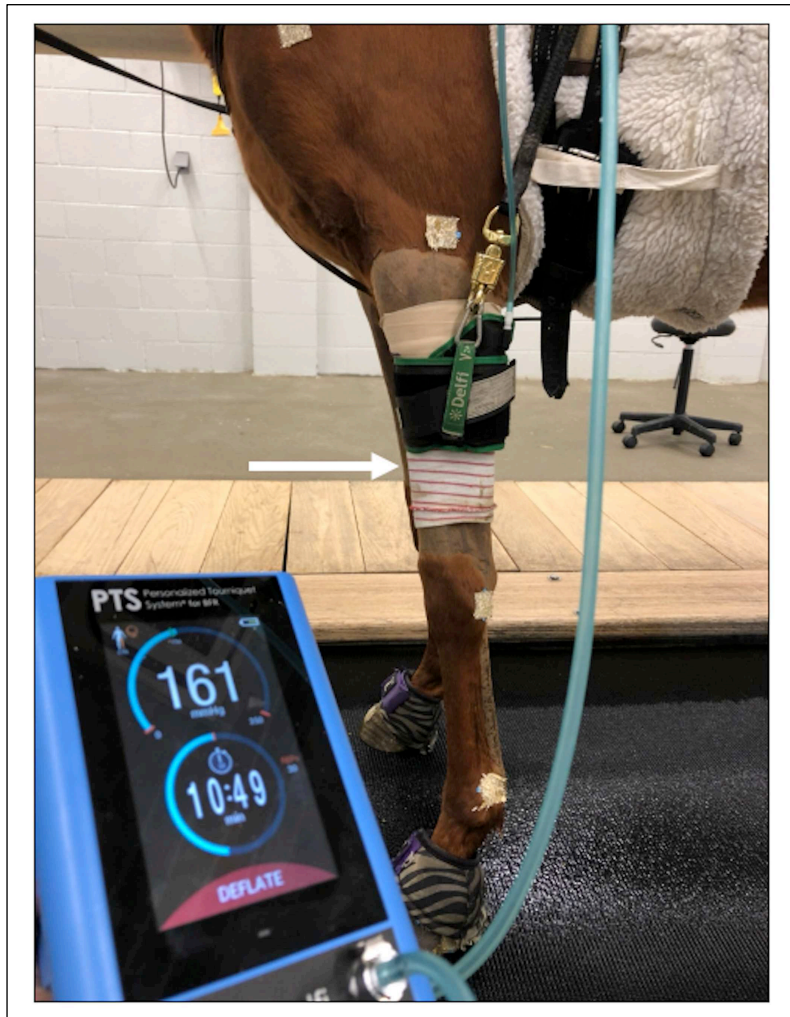
Fig 6.2. Application of a limb protection sleeve (white arrow) secured with elastic adhesive tape and inflated BFR cuff to the left forelimb of a horse in preparation for walk exercise. With light suspension, the band remained in position within the proximal antebrachium at 80% vascular occlusion. The personalized tourniquet system (PTS) developed by Delfi Medical Innovations, Inc. dynamically adjusted pressure to maintain 80% LOP pressure during all BFR sessions.

Each BFR exercise session began with a 3-minute warm-up period at a velocity of 3.5-3.7

mph (brisk walk, with no BFR cuff or limb protection sleeve). Following the 3-minute warm-up

period, the limb protection sleeve was secured with elastic adhesive tape, the PTS was placed

and the doppler-determined 80% vascular occlusion was applied to the BFR-exposed forelimb.

The randomly assigned contralateral (control) forelimb of each horse was not exposed to a limb protection sleeve or any BFR occlusion. Horses then walked at a velocity of 3.5-3.7 mph for a total walk time of 10 minutes at the following interval protocol: 4-minutes walk, 1-minute rest (standing quietly on the land treadmill), 3-minutes walk, 1-minute reset, 3-minutes walk [11-12]. The PTS remained inflated for the duration of the walk-rest exercise protocol (constant operator supervision during each BFR session and machine prompts confirmed successful cuff inflation for the entire walk period). Following the session, the PTS was immediately deflated, removed and the horse underwent a 3-minute supervised recovery period (standing quietly in the barn aisle) before returning to its stall. BFR walking exercise was performed 5 days/week for the 56-day study period. Cuff leak tests were performed, and pressure readings were validated once weekly with a Mercury manometer throughout the duration of the study to ensure accurate pressure delivery and cuff maintenance.

Clinical Evaluation:

Both forelimbs of all horses were evaluated for clinically apparent swelling, dermatitis, sensitivity and vascular thrombosis of the median artery and vein (via grey-scale ultrasound) on study dates 0, 28 and 56 (Figure 6.3). Forelimbs were palpated in standard fashion and any evidence of flexor tendon thickening or sensitivity was noted. Additionally, palpable effusion of the radiocarpal and middle carpal joints was graded on a 0 to 4 scale (0 = no effusion; 4 = marked effusion). Clinical lameness evaluations were also performed on study dates 0, 28 and 56 (Figure 6.3) with lameness subjectively graded using the American Association of Equine Practitioners (AAEP) scale of 0 to 5. All passive and clinical examinations were performed by an

experienced, board-certified specialist in equine sports medicine and rehabilitation (DACVSMR) blinded to forelimb BFR-exposure assignment.
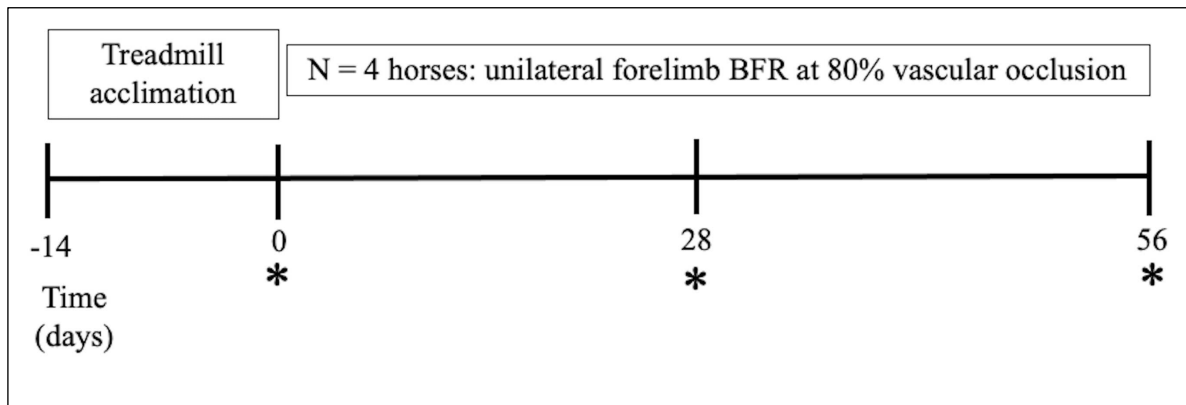
Fig 6.3: Following 14 days of treadmill acclimation, unilateral forelimb BFR walking exercise at 80% vascular occlusion was performed once/day for 5 days/week for a 56-day study period. On days 0, 28 & 56, clinical, kinetic and kinematic evaluations were performed (*). Doppler limb occlusion pressure (LOP) readings were obtained daily immediately prior to BFR walking sessions.

Kinetic Gait Analysis:

Kinetic and kinematic gait analysis was performed on study dates 0, 28 and 56 (Figure 6.3). Specifically, ground reaction forces (GRFs) for all 4 limbs were recorded using 2 strain-gauge based force platforms (60 x 90-cm) mounted sequentially in an isolated concrete base in the center of a 25-m runway as previously described [17]. A kinetic trial was considered successful when ipsilateral thoracic and pelvic limb pairs contacted the center of a single force platform. Five valid trials were collected during each time point. Orthogonal GRF data were sampled at 2000 Hz; however, only the vertical and craniocaudal GRFs were analyzed for this study. The following kinetic parameters were calculated from each trial: stance duration, peak vertical, braking and propulsive forces and impulses and vertical loading rates. Kinetic variables were averaged across the five trials and normalized to subject body mass and expressed as N/kg or Ns/kg.

Kinematic Gait Analysis:

The Orthopaedic Research Center Gait Analysis Laboratory equipped with 10 Oqus 7, Qualysis 3-D motion capture cameras centered around the capture volume containing the force platforms was utilized for all kinematic gait analysis. The Qualysis track manager software recorded and calculated real time 2-D with 6 degrees of freedom motion data. The software also supported the force plates so that the analog signals and motion capture were synced and directly correlated to each other. For data collection and analysis, 12.7mm retro-reflective markers were adhered to the skin over the centers of joint rotation as previously described [17]. Once identified, each center of joint rotation was clipped and marked with permanent red lacquer to ensure consistent marker placement for subsequent gait analyses. Thoracic limb joint angles were calculated on the basis of the anatomic flexor surface of each joint. Raw coordinate data was filtered with a low-pass fourth-order recursive Butterworth filter at 12 Hz. Kinematic variables calculated for each trial included range of motion, maximum and minimum joint angles during the stance and swing phases and time to peak joint angles during each stride. All kinetic and kinematic gait analysis data acquisition was performed by a board-certified specialist in equine sports medicine and rehabilitation (DACVSMR) experienced in objective gait analysis and blinded to treatment groups.

Statistical Analysis:

Following professional statistical consultation, all statistical analysis was performed by a board-certified specialist in equine sports medicine and rehabilitation (DACVSMR) using the

software package RStudio[6]. To investigate the relationships between BFR exposure and response variable of kinetic, kinematic and subjective lameness, a linear mixed model was fit. To account for the design of data collection, the model included fixed effects of treatment, date and treatment by date and random effect of horse. Diagnostic plots were used to assess assumptions of equal variance and normality. Based on these plots, assumptions were met. Comparisons across date and exposure were conducted utilizing the lmer4 and emmeans packages. Tukey's adjustment of *P*-values for pairwise comparisons were used. To evaluate mean LOP differences between horses, a one-way analysis of variance (ANOVA) with post-hoc Tukey's adjustment of *P* values for pairwise comparisons was utilized. Mean LOP differences between left and right forelimbs was evaluated using a Student's t-test. Statistical significance was considered *P* < 0.05 for all analyses.

6.4 Results

Clinical Evaluation:

A total of two left and two right forelimbs (n = 4 forelimbs) of four horses (n = 4 horses, three mares and one gelding, ages 2-3 years) were exposed to 40 BFR-walk sessions over a 56-day study period. No evidence of venous or arterial thrombosis was noted in any horse at any evaluation timepoint based on clinical and/or ultrasonographic evaluation. No evidence of dermatitis, swelling, thickening or sensitivity was noted on standard forelimb palpation evaluation. No statistically significant differences in forelimb lameness were appreciated over time (Table 6.1A, *P* > 0.05) or between BFR-exposed and control (contra-lateral) limbs (Table 6.1B, *P* > 0.05). None of the forelimbs demonstrated any subjectively assessed radiocarpal or middle carpal joint effusion > 0 at any study time point (Table 6.2). All radiocarpal and middle

---

[6] R-project®, R Foundation for Statistical Computing Vienna, Austria

carpal effusion scores and forelimb AAEP lameness values for all study dates are reported in

Table 6.2.

Table 6.1: Reported estimates, standard errors (SE) and *P*-values based on the results of a linear mixed model with Tukey's pairwise comparisons for subjectively assessed lameness scores between the various study time points (Table 6.1A) and between BFR-exposed and control (contra-lateral) forelimbs at all study time points (Table 6.1B). No statistically significant differences in forelimb lameness were appreciated over time (Table 6.1A, *P* > 0.05) or between BFR-exposed and control (contra-lateral) forelimbs (Table 6.1B, *P* > 0.05).

Table 6.1A: Tukey's pairwise comparison values comparing subjective lameness scores between various study time points for BFR-exposed and control (contra-lateral) forelimbs.

	Control (Contra-lateral) Limbs			BFR Limbs		
Study Date Comparison	Estimate	Standard Error (SE)	*P* value	Estimate	Standard Error (SE)	*P* value
0 vs 28	-0.25	0.54	0.89	0	0.54	1.0
0 vs 56	0.25	0.54	0.89	-0.63	0.54	0.50
28 vs 56	0.50	0.54	0.64	-0.63	0.54	0.50

Table 6.1B: Tukey's pairwise comparison values comparing subjective lameness scores between BFR-exposed and control (contra-lateral) forelimbs at evaluated study time points of 0, 28 and 56 days.

Study Date	Estimate	Standard Error (SE)	*P* value
0	0.75	0.54	0.19
28	1.0	0.54	0.09
56	-0.13	0.54	0.82

Table 6.2: Table summarizing subjectively assessed radiocarpal/middle carpal joint effusion and forelimb lameness at all evaluated time points (days 0, 28 and 56). All examinations were performed by an experienced, board-certified specialist in equine sports medicine and rehabilitation (DACVSMR) blinded to forelimb treatment groups. Radiocarpal/middle carpal joint effusion was graded on a 0 to 4 scale (0 = no effusion; 4 = marked effusion); forelimb lameness was recorded using the American Association of Equine Practitioners (AAEP) scale of 0 to 5.

Horse	Forelimb *indicates BFR-exposed forelimb	Study Date	Radiocarpal & Middle Carpal Joint Effusion (Scale of 0 to 4)	Grade of Forelimb Lameness (0 to 5 AAEP Scale)
	LF	0	0	0
		28	0	0
		56	0	0
2	RF*	0	0	0
		28	0	0
		56	0	1
	LF	0	0	0
		28	0	2
		56	0	0
4	RF*	0	0	0
		28	0	0
		56	0	1.5
	*LF	0	0	0
		28	0	0
		56	0	0

6		0	0	1.5
	RF	28	0	2
		56	0	2
		0	0	0
	*LF	28	0	0
		56	0	0
7		0	0	1.5
	RF	28	0	0
		56	0	0

Kinematic & Kinetic Gait Analysis:

No significant differences in a total of 20 evaluated kinematic/kinetic forelimb gait parameters on study days 0, 28 and 56 were observed in BFR-exposed limbs compared to control (contra-lateral) limbs over time ($P > 0.05$). Estimates, standard errors and P-values for all pair-wise comparisons are presented in Table 6.3.

Table 6.3: Reported estimates, standard errors (SE) and *P*-values based on the results of a linear mixed model with Tukey's pairwise comparisons for all evaluated kinematic and kinetic gait parameters comparing the various study time points (0, 28 and 56 days) of blood flow restriction (BFR) exposure in four horses.

Gait Parameter	Study Date Comparison	Estimate	Standard Error (SE)	*P* value
Stance duration (ms)	0 vs 28	13.00	8.35	0.27
	0 vs 56	-4.25	8.35	0.87
	28 vs 56	-17.25	8.35	0.10
Stride Length (m)	0 vs 28	-0.11	0.06	0.12
	0 vs 56	-.03	0.06	0.83
	28 vs 56	0.08	0.06	0.35
Velocity (s)	0 vs 28	-0.13	0.08	0.24
	0 vs 56	-0.00	0.08	0.99
	28 vs 56	0.13	0.08	0.25
Head Height Stance Phase (m)	0 vs 28	-0.0003	0.01	0.99
	0 vs 56	-0.005	0.01	0.92
	28 vs 56	-0.01	0.01	0.65

Head Height Swing Phase (m)	0 vs 28	-0.03	0.01	0.13
	0 vs 56	-0.008	0.01	0.83
	28 vs 56	0.02	0.01	0.34
Peak Vertical Force (N/kg)	0 vs 28	-4.06	0.29	0.34
	0 vs 56	0.12	0.29	0.91
	28 vs 56	0.52	0.29	0.17
Peak Braking Force (N/kg)	0 vs 28	-0.02	0.12	0.98
	0 vs 56	-0.05	0.12	0.89
	28 vs 56	-0.03	0.12	0.96
Peak Propulsion Force (N/kg)	0 vs 28	-0.07	0.10	0.79
	0 vs 56	-0.02	0.10	0.99
	28 vs 56	0.05	0.10	0.88
Vertical Impulse (Ns/kg)	0 vs 28	0.01	0.05	0.99
	0 vs 56	-0.003	0.05	0.99
	28 vs 56	-0.01	0.05	0.97
Braking Impulse (Ns/kg)	0 vs 28	-4.68×10^3	0.02	0.95
	0 vs 56	-3.02×10^3	0.02	0.98
	28 vs 56	1.66×10^3	0.02	0.99
Propulsion Impulse (Ns/kg)	0 vs 28	-0.004	0.01	0.93
	0 vs 56	-0.003	0.01	0.96
	28 vs 56	0.001	0.01	0.99
Shoulder Range of Motion	0 vs 28	-0.78	1.27	0.84
During Stance Phase (degrees)	0 vs 56	-0.23	1.27	0.98

	28 vs 56	0.50	1.27	0.92
Elbow Range of Motion During	0 vs 28	1.22	1.87	0.79
Stance Phase (degrees)	0 vs 56	0.79	1.87	0.91
	28 vs 56	-0.42	1.87	0.97
Carpal Range of Motion	0 vs 28	1.56	1.21	0.41
During Stance Phase (degrees)	0 vs 56	1.42	1.21	0.48
	28 vs 56	-0.15	1.21	0.99
Fore Fetlock Range of Motion	0 vs 28	0.19	1.2	0.99
During Stance Phase (degrees)	0 vs 56	1.18	1.2	0.59
	28 vs 56	0.99	1.2	0.69
Shoulder Range of Motion	0 vs 28	-0.68	1.31	0.86
During Swing Phase (degrees)	0 vs 56	-0.03	1.31	0.99
	28 vs 56	0.65	1.31	0.87
Elbow Range of Motion During	0 vs 28	-0.14	1.8	0.99
Swing Phase (degrees)	0 vs 56	-0.64	1.8	0.93
	28 vs 56	-0.50	1.8	0.96
Carpal Range of Motion	0 vs 28	1.55	2.13	0.75
During Swing Phase (degrees)	0 vs 56	-0.78	2.13	0.93
	28 vs 56	-2.33	2.13	0.52
Fore Fetlock Range of Motion	0 vs 28	0.67	3.06	0.97
During Swing Phase (degrees)	0 vs 56	2.75	3.06	0.65
	28 vs 56	2.08	3.06	0.78

Limb Occlusion Pressure Measurements:

Forty LOP readings for each forelimb (n = 4) were obtained for a total of 160 readings of four horses over the 56-day study period. Mean LOP values across all timepoints in mm Hg with corresponding standard deviation values for each horse were as follows: 172.8 ± 17.1, 174.8 ± 19.3, 200.7 ± 15.6, 208.3 ± 12.1, respectively. Mean LOP and standard deviation across all readings was 189.1 ± 22.2mm Hg with all readings graphically depicted in Figure 6.4. Statistically significant differences in pairwise comparisons of mean LOP values between horses were appreciated for which mean differences, 95% confidence intervals (CIs) and *P*-values reported in Table 6.4. A statistically significant difference in mean LOP values between measured left and right forelimbs was appreciated, with a mean of 173.78 mm Hg for right forelimbs and 204.48 mm Hg for left forelimbs, respectively (*P* <0.0001).

No cuff leaks were identified on weekly inspection, and all cuff pressure readings were within 2mm of the Mercury manometer value indicating accurate pressure delivery and maintenance.

Table 6.4: Mean limb occlusion pressure (LOP) differences between horses with upper and lower 95% confidence intervals and *P*-values based on one-way ANOVA and post-hoc Tukey's pairwise comparisons.

| Between Horse Comparison	Mean Limb Occlusion Pressure (LOP) Difference	Lower 95% Confidence Interval Value	Upper 95% Confidence Interval Value	*P*-value
Horse 4 vs. Horse 2	2.00	-7.45	11.45	0.95
Horse 6 vs. Horse 2	27.93	18.47	37.38	<0.0001
Horse 7 vs. Horse 2	35.48	26.02	44.93	<0.0001
Horse 6 vs. Horse 4	25.93	16.47	35.38	<0.0001
Horse 7 vs. Horse 4	33.48	24.02	42.93	<0.0001
Horse 7 vs. Horse 6	7.55	-1.90	17.00	0.17
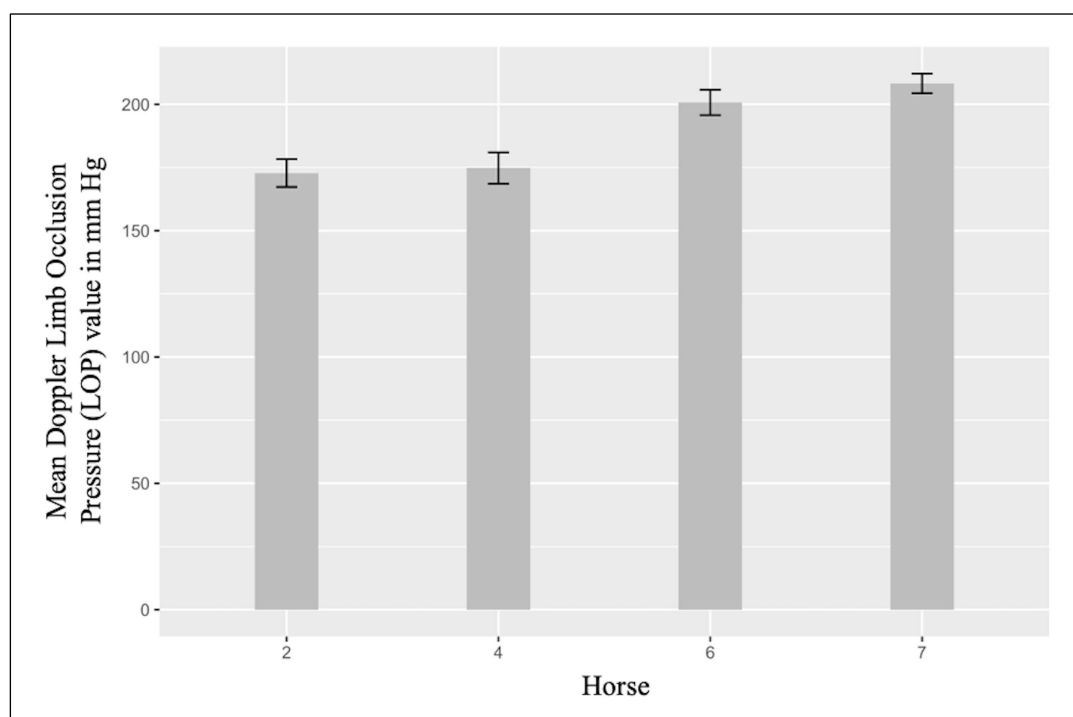
Fig 6.4: Mean doppler limb occlusion pressure (LOP) values and 95% confidence intervals for each horse (n = 4) during the 56-day study period.

6.5 Discussion

This study sought to explore safety, patient tolerance and general suitability of this novel rehabilitation modality for horses prior to clinical incorporation through assessment of longitudinal subjective and objective forelimb gait analyses in addition to clinical evaluations. The results of this pilot investigation indicate that BFR exposure did not alter or negatively impact forelimb biomechanical gait parameters assessed in this four-horse study population. Complications related to BFR such as consistent forelimb lameness, thrombosis or dermatitis were not appreciated. Mean LOP and standard deviation values across all readings were 189.1 ± 22.2mm Hg. This data suggests that occlusion pressures of 75-151 mm Hg would likely simulate a range of 50-80% vascular occlusion in horses, but significant differences between mean LOP values between horses and measured left and right forelimbs were noted suggesting that the inherent physiologic variation appreciated warrants continued incorporation of individual patient pressures for optimized BFR application.

No statistically significant differences in subjectively-assessed forelimb lameness were appreciated over time (Table 6.1A,) or between BFR-exposed and control (contra-lateral) limbs (Table 6.1B). No significant differences in any of the objectively assessed (kinetic/kinematic) forelimb gait parameters were observed in BFR-exposed limbs compared to control (contra-lateral) limbs over time (Table 6.3). Subjective lameness evaluations suggested that mild forelimb lameness was present in the BFR-exposed limbs of two horses at the 56-day evaluation only, for which corresponding changes in objective gait parameters were not appreciated. Additionally, mild (consistent) forelimb lameness was also observed in the non-BFR exposed

limbs that did not worsen over time nor result in deteriorated kinetic/kinematic gait parameters assessed over time, suggesting that the utilized study horse population demonstrated mild degrees of oscillating forelimb lameness in absence of BFR exposure. Inherent differences between subjective and objective gait analysis agreement have been well documented, but other potential explanations may be attributed to a source of mild forelimb lameness unrelated to BFR application, such as daily treadmill exposure itself. Study inclusion criteria required that horses demonstrate no evidence of current or previous osseous or soft tissue forelimb abnormalities on baseline (prior to study day 0) lameness evaluation and ultrasonographic evaluation of the forelimb flexor tendons, accessory ligament of the deep digital flexor tendon and carpal canal, but further radiographic evaluation may have also aided in further patient selection. None of the horses in this study were shod, which may have also affected forelimb soundness.

None of the forelimbs evaluated in this study demonstrated any subjectively assessed radiocarpal or middle carpal joint effusion > 0 at any study time point. Evaluation of the carpal joints specifically was selected due to its close anatomic proximity to BFR cuff application within the mid-antebrachium. Given that no significant differences for any of the evaluated subjective or objective gait parameters were appreciated over time or between BFR and control (contralateral) limbs, and complications related to BFR cuff application such as thrombosis, laminitis, dermatitis or soft tissue swelling were not appreciated, the authors feel it is reasonable to conclude that the application of unilateral forelimb BFR at 80% LOP over a 56-day study period did not alter or negatively impact gait or clinically relevant parameters assessed in this four-horse study population. The safety of BFR exercise in humans is a source of ongoing investigation [14,18-20] with focus being placed on central and peripheral cardiovascular responses, muscle damage, oxidative stress and nerve conduction responses in comparison to

regular exercise [19]. Longer term studies to elucidate the chronic effects of BFR are still

needed, but human providers acknowledge key patient contra-indications to be that of

neuropathies, known clotting disorders and a predisposition to rhabdomyolysis [15,19].

Complications related to pressure-specific equine BFR use were not expected to be discovered

by the authors, but were also completely unknown.

This exercise protocol utilized herein was adapted from human walk protocols [14] in

terms of duration, frequency of application (5 days/week), rest periods (cuff inflated at rest), and

that previously utilized by our research group that demonstrated SDF muscle oxidative capacity

changes over a 10-day study period [11-12]. Given that SDF muscle oxidative capacity increases

have been found to be consistent with acute metabolic adaptations of increased mitochondrial

density and an improved ability to oxidize fuels [11-12], and similar equine walk protocols (10

minutes) have also demonstrated elevations in GH and muscular hypertrophy [10], this exercise

protocol was utilized to determine any associated safety considerations related to its use. Further

tissue analysis that is currently underway can also be expected to guide safety considerations at

the tissue-specific level [Johnson, unpublished data]. Additionally, this walk protocol is similar

to hand-walking protocols in current clinical use for a variety of equine musculoskeletal injuries

(hand-walk 10-15 minutes once daily, for example). Further exercise prescription iterations may

have yielded different results, but authors felt this level of BFR exercise intensity was reasonable

to that previously reported for both humans and horses.

Human BFR application in the rehabilitative setting suggests that occlusion percentages

of 40-80% will yield maximal therapeutic benefit, with incorporation of the lowest occlusion

pressure possible being favored by clinicians due to improved patient comfort during BFR

sessions [14,17]. In general, 80% occlusion is recommended for lower extremity use and 50% is

advised for use on upper extremities, but specific pressures are widely varied in the human literature and prescription is often highly clinician, patient and injury-dependent [15]. Cuff width and limb circumference are inconsistently accounted for in human BFR investigations, making it difficult to draw conclusions regarding specific pressures [19]. Consequently, the higher end of vascular occlusion (80% LOP) was used in this study to assess for clinical complications related to the highest occlusion pressures that would theoretically be used in the equine clinical setting. The authors acknowledge that tourniquet use has been commonly utilized for certain procedures such as regional limb perfusions or in the surgical setting, but this is the first report of modernized human BFR equipment being utilized to deliver equine, patient-specific occlusion percentages for walk application. One previous equine BFR investigation utilized 200-230mm Hg cuff pressure to deliver bilateral forelimb BFR at a walk pace six unfit Standardbred mares [9], but the data reported herein suggests that occlusion pressures of 75-151 mm Hg would likely simulate a range of 50-80% vascular occlusion in horses (far less than that previously utilized). Patient-specific delivery of BFR occlusion percentages (instead of applying blanket pressures to all patients) is considered the standard of care in human patients due to improved therapeutic outcomes, increased comfort and minimized safety risks [14-15]. Additionally, using a personalized tourniquet pressure for each patient lessens the need to account for other BFR use variables such as cuff width or limb size [15]. While there is still ongoing research into optimized BFR application in human orthopedic rehabilitation, considering these variables in the equine clinical setting will help expedite its safe and efficacious use.

Specific features of the herein utilized BFR cuff and corresponding equipment that make it quite different to that of standard (standing) tourniquet application and that previously investigated for equine BFR use [9-10] is the presence of sensors that line the inner most portion

of the cuff that allow the dynamic measurement and real-time adjustment of subsequently delivered pressure. Specifically, the rapid addition or removal of pressure that occurs instantaneously with corresponding limb movement results in a contoured, inflated fit during locomotion. The even distribution of pressure within the cuff allows for improved patient comfort in contrast to traditional rubber/neoprene tourniquets that often inadvertently tighten over anatomic regions lacking muscular cover (boney prominences, for example) or unevenly distribute pressure. Additionally, with the ability to set and modify pressure through machine prompts, adjustments in delivered pressure offer the clinician a way to closely titrate the amount of occlusion. Transient forelimb cutaneous vessel distension and persistent vessel engorgement was readily visibly appreciable during BFR sessions (Figure 6.5). With light suspension of the inflated BFR cuff, it was the authors' impression that the cuff stayed in position without major slippage (slippage estimated to be less than 1.5 inches), gapping or loosening in reference to a marker line denoting initial proximal to distal site of application (Figure 6.5C). The designated pressure of each cuff was verified to have been delivered at the end of each walking session through machine prompts and the ability of the cuff to stay in place unassisted.

Fig 6.5: Pre (6.5A) and post (6.5B) occlusion images of the left forelimb during limb occlusion pressure (LOP) determination demonstrating visible cutaneous vessel engorgement (yellow arrows) distal to the site of cuff application. Persistent vessel engorgement distal to the limb protection sleeve was commonly noted during BFR walking exercise at 80% vascular occlusion (6.5C, white arrow) as was adequate cuff positioning in reference to a marker line denoting initial proximal to distal site of cuff application (6.5C, red arrow).

In this investigation, LOP readings for each equine BFR assigned forelimb were obtained daily immediately prior to each BFR session via Doppler ultrasound to ensure that patient-specific pressures were utilized for each session. Doppler ultrasound is widely utilized in human and veterinary medicine to determine blood pressure, but it's application in the standing, un-sedated horse is much less common. Short-term beneficial effects of BFR on equine superficial digital flexor (SDF) muscle oxidative capacity over a 10-day study period utilizing patient-specific pressures determined through machine prompts and confirmed with power doppler grey-scale ultrasound previously demonstrated large vessel stasis just distal to the site of cuff application [11-12], but the study described herein utilizes even further improved LOP determination techniques with the incorporation of Doppler ultrasound. Specifically, the same observer obtained all Doppler readings in a systematic manner, and most importantly was blinded to the real-time readings to prevent any bias in continuity of measurements. Our pilot

study results suggest significant differences in pressure readings exist between horses and between the measured left and right forelimbs. It is also the authors' impression that environmental stimuli, time of day, limb position and patient habituation to the process of pressure determination followed by BFR exercise all likely influence variation in daily pressure readings (Figure 6.6). Also noteworthy is the fact that doppler values for BFR-exposed forelimbs only (n = 4) were measured daily (in contrast to both left and right forelimb LOP measurements being taken on each horse, n = 8). This study design was elected to ensure that vascular occlusion was applied only to BFR-exposed forelimbs with each contra-lateral limb serving as an internal (unoccluded) control for clinical examination purposes and longitudinal monitoring. It would seem worthwhile, however, to determine left compared to right forelimb LOP variations within the same horse as a next investigative step. Human limb LOP values have historically been obtained at weekly intervals for daily clinical use in a supine position with pressure reading differences documented as dependent upon limb and body position [21]. A recent human investigation assessing LOP variability of lower-extremity BFR found that LOP values were not different between legs, but did vary significantly between participants [22]. The herein reported standard deviation of roughly 22mm Hg across all LOP readings of all horses in this small pilot investigation provides initial insight into the variability that might be expected in LOP readings for subsequent clinical use. Further investigation incorporating repeated measures of both left and right forelimbs using a larger number of horses will, however, be required to determine the need for daily vs. weekly LOP measurements.
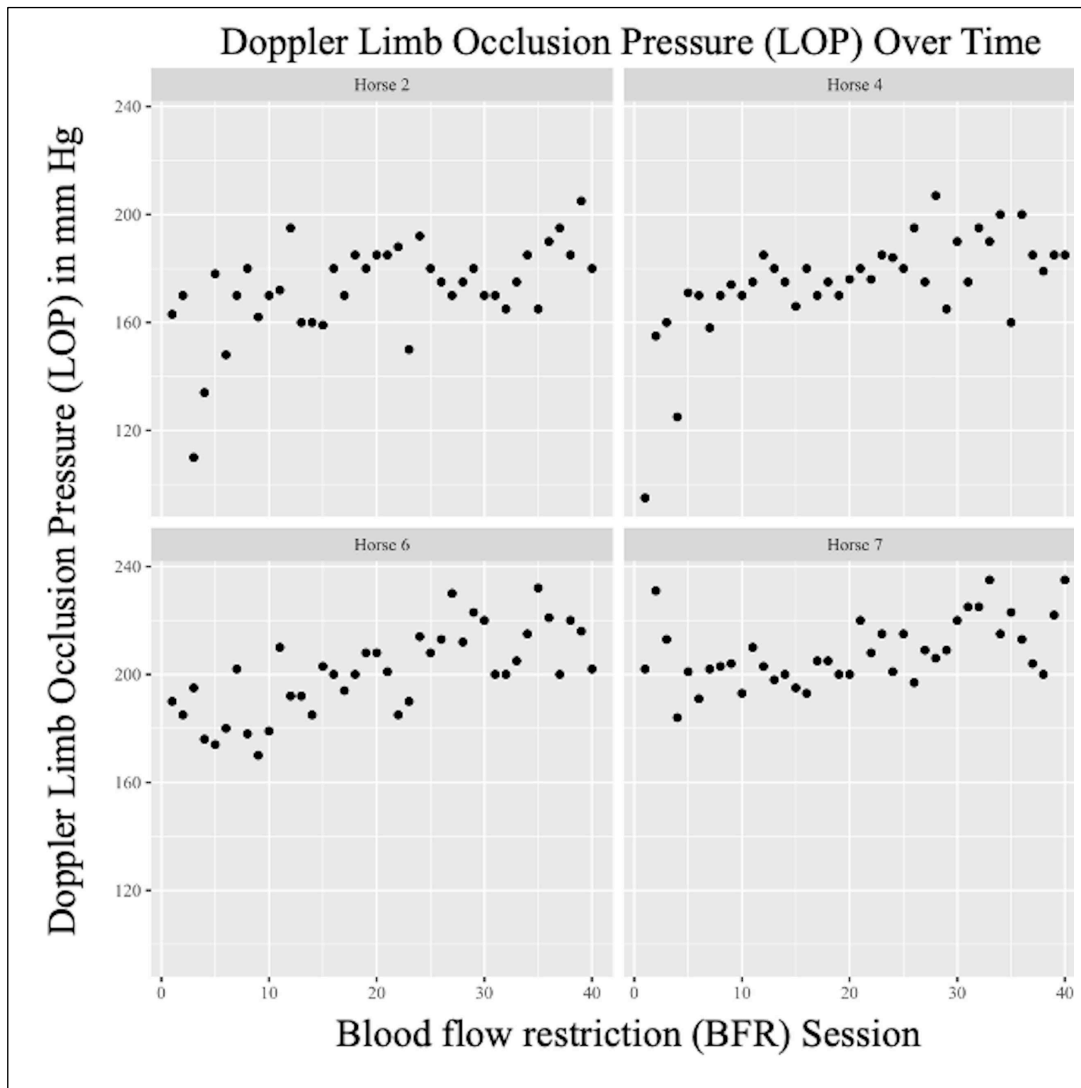
Fig 6.6: Limb occlusion pressure (LOP) values in mm Hg determined via daily Doppler ultrasound evaluation in 4 horses over 40 BFR sessions. Statistically significant differences between horses were noted (Table 2), with variations in daily readings also noted (standard deviation of roughly 22mm Hg across all readings).

The herein utilized patented cuff-sensor technology engineered by Delfi is capable of measuring human limb occlusion pressure (LOP) with an accuracy of 1mm Hg and precision ± 12mm Hg of Doppler ultrasound [16,21] through machine prompts alone, but its systematic pressure readings for use in the standing horse have not yet been validated and hence was the authors' motivation to incorporate Doppler ultrasound pressure confirmation. As technology

evolves for equine-specific use, its clinical BFR use in horses would be facilitated by the ability to easily obtain an accurate LOP measurement in the standing, un-sedated horse while in consistent (square) limb position, which is still commercially unavailable.

There are several limitations the authors would like to acknowledge including statistical assessment of only forelimb biomechanical gait parameters. Statistical evaluation of hindlimb biomechanical gait data may have been helpful to help evaluate for compensatory gait patterns secondary to forelimb BFR exposure, but qualitative observations of the hindlimb gait data suggested a lack of clinically relevant conclusions so formal statistical analysis was not pursued. Although Doppler pressure readings have been documented as accurate in both human and veterinary medicine, there is likely inherent variation of readings between limbs, horses and experience of observers. Optimal occlusion percentages and subsequent walk protocols for BFR application in the clinical setting as has been investigated in humans are still unknown for the horse. The occlusion percentage (80%) utilized herein was extrapolated from human practice in addition to other BFR variables (cuff width, cuff length, etc). Also noteworthy is that although Delfi PBFRR machine prompts indicated that designated pressures were successfully dynamically delivered during BFR walk exercise, it's impossible to know whether this pressure reflected 80% physiologic occlusion while horses were on the treadmill at a walk (perhaps their blood pressures inherently differed from immediately prior to exercise compared to those during exercise, for example). Specific interface pressures as have been described for human BFR use [21] need to be investigated in the horse, potentially by placing an intra-arterial catheter in the forelimb with real-time measurements obtained during exercise, which may prove difficult. Additionally, this study utilized a standard human BFR cuff for equine application. An equine-specific forelimb BFR cuff has since been developed which will optimize anatomic fit and may

167

even facilitate automated LOP readings to eliminate the need for Doppler evaluation (once validated). Further advancements in equine-specific BFR technology can be expected to improve ease of clinical use. Lastly, this study utilized a study group of 4 horses exposed to unilateral forelimb BFR at a walk pace using a previously utilized protocol [11-12] for pilot investigative purposes. A post-priori power calculation using published kinetic/kinematic differences of aquatic therapy compared to control exercise [17] suggests that our sample size of four limbs has a 0.5 power with an effect size of 1.3. This lack of statistical power highlights the need for continued investigation incorporating data from more horses to draw conclusions beyond pilot investigation alone. To confidently assert safety by having a study design with >90% power, a total of 10 limbs would have been needed and should motivate additional work in the field moving forward. In summary, a larger study population using varied occlusion percentages, a different exercise protocol or further LOP investigations over a longer study period may have yielded different results.

In conclusion, this is the first controlled study in horses to investigate both subjective and objective forelimb biomechanical gait alterations related to the use of forelimb BFR at 80% vascular occlusion. The herein limb occlusion pressure values are also the first reported forelimb pressure readings in standing, un-sedated horses that may be useful for the clinician looking to incorporate BFR into professional rehabilitation programs. Our results suggest that differences between horses and measured forelimbs still necessitate patient-specific pressure readings in lieu of blanket pressure applications. Further investigation into occlusion percentages related to optimal clinical outcomes for a variety of injuries represent a source of ongoing investigation.

References

1. Laurentino GC, Ugrinowitsch C, Roschel H, et al. Strength training with blood flow restriction diminishes myostatin gene expression. *Med Sci Sports Exer* 2012; 406-412.

2. Tennent D, Hylden C, Johnson A, et al. Blood flow restriction training after knee arthroscopy: a randomized controlled pilot study. *Clin J Sport Med* 2017;27(3):245-252.

3. Yow BG, Tennet DJ, Dowd TC, et al. Blood flow restriction training after achilles tendon rupture. *J Foot Ankle Surg* 2018;57:635-638.

4. Shimizu R, Hotta K, Yamamoto S, et al. Low-intensity resistance training with blood flow restriction improves vascular endothelial function and peripheral blood circulation in healthy elderly people. *Eur J Appl Physiol* 2016;116:749-757.

5. Patterson SD, Brandner CR. The role of blood flow restriction training for applied practitioners: a questionnaire-based survey. *J Sports Sci* 2018;36(2):123-130, doi: 10.1080/02640414.2017.1284341.

6. Cognetti DJ, Sheean AJ, Owens JG. Blood flow restriction therapy and its use for rehabilitation and return to sport: Physiology, application, and guidelines for implementation. *Arthroscopy, Sports Med & Rehabil* 2022;4(1):e71-e76.

7. Lowery R, Joy J, Loenneke J, et al. Practical blood flow restriction training increases muscle hypertrophy during a periodized resistance training programme. *Scand Soc Clin Phys Nuc Med* 2013;34(4):317-321.

8. Amano S, Ludin AFM, Clift R, et al. Effectiveness of blood flow restricted exercise compared with standard exercise in patients with recurrent low back pain: study protocol for a randomized controlled trial. *Trials* 2016;17:81.

9. Abe T, Kearns C, Manso Filho H, et al. Acute vascular occlusion in horses: effects on skeletal muscle size and blood flow. *Equine & Comp Ex Phys* 2004;4:239-243.

10. Abe T, Kearns C, Manso Filho H, et al. Muscle, tendon and somatotropin responses to the restriction of muscle blood flow induced by KAATSU-walk training. *Eq Ex Phys* 2006;36:345- 348.

11. Johnson SA, Chicco AJ, Selberg KT, et al. Short-term effects of blood flow restriction training on equine skeletal muscle oxidative capacity. In: *Orthop Res Soc* Annual Meeting, Poster Presentation, Feb 12-16, 2021.

12. Navas de Solis C, Gabbett T, King MR, et al. Science in brief: The Dorothy Havemeyer International Workshop on poor performance in horses: Recent advances in technology to improve monitoring and quantification. *Equine Vet J* 2022;54:844-846.

13. Johnson SA, Bell S Schnabel LS, et al. Frontiers in Athletic Rehabilitation: What is Translatable to the Horse? In: *Proceedings* American Association of Equine Practitioners Annual Convention, December 4-8, 2021.

14. Patterson, SD, Hughes L, Warmington S, et al. Blood flow restriction exercise: considerations of methodology, application, and safety. *Frontiers Phys* 2019;10(533):1-15. doi: 10.3389/fphys.2019.00533.

15. Owens JO. Personalized blood flow restriction rehabilitation. Owens Recovery Science Personalized Blood Flow Restriction Manual 2018;110-116.

16. Masri BA, Day B, Younger, AS, et al. Technique for measuring limb occlusion pressure that facilitates personalized tourniquet systems: a randomized trial. *J Med Biol Eng* 2016;36:644-650.

17. King MR, Haussler KK, Kawcak CE, et al. Biomechanical and histologic evaluation of the effects of underwater treadmill exercise on horses with experimentally induced osteoarthritis of the middle carpal joint. *Am J Vet Res* 2017;78:558-569.

18. Clark, B. C., Manini, T. M., Hoffman, R. L., Williams, P. S., Guiler, M. K., Knutson, M. J., Kushnick, M. R. (2011). Relative safety of 4 weeks of blood flow-restricted resistance exercise in young, healthy adults. *Scand J Med Sci Sports, 21*(5), 653-662.

19. Loenneke, J. P., Wilson, J. M., Wilson, G. J., Pujol, T. J., & Bemben, M. G. (2011). Potential safety issues with blood flow restriction training. *Scand J Med Sci Sports, 21*(4), 510-518. doi: 10.1111/j.1600- 0838.2010.01290.x

20. Horiuchi, M., & Okita, K. (2012). Blood flow restricted exercise and vascular function. *Int J Vasc Med, 2012*, 543218. doi: 10.1155/2012/543218

21. Hughes L, Rosenblatt B, Gissane C, et al. Interface pressure, perceptual, and mean arterial pressure responses to different blood flow restriction systems. *Scan J Med Sci Sports* 2018;28:1757-1765.

22. Evin A, Mahoney S, Wagner M, et al. Limb occlusion pressure for blood flow restricted exercise: Variability and relations with participant characteristics. *Phys Therapy In Sport* 2021;47:78-84.

CHAPTER 7 - Blood Flow Restriction Training & Its Musculoskeletal Effects

7.1 Introduction

Human musculoskeletal injuries occur frequently, equating to greater than $600 billion of expenses in the United States alone [1]. Similarly, equine musculoskeletal injuries are estimated to affect 60% of all athletic horses, resulting in associated costs of approximately $420 billion per year [2-4]. In both humans and horses, orthopedic injuries often result in periods of mandatory rest depending on the severity and type of injury. Rapid declines in muscular strength compound the original injury's morbidity and predispose patients to subsequent loss of physical function.

Low load exercise training with blood flow restriction (BFR) is revolutionizing how human strength coaches are conditioning athletes for competition. Through application of a specialized tourniquet to temporarily reduce blood flow to an exercising limb, athletes are able to increase strength and produce muscular hypertrophy using only light weights or low-intensity exercise (walking) [5-6]. Reducing exercise intensity while minimizing muscle atrophy through the use of BFR has also been proposed as a progressive clinical rehabilitation tool for a variety of human conditions including knee osteoarthritis [7], soft tissue injuries [8] and geriatric sarcopenia [9]. Despite BFR's widespread clinical use to maintain muscular strength and function for these conditions, little is known about its concurrent tissue-specific effects on that other than muscle (tendon, cartilage, subchondral bone). Additionally, its use has not been validated in horses. Therefore, the overarching goal of this project was to determine comprehensive musculoskeletal effects of equine BFR, specifically on articular cartilage, tendon, muscle and bone as safety validation for equine use and human translational investigation. The

orthopedic similarities of horses and humans for translational research are well-documented [10]; equine BFR use would represent not only an untapped resource for horses of all ages and morbidities, but also an avenue through which translational information can be obtained.

7.2 Experimental Animals & Study Design

Experimental Animals:

This study was a controlled prospective experiment. All study methods were conducted in compliance with the University's Institutional Animal Care and Use Committee (IACUC, protocol #1013). Enrolled horses (n = 8: six mares, one gelding and one stallion, ages 2-3 years) were purchased from an outside vendor and showed no evidence of current or previous osseous or soft tissue forelimb abnormalities on baseline lameness evaluation and ultrasonographic evaluation of the forelimb flexor tendons, accessory ligament of the deep digital flexor tendon and carpal canal. All horses were acclimated to a treadmill through once daily exposures to an Equigym high-speed treadmill for 14 days [11]. This exposure consisted of a 10-minute exercise period (brisk walk at a velocity of 3.5-3.7 mph), followed by a five-minute rest period. Horses were also acclimated to the application of a surcingle during this time.

Horses were randomly assigned to left or right forelimb BFR application using a random number generator. A total of two left and two right forelimbs (n = 4 forelimbs) of four horses (three mares and one gelding) were exposed to 40 BFR-walk sessions on a treadmill over a 56-day study period with their contralateral forelimbs (n = 4, two left and two right forelimbs) serving as untreated controls (not exposed to a limb protection sleeve or any BFR occlusion), Figure 7.1.
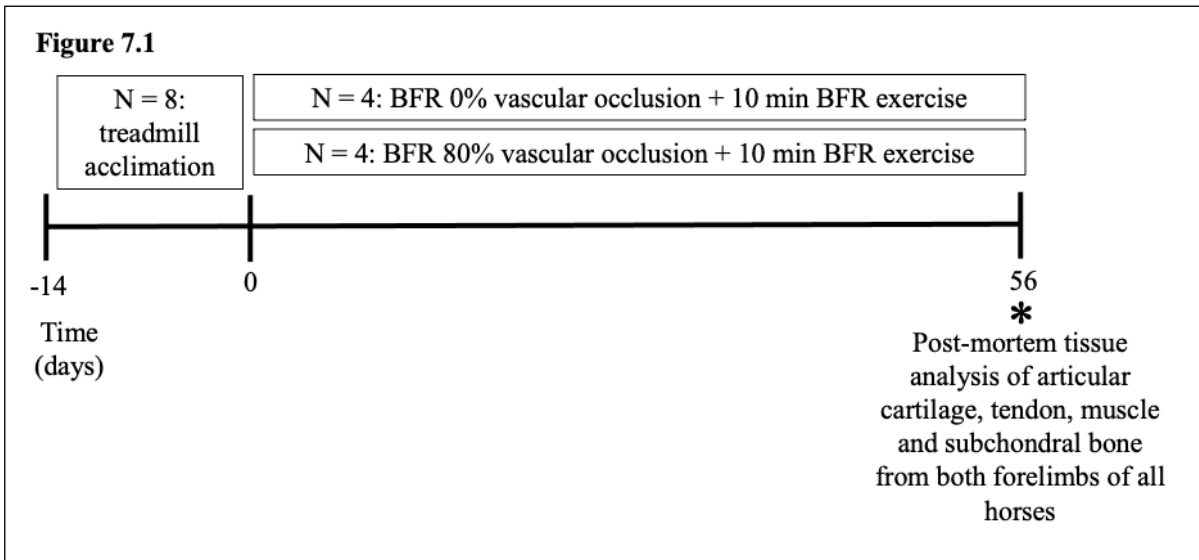
Figure 7.1: Blood flow restriction (BFR) exercise was performed once/day for 5 days/week for a 56-day study period. A total of two left and two right forelimbs (n = 4 forelimbs) of four horses were exposed to 40 BFR-walk sessions with their contralateral forelimbs (n = 4, two left and two right forelimbs) serving as untreated controls (not exposed to a limb protection sleeve or any BFR occlusion) Similarly, a total of two left and two right forelimbs (n = 4 forelimbs) of four horses were exposed to 40 sham cuff walk sessions with their contralateral forelimbs (n = 4, two left and two right forelimbs) serving as untreated controls. All horses randomly assigned to the control group (n = 4 horses) were exposed to the same treadmill exercise as horses in the BFR group, but with a lightly suspended, non-inflated cuff applied as a sham treatment to a randomly assigned forelimb. Comprehensive post-mortem tissue analysis was performed following the final BFR session on day 56.

Similarly, a total of two left and two right forelimbs (n = 4 forelimbs) of four horses

(three mares and one stallion, ages 2-3 years) were exposed to 40 sham cuff walk sessions on a

treadmill over the 56-day study period with their contralateral forelimbs (n = 4, two left and two

right forelimbs) serving as untreated controls (Figure 7.1). All horses randomly assigned to the

control group (n = 4 horses) were exposed to the same treadmill exercise as horses in the BFR

group, but with a lightly suspended, non-inflated cuff applied as a sham treatment to a randomly

assigned forelimb (n = 4 horses, 4 sham limbs). The uninflated cuff was maintained in position

with light suspension, and the same limb protection sleeve was applied underneath each

uninflated cuff. The randomly assigned contralateral (control) forelimb of each horse was not exposed to a limb protection sleeve or any BFR occlusion.

Limb Occlusion Pressure Determination:

For limbs randomly assigned to BFR exposure (n = 4 horses, 4 exposed forelimbs), limb occlusion pressures (LOP) were obtained immediately prior to each daily session by Doppler evaluation. The LOP was defined as the amount of pressure required to achieve 100% vascular occlusion. A standard human BFR cuff manufactured by Delfi Medical Innovations[7], Inc was utilized for all aspects of LOP assessment and BFR delivery for this study. Specifically, the Delfi Personalized Blow Flow Restriction Rehabilitation (PBFRR) blood pressure cuff was placed 6 inches distal to the olecranon within the mid to proximal antebrachium, at the same location as the cuff placement during BFR walk sessions. The piezoelectric doppler probe was placed just distal to the blood pressure cuff and positioned so a clear distal pulse of the median artery was heard [12-13]. The blood pressure cuff was then inflated using the manual pressure regulator option on the Delfi system up to the pressure at which the distal pulse was no longer audible [12-14]. The value in mmHg for which the pulse of the median artery was no longer audible was then recorded as the LOP and utilized to calculate the specified 80% vascular occlusion. Resurgence of the median artery pulse with cuff deflation was confirmed for all successful Doppler readings to ensure probe placement remained accurate. All LOP determinations were measured by the same observer blinded to real-time numeric LOP measurements with horses in a standing, (un-sedated) square position within the same barn location [13].

Blood Flow Restriction Exercise:

---

[7] Delfi Medical Innovations, Inc. Vancouver, BC, Canada

174

The previously described blood pressure cuff was placed 6 inches distal to the olecranon within the mid to proximal antebrachium (Figure 7.2) during walk exercise [12-13]. All BFR limbs were appropriately fitted to an Easi-Fit Tourniquet Cuff 24" in circumference as previously described [12-13]. The personalized tourniquet system (PTS) matching limb protection sleeve was applied underneath each tourniquet and secured with elastic adhesive tape to circumvent any inadvertent dermatitis (Figure 7.1). A small bungee (elastic) cord was used to suspend the cuff to a surcingle ring to avoid any cuff slippage. Each BFR session was performed by the same investigator who has clinical experience in the use of the PTS, completed the Owens Recovery Science BFR certification course and initial pilot experimentation [12-13]. The contralateral forelimb was not exposed to cuff application to serve as an internal (unexposed) control.

Each BFR exercise session began with a 3-minute warm-up period at a velocity of 3.5-3.7 mph (brisk walk, with no BFR cuff). Following the 3-minute warm-up period, the limb protection sleeve was secured, the PTS was placed and the doppler-determined 80% vascular occlusion was applied to the BFR-exposed forelimb (Figure 7.1). Horses then walked at a velocity of 3.5-3.7 mph for a total walk time of 10 minutes at the following interval protocol: 4-minutes walk, 1-minute rest (standing quietly on the land treadmill), 3-minutes walk, 1-minute reset, 3-minutes walk [12-13]. The PTS remained inflated for the duration of the walk-rest exercise protocol. Following the session, the PTS was immediately deflated, removed and the horse underwent a 3-minute supervised recovery period (standing quietly in the barn aisle) before returning to its stall. BFR walking exercise was performed 5 days/week for the 56-day study period. Cuff leak tests were performed, and pressure readings were validated once weekly

with a Mercury manometer throughout the duration of the study to ensure accurate pressure
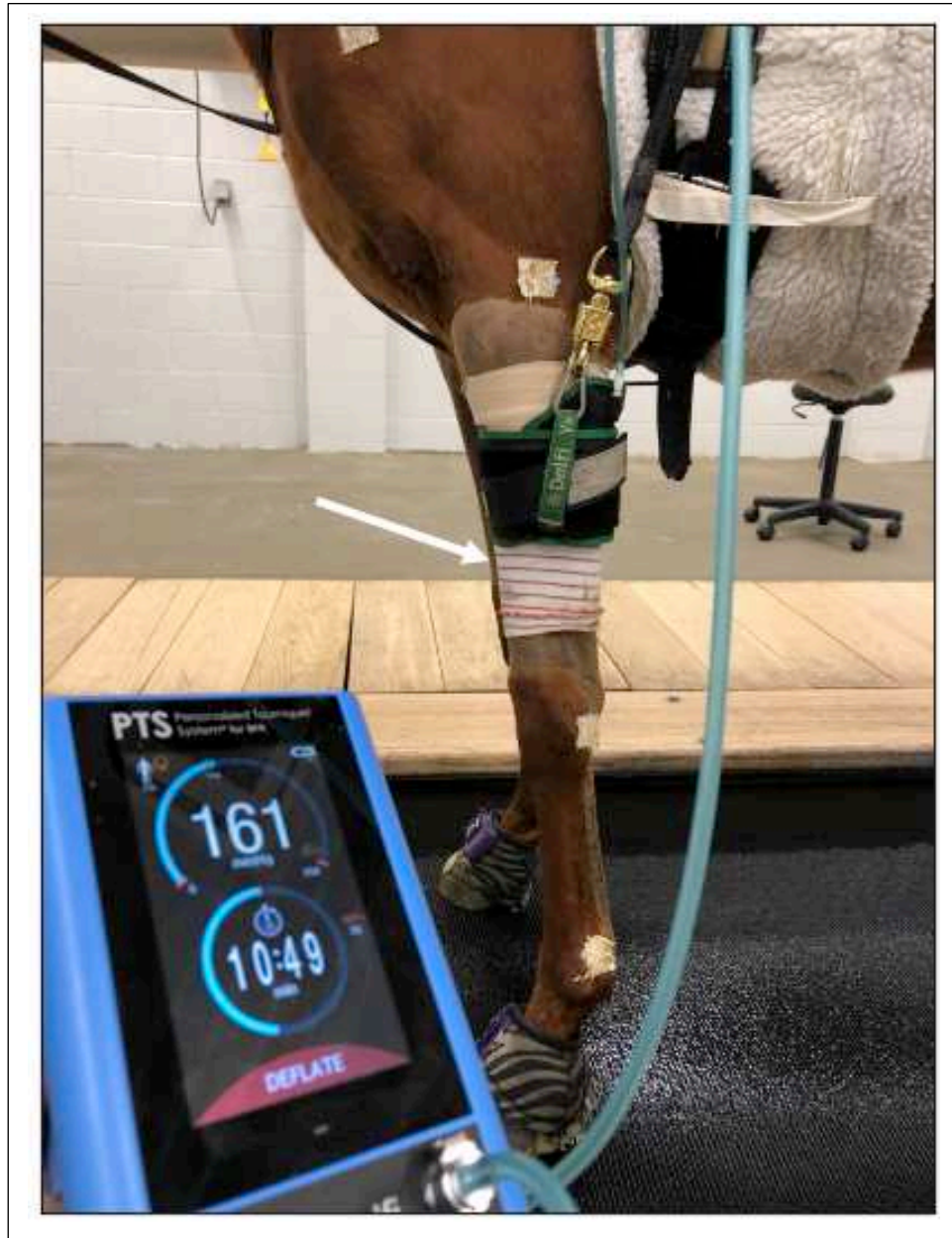
delivery and cuff maintenance.

Figure 7.2: Application of a limb protection sleeve (white arrow) secured with elastic adhesive tape and inflated BFR cuff to the left forelimb of a horse in preparation for walk exercise. The personalized tourniquet system (PTS) adjusts pressure dynamically to maintain individual levels of occlusion based on daily measured limb occlusion pressures (LOP).

7.3 BFR's Effects on the Equine Superficial Digital Flexor Tendon (SDFT)

BFR's Effects on the Equine Superficial Digital Flexor Tendon Materials & Methods:

Non-Destructive Biomechanical Testing:

On day 56, all horses were humanely euthanized and forelimb superficial digital flexor tendons (SDFTs) were carefully harvested from the proximal myotendinous junction (MTJ) to the level of the proximal sesamoid bones. The CSA of all tendons was measured at five regions of interest (ROI) using an area micrometer and applied plunger pressure of 0.12 MPa following equilibrium for 2 minutes [15]. These measurements were averaged and used to normalize load data to calculate tissue stress. Tendons were gripped at a standardized 15cm gauge length using custom cryo-grips maintained between -20°C to -30°C in a servo-hydraulic load frame (Model 858, MTS Corp, Eden Prairie, MN) (Figure 7.3). Prior to initiation of biomechanical testing, a static preload of 20N was applied to each tendon for a duration of two minutes, at which point a reference gage length was measured and recorded for purposes of strain normalization. Tendons were then preconditioned from 50-1000N (approximately 12-25% failure load) for 10 cycles, followed by five quasi-static loading cycles from 50-2500N (approximately 12-40% failure load) at 25N/sec loading rate. All data was sampled at 100Hz, and stiffness and elastic modulus were calculated for all five loading cycles.
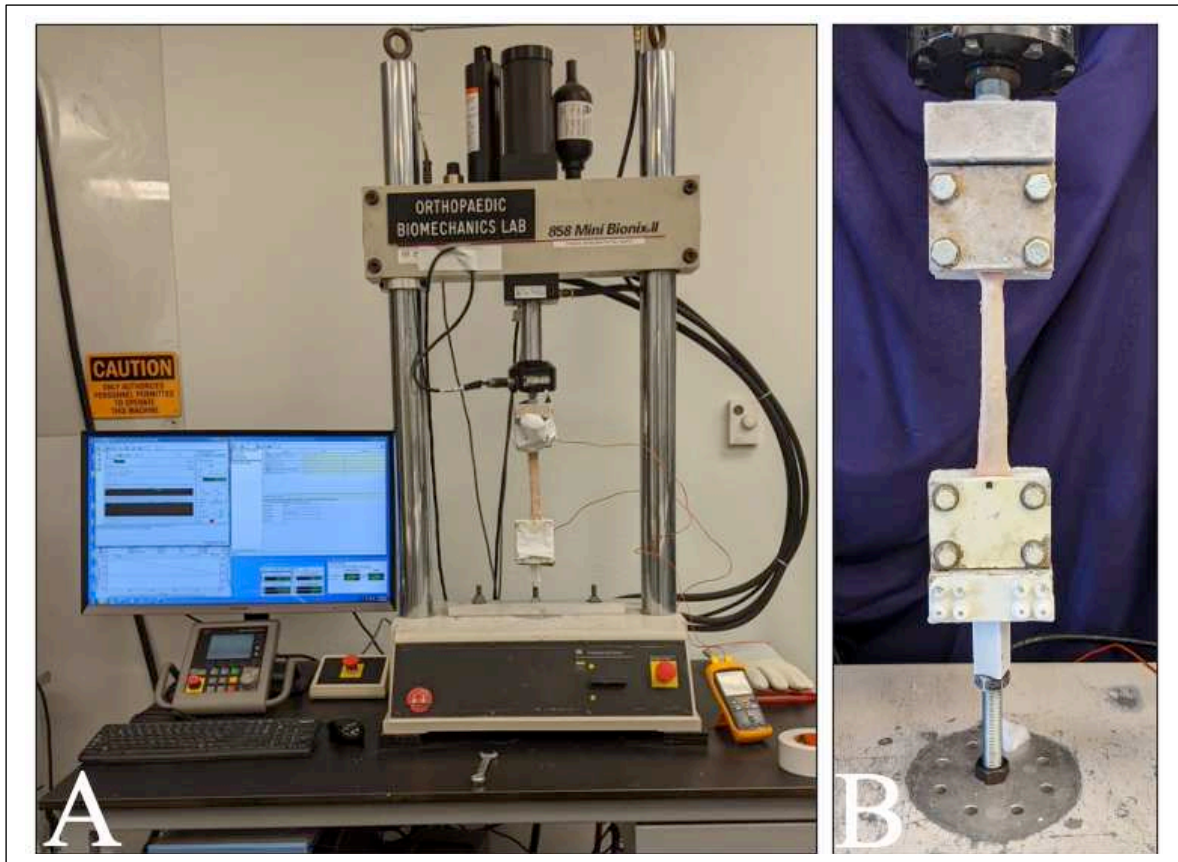
Figure 7.3: A) Non-destructive biomechanical testing apparatus (Model 858, MTS Corp, Eden Prairie, MN) used to measure superficial digital flexor tendon (SDFT) cross-sectional area (CSA), stiffness and resultant elastic modulus. B) Tendons were gripped at standardized 15cm gauge length using custom cryo-grips maintained between -20°C to -30°C in a servo-hydraulic load frame.

Histologic Evaluation:

Following non-destructive biomechanical evaluation, forelimb SDFTs at five determined levels (Figure 7.4) were fixed in 10% neutral buffered formalin, embedded in paraffin, sectioned (5μm; longitudinal) and stained with Toluidine Blue (TolBlue) and Hematoxylin and Eosin (H&E). Tissue harvest for level five corresponding to the MTJ region was collected from the SDF muscle-SDFT complex prior to trimming for biomechanical testing (the SDF MTJ was not biomechanically tested). Tendon specimens corresponding to levels 1-4 were harvested in relation to the biomechanically utilized 15cm gauge length excluding the freezing artifact,

leaving approximately 13cm of SDFT that was then divided equally into levels 1-4 for histopathologic analysis. Specimens were qualitatively scored by a board-certified veterinary pathologist blinded to treatment groups using modified (to allow for half grades) Bonar and Movin scoring criteria for levels 1-4 (Table 7.1, Figure 7.4) [16-17]. Level 5 was scored using a modified (to allow for half grades) scale of 0-3 for ground substance, fibrosis and vascularity (Table 7.1) [18].
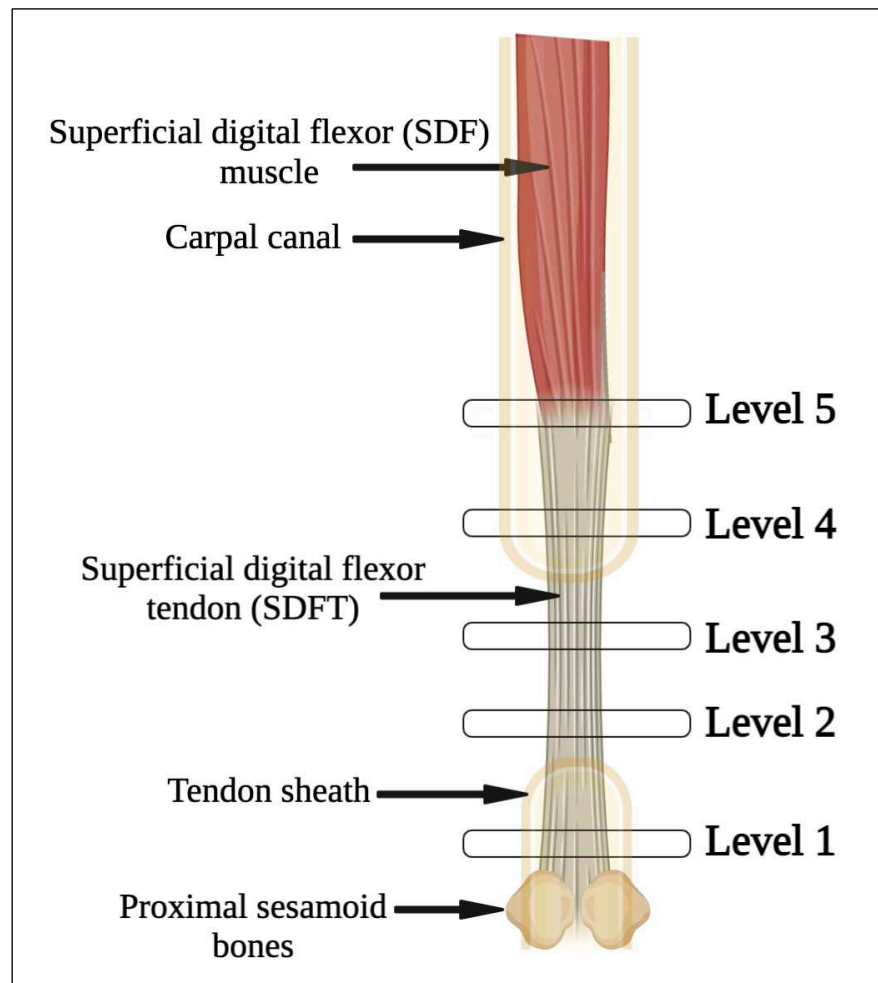
Figure 7.4: Five levels of superficial digital flexor tendon harvest for histopathologic analysis (Toluidine blue and hematoxylin and eosin staining). Level 1: proximal to proximal sesamoid bones (intra-thecal); Level 2: distal-metacarpal region (extra-thecal); Level 3: mid-metacarpal region (extra-thecal); Level 4: distal end of carpal canal (intra-thecal); Level 5: musculotendinous junction (MTJ) of the superficial digital flexor muscle and tendon.

Table 7.1: Bonar and Movin scoring criteria (0-3) used to assess levels 1-4 of superficial digital flexor tendon (SDFT) samples. Level 5 (musculotendinous junction, MTJ) was scored using a previously reported scale of 0-3 (Sikes et al 2021). All samples were scored by a board-certified veterinary pathologist blinded to treatment groups.

Bonar Scale	Grade			
	0	1	2	3
Tenocytes	Inconspicuous elongated spindle shaped nuclei with no obvious cytoplasm at light microscopy	Increased roundness: nucleus becomes more ovoid to round in shape without conspicuous cytoplasm	Increased roundness and size: the nucleus is round, slightly enlarged and a small amount of cytoplasm is visible	Nucleus is round, large with abundant cytoplasm and lacuna formation (chondroid change)
Ground substance	No stainable ground substance	Stainable mucin between fibers, but bundles still discrete	Stainable mucin between fibers with loss of clear demarcation of bundles	Abundent mucin throughout with inconspicuous collagen staining
Collagen	Collagen arranged in tightly cohesive well demarcated bundles with a smooth dense bright homogeneous polarization pattern and normal crimping	Diminished fiber polarization: separation of individual fibers with maintenance of demarcated bundles	Bundle changes: separa- tion of fibers with loss of demarcation of bundles giving rise to expansion of the tissue overall and clear loss of normal polarization pattern	Marked separation of fibers with complete loss of architecture
Vascularity	Inconspicuous blood vessels coursing between bundles	Occasional cluster of capillaries, less than 1 per 10 high power fields	1-2 clusters of capillaries per 10 high power fields	Greater than 2 clusters per 10 high power fields

Movin Scale	Grade			
	0	1	2	3
Fiberstructure	Normal	Slightly abnormal	Moderately abnormal	Markedly abnormal
Fiber arrangement	Normal	Slightly abnormal	Moderately abnormal	Markedly abnormal
Rounding of the nuclei	Normal	Slightly abnormal	Moderately abnormal	Markedly abnormal
Regional variations in cellularity	Normal	Slightly abnormal	Moderately abnormal	Markedly abnormal
Increased vascularity	Normal	Slightly abnormal	Moderately abnormal	Markedly abnormal
Decreased collagen stainability	Normal	Slightly abnormal	Moderately abnormal	Markedly abnormal
Hyalinization	Normal	Slightly abnormal	Moderately abnormal	Markedly abnormal
GAG content	Normal	Slightly abnormal	Moderately abnormal	Markedly abnormal
General description	0 to 8 (normal to slight tendon changes)		9 to 16 (moderate changes)	17 to 24 (severe changes)

Musculotendinous Junction (MTJ) Scoring Criteria, Appendix 3 Sikes et al 2021	Grade			
	0	1	2	3
Ground substance	Absent/normal	Mild myxomatous degeneration mildly separating collagen bundles	Moderate myxomatous degeneration disrupting or effacing collagen fiber organization	Marked myxomatous degeneration effacing collagen bundles with cartilaginous and/or osseous metaplasia and or enthesophytes at tendon insertion
Fibrosis	Normal	Mildly increased numbers of interstitial fibroblasts with maintenance of	Fibroblasts disrupt collagen fiber organization and/or fiber polarization	Fibroblasts efface collagen fibers

		fiber organization		
Vascularity	Normal	1-2 cross-sectional vascular profiles per high powered field	3-6 cross-sectional vascular profiles per high powered field	Over 7 cross-sectional vascular profiles per high powered field

Biomechanical Statistical Analysis:

Statistical analysis was performed in GraphPad Prism 9.0.0 (San Diego, CA). Significance in biomechanical parameters between treatment groups was analyzed using a mixed-effects comparison analysis of variance (ANOVA) with Tukey's post-hoc tests. A *P*-value of less than 0.05 was considered statistically significant.

BFR's Effects on the Equine Superficial Digital Flexor Tendon Results:

Non-Destructive Biomechanical Analysis:

No statistically significant differences in SDFT CSA were appreciated between treatment groups ($P = 0.46$, Figure 7.5A), however a slight trend ($P = 0.07$) for increased CSA was noted between the BFR limb compared to its contralateral unexposed forelimb (Figure 7.5A). Statistically significant differences in SDFT stiffness for both first ($P = 0.02$, Figure 7.5B) and last cycles ($P = 0.03$, Figure 7.5C) were appreciated within the BFR treated group only, with BFR exposed forelimbs being significantly more stiff than the contralateral unexposed forelimbs. No significant differences were appreciated between treatment groups in elastic modulus for the first ($P = 0.49$, Figure 7.5D) or last cycles ($P = 0.40$, Figure 7.5E).
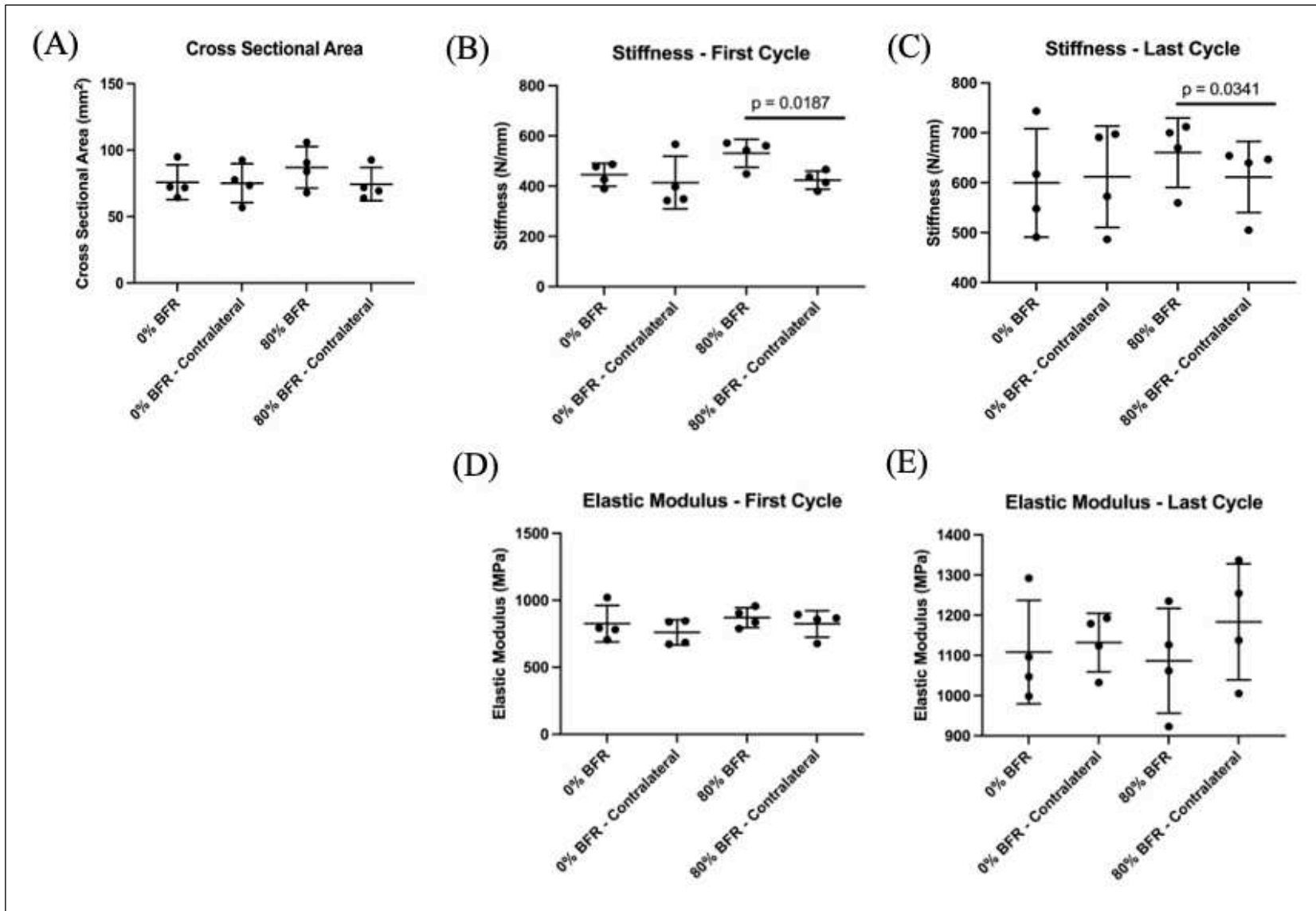
Figure 7.5: Measured biomechanical parameters including (A) Cross-Sectional Area, (B) First and (C) Last Cycle Stiffness (N/mm), and (D) First and (E) Last Cycle Elastic Modulus (MPa). Data presented as mean +/- STD with significant differences between groups marked.

Histologic Evaluation:

No consistent qualitative histologic differences were appreciated between treatment groups according to the utilized Bonar, Movin or MTJ evaluation criteria. Levels two and four of one BFR-exposed limb (horse 6, left forelimb) were given scores of 0.5 on the Movin scale for fiber structure, fiber arrangement, rounding of nuclei, regional variations in cellularity and glycosaminoglycan (GAG) content for resultant total Movin scores of 2.5 (normal to slight tendon changes, Table 7.2A). Level three of one BFR-exposed limb (horse 4, right forelimb) was given a 0.5 score on the Movin scale for increased vascularity (Table 7.2A). All remaining scores for BFR limbs according to Movin criteria were found to be zero, with all scores reported in Table 7.2A. Control limbs contralateral to BFR limbs were all assigned Movin total scores of zero (Table 7.2B). Levels two and three of one sham-exposed limb (horse 1, left forelimb) were given scores of 0.5 on the Movin scale for fiber structure, fiber arrangement, rounding of nuclei, regional variations in cellularity and glycosaminoglycan (GAG) content for resultant total Movin scores of 2.5 (normal to slight tendon changes, Table 7.2C). All remaining scores for sham-exposed limbs according to Movin criteria were found to be zero. Level three of one control limb contralateral to the sham limb (horse 3, right forelimb) was assigned scores of 0.5 for fiber structure, fiber arrangement and decreased collagen stainability, and scores of 1 for rounding of nuclei, regional variations in cellularity and GAG content for a total Movin score of 4.5 (normal to slight tendon changes, Table 7.2D).

Levels two and four of one BFR exposed limb (horse 6, left forelimb) was given a score of 0.5 for tenocytes, ground substance and collagen on the Bonar score. Level three of one BFR exposed limb (horse 4, right forelimb) was given a Bonar score of 0.5 for vascularity. All remaining Bonar scores for BFR exposed limbs were zero and are reported in Table 7.3A. Control

184

limbs contralateral to BFR limbs were all assigned Bonar scores of zero (Table 7.3B). Levels two and three of one sham-exposed limb (horse 1, left forelimb) were given Bonar scores of 0.5 for tenocytes, ground substance and collagen (Table 7.3C). All remaining Bonar scores for sham-exposed were zero. Level three of one control limb contralateral to a sham limb (horse 3, right forelimb) was given Bonar scores of 1 for tenocytes, ground substance and collagen. The remaining Bonar scores for control limbs contralateral to sham limbs were otherwise zero (Table 7.3D).

One MTJ region (level 5) of one BFR exposed limb (horse 7, left forelimb) was given a score of 0.5 for fibrosis with all other scores being zero (Table 7.4A). One control limb contralateral to a BFR limb at the MTJ region (horse 6, right forelimb) was given a 1.5 score for fibrosis while another control limb contralateral to its BFR limb (horse 7, right forelimb) was given a score of 0.5 for fibrosis (Table 7.4A). Two MTJ regions of two sham-exposed limbs (horse 1 left forelimb and horse 3 left forelimb, respective) were assigned fibrosis scores of 1 (Table 7.4B). One MTJ region of one control limb contralateral to its sham limb (horse 3, right forelimb) was assigned a fibrosis score of 1 (Table 7.4B).

Table 7.2A: Movin scoring for all histologically evaluated levels of limbs exposed to blood flow restriction (BFR) training over a 56-day study period.

Horse, Limb	Level	Fiber Structure	Fiber Arrangement	Rounding of Nuclei	Regional Variations in Cellularity	Increased Vascularity	Decreased Collagen Stainability	Hyalinization	GAG Content	Total Movin Score
					BFR Limbs					
					Movin Scoring Criteria					
2, RF	1	0	0	0	0	0	0	0	0	0
	2	0	0	0	0	0	0	0	0	0
	3	0	0	0	0	0	0	0	0	0
	4	0	0	0	0	0	0	0	0	0
	5	0	0	0	0	0	0	0	0	0
4, RF	1	0	0	0	0	0	0	0	0	0
	2	0	0	0	0	0	0	0	0	0
	3	0	0	0	0	0.5	0	0	0	0.5
	4	0	0	0	0	0	0	0	0	0
	5	0	0	0	0	0	0	0	0	0
6, LF	1	0	0	0	0	0	0	0	0	0
	2	0.5	0.5	0.5	0.5	0	0	0	0.5	2.5
	3	0	0	0	0	0	0	0	0	0
	4	0.5	0.5	0.5	0.5	0	0	0	0.5	2.5
	5	0	0	0	0	0	0	0	0	0
7, LF	1	0	0	0	0	0	0	0	0	0
	2	0	0	0	0	0	0	0	0	0
	3	0	0	0	0	0	0	0	0	0
	4	0	0	0	0	0	0	0	0	0
	5	0	0	0	0	0	0	0	0	0

Table 7.2B: Movin scoring for all histologically evaluated levels of control limbs contralateral to BFR limbs over a 56-day study period.

Horse, Limb	Level	Fiber Structure	Fiber Arrangement	Rounding of Nuclei	Regional Variations in Cellularity	Increased Vascularity	Decreased Collagen Stainability	Hyalinization	GAG Content	Total Movin Score
					Control Limbs Contralateral to BFR Limbs					
					Movin Scoring Criteria					
2, LF	1	0	0	0	0	0	0	0	0	0
	2	0	0	0	0	0	0	0	0	0
	3	0	0	0	0	0	0	0	0	0
	4	0	0	0	0	0	0	0	0	0
	5	0	0	0	0	0	0	0	0	0
4, LF	1	0	0	0	0	0	0	0	0	0
	2	0	0	0	0	0	0	0	0	0
	3	0	0	0	0	0	0	0	0	0
	4	0	0	0	0	0	0	0	0	0
	5	0	0	0	0	0	0	0	0	0
6, RF	1	0	0	0	0	0	0	0	0	0
	2	0	0	0	0	0	0	0	0	0
	3	0	0	0	0	0	0	0	0	0
	4	0	0	0	0	0	0	0	0	0
	5	0	0	0	0	0	0	0	0	0
7, RF	1	0	0	0	0	0	0	0	0	0
	2	0	0	0	0	0	0	0	0	0
	3	0	0	0	0	0	0	0	0	0
	4	0	0	0	0	0	0	0	0	0
	5	0	0	0	0	0	0	0	0	0

Table 7.2C: Movin scoring for all histologically evaluated levels of sham-exposed limbs over a 56-day study period. '.' Indicates tissue shearing that precluded histologic grading.

Horse, Limb	Level	Fiber Structure	Fiber Arrangement	Rounding of Nuclei	Regional Variations in Cellularity	Increased Vascularity	Decreased Collagen Stainability	Hyalinization	GAG Content	Total Movin Score
					0% BFR, Sham Limbs					
					Movin Scoring Criteria					
1, LF	1	0	0	0	0	0	0	0	0	0
	2	0.5	0.5	0.5	0.5	0	0	0	0.5	2.5
	3	0.5	0.5	0.5	0.5	0	0	0	0.5	2.5
	4	.	.	.	.	.	.	.	.	.
	5	0	0	0	0	0	0	0	0	0
3, LF	1	0	0	0	0	0	0	0	0	0
	2	0	0	0	0	0	0	0	0	0
	3	0	0	0	0	0	0	0	0	0
	4	0	0	0	0	0	0	0	0	0
	5	0	0	0	0	0	0	0	0	0
5, RF	1	0	0	0	0	0	0	0	0	0
	2	0	0	0	0	0	0	0	0	0
	3	0	0	0	0	0	0	0	0	0
	4	0	0	0	0	0	0	0	0	0
	5	.	.	.	.	.	.	.	.	.
8, RF	1	0	0	0	0	0	0	0	0	0
	2	0	0	0	0	0	0	0	0	0
	3	0	0	0	0	0	0	0	0	0
	4	0	0	0	0	0	0	0	0	0
	5	0	0	0	0	0	0	0	0	0

Table 7.2D: Movin scoring for all histologically evaluated levels of control limbs contralateral to sham-exposed limbs over a 56-day study period.

Horse, Limb	Level	Fiber Structure	Fiber Arrangement	Rounding of Nuclei	Regional Variations in Cellularity	Increased Vascularity	Decreased Collagen Stainability	Hyalinization	GAG Content	Total Movin Score
					Control Limbs Contralateral to Sham Limbs					
					Movin Scoring Criteria					
1, RF	1	0	0	0	0	0	0	0	0	0
	2	0	0	0	0	0	0	0	0	0
	3	0	0	0	0	0	0	0	0	0
	4	0	0	0	0	0	0	0	0	0
	5	0	0	0	0	0	0	0	0	0
3, RF	1	0	0	0	0	0	0	0	0	0
	2	0	0	0	0	0	0	0	0	0
	3	0.5	0.5	1	1	0	0.5	0	1	4.5
	4	0	0	0	0	0	0	0	0	0
	5	0	0	0	0	0	0	0	0	0
5, LF	1	0	0	0	0	0	0	0	0	0
	2	0	0	0	0	0	0	0	0	0
	3	0	0	0	0	0	0	0	0	0
	4	0	0	0	0	0	0	0	0	0
	5	0	0	0	0	0	0	0	0	0
8, LF	1	0	0	0	0	0	0	0	0	0
	2	0	0	0	0	0	0	0	0	0
	3	0	0	0	0	0	0	0	0	0
	4	0	0	0	0	0	0	0	0	0
	5	0	0	0	0	0	0	0	0	0

Table 7.3A: Bonar scoring for all histologically evaluated levels of limbs exposed to blood flow restriction (BFR) training over a 56-day study period.

Horse, Limb	Level	Tenocytes	Ground Substance	Collagen	Vascularity	Total
			BFR Limbs			
			Bonar Scoring Criteria			
2, RF	1	0	0	0	0	0
	2	0	0	0	0	0
	3	0	0	0	0	0
	4	0	0	0	0	0
	5	0	0	0	0	0
4, RF	1	0	0	0	0	0
	2	0	0	0	0	0
	3	0	0	0	0.5	0.5
	4	0	0	0	0	0
	5	0	0	0	0	0
6, LF	1	0	0	0	0	0
	2	0.5	0.5	0.5	0	1.5
	3	0	0	0	0	0
	4	0.5	0.5	0.5	0	1.5
	5	0	0	0	0	0
7, LF	1	0	0	0	0	0
	2	0	0	0	0	0
	3	0	0	0	0	0
	4	0	0	0	0	0
	5	0	0	0	0	0

Table 7.3B: Bonar scoring for all histologically evaluated levels of control limbs contralateral to BFR limbs over a 56-day study period.

Horse, Limb	Level	Tenocytes	Ground Substance	Collagen	Vascularity	Total
			Control Limbs Contralateral to BFR Limbs			
			Bonar Scoring Criteria			
2, LF	1	0	0	0	0	0
	2	0	0	0	0	0
	3	0	0	0	0	0
	4	0	0	0	0	0
	5	0	0	0	0	0
4, LF	1	0	0	0	0	0
	2	0	0	0	0	0
	3	0	0	0	0	0
	4	0	0	0	0	0
	5	0	0	0	0	0
6, RF	1	0	0	0	0	0
	2	0	0	0	0	0
	3	0	0	0	0	0
	4	0	0	0	0	0
	5	0	0	0	0	0
7, RF	1	0	0	0	0	0
	2	0	0	0	0	0
	3	0	0	0	0	0
	4	0	0	0	0	0
	5	0	0	0	0	0

Table 7.3C: Bonar scoring for all histologically evaluated levels of sham-exposed limbs over a 56-day study period. '.' Indicates tissue shearing that precluded histologic grading.

Horse, Limb	Level	Tenocytes	Ground Substance	Collagen	Vascularity	Total
			0% BFR, Sham Limbs			
			Bonar Scoring Criteria			
1, LF	1	0	0	0	0	0
	2	0.5	0.5	0.5	0	1.5
	3	0.5	0.5	0.5	0	1.5
	4	.	.	.	.	.
	5	0	0	0	0	0
3, LF	1	1.5	0	0	0	0
	2	0	0	0	0	0
	3	0	0	0	0	0
	4	0	0	0	0	0
	5	0	0	0	0	0
5, RF	1	0	0	0	0	0
	2	0	0	0	0	0
	3	0	0	0	0	0
	4	0	0	0	0	0
	5	.	.	.	.	.
8, RF	1	0	0	0	0	0
	2	0	0	0	0	0
	3	0	0	0	0	0
	4	0	0	0	0	0
	5	0	0	0	0	0

Table 7.3D: Bonar scoring for all histologically evaluated levels of control limbs contralateral to sham-exposed limbs over a 56-day study period.

Horse, Limb	Level	Tenocytes	Ground Substance	Collagen	Vascularity	Total
			Control Limbs Contralateral to Sham Limbs			
			Bonar Scoring Criteria			
1, RF	1	0	0	0	0	0
	2	0	0	0	0	0
	3	0	0	0	0	0
	4	0	0	0	0	0
	5	0	0	0	0	0
3, RF	1	0	0	0	0	0
	2	0	0	0	0	0
	3	1	1	1	0	3
	4	0	0	0	0	0
	5	0	0	0	0	0
5, LF	1	0	0	0	0	0
	2	0	0	0	0	0
	3	0	0	0	0	0
	4	0	0	0	0	0
	5	0	0	0	0	0
8, LF	1	0	0	0	0	0
	2	0	0	0	0	0
	3	0	0	0	0	0
	4	0	0	0	0	0
	5	0	0	0	0	0

Table 7.4A: Musculotendinous junction (MTJ) scoring for all limbs exposed to blood flow restriction (BFR) training and their contralateral (control) limbs over a 56-day study period.

| | BFR Limbs | | | |
| | MTJ Scoring Criteria | | | |
Horse, Limb	Level	Ground Substance	Vascularity	Fibrosis
2, RF	5	0	0	0
4, RF	5	0	0	0
6, LF	5	0	0	0
7, LF	5	0	0	0.5
	Control Limbs Contralateral to BFR Limbs			
2, LF	5	0	0	0
4, LF	5	0	0	0
6, RF	5	0	0	1.5
7, RF	5	0	0	0.5

Table 7.4B: Musculotendinous junction (MTJ) scoring for all sham-exposed limbs and their contralateral (control) limbs over a 56-day study period.

| | 0% BFR, Sham Limbs | | | |
| | MTJ Scoring Criteria | | | |
Horse, Limb	Level	Ground Substance	Vascularity	Fibrosis
1, LF	5	0	0	1
3, LF	5	0	0	1
5, RF	5	0	0	0
8, RF	5	0	0	0
	Control Limbs Contralateral to Sham Limbs			
1, RF	5	0	0	0
3, RF	5	0	0	1
5, LF	5	0	0	0
8, LF	5	0	0	0

BFR's Effects on the Equine Superficial Digital Flexor Tendon Discussion:

This study is the first of its kind to demonstrate that BFR applied at the muscular level results in concurrent tendon property changes in horses, thereby suggesting utility for BFR in tendon rehabilitation strategies. Specifically, intra-horse differences in SDFT stiffness were appreciated, with tendons exposed to BFR demonstrating increased stiffness relative to contralateral counterparts. This was associated with a trend in increased CSA, which resulted in no differences seen in elastic modulus. While numerous studies in both humans [5, 19] and horses [12, 20-22] have documented physiologic responses of muscle to BFR exposure, investigations to assess BFR's concurrent, tendon-specific effects are more sparse [20, 23-26]. Additionally, current *in-vivo* investigative techniques lack sensitivity to detect changes in biomechanical and histologic responses over multiple tendinous locations that would ultimately help determine adaptive responses to BFR [14, 23-24, 27]. This study demonstrates no negative impact of BFR on mechanical strength of the equine SDFT over a 56-day study period, with evidence in this small cohort to suggest that BFR resulted in increased tendon stiffness with a trend for increased tendon CSA. Additionally, evidence of histologic tendinous damage as a result of BFR exposure was not appreciated.

Superficial digital flexor tendon overuse injuries remain a frequent and frustrating cause of morbidity in athletic horses [28-31]. Tendon injury was implicated as the primary reason for retirement of Thoroughbred racehorses over a twelve-year epidemiologic study period in Hong Kong [32]. Similarly, event horses were most commonly unable to compete due to tendon or ligament injury in the United Kingdom [33]. Despite long periods of convalescence, re-injury rates as high as 82% in slight, moderate or severe SDFT injuries have been documented [34]. While mechanistic focus has historically implicated the role of progressive microdamage of

collagen fibrils, investigators have recently concluded that tendon injury may not be due exclusively to tendon weakness, but rather is the result of functional deficiencies through the entire superficial digital flexor (SDF) muscle-tendon complex [35-37]. The SDF muscle specifically is known for attenuating high-frequency vibrations of the forelimb [38] and enhancing elastic energy storage [38-39]. Cumulatively, these features suggest that the SDF muscle-tendon unit comprises a biomechanically critical limb-spring system that reduces the metabolic cost of locomotion [39-40]. Recent metabolic studies, however, have documented the predisposition of the SDF muscle to early onset of fatigue [37, 41]. This fatigue-predisposition compounds the SDF muscle's inability to accommodate large biomechanical forces during maximal exercise [35, 40], leading to inherent, potentially catastrophic limitations of the SDF muscle-tendon unit. Additionally, when exercise can be safely initiated following SDFT injury, it is usually at a much lower intensity than pre-injury. Due to the inability to predict spontaneous overexertion, rehabilitation protocols are often much more conservative than they likely have to be. The resultant disuse then initiates a cascade of secondary SDF muscle weakness, decreases in intra-tendinous collagen mass, increases in the scar tissue protein glycosaminoglycan (GAG) and resultant biomechanical weakness. Strengthening the SDF muscle-tendon complex would allow its tendon to return and store elastic energy more efficiently, making it an attractive target for preventative and rehabilitative strategies.

Subsequent equine rehabilitation efforts have been directed at improving strength of the SDF muscle-tendon complex as a therapeutic strategy during tendinopathy convalescence [37]. Commonly used rehabilitation modalities such as underwater treadmill and conventional treadmill exercise, however, have failed to affect SDF muscle metabolic responses over four- and eight-week time periods [37, 41], suggesting that neither modality alone increases muscle

oxidative capacity to the same extent as other forms of resistance training [42]. An array of therapeutic options including mesenchymal stem cells (MSCs), high-intensity laser therapy and extra-corporeal shockwave therapy are available for injured tendons; however, these modalities have not been shown to improve cellular or functional health of the entire muscle-tendon complex long-term, limiting their effectiveness in a global rehabilitation approach. Despite the utilized therapy, the rehabilitation period is still prolonged, potentiating the cascade of secondary weakness and lose of biomechanical strength through the SDF muscle-tendon complex. An effective rehabilitative modality that would improve tendinopathic features at the cellular level and increase mechanical strength of the SDF muscle-tendon complex is currently lacking, but would be hugely impactful due to: 1) improved healing, 2) quicker returns to function and 3) decrease associated economic losses.

The biomechanical effects of BFR on the equine SDFT as reported herein are exciting, and similar to a recent human investigation that documented increases in both Achilles tendon CSA and stiffness, but no change in elastic modulus following 50% BFR exposure [23]. Specifically, Achilles myotendinous adaptations after 14 weeks of strength training were investigated in 55 male volunteers [23]. Similar to equine methodology described herein, investigators determined arterial occlusion pressures (AOP) in a standing position using Doppler ultrasound, then utilized a subsequent cuff pressure at 50% of each individual's AOP (in comparison to 80% LOP as described herein). Authors noted adaptive changes in Achilles tendon properties following low-load resistance training with BFR to be comparable to that of traditional high-load resistance training, which is of particular relevance to those patients who may not tolerate heavy training loads, but would still benefit from improvements in myotendinous function [23]. Noteworthy, however, was the incorporation of progressively

increased loads (weight) in the BFR group, which is different than the static walking exercise utilized for horses herein. It is possible that a different exercise protocol in terms of duration, frequency, speed or addition of a limb weight may have yielded different results in our group of horses. Interestingly, when this same group of investigators evaluated the effects of 14 weeks of BFR compared to high-load training on patellar tendon adaptations, they described similar findings (comparable changes in patellar tendon stiffness and similar increases in patellar tendon CSA between the two groups) [24].

Also of interest is the mechanism and timing for which these acute responses in Achilles tendon thickness (CSA) occur in relation to BFR exposure [25-26]. In contrast to our findings here, Picon-Martinez *et al* described statistically significant decreases in Achilles tendon thickness immediately, 60 minutes and 24 hours post BFR exposure (at 30% of an individual's AOP) [26]. These authors speculated that movement of fluid into the tendon that may occur with exposure to BFR may ultimately reduce the amount of free water, thereby transiently reducing tendon CSA [26]. They also describe that the inclusion of BFR into the *continuum* of tendon rehabilitative strategies may be ideal due to the lack of inflammatory response and ability to only place low-load mechanical stresses on joints [26]. Similarly, Chulvi-Medrano et al also postulated that acute responses in Achilles tendon thickness following exposure to BFR may be due to intratendinous fluid movement [25]. It is possible that inherent morphometric differences in human Achilles structure compared to that of the equine SDFT resulted in conflicting CSA findings, or that exercise differences (percentage of occlusion, incorporation of weighted exercise, etc) also affected our results.

To date, previous investigations have not incorporated histologic evaluation of tendons exposed to BFR compared to unexposed controls. Of particular interest in relation to BFR

exposure was the evaluation of tendinous cellularity, neovascularization and GAG deposition. The study design utilized herein allowed comparison of four total treatment exposures: 1) BFR, 2) contralateral limb of BFR exposure, 3) sham (control) and 4) contralateral limb of sham exposure over five tendinous sites including the MTJ. No consistent qualitative histologic differences were appreciated between treatment groups according to the utilized Bonar, Movin or MTJ evaluation criteria leading us to conclude that the BFR exercise protocol utilized did not manifest as detrimental changes at the cellular level. While significant histologic changes in this population of normal tendons was not expected, it was surprising that no major differences in neovascularization were appreciated. Similar histologic evaluation of naturally occurring tendon injury or experimental models of tendinopathy exposed to BFR represent logical next steps to further characterize injury responses.

The most consistently documented therapeutic benefits of BFR within the human literature are muscular hypertrophy and subsequent increases in strength secondary to elevated levels of growth hormone (GH) [43-44]. The metabolic accumulation of GH has been demonstrated to reach supraphysiologic levels (290 times that of baseline) during human BFR training and is thought to be the main activator of resultant muscular hypertrophy [43-44]. Pertinent to the muscle-tendon complex, GH has been documented to play a direct role in increased muscle and tendon collagen synthesis after exercise [45]. Given that GH plays a direct role in increased muscle and tendon collagen synthesis following exercise [45], and BFR use in horses has been demonstrated to result in elevations in GH and muscular hypertrophy [20], it's reasonable to hypothesize that BFR incorporation may augment healing of the equine SDF muscle-tendon complex to a greater extent than exercise alone, but direct insight at the

199

mechanistic level in horses is still lacking. This type of further mechanistic investigation represents a promising source of future investigation opportunities.

Study limitations include short-term comparisons in a small sample population without correlation to performance outcome measures. This study thus far has demonstrated no negative impact of BFR on mechanical strength of the equine SDFT over a 56-day study period, with evidence in this small cohort to suggest that BFR resulted in increased tendon stiffness with a trend for increased tendon CSA in absence of consistent histologic changes.

7.4 BFR's Effects on Equine Articular Cartilage

BFR's Effects on Equine Articular Cartilage Materials & Methods:

Following macroscopic evaluation as previously described [46], articular cartilage sections (5mm biopsies) were collected from each third carpal bone [47] and processed for routine histologic analysis (hematoxylin and eosin (H&E) and safranin O fast green (SOFG)), then macroscopically and microscopically graded as previously described [46]. Osteochondral fragments measuring 3mm in diameter were also harvested from the third carpal bone and analyzed for live cells and glycosaminoglycan (GAG) content from sites previously described [47]. The live/dead viability was determined using the live/dead staining reagent[8]. The total content of sulfated GAG was determined by 1,9 dimethylmethylene blue (DMMB) binding as described previously [47, 48-49].

To investigate the relationships between BFR exposure and response variables of live cell viability percentage and GAG levels, a linear mixed model was fit. To account for the design of data collection and paired limbs, the model included fixed effects of treatment and random effect

---

[8] Thermo Fisher Scientific, Waltham, MA, Catalog #L3224

of horse. Diagnostic plots were used to assess assumptions of equal variance and normality. Based on these plots, assumptions were met. Comparisons across exposure were conducted utilizing the lmer4 and emmeans packages. Tukey's adjustment of *P*-values for pairwise comparisons were used.

BFR's Effects on Equine Articular Cartilage Results:

 Qualitative differences between treatment groups for macroscopically assessed criteria were not appreciated between treatment groups. Specifically, the macroscopically assessed criteria (scale of 0 (normal) to 4 (severe), Tables 7.5 and 7.6), only one limb was assigned a total erosion score of one, with all other limbs scoring zero. This limb belonged to a sham limb (Table 7.6). Two control limbs contralateral to the BFR exposed forelimbs were given a total hemorrhage score of one (Table 7.5). One sham limb was assigned a partial thickness erosion score of 2, while one limb contralateral to a sham limb (control limb) was given a score of one (Table 7.6). All remaining macroscopically assessed histologic grades for all limbs were found to be zero (normal).

 Qualitative differences between treatment groups for microscopically assessed criteria were not appreciated between treatment groups. Specifically, none of the BFR-exposed limbs demonstrated any level of chondrocyte necrosis or fibrillation fissuring (Table 7.5). All BFR-exposed limbs were given a score of 1 for clustered complex chondrone formation, with their contralateral limbs all given scores of 0. Three of the four BFR-exposed limbs were assigned focal cell loss scores of zero, while one was given a score of one. Two of the BFR-exposed limbs were given SOFG scores of 3, with the other two being zero. Total histologic scores for BFR limbs ranged from 1-5 (Table 7.5) while their contralateral unexposed counterparts (control

limbs) ranged from 0-3 (Table 7.5). All macroscopic and microscopic grades are reported in Tables 7.5 and 7.6.

No statistically significant differences in any evaluated GAG or live cell viability values between treatment groups were appreciated ($P > 0.05$), with all estimates, standard errors (SE) and P-values reported in Table 7.7. Means and standard deviations (SDs) for DMMB based on dry weight (mg) for BFR-exposed limbs and their contralateral (control) counterparts were found to be 512.8 ± 326.15 and 325.75 ± 266.91, respectively (Figure 7.6). DNA content for BFR-exposed limbs in comparison to the sham BFR-exposed limbs was 1.74 ± 0.10 and 1.59 ± 0.31, respectively. Percentage of live cell viability for BFR-exposed, their contralateral (control) limbs, sham BFR limbs and their contralateral (control) limbs was found to be 87.66 ± 11.10, 84.71 ± 7.56, 89.56 ± 5.44 and 93.85 ± 4.95, respectively. All reported means and standard deviations are reported in Figure 7.6.

Table 7.5: Macroscopic and microscopic histologic grading of Safranin O (SAFOG) and hematoxylin and eosin (H&E) stained articular cartilage samples taken from the third carpal bone of limbs exposed to 80% forelimb blood flow restriction (BFR) in contrast to their contralateral forelimbs (control limbs). Study horses 2, 4, 6 and 7 were randomly assigned to the BFR study group, with their respective forelimb also denoted (left forelimb (LF), right forelimb (RF)). All scoring was graded on a 0 (normal) to 4 (severe) scale.

	BFR Limbs											
	Macroscopic Grading						Microscopic Grading					
Horse	Total Erosion Score	Total Hemorrhage Score	Full Thickness Erosion	Partial Thickness Erosion	Kissing Lesion	Synovial Adhesion	Chondrocyte Necrosis	Cluster Complex Chondrone Formation	Fibrillation Fissuring	Focal Cell Loss	SAFOG Stain Uptake	Total Histo Score
2 (RF)	0	0	0	0	0	0	0	1	0	0	3	4
4 (RF)	0	0	0	0	0	0	0	1	0	0	0	1
6 (LF)	0	0	0	0	0	0	0	1	0	0	0	1
7 (LF)	0	0	0	0	0	0	0	1	0	1	3	5
	Control Limbs Contralateral to BFR Limbs											
2 (LF)	0	1	0	0	0	0	0	0	0	0	2	2
4 (LF)	0	1	0	0	0	0	0	0	0	2	1	3
6 (RF)	0	0	0	0	0	0	0	0	0	0	2	2
7 (RF)	0	0	0	0	0	0	0	0	0	0	0	0

Table 7.6: Macroscopic and microscopic histologic grading of Safranin O (SAFOG) and hematoxylin and eosin (H&E) stained articular cartilage samples taken from the third carpal bone of limbs exposed to 0% (sham) forelimb blood flow restriction (BFR) in contrast to their contralateral forelimbs (control limbs). Study horses 1, 3, 5 and 8 were randomly assigned to the 0% (sham) study group, with their respective forelimb also denoted (left forelimb (LF), right forelimb (RF). All scoring was graded on a 0 (normal) to 4 (severe) scale.

	0% BFR, Sham Limbs											
	Macroscopic Grading						Microscopic Grading					
Horse	Total Erosion Score	Total Hemorrhage Score	Full Thickness Erosion	Partial Thickness Erosion	Kissing Lesion	Synovial Adhesion	Chondrocyte Necrosis	Cluster Complex Chondrone Formation	Fibrillation Fissuring	Focal Cell Loss	SAFOG Stain Uptake	Total Histo Score
1 (LF)	1	0	0	2	0	0	0	1	0	0	1	2
3 (LF)	0	0	0	0	0	0	0	1	2	1	1	3
5 (RF)	0	0	0	0	0	0	0	2	0	0	0	2
8 (RF)	0	0	0	0	0	0	0	0	0	0	4	4
	Control Limbs Contralateral to Sham Limbs											
1 (RF)	0	0	0	0	0	0	0	1	0	0	4	5
3 (RF)	0	0	0	1	0	0	0	1	0	1	1	3
5 (LF)	0	0	0	0	0	0	0	1	0	0	3	4

8 (LF)	0	0	0	0	0	0	0	0	0	0	0	2

Table 7.7: Reported estimates, standard errors (SE) and *P*-values based on the results of a linear mixed model with Tukey's pairwise comparisons for evaluated cartilage parameters comparing study groups of 80% blood flow restriction (BFR) exposure, controls (no BFR or sham cuff) and 0% BFR (sham cuff) exposure. Evaluated cartilage parameters were dimethylmethylene blue assay (DMMB) based on dry weight (mg) and DNA (DMMB DNA, µg/mL), DNA content (µg/mL), Hoescht concentration (µg/mL) and the percentage of live cell viability (live percent).

Cartilage Parameter	Study Group Comparison	Estimate	Standard Error	*P*-value
DMMB Dry Weight	Control vs. 0% BFR	-46.1	87.9	0.86
	Control vs. 80% BFR	-203.1	87.9	0.12
	0% BFR vs. 80% BFR	-156.9	123.8	0.45
DMMB DNA	Control vs. 0% BFR	-3.44	7.02	0.88
	Control vs. 80% BFR	-4.59	7.02	0.80
	0% BFR vs. 80% BFR	-1.15	9.92	1.00
DNA Content	Control vs. 0% BFR	0.0023	0.15	1.00
	Control vs. 80% BFR	-0.088	0.15	0.82
	0% BFR vs. 80% BFR	-0.09	0.20	0.89
Hoescht	Control vs. 0% BFR	0.047	2.92	1.00
	Control vs. 80% BFR	-1.76	2.92	0.82
	0% BFR vs. 80% BFR	-1.80	3.96	0.89
Live Percent	Control vs. 0% BFR	-0.28	5.28	1.00
	Control vs. 80% BFR	1.62	5.28	0.95
	0% BFR vs. 80% BFR	1.90	6.68	0.95

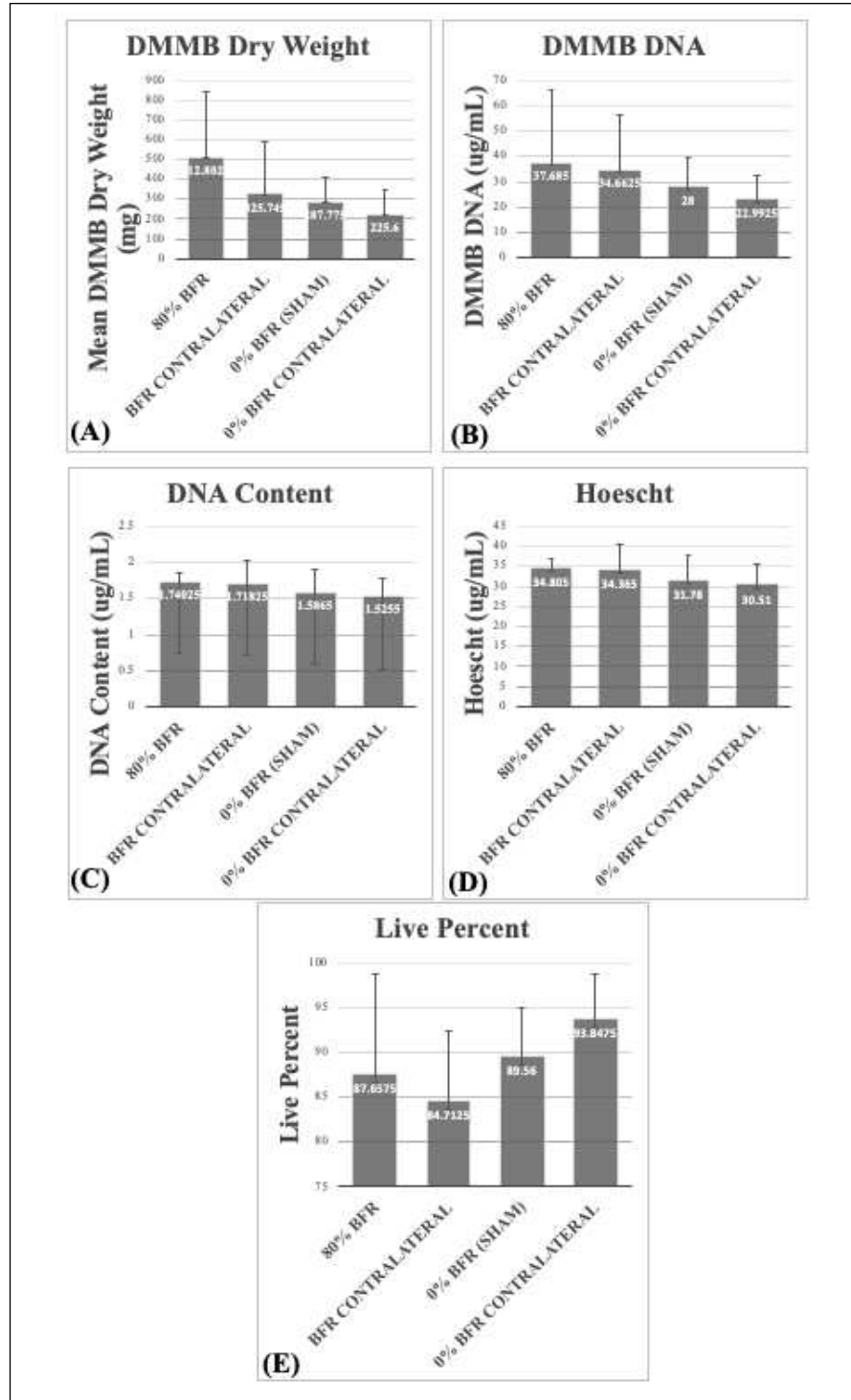**Figure 7.6:** Measured glycosaminoglycan (GAG) cartilage parameters including (A) dimethylmethylene blue assay (DMMB) based on dry weight (mg), (B) DNA (DMMB DNA, μg/mL), (C) DNA content (μg/mL), (D) Hoescht concentration (μg/mL) and (E) percentage of live cell viability (live percent). Data presented as mean +/- STD. No significant differences between groups were noted ($P > 0.05$) based on the results of a linear mixed model.

BFR's Effects on Equine Articular Cartilage Discussion:

The results of this portion of the investigation demonstrate no deleterious effects of BFR walking exercise on articular cartilage based on morphologic, live cell viability and biochemical methods (SOFG and DMMB) to determine GAG content of the third carpal bone. While widespread safety conclusions cannot be extrapolated, these results are exciting and represent the first report of cellular-level effects of BFR on articular cartilage, specifically that of the joint most distal to the site of cuff application. Realization of BFR's physiologic effects on articular cartilage are currently unknown, but would help guide its safe orthopedic use in humans and horses.

Improving muscular strength in absence of high-intensity exercise through the use of BFR training has become a key rehabilitative modality utilized by human physical therapists to restore muscle strength following arthroscopy. Specifically, this low-intensity training promotes a faster return to physical function and less co-morbidity in human patients by mitigating arthrogenic muscle inhibition [7, 50-52] that would otherwise delay or prohibit full return to orthopedic function. Subsequently, BFR has become a post-operative modality for human knee osteoarthritis [53-54] and anterior cruciate ligament (ACL) reconstruction [7, 50-52]. Despite BFR's increasingly widespread use to maintain muscular strength and function in the crucial post-operative period, BFR's effects specifically on articular cartilage properties are unknown. Hence, without investigation of BFR's concurrent effects on cartilage, it's clinical use has been based on speculation that it does not negatively affect articular cartilage cellular matrix. The results of our investigation suggest that based on morphologic, live cell viability and biochemical methods to determine GAG content of the third carpal bone, no downstream deleterious effects

207

related to BFR exposure were appreciated. When GAG levels were evaluated via DMMB methods, no significant differences between treatment groups were appreciated (Table 7.7). Qualitative observations of SOFG stain uptake found that BFR limbs demonstrated a mean SOFG stain uptake score of 1.5, compared to their control limbs contralateral limbs' mean of 1.25, while sham limbs and their contralateral limbs were found to have means of 1.5 and 2 respectively (Tables 7.6, 7.7). Given that the semi-quantitative evaluated binding of SOFG is considered to have a linear relationship with GAG [55], yet is less reliable and repeatable than GAG biochemical methods [47], our morphologic and biochemical findings are in accordance with each other that group differences were equivocal. While detrimental effects at the articular cartilage level as a result of BFR exposure were not expected, because cartilaginous health relies heavily on diffusion for nutrient supply and waste removal, any stimulus that may subsequently alter vascular, lymphatic or neural blood supply warrants safety investigation as a physiotherapeutic modality.

The motivation to utilize BFR application post-arthroscopy in people stems from the ability to provide an effective rehabilitation tool that does not place heavy loads and force through the tibiofemoral joint [52]. In particular, substantial skeletal muscle atrophy ensues following anterior cruciate ligament (ACL) tears and osteoarthris (OA) due to changes in muscle protein balance and satellite cell abundance [52], for which BFR has been shown to dramatically improve [51-52]. Despite significant insight into the muscular and beneficial functional effects of BFR post meniscal repair or chondral restoration surgery [56], there is little information about tissue level effects. Equine athletes experience similar injuries with meniscal tears [57-59] and osteoarthritis [3] representing significant sources of equine morbidity requiring more optimized rehabilitative solutions. The objective of this study was to investigate the health of articular

cartilage following BFR training, which are currently unknown in both humans and horses. While BFR's treatment efficacy for specific equine injuries still remains unknown, our results suggest that BFR muscular application does not cause substantial harm to normal (healthy) articular cartilage.

Limitations of this study include a small study population evaluating BFR's effects in only healthy articular cartilage without analysis of synovial fluid or cartilage biomechanics. Further investigations incorporating more robust tissue analysis in osteoarthritic cartilage or various experimental injury models represent logical next investigative steps.

7.5 BFR's Effects on Equine Subchondral Bone

BFR's Effects on Equine Subchondral Bone Materials & Methods:

Following euthanasia, both forelimbs of all horses were harvested at the level of the scapulohumeral joint and a post-mortem computed tomographic (CT) evaluation was performed (Siemens Somatome Definition AS 64). To evaluate bone density, a region of interest (ROI) 4mm distal to the articular surface was drawn around the entire circumference of the third carpal bone using the free-hand ROI tool. Hounsfield Units (HU) readings of each third carpal bone were then recorded. All ROI's and subsequent HU readings were determined by a board-certified veterinary radiologist blinded to treatment groups. Following CT evaluation, soft tissues were removed and gross lesions of all third carpal bones were recorded and photographed. Osteochondral samples from the third carpal bones were harvested, paraffin embedded and stained with H&E for histologic assessment.

Follow professional statistical consultation, all statistical analysis was performed by a board-certified specialist in equine sports medicine and rehabilitation (DACVSMR) using the

software package RStudio[9]. To investigate the relationships between BFR exposure and response variable of HU, a linear mixed model was fit. To account for the design of data collection, the model included fixed effect of treatment and random effect of horse. Diagnostic plots were used to assess assumptions of equal variance and normality. Based on these plots, assumptions were met. Comparisons across exposure were conducted utilizing the lmer4 and emmeans packages. Tukey's adjustment of P-values for pairwise comparisons were used.

BFR's Effects on Equine Subchondral Bone Results:

No statistically significant differences in HU readings between treatment groups were found ($P > 0.05$). Mean HU readings for third carpal bones of limbs exposed to BFR was 948.42 ± 254.14 with the contralateral third carpal bones demonstrating a mean HU of 908.17 ± 145.48 (Figure 7.7A). Mean HU readings for third carpal bones of limbs exposed to sham cuff exposure was 926.97 ± 314.44 with the contralateral third carpal bones demonstrating a mean HU of 870.80 ± 28.40. All mean HU's and standard deviations are presented in Figure 7.7A-7.7C. At the time of this publication, histologic analysis (H&E) of third carpal subchondral bone samples is pending.

---

[9] R-project®, R Foundation for Statistical Computing Vienna, Austria
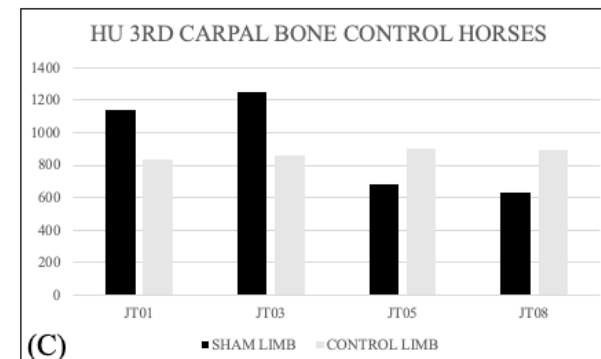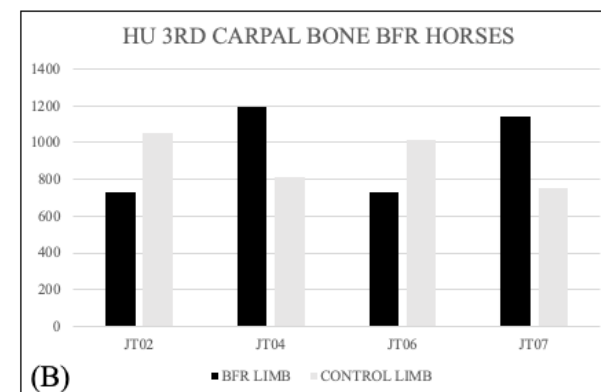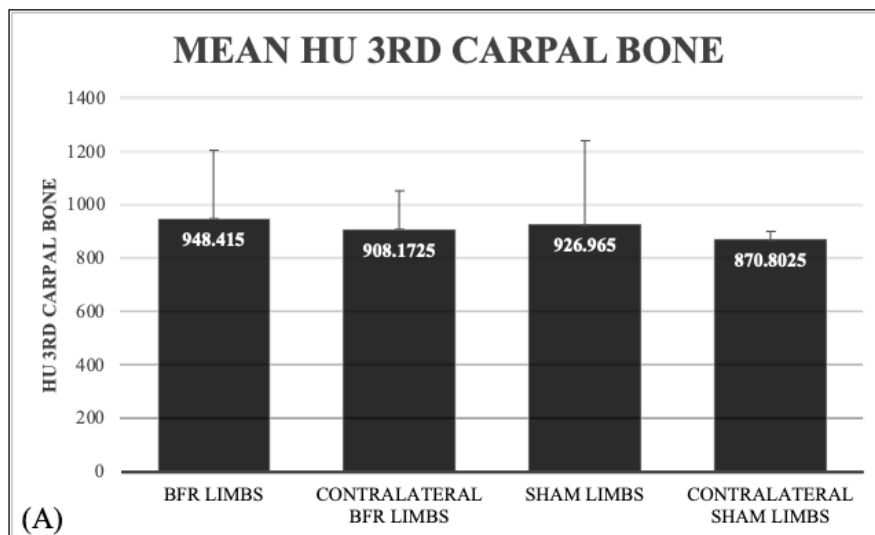
Figure 7.7: (A) Mean Hounsfield Units (HU) and standard deviations as a measure of bone density across the four treatment exposures (BFR, contralateral BFR limbs, sham limbs and contralateral sham limbs). No statistically significant differences in HU readings between exposures was found based on the results of a linear mixed model with Tukey's pairwise adjustment ($P > 0.05$). (B) HU measurements for BFR-exposed third carpal bones compared to their contralateral (unexposed limbs). (C) HU measurements for sham-exposed third carpal bones compared to their contralateral (non sham-exposed) limbs.

BFR's Effects on Equine Subchondral Bone Discussion:

The results of this investigation suggest that no statistically significant changes in (normal) bone density as assessed on post-mortem CT evaluation occurred as a result of exposure to 40 BFR walking sessions. With a small study population and wide standard deviations, it is not surprising that statistically significant differences were not appreciated. Regardless, this experimental design enabled the comparison of four exposure groups, that specifically of: 1) BFR, 2) forelimbs contralateral to BFR exposure, 3) sham limbs and 4) forelimbs contralateral to sham limbs. It was interesting to note that despite the lack of significant differences in HU readings between BFR and sham-exposed limbs, the paired forelimbs of all horses consistently demonstrated appreciable differences that seemingly were unrelated to BFR or sham cuff application (Figure 7.7). The reason for this remains unknown, but a possible explanation is that horses may have inherent physiologic variation related to handed-ness that manifests itself as preferential loading of one forelimb over the other. Baseline CT evaluation would have helped identify if these left to right differences existed prior to any BFR or exercise exposure had it been monetarily feasible.

The downstream effects BFR may have on osseous remodeling is a source of ongoing investigation [60], and of particular interest to those clinicians incorporating its use into post-fracture repair rehabilitation. While direct mechanistic insight is still lacking, three theories currently exist that implicate BFR exposure to improved osseous healing including that of: 1) Supraphysiologic increases in growth hormone (GH) [44, 60], 2) Alterations in the interstitial fluid flow (IFF) [61] and 3) Increases in vascular endothelial growth factor (VEGF) [61].

In a distraction osteogenesis model of micropigs, exogenously administered GH improved callus formation and overall bone formation [62]. Similarly, a clinical trial in 406

human patients with closed tibial fractures found a 26% decrease in healing time in the group receiving GH (95 days) compared to the placebo group (129 days) [63]. With clinical trials still lacking to substantiate this direct triangular correlation between BFR, GH and improved osseous healing, the (likely multi-factorial) etiology remains unknown. Another potential explanation could be that the increases in GH and subsequent improvements in muscular size and function as a result of BFR exposure optimize mechanical loading of the bone itself. With bone having been demonstrated to be highly deformable to mechanical loading (Wolf's Law), muscle contractions and gravitational forces [64-65], the ability of alterations in vascular flow (in a variety of capacities) to positively affect bone density in animal fracture models has been a source of ongoing investigation [66-69].

Albeit different than clinically utilized BFR, early venous occlusion models in dogs [70] and goats [66] demonstrated increases in bone density and new bone formation compared to controls [66, 70]. Similarly, femoral vein ligation resulted in increased bone mineral content in a rat hindlimb suspension model, with authors motivated to investigate how alterations in interstitial fluid flow (IFF) affect bone remodeling [67]. As pneumatic cuff technology and methodology evolved with the ability to incorporate intermittent pneumatic compression (IPC) techniques, animal models were utilized to investigate how alterations in blood flow affected the experimentally-induced fracture healing process [68-69]. When mid-tibial osteotomies with a 3-mm gap were induced in 30 rabbits followed by IPC vs. no IPC, an increase in callus area (32.2% larger) and mineral content (49.7%) at the osteotomy gap site was observed only in rabbits receiving IPC [68]. Additionally, improved biomechanical properties in the IPC group were noted (torsional stiffness, maximum torque, angular displacement at maximum torque and energy required to failure) [68]. A similar investigation that created ostectomies in the radii of 30

male beagles followed by cyclic IPC (5 minutes occlusion followed by 2.5 minutes deflation performed 100 times per day for 8 weeks) found a significantly increased bone mineral content in the group receiving IPC compared to the sham cuff group in absence of soft tissue complications [69]. Authors concluded that IPC may be useful to treat "difficult to heal" fractures [69].

Lastly, mechanisms to increase VEGF and bone biomarkers (bone alkaline phosphate, BAP) have motivated investigations into BFR's subsequent mechanistic effects [71-72]. When healthy men walked on a treadmill twice per day for 3 weeks with or without blood flow occlusion pressure cuffs on their thighs, serum BAP was increased 10.8% in the group walking with cuffs compared to only 0.3% in the control-walk group [71]. Interestingly, no significant change in serum insulin-like growth factor 1 (IGF-1) was noted for either group. These findings are in contrast to an investigation looking at only a single bout of vascular restriction during low intensity resistance exercise for which no changes in serum BAP were noted [72].

There are many ways in which this aspect of the study could have been improved, the most notable of which would be through incorporation of baseline (study day 0) CT evaluation. Additionally, healthy bone may not respond to BFR exposure as dramatically as damaged (unhealthy bone), negating any effects we may have been able to appreciate on CT evaluation alone. Regardless, our results thus far suggest that significant changes in bone density as assessed on CT evaluation did not occur as a result of BFR exposure over a 56-day study period. Because the horse remains a promising avenue for translational orthopedic research, further investigations into bone-related mechanisms of action are expected through potential incorporation of cast (disuse) models or experimental fracture creation.

7.6 BFR's Effects on Equine Muscle Fiber Oxidative Capacity

BFR's Effects on Equine Muscle Fiber Oxidative Capacity Materials & Methods:

Following euthanasia and post-mortem CT imaging, both forelimb superficial digital flexor (SDF) muscles just distal to the level of cuff application but proximal to the MTJ were isolated and harvested for processing. Mitochondrial metabolism as a measure of the muscle's oxidative capacity to make usable energy was evaluated using a previously described method [73]. Muscle fiber bundles were prepared using two Oxygraph-2k high-resolution respirometers [74]. Oxygen flux was monitored in real-time by resolving changes in the negative time derivative of the chamber oxygen concentration signal normalized to fiber wet weight following standardized instrumental and chemical background calibrations. All samples were run in duplicate and averaged. Any fiber preparations exhibiting a greater than 10% increase in flux in response to cytochrome c (indicating loss of outer mitochondrial membrane integrity) was excluded.

Follow professional statistical consultation, all statistical analysis was performed using the software package RStudio[10]. To investigate the relationships between BFR exposure and response variables of carbohydrate oxygen consumption rate (carb OXPHOS), fatty acid oxygen consumption rate (fatty acid OXPHOS) and reactive oxygen species (ROS) release, a linear mixed model was fit. To account for the design of data collection, the model included fixed effect of treatment and random effect of horse. Diagnostic plots were used to assess assumptions of equal variance and normality. Based on these plots, assumptions were met. Comparisons across exposure were conducted utilizing the lmer4 and emmeans packages. Tukey's adjustment of *P*-values for pairwise comparisons were used.

---

[10] R-project®, R Foundation for Statistical Computing Vienna, Austria

BFR's Effects on Equine Muscle Fiber Oxidative Capacity Results:

No statistically significant differences in any evaluated muscle oxidative capacity values were appreciated between treatment groups ($P > 0.05$), with all estimates, standard errors (SE) and *P*-values reported in Table 7.8. Means and standard deviations (SDs) for carb OXPHOS for BFR-exposed limbs in comparison to sham limbs were found to be 62.9 ± 5.65 and 60.04 ± 15.44, respectively (Figure 7.8). Similarly, fatty acid OXPHOS values were found to be 33.97 ± 6.0 and 35.85 ± 11.67 for BFR vs sham limbs (Figure 7.8). Mean ROS release values for all study groups was 0.001 (Figure 7.9). All reported means and standard deviations are reported in Figures 7.8 and 7.9.

Table 7.8: Reported estimates, standard errors (SE) and *P*-values based on the results of a linear mixed model with Tukey's pairwise comparisons for all evaluated muscle oxidative capacity parameters comparing study groups of 80% blood flow restriction (BFR) exposure, controls (no BFR or sham cuff) and 0% BFR (sham cuff) exposure. Evaluated muscle oxidative capacity parameters were carbohydrate oxygen consumption rate (Carb OXPHOS) during ATP production ($pmmolO_2/mg/sec$), fatty acid oxygen consumption rate (Fatty Acid OXPHOS) during ATP production($pmmolO_2/mg/sec$), and muscle respirometry data normalized to oxygen consumption rates then expressed as reactive oxygen species (ROS/O_2) release.

Muscle Parameter	Study Group Comparison	Estimate	Standard Error	*P*-value
Carb OXPHOS ($pmmolO_2/mg/sec$)	Control vs. Sham	-1.52	6.26	0.97
	Control vs. BFR	-3.13	6.26	0.87
	Sham vs. BFR	-1.61	8.38	0.98
Fatty Acid OXPHOS ($pmmolO_2/mg/sec$)	Control vs. Sham	-0.075	3.47	0.98
	Control vs. BFR	8.485	3.47	0.10
	Sham vs. BFR	8.560	4.9	0.25
ROS Release (ROS/O_2)	Control vs. Sham	-0.000141	0.000143	0.61
	Control vs. BFR	0.000164	0.000143	0.52
	Sham vs. BFR	0.000306	0.000202	0.35
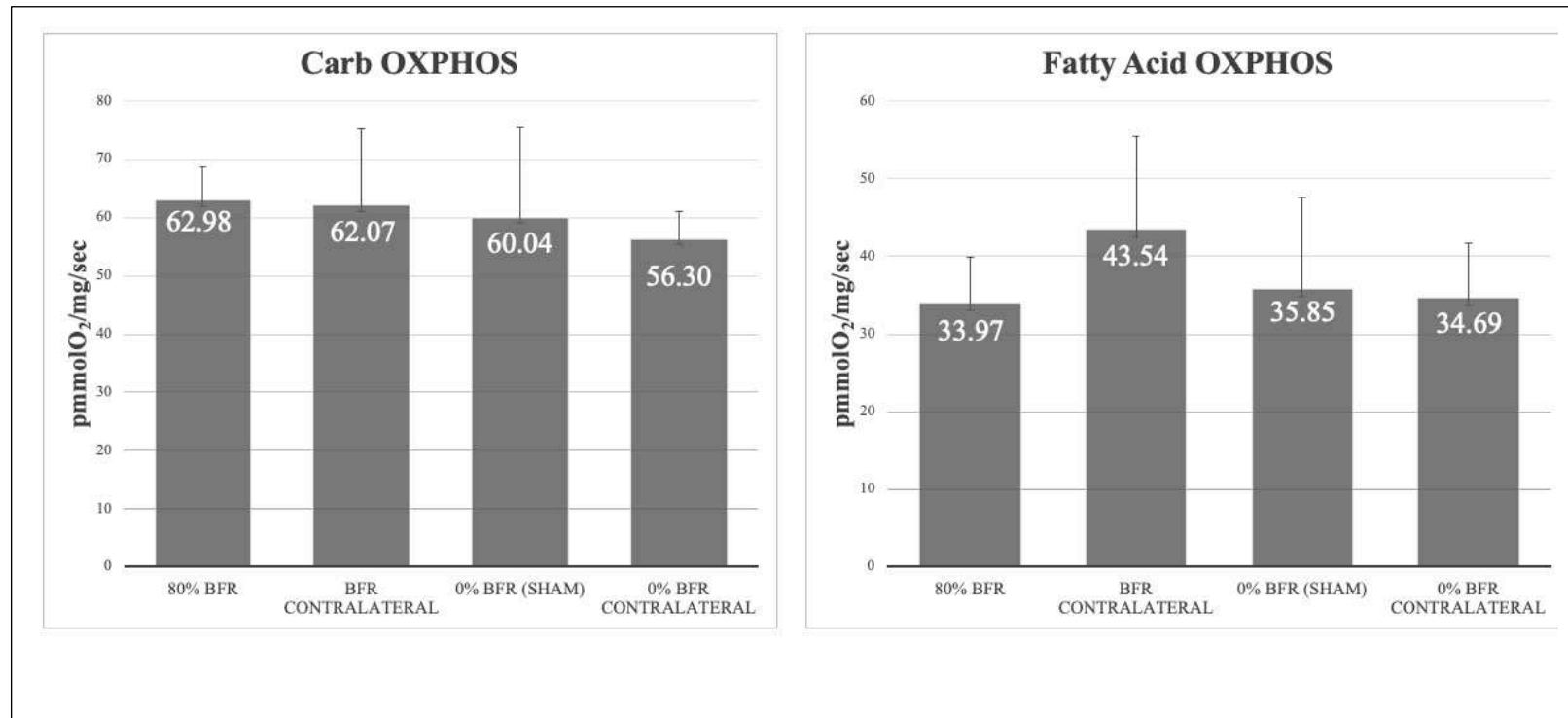
Figure 7.8: Measured muscle oxidative capacity parameters OF (A) carbohydrate oxygen consumption rate (Carb OXPHOS) during ATP production (pmmolO$_2$/mg/sec) and (B) fatty acid oxygen consumption rate (Fatty Acid OXPHOS) during ATP production(pmmolO$_2$/mg/sec). Data presented as mean +/- STD. No significant differences between groups were noted ($P > 0.05$) based on the results of a linear mixed model.
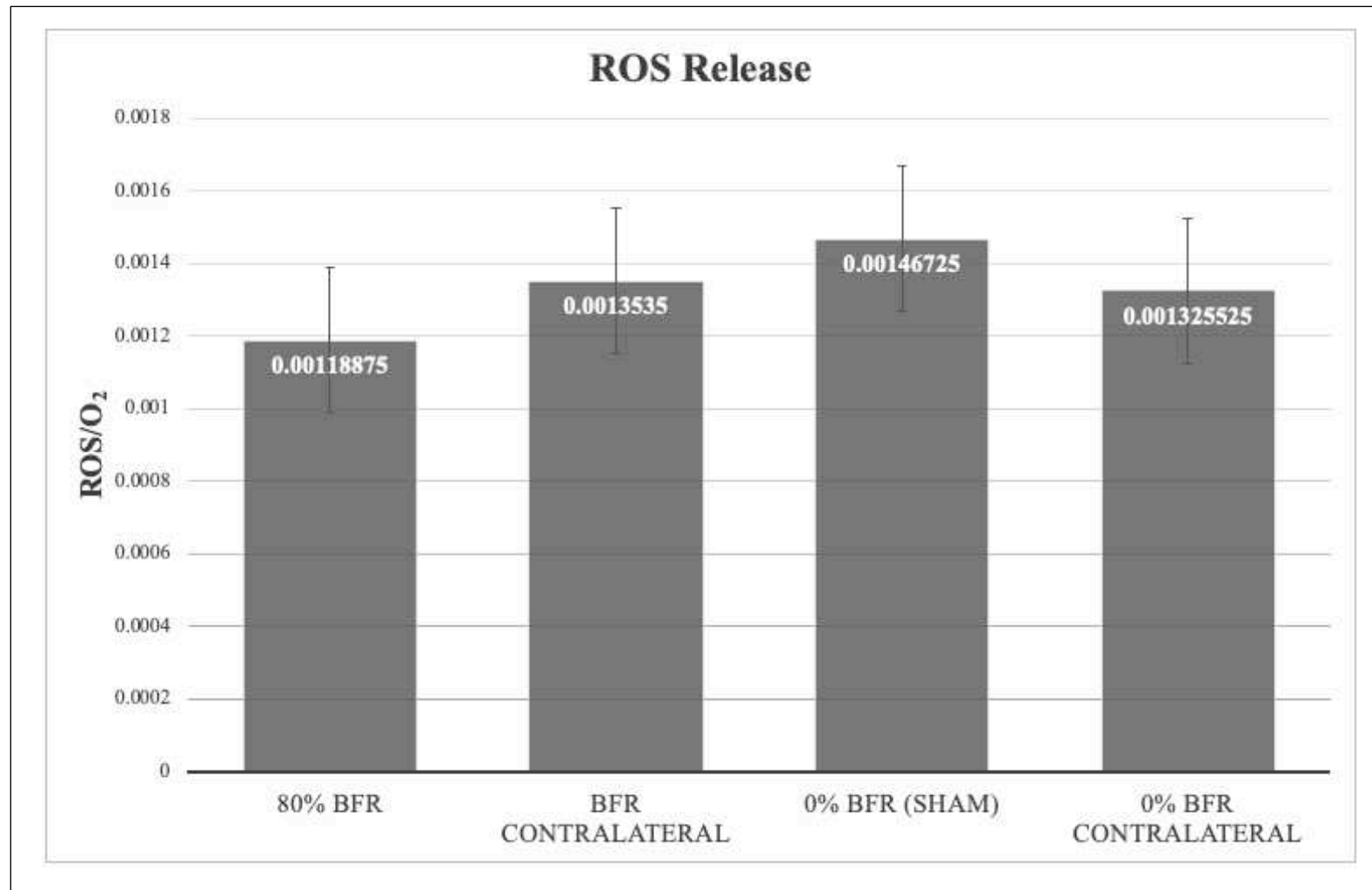
Figure 7.9: Measured muscle respirometry data normalized to oxygen consumption rates then expressed as reactive oxygen species (ROS/O_2) release. Data presented as mean +/- STD. No significant differences between groups were noted ($P > 0.05$) based on the results of a linear mixed model.

BFR's Effects on Equine Muscle Fiber Oxidative Capacity Discussion:

The findings of this investigation suggest that no consistent alterations in SDF muscle mitochondrial density were apparent 56-days following forelimb BFR exposure. It is suspected that early-phase muscle remodeling that manifests as changes in mitochondrial density does not persist with more chronic BFR exposure.

The results herein that demonstrate a lack of metabolic adaptive differences between BFR and sham cuff exposure are interesting, and in contrast to our expected findings. Specifically, our previous 10-day pilot investigation demonstrated significant increases in oxidative capacity of carbohydrate and fatty acid fuel sources with lower H_2O_2 release rates in the superficial digital flexor (SDF) muscle (as measured before vs. after 10 days of 80% BFR walk exercise with the same protocol used herein). Cumulatively, these findings indicated acute metabolic adaptations of increased mitochondrial density and an improved ability to oxidize fuels [12]. With these exciting findings in such a short study period, we were motivated to define more long-term (chronic) metabolic effects, and specifically to compare muscular adaptations to that of a sham cuff treatment group (instead of within-horse differences before vs. after exposure). Potential explanations for this lack of significant differences between treatment groups may be attributed to chronic remodeling that doesn't manifest itself as changes in mitochondrial density, or that more early-phase adaptations were simply missed by a single sampling time point at study day 56. It could also be that treadmill exposure itself neutralized metabolic changes related specifically to BFR usage. Similarly, other rehabilitative modalities sch as underwater treadmill and conventional treadmill exercise have also failed to affect SDF muscle metabolic responses over four and eight-week time periods [37, 41]. Given that such small muscle mass exists in equine limbs, clinical improvements appreciated with the use of such rehabilitative technology

may in fact may not be attributed to muscular metabolic changes, but rather another mechanism of physiologic healing (for example, more symmetric limb loading).

The most consistently documented therapeutic benefits of BFR within the human literature are muscular hypertrophy and subsequent increases in strength secondary to elevated levels of growth hormone (GH) [43-44]. The metabolic accumulation of GH has been demonstrated to reach supraphysiologic levels (290 times that of baseline) during human BFR training and is thought to be the main activator of resultant muscular hypertrophy [43-44]. Recently, early metabolic responses after BFR were demonstrated to result in increases of pyruvate, lactate, alanine and succinate [75]. Increases of these metabolites specifically have been implicated as beneficial in muscle regeneration and muscle protein synthesis, giving credence to their potential role in improved muscular strength and function with incorporation of BFR [76-77]. While not related to BFR usage, the role of hypoxia in physiologic adaptation of skeletal muscle energy metabolism has also described [73]. Blood flow restriction cuff placement and type of exercises employed thereafter is the most significant application difference between human and equine use. It is possible that significantly less large muscle-group access in the horse compared to that of the human will subsequently affect muscular metabolic adaptive responses. Additionally, evaluating metabolic oxidative capacity of only the SDF muscle just distal to the site of cuff application limits conclusions regarding more proximal musculature (such as the triceps) response to BFR. A more robust metabolite approach may reveal if similar metabolic responses occur in horses, even in absence of changes in mitochondrial density.

In conclusion, the muscular adaptations behind BFR use in the horse remain largely unknown, but do not seem to manifest as increases in mitochondrial density or significant

oxidative capacity changes in the SDF muscle just distal to the site of cuff application over 56 days of BFR exposure.

7.7 Conclusion

In summary, this pilot investigation exploring musculoskeletal effects of BFR suggests that it may increase normal equine tendon stiffness and is not detrimental to measured articular cartilage properties or subchondral bone density. When assessing muscle oxidative capacity and reactive oxygen species (ROS) release, we were able to demonstrate that early-phase muscle remodeling (10 days) may not manifest as changes in mitochondrial density that persist with more chronic (56 days) BFR exposure. This work will hopefully provide foundational, much-needed insight into the downstream effects of BFR on tendon, articular cartilage, and subchondral bone to compliment the existing body of work demonstrating beneficial muscle effects.

References

1. Whiting WC, Zernicke RF. Overview and perspectives on injury. In: Biomechanics of musculoskeletal injury. 2nd ed. Human Kinetics;2008:2-15.

2. Caron JP. Osteoarthritis. In: Ross MW, Dyson SJ, eds. Diagnosis and management of lameness in the horse. 2nd ed. Elsevier Saunders;2011:655-668.

3. Caron JP, Genovese RL. Principles and practices of joint disease treatment. In: Ross MW, Dyson SJ, eds. Diagnosis and management of lameness in the horse. Philadelphia, PA: Elsevier; 2003.

4. USDA lameness and laminitis in U.S. horses. USDA: APHIS: VS CEAH. Fort Collins, CO: National Animal Health Monitoring System; 2000. N318.0400.

5. Kawada S. What phenomena do occur in blood flow-restricted muscle? *Int. J. KAATSU Training Res* 2005;1:37-44.

6. Laurentino GC, Ugrinowitsch C, Roschel H, et al. Strength training with blood flow restriction diminishes myostatin gene expression. *Med Sci Sports Exer* 2012; 406-412.

7. Tennent D, Hylden C, Johnson A, et al. Blood flow restriction training after knee arthroscopy: a randomized controlled pilot study. *Clin J Sport Med* 2017;27(3):245-252.

8. Yow BG, Tennet DJ, Dowd TC, et al. Blood flow restriction training after achilles tendon rupture. *J Foot Ankle Surg* 2018;57:635-638.

9. Shimizu R, Hotta K, Yamamoto S, et al. Low-intensity resistance training with blood flow restriction improves vascular endothelial function and peripheral blood circulation in healthy elderly people. *Eur J Appl Physiol* 2016;116:749-757.

10. McIlwraith, C. W., D. D. Frisbie, and C. E. Kawcak. The horse as a model of naturally occurring osteoarthritis. *Bone Joint Res* 2012;1(11): 297-309.

11. King MR, Haussler KK, Kawcak CE, et al. Effect of underwater treadmill exercise on postural sway in horses with experimentally induced carpal joint osteoarthritis. *Am J Vet Res* 2013;74:971-982.

12. Johnson SA, Chicco AJ, Selberg KT, et al. Short-term effects of blood flow restriction training on equine skeletal muscle oxidative capacity. In: *Orthop Res Soc* Annual Meeting, Poster Presentation, Feb 12-16, 2021.

13. Johnson SA, Frisbie DD, Griffenhagen GM, King MR. Equine blood flow restriction training: Part I safety validation. *Equine Vet J*, 2022;Minor revisions submitted 10.5.22.

14. Masri BA, Day B, Younger, AS, et al. Technique for measuring limb occlusion pressure that facilitates personalized tourniquet systems: a randomized trial. *J Med Biol Eng* 2016;36:644-650.

15. McGilvray, K.C., Santoni, B.G., Turner, A.S., Bogdansky, S., Wheeler, D.L., Puttlitz, C.M. Effects of ^{60}Co gamma radiation dose on initial structural biomechanical properties of ovine bone-patellar tendon-bone allografts. *Cell Tissue Bank* 2010; **12**, 89-98.

16. Movin T, Gad A, Reinholt F, et al. Tendon pathology in long-standing achillodynia. Biopsy findings in 40 patients. *Acta Orthop Scand* 1997;68:170-175.

17. Cook J, Feller J, Bonar S, et al. Abnormal tenocyte morphology is more prevalent than collagen disruption in asymptomatic athletes' patellar tendons. *J Orthop Res* 2004;22:334-338.

18. Sikes KJ, Andrie KM, McConnell A, et al. Clinical and histologic manifestations of a novel rectus femoris myotendinous juction injury in rats. *Musc Lig Tend J* 2021;11(4):600-613.

19. Laurentino GC, Ugrinowitsch C, Roschel H, et al. Strength training with blood flow restriction diminishes myostatin gene expression. *Med Sci Sports Exer* 2012; 406-412.

20. Abe T, Kearns C, Manso Filho H, et al. Muscle, tendon and somatotropin responses to the restriction of muscle blood flow induced by KAATSU-walk training. *Eq Ex Phys* 2006;36:345- 348.

21. Navas de Solis C, Gabbett T, King MR, et al. Science in brief: The Dorothy Havemeyer International Workshop on poor performance in horses: Recent advances in technology to improve monitoring and quantification. *Equine Vet J* 2022;54:844-846.

22. Johnson SA, Bell S Schnabel LS, et al. Frontiers in Athletic Rehabilitation: What is Translatable to the Horse? In: *Proc* American Association of Equine Practitioners Annual Convention, December 4-8, 2021.

23. Centner C, Lauber B, Seynnes OR, et al. Low-load blood flow restriction training induces similar morphological and mechanical Achilles tendon adaptations compared with high-load resistance training. *J Appl Physiol* 2019;127:1660-1667.

24. Centner C, Jerger S, Lauber B, et al. Low-load blood flow restriction and high-load resistance training induce comparable changes in patellar tendon properties. *Med Sci Sports Ex* 2021; doi:10.1249/MSS.0000000000002824.

25. Chulvi-Medrano I, Picon-Martinez M, Cortell-Tormo JM, et al. Different time course of recovery in Achilles tendon thickness after low-load resistance training with and without blood flow restriction. *J Sport Rehabil* 2020;30(2):300-305.

26. Picon Martinez M, Medrano-Chulvi I, Cortell-Tormo JM. Acute effects of resistance training with blood flow restriction on Achilles tendon thickness. *J Human Kinetics* 2021;78:101-109.

27. Wiesinger HP, Kosters A, Muller E, et al. Effects of increased loading on in-vivo tendon properties: a systematic review. *Med Sci Sports Exerc* 2015;47:1885-1895.

28. Williams, RB, Harkins, LS, Hammond, CJ, et al. Racehorse injuries, clinical problems and fatalities recorded on British racecourses from flat racing and National Hunt racing during 1996, 1997 and 1998. *Equine Vet J* 2001;33(5): 478-86.

29. Godwin, EE, Young, NJ, Dudhia, J, et al. Implantation of bone-marrow derived mesenchymal stem cells demonstrates improved outcome in horses with overstrain injury of the superficial digital flexor tendon. *Equine Vet J* 2012;44:25-32.

30. Palmer, S, Genovese, R, Longo, L, et al. Practical management of superficial digital flexor tendonitis in the performance horse. *Vet Clin N Am Equine Pract* 1994;10: 425-482.

31. Sarrafian, TL, Case, JT, Kinde H, et al. Fatal musculoskeletal injuries of Quarter Horse racehorses: 314 cases (1990-2007). *J Am Vet Med Assoc* 2012; 241(7): 935-942.

32. Lam, KH, Parkin, TDH, Riggs, CM, et al. Descriptive analysis of retirement of Thoroughbred racehorses due to tendon injuries at the Hong Kong Jockey Club (1992-2004). *Equine Vet J* 2007; 39(2): 143-148.

33. Singer, ER, Barnes, J, Saxby, F, et al. Injuries in the event horse: Training versus competition. *Vet J* 2008;175(1): 76-81.

34. Genovese, R. Quantitative sonographic assessment in the clinical management of superficial digital flexor injuries in Thoroughbred racehorses. In: *Proc Am Assoc Equine Pract* 1997 Annual Convention, December 7-10 1997:43;285.

35. Butcher MT, Hermanson JW, Ducharme NG, et al. Superficial digital flexor tendon lesions in racehorses as a sequela to muscle fatigue: A preliminary study. *Equine Vet J* 2007;39(6):540-545.

36. Patterson-Kane JC, Becker DL, Rich T. The pathogenesis of tendon microdamage in athletes: the horse as a natural model for basic cellular research. *J Comp Pathol* 2012;147:227– 247.

37. Firshman AM, Borgia LA, Valberg SJ. Effects of training at a walk on conventional and underwater treadmills on fiber properties and metabolic responses of superficial digital flexor and gluteal muscles to high-speed exercise in horses. *Am J Vet Res* 2015;76:1058-1065.

38. Wilson AM, McGuigan MP, Su A, et al. Horses damp the spring in their step. *Nature* 2001;414:895-899.

39. Butcher MT, Hermanson JW, Ducharme NG, et al. Contractile behavior of the forelimb digital flexors during steady-state locomotion in horses (Equus caballus): An initial test of muscle architectural hypotheses about in vivo function. *Comp Biochem Physiol, Part A* 2009:100-114.

40. Zarucco L, Taylor KT, Stover SM. Determination of muscle architecture and fiber characteristics of the superficial and deep digital flexor muscles in the forelimbs of adult horses. *Am J Vet Res* 2004;65(6):819-828.

41. Borgia LA, Valberg SJ, Essen-Gustavsson B. Differences in the metabolic properties of gluteus medius and superficial digital flexor muscles and the effect of water treadmill training in the horse. *Equine Vet J* 2010;42(38):665-670.

42. Gottlieb M, Essen-Gustavsson B, Lindholm A, et al. Effects of a draft-loaded interval-training program on skeletal muscle in the horse. *Am Phys Soc* 1989:570-577.

43. Pierce J, Clark B, Ploutz-Snyder L, et al. Growth hormone and muscle function responses to skeletal muscle ischemia. *J Appl Physiol* 2006;101:1588-1595.

44. Takarada Y, Nakamura Y, Argua S, et al. Rapid increases in plasma growth hormone after low-intensity resistance exercise with vascular occlusion. *J Appl Physiol* 2000;88:61-65.

45. Doessing S, Heinemeier KM, Holm L, et al. Growth hormone stimulates the collagen synthesis in human tendon and skeletal muscle without affecting myofibrillar protein synthesis. *J Physiol* 2010;588:341-51.

46. McIlwraith CW, Frisbie DD, Kawcak CE. The OARSI histopathology initiative – recommendations for histological assessments of osteoarthritis in the horse. *Osteoarthritis Cart* 2010;18:S93-S105.

47. Frisbie DD, Kawcak C, Trotter G, et al. Effects of triamcinolone acetonide on an in-vivo equine osteochondral fragment exercise model. *Equine Vet J* 1997;29:349-359.

48. Miller RE, Grodzinsky AJ, Barrett MF, et al. Effects of the combination of microfracture and self-assembling peptide filling on the repair of a clinically relevant trochlear defect in an equine model. *J Bone Joint Surg Am* 2014;96:1601-9.

49. Farndale RW, Sayers CA, Barrett AJ, et al. A direct spectrophotometric microassay for sulfated glycosaminoglycans in cartilage cultures. *Connect Tissue Res* 1982;9(4):247-248. Epub 1982 Jan 1.

50. DePhillipo NN, Kennedy MI, Aman ZS, et al. The role of blood flow restriction therapy following knee surgery: Expert opinion. Arthroscopy: *J Arthro Rel Surg* 2018;34(8):2506-2510.

51. Erickson LN, Hickey Lucas KC, Davis K, et al. Effect of blood flow restriction training on quadriceps muscle strength, morphology, physiology and knee biomechanics before and after anterior cruciate ligament reconstruction: protocol for a randomized clinical trial. *Physical Therapy* 2019;99(8):1010-1019.

52. Hughes L, Rosenblatt B, Paton B, et al. Blood flow restriction training in rehabilitation following anterior cruciate ligament reconstructive surgery: A review. *Tech in Orthop* 2018;33(2): 106-113.

53. Ferraz RB, Gualano B, Rodrigues R, et al. Benefits of resistance training with blood flow restriction in knee osteoarthritis. *Med Sci Sports Exerc* 2018;50(5): 897-905.

54. Ferlito JV, Pecce SAP, Oselame L, et al. The blood flow restriction training effect in knee osteoarthritis people: a systematic review and meta-analysis. *Clinical Rehabilitation* 2020; 34(11): 1378-1390.

55. Rosenberg. L. Chemical basis for the histological use of safranin o in the study of articular cartilage. *J Bone Jr Surg* 1971*;*53-A: 69-82.

56. Mason, JS, Crowell MS, Brindle RA, et al. The effect of blood flow restriction training on muscle atrophy following meniscal repair or chondral restoration surgery in active duty military: a randomized controlled trial. *Journal of Sport Rehabilitation* 2021;31(1): 77-84.

57. Walmsley J, Phillips T, Townsend H. Meniscal tears in horses: an evaluation of clinical signs and arthroscopic treatment of 80 cases. *Equine Vet J* 2003:35(4);402-406.

58. Ferris D, Frisbie D, Kisiday J, McIlwraith C et al. Clinical outcome after intra-articular administration of bone marrow derived mesenchymal stem cells in 33 horses with stifle injury. *Vet Surg* 2014: 43; 255-265.

59. Croxford AK, Parker RA, Burford JH, et al. Chondromalacia of the cranial medial femoral condyle; its occurrence and association with clinical outcome in a population of adult horses with stifle lameness. *Equine Vet J* 2020;52:379-383.

60. Owens JO. Personalized blood flow restriction rehabilitation. *Owens Recovery Science* 2018.

61. Loenneke JP, Young KC, Fahs CA, et al. Blood flow restriction: rationale for improving bone. *Med Hypotheses, 2012;78*(4): 523-527.

62. Bail H, Raschke MJ, Kolbeck SF, et al. Recombinant growth hormone increasus callus maturation time in distraction osteogenesis—a histomorphometric study. *Langenbecks Archiv für Chirurgie*. 1998;115(supplement I):675–680.

63. Raschke M, Rasmussen MH, Govender S, et al. Effects of growth hormone in patients with tibial fracture: a randomised, double blind, placebo-controlled clinical trial. *Eur J Endocrinol* 2007;156:341–351.

64. Frost HM. From Wolff's law to the Utah paradigm: insights about bone physiology and its clinical applications. *Anat Rec* 2001;262:398–419.

65. Turner CH. Three rules for bone adaptation to mechanical stimuli. *Bone* 1998;23:399–407.

66. Welch RD, Johnston 2nd CE, Waldron MJ, et al. Bone changes associated with intraosseous hypertension in the caprine tibia. *J Bone Joint Surg Am* 1993;75:53–60.

67. Bergula AP, Huang W, Frangos JA. Femoral vein ligation increases bone mass in the hind limb suspended rat. *Bone* 1999;24:171–7.

68. Park SH, Silva M. Effect of intermittent pneumatic soft-tissue compression on fracture–healing in an animal model. *J Bone Joint Surg Am* 2003;85:1446 53.

69. Hewitt JD, Harrelson JM, Dailiana Z, et al. The effect of intermittent pneumatic compression on fracture healing. *J Orthop Trauma* 2005;19:371–6.

70. Kelly PJ, Bronk JT. Venous pressure and bone formation. *Microvasc Res* 1990;39:364–75.

71. Beekley MD, Sato Y, Abe T. KAATSU-walk training increases serum bone specific alkaline phosphatase in young men. *Int J KAATSU Training Res* 2005;1:77–81.

72. Bemben DA, Palmer IJ, Abe T, et al. Effects of a single bout of low intensity KAATSU resistance training on markers of bone turnover in young men. *Int J KAATSU Training Res* 2007;3:21–6.

73. Chicco AJ, Le CH, Gnaiger E, et al. Adaptive remodeling of skeletal muscle energy metabolism in high-altitude hypoxia: Lessons from AltituteOmics. *J Biol Chem* 2018;293(18):6659-6671.

74. Pesta D, Gnaiger E. High-resolution respirometry: OXPHOS protocols for human cells and permeabilized fibers from small biopsies of human muscle. *Methods Mol Biol* 2012;810:25-58.

75. Valerio DF, Berton R, Conceicao MS, et al. Early metabolic response after resistance exercise with blood flow restriction in well-trained men: a metabolomics approach. *Appl Physiol Nutr Metab* 2018;43:240-246.

76. Tsukamoto S, Shibasaki A, Naka A, et al. Lactate promotes myoblast differentiation and myotube hypertrophy via a pathway involving myoD in vitro and enhances muscle regeneration in vivo. *Int J Mol Sciences* 2018;19:3649.

77. Yuan Y, Xu Y, Xu J, et al. Succinate promotes skeletal muscle protein synthesis via Erk1/2 signaling pathway. *Mol Med Reports* 2017;16:7361-7366.

CHAPTER 8 - Concluding Remarks and Future Directions

Tendon injuries in the horse remain a challenge for veterinary practitioners to accurately diagnose, prognose and treat in absence of re-injury. The body of work herein describes a lineage of investigations pertinent to tendinopathic diagnostic and rehabilitative methods. Through incorporation of various experimental tendinopathic models using diagnostic imaging and morphologic outcomes, insight into lesion detection and staging has been realized. These studies were followed by investigation into the role of therapeutic exercise and lastly the novel rehabilitative modality of blood flow restriction (BFR) training for use in the horse. The ability of the horse to serve as a translational model for further BFR investigations such as sensor validation, incorporation of experimental models of injury and clinical trials are promising avenues of further study.

Beginning with an equine surgical superficial digital flexor (SDF) tendinopathic model to investigate the diagnostic utility of computed tomography (CT), magnetic resonance imaging (MRI) and ultrasound (US) [1], we have demonstrated that non-contrast enhanced CT most closely correlated with sub optimal healing and that T2-weighted hyperintensity on MRI indicates tendinous hypercellularity even in the more chronic stages of healing. In contrast to other published equine investigations [2,3], contrast-enhanced CT and MRI evaluation was not relevant to end-point tissue analysis and were not useful to predict ongoing physiologic events for longitudinal tendinopathic evaluation. As a basis for further model development, the biomechanical properties of these tendons were then compared to that of uninjured equine tendons which demonstrated detrimental increases in elastic modulus and cross-sectional area (CSA) not only at the site of lesion creation, but also proximal and distal consistent with global

tendinopathic change. Through this work, the features of this surgical model have now been longitudinally evaluated from diagnostic imaging, histopathologic, biochemical and biomechanical perspectives.

Subsequently, the emerging diagnostic imaging modality of elastography and its ability to differentiate tissue deformability characteristics was investigated using an equine collagenase model of deep digital flexor (DDF) tendinopathy [4]. Tissue-specific differences between deep digital flexor tendons (DDFTs) treated with mesenchymal stem cells (MSCs) were apparent biochemically, but unfortunately not predicted by elastography. With a weak correlation to corresponding intra-tendinous glycosaminoglycan (GAG), DNA and collagen content, elastography's ability to predict physiologic tendinous characteristics within this anatomic region remains limited.

The therapeutic benefits of various exercise protocols in terms of grade and speed were then related to exercise capacity, morphology and mechanical outcomes using an established model of murine tendinopathy. This investigation was motivated to help define exercise parameters most beneficial to tendon healing, which are currently unknown for clinical tendinopathic exercise prescription. Specifically, exercise at a fast, flat speed was most detrimental to tendon healing, and higher levels of systemic collagen X (COLX) were found in mice exercised (at any speed or grade) in comparison to those cage-rested. These findings ultimately advance the understanding of how the intensity of exercise correlates to tendon injury and healing in a chronic tendon injury model, for which there currently is no peer-reviewed evidence to support.

The final chapters herein move away from tendinopathic injury models and into the realm of safety validation of the novel rehabilitative modality BFR. With substantial work in humans

demonstrating efficacy in BFR's ability to improve muscle size and strength in absence of damaging loads [5] the motivation to evaluate its safe musculoskeletal application in healthy horses serves as a crucial first investigative step to further evaluate its efficacious use within the equine rehabilitative setting. Additionally, very little is known about BFR's downstream effects on a variety of musculoskeletal tissue types (tendon, bone, cartilage). Through this initial pilot investigation, we have now produced evidence to suggest that BFR increases normal equine tendon stiffness. Additionally, we were unable to detect differences in normal articular cartilage or subchondral bone density as a result of BFR exposure. When assessing muscle oxidative capacity and reactive oxygen species (ROS) release, we were able to demonstrate that early-phase muscle remodeling (10 days) may not manifest as changes in mitochondrial density that persist with more chronic (56 days) BFR exposure. We were also able to document currently unknown limb occlusion pressure (LOP) values in the standing, unsedated horse and demonstrate that BFR exposure did not result in forelimb biomechanical dysfunction. With the well documented orthopedic similarities between humans and horses and the ability to sample tissues at a more cellular level, the horse represents a promising avenue for further translational BFR research.

Blood flow restriction training is perhaps one of the most exciting, novel rehabilitative modalities for use in horses because it advances beyond the traditional physical therapy pillars of rest, ice and compression. With specific advantages for horses only able to perform a limited amount of exercise, the ability to "biohack" the system with BFR to maintain global strength, protect damaged tissues and even encourage healing at the cellular level is exciting and warrants careful consideration. In terms of subsequent equine BFR use and clinical prescription, the three

areas requiring significant further investigation include that of: 1) Sensor validation, 2) Incorporation of experimental models of injury and 3) Pursuit of clinical trials.

Specifically, the limb occlusion pressure (LOP) is defined as the minimum amount of pressure required to occlude vascular flow (pressure resulting in complete venous occlusion and arterial occlusion). Subsequent occlusion percentages are then calculated from this LOP value to safely and effectively deliver BFR. In our equine investigation herein, LOP readings for each equine forelimb were obtained daily via Doppler ultrasound to ensure that patient-specific pressures were utilized for each BFR session. Patented cuff-sensor technology engineered by Delfi is capable of measuring human LOP values with an accuracy of 1mm Hg and precision +/- 12mm Hg of Doppler ultrasound [6,7]. We have found in horses that the absolute (Doppler ultrasound measurement) pressure detected was 24 +/- 17mm Hg higher than predicted by the Delfi unit's software and monitoring system. Additionally, human limb LOP values are routinely obtained in a supine position with pressure reading differences documented as dependent upon limb and body position [8]. Clinical use in horses would require LOP measurement to be accurately obtained while standing, but limb position while obtaining LOP readings will likely vary. Therefore, the validation of an automated equine-specific tourniquet system capable of accurately (within 5mm Hg) and precisely (minimal variance around the predicted number, +/- 10mm Hg) measuring equine LOP BFR in a variety of limb positions is critically needed and would optimize system performance and thus subsequent therapeutic results. Equine-specific cuff design features would also facilitate ease of clinical use, ensure accuracy of delivered pressures and improve patient comfort. Validation of an equine-specific BFR tourniquet with associated sensor technology and refined measurement acquisition parameters would ultimately serve as a gateway for further safe, veterinary use.

With safety in a variety of musculoskeletal tissue types now having been explored, the next investigative step lies in the incorporation of experimental injury models and clinical trials to further refine equine BFR use. The investigation of BFR in the surgical tendinopathy model used herein [1] to investigate BFR's effects on tendinopathic healing, the previously described ostechondral fragment model [9-11] to evaluate its effects on articular cartilage repair or even a cast model to simulate disuse osteopenia [12] to assess effects on bone density would be exciting avenues to pursue. Additionally, clinical trials comparing efficacy of currently utilized therapeutics to that of BFR for treatment of frequent sources of lameness such as proximal suspensory desmopathy would also be hugely valuable. Mechanistically-driven investigations would logically incorporate the exploration of systemic vs. peripheral metabolomic profiles before, during and after cuff application at a variety of LOP percentages to help refine protocol development. Particular metabolites of interest would be lactate, succinate, alanine and glutamate based on relevant findings with human BFR use [13-16]. Specifically, succinate and lactate have been implicated in altering beneficial down-stream muscle protein synthesis signaling pathways, while alanine and glutamine are markers of muscle catabolism [13-16]. Lastly, various intermittent pneumatic compression (IPC) and BFR exercise protocols in terms of frequency, type of exercise, duration, cuff width and occlusion levels also need to be defined. These types of "best practices" experiments provide exponential sources of BFR investigative opportunities. Given that upwards of 70% of all equine athletes will sustain a musculoskeletal injury during their career, validating and refining techniques such as BFR could greatly enhance the health, welfare and general well-being of a vast number of horses.

The series of experiments herein represent imperfect, yet important investigative first-steps to a greater lineage of future work within the field of translational orthopedic rehabilitation.

Pursuant to the study of tendinopathy, inherent limitations of experimentally induced injury as it relates to clinical disease must be acknowledged. Additionally, incorporation of a more mechanistic focus to investigate the pathogenesis of tendon injury and/or healing at the cellular level in naturally occurring tendon injury may have helped correlate experimental findings to that of spontaneous injury. Regarding the investigation of BFR as a rehabilitative aide for horses, a graduated exercise protocol similar to that which is used in human rehabilitation programs may have yielded different results. Incorporation of corresponding electromyography (EMG) of the SDF muscle and similar (yet more robust) analysis of more muscles of the thoracic sling and girdle would have expanded our conclusions tremendously. Functional outcomes related to BFR's use will also need to be investigated in the future to establish its utility as a true therapeutic aide in horses. Albeit imperfect, the body of work herein was performed to enhance the orthopedic welfare of the horse through investigation of how we may be better suited to detect, stage and rehabilitate tendon injuries specifically. The resultant base of knowledge gained will hopefully continue to cultivate the interdisciplinary collaboration between human and equine orthopedic experts to further advancements within the translational rehabilitative world.

References

1. Johnson SA, Valdez-Martinez A, Turk P, et al. Longitudinal tendon healing as assessed with multi-modality advanced imaging and tissue analysis. *Equine Vet J* 2021;00:1-16.

2. Puchalski SM, Galuppo LD, Hornof WJ, et al. Intraarterial contrast-enhanced computed tomography of the equine distal extremity. *Vet Radiol* 2007;48:21–9.

3. Puchalski SM, Galuppo LD, Clifton DP, Wisner ER. Use of contrast-enhanced computed tomography to assess angiogenesis in deep digital flexor tendonopathy in a horse. *Vet Radiol* 2009;50:292–7.

4. Johnson SA, Biscoe EW, Eilertson KE, Lutter JD, Schneider RK, Roberts GD, Cary JA, Frisbie DD. Tissue predictability of elastography is low in collagenase induced deep digital flexor tendinopathy. *Vet Radiol Ultrasound* 2021;1-13.

5. Pierce J, Clark B, Ploutz-Snyder L, et al. Growth hormone and muscle function responses to skeletal muscle ischemia. *J Appl Physiol* 2006;101:1588-1595.

6. Masri BA, Day B, Younger, AS, et al. Technique for measuring limb occlusion pressure that facilitates personalized tourniquet systems: a randomized trial. *J Med Biol Eng* 2016;36:644-650.

7. Hughes L, Rosenblatt B, Gissane C, et al. Interface pressure, perceptual, and mean arterial pressure responses to different blood flow restriction systems. *Scan J Med Sci Sports* 2018;28:1757-1765.

8. Hughes L, Jeffries O, Waldron M, et al. Influence and reliability of lower-limb arterial occlusion pressure at different body positions. *Peer J* 2018;6:e4697. doi10.7717/pperj.4697.

9. Frisbie DD, Kawcak C, Trotter G, et al. Effects of triamcinolone acetonide on an in-vivo equine osteochondral fragment exercise model. *Equine Vet J* 1997;29:349-359.

10. Kawcak CE, Frisbie D, Trotter G, et al. Effects of intravenous administration of sodium hyaluronate on carpal joints in exercising horses after arthroscopic surgery and osteochondral fragmentation. *Am J Vet Res* 1997;58:1132–1140.

11. Foland JW, McIlwraith CW, Trotter G, et al. Effect of betamethasone and exercise on equine carpal joints with osteo- chondral fragments. *Vet Surg* 1994;23:369–376.

12. Stewart HL, Werpy NM, McIlwraith CW, et al. Physiologic effects of long-term immobilization of the equine distal limb. *Vet Surg* 2020;49(5):840-851.

13. Kawada, S. What phenomena do occur in blood flow-restricted muscle? Int. J. KAATSU Training Res 2005;1:37-44.

14. Valerio DF, Berton R, Conceicao MS, et al. Early metabolic response after resistance exercise with blood flow restriction in well-trained men: a metabolomics approach. *Appl Physiol Nutr Metab* 2018;43:240-246.

15. Tsukamoto S, Shibasaki A, Naka A, et al. Lactate promotes myoblast differentiation and myotube hypertrophy via a pathway involving myoD in vitro and enhances muscle regeneration in vivo. *Int J Mol Sciences* 2018;19:3649.

16. Yuan Y, Xu Y, Xu J, et al. Succinate promotes skeletal muscle protein synthesis via Erk1/2 signaling pathway. *Mol Med Reports* 2017;16:7361-7366.

Subjective Grading Scale	Subjective Grading Scale Description	Standard CT Reference Image (left) & Arterial CECT Phase (right)	Standard CT Reference Image (left) & Venous CECT Phase (right)	Standard CT Reference Image (left) & Delayed CECT Phase (right)
0 = No Contrast Enhancement	No contrast enhancement appreciated			
1 = Very Mild	Small, faint and few vessels migrating into or around the lesion comprising 10-25% overall hyperattenuation			
2 = Mild	Small, faint but several vessels migrating into or around the lesion, comprising 26-25% overall hyperattenuation			
3 = Moderate	Several medium-sized hyperattenuating vessels migrating into or around the lesion, comprising 46-75% overall hyperattenuation			
4 = Marked	Most of the lesion is intensely hyperattenuated by vessels migrating into or around the lesion, comprising 76-100% overall hyperattenuation			

Supplementary Figure 9.1: Grading criteria used to subjectively grade computed tomography (CT) attenuation on various post contrast-enhanced computed tomography (CECT) phases (arterial, venous, delayed) at center of lesion induction. Corresponding limb standard phase CT images provided for pre-contrast comparison. Representative images are from various limbs at the two month evaluation timepoint.

Supplementary Figure 9.2: Equations and associated units of measurement used to calculate stress (A), strain (B) and elastic modulus (C) for each superficial digital flexor tendon (SDFT) region of interest (ROI).

The three equations in the figure are:

$$\text{Stress (MPa)} = \frac{\text{Force}_{MTS}(N)}{\text{Cross Sectional Area}_{AOI\ Specific}(mm^2)}$$

$$\text{Strain}\left(\frac{mm}{mm}\right) = \frac{\text{Length}_{Initial} - \text{Length}_{Instantaneous}}{\text{Length}_{Initial}}$$

$$\text{Modulus}_{Elastic} = \frac{\text{Stress}_{Linear\ Region}}{\text{Strain}_{Linear\ Region}}$$

MRI CSA Lesion Measurements Over Time

	0	1	2	4	6	9	12
T1	0.190	0.466	0.622	0.915	1.075	0.447	0.210
PD	0.181	0.460	0.547	0.690	0.772	0.093	0.088
T2	0.163	0.435	0.290	0.021	0.280	0.000	0.051
STIR	0.202	0.484	0.557	0.913	0.818	0.000	0.053
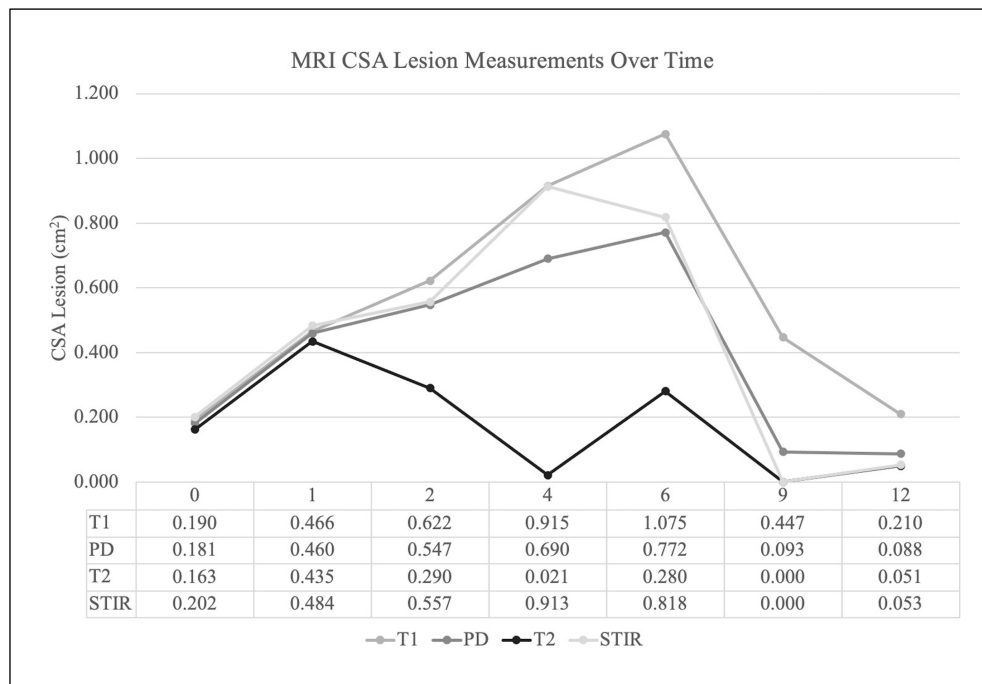
Supplementary Figure 9.3: Average lesion cross sectional area (CSA) measurements (cm^2) across all limbs (n=16) obtained from various magnetic resonance imaging (MRI) sequences (proton density (PD), T1-weighted (T1), T2-weighted (T2) and short-tau inversion recovery (STIR)) over the 12 month study period (0-12).
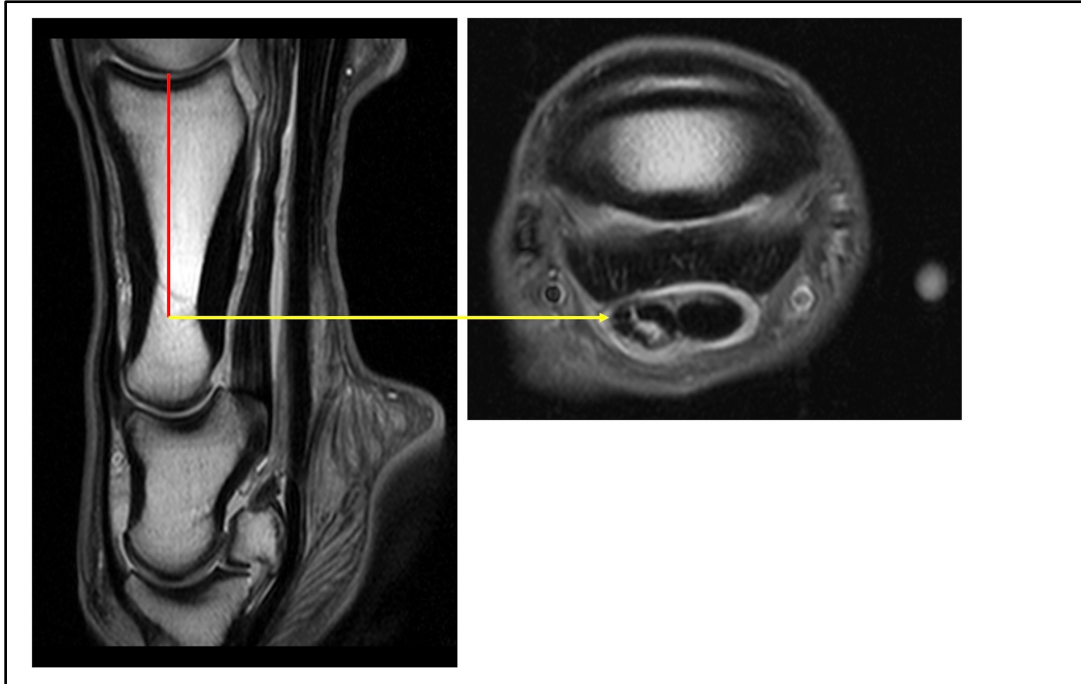
Supplementary Figure 9.4: All post-mortem, day 214 magnetic resonance (MR) images were evaluated to identify the most affected site of deep digital flexor tendon (DDFT) injury (yellow arrow). This location relative to the metacarpophalangeal joint at the most distal aspect of the third metacarpal bone (MC3) with the dorsal cortices of MC3, the proximal phalanx, middle phalanx and distal phalanx aligned was then recorded (red line) and used as the center of evaluation for subsequent biochemical analysis.